# PHOTO-INDUCED STRUCTURAL TRANSFORMATIONS IN SOL-GEL DERIVED SILICA-METHACRYLATE COMPOSITES

*Kalaichelvi Saravanamuttu*

Department of Chemistry
McGill University, Montréal, Quebec, Canada

December 2000

A thesis submitted to the Faculty of Graduate Studies and Research in partial fulfilment of the requirements for the degree of Doctor of Philosophy

0-612-75677-7

*Repression is a seamless garment;*
*- Salman Rushdie*

# ABSTRACT

We describe our investigations into photochemical and micro-structural characteristics of sol-gel derived silica-methacrylate composites (SAC). Upon irradiation with UV light, thin SAC films undergo spatially localised increases of the index of refraction, a macroscopic property that has been used in the photo-lithography of passive integrated optics devices. Our spectroscopic studies indicate that UV initiated free-radical polymerisation of methacrylate substituents trigger further growth and densification of the silica host. This advances our molecular level understanding of photo-reactions in hybrid organo-silica networks.

We examine laser-initiated organic chain growth in SAC planar waveguides. Optical modes initiate polymerisation of methacrylate substituents along the propagation path. In turn, the nascent reaction medium presents a non-uniform refractive index profile to the guided laser beam. Spatially localised and intensity-dependent refractive index changes create a lens-like profile in the medium. As a result, the beam self-focuses along its propagation axis without diffraction.

We describe oriented organic chain growth in the nonlinear optical and highly anisotropic reaction field provided by a linearly polarised, self-focusing laser beam. A self-focusing laser beam induces an anisotropy in the refractive index profile of SAC waveguides. We characterise laser-induced birefringence in the hybrid network through polarised waveguide Raman spectroscopy and optical birefringence measurements.

Long-range periodic self-organisation in sol-gel derived silica acrylate composites formed in the absence of external templates was observed for the first time. Significantly, the periodicity associated with this structure is approximately 200 nm, approaching the optical wavelength regime.

# RÉSUMÉ

Nous presentons nos investigations des propriétés photochimiques et structurelles des composites silica-methacrylate (SAC) obtenu par procédé sol-gel. Apres exposition à la lumiere UV, une augmentation d'indice de refraction est observé dans films de ces materiaux hybride, une charactere qui est utlisé pour fabrication des element des optique intégrée. Nos investigations spectroscopiques indiquent que le polymerisation des unitues organiques dans le composite active les condensations entre les groups alkoxides dans le composite.

Polymerisation dans les guides d'ondes des composites SAC peut etre active par la lumiere guidee 'un laser a ion d'argon. Les reactions presentes une changement d'indice de reaction continuelles dans le film. Par consequence, nous avons observé des characteres auto-focussant du laser.

Nous descrivons que la lumiere auto-focussant introduit une anisotropie dans le SAC film Cette birefringence a été characterisée par le spectroscopie Raman de guides d'ondes polarisée.

Nous avons observé l'organisation periodique dans SAC composites. C'est le premier example d'ordre dans une composite derivé par procédé sol-gei dans l'absence des templates externals.

# ACKNOWLEDGEMENTS

I am grateful to Prof. Mark P. Andrews for membership in his research group in both my undergraduate and graduate years. His enthusiasm, advice and contagious delight at Science, during the course of research and in the preparation of my thesis are deeply appreciated.

The assistance of the following people on technical aspects of this research project is gratefully acknowledged. Dr. Fred Morin for acquiring solid-state $^{29}$Si NMR spectra. Rick Rossi for resuscitating the spin-coater on several occasions. Fred Kluck and Mr. Bill Bastian created and repaired several components for the optical assemblies. Helen Campbell from the Department of Mining and Metallurgical Sciences for training sessions on the scanning electron microscope and advice on acquiring micrographs. Prof. Vali, Jeanni and Caroline of the Department of Anatomy for their invaluable assistance with sample preparation and acquiring transmission electron micrographs. Glen Poirier for training sessions on the atomic force microscope. Peyman Meshkinfam for assistance with acquiring an optical micrograph and in fibre-coupling experiments. Dr. Serge Pelissier and Dr. Daniel Blanc for their help and advice with the prism-coupling set-up. Jean Francois Nadeau for training on the ArF excimer laser, the optical set-up for Bragg grating inscription and the optical spectrum analyser. His lifts to the workplace on numerous wintry, Saturday mornings will be warmly remembered.

Liberal use of UV-Vis spectrophotometers belonging to Prof. R. Kazlauskas and Prof. A. Kakkar, the IR spectrometer in the laboratory of Prof. J. Gleason, the polarised optical microscope, camera and IR polariser from the laboratories of Prof. Brown and Millipore™ water from the laboratory of Prof. B. Lennox is gratefully acknowledged.

I am indebted to Prof. J. Hogan for his powerful support during my final undergraduate year. I thank Dr. G. Wilzcek for her advice and for making me aware of the Dance of Anger. I also thank all the members of Room 348, past and present, for their humour and goodwill.

I am grateful to Prof. Ignacio Vargas-Baca, my harshest and most valued critic, for his interest, intuition and guidance with many aspects of my work and in particular, for the long hours spent capturing sunbeams, opalescence and elusive optical modes on film. I am thankful to Ngiap-Kie Lim for his realism and kindness during our years at McGill.

I especially thank Evelyn Martins for her grace, compassion and friendship through all things. Her consistent encouragement, invaluable assistance in the preparation of this thesis as well as her patient and careful proof reading of numerous versions of this *in*organic manuscript are most gratefully acknowledged.

Finally, I am forever indebted to my parents and Nagulan for their unfailing support, tolerance and generosity throughout my school years, and especially Amma and Dadda, for strength.

# TABLE OF CONTENTS

## 1. INTRODUCTION

2. PHOTO-INDUCED STRUCTURAL TRANSFORMATIONS IN SOL-GEL DERIVED COMPOSITE THIN FILMS - IMPLICATIONS FOR INTEGRATED-OPTICS DEVICE FABRICATION

## 3. *IN SITU* WAVEGUIDE RAMAN SPECTROSCOPY OF PHOTO-REACTIONS IN SOL-GEL DERIVED SILICA-METHACRYLATE THIN FILMS

## 4. SELF-FOCUSSING OF LIGHT IN HYBRID SILICA-METHACRYLATE NANOCOMPOSITES

**5. UNEXPECTED SELF-ORGANISATION IN A CLASS OF SOL-GEL DERIVED SILICA-METHACRYLATE COMPOSITES**

**6. ORIENTED POLYMER GROWTH WITH POLARISED, SELF-FOCUSING LIGHT IN SILICA-METHACRYLATE WAVEGUIDES**

## 7. CONCLUSIONS, SUGGESTIONS FOR FUTURE RESEARCH AND CONTRIBUTIONS TO ORIGINAL KNOWLEDGE

# LIST OF FIGURES AND TABLES

# 1. INTRODUCTION

## 1.1 LIGHT-BASED COMMUNICATIONS SYSTEMS

Photonics technology has had significant impact on long distance communications. More information is being dispensed faster and further than ever before through fibre-optic networks that support large sectors of telecommunications systems. Modulated pulses of near infrared (NIR) light propagating through $SiO_2$ fibres, courier digital information between computers and telephones throughout the globe. Photons have proved to be efficient data carriers because they travel faster than electrons, can be resolved into a spectrum of wavelengths, each with information carrying capacity, and do not interact with each other, reducing energy loss and cross talk.

### 1.1.1 Silica – the medium of light transport

The $SiO_2$ optical fibre is the fundamental optical element of both the terrestrial and transoceanic branches of the communication backbone. Indeed, within the next five years the total length of fibre installed in these systems, will suffice to encircle the Earth fifteen times[1]. Low-loss $SiO_2$ fibres for optical transmission were first created in 1970 by researchers at Corning[2]. These hair-fine, cylindrical filaments coated with a low refractive index (n) cladding, served as passive waveguides for visible and infrared (IR) light. A simple representation of waveguiding in these structures is shown in Figure 1.1.

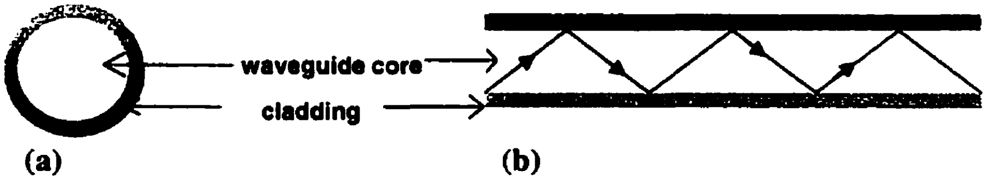

**Figure 1. 1 a)** circular and **b)** longitudinal cross section of an optical fibre consisting of a high refractive index core surrounded by a lower refractive index cladding. The zigzag path of waveguided light is schematised in b).

A laser beam that is coupled into the circular waveguide continuously suffers total internal reflection (TIR) at the core/cladding interfaces. As a result, the beam is confined to the glass core and propagates in a zigzag path (*i.e.* is guided) over long distances, without significant attenuation. In this way, the NIR wavelengths used in telecommunications, namely 0.83, 1.3 and 1.5 μm, propagate as guided optical waves through $SiO_2$ optical fibres, a gram of which may extend to 500 kilometres[3].

Fuelled by the tremendous user appetite for bandwidth (data rates), considerable research and industrial activity has been devoted to increasing the data carrying capacity of the $SiO_2$ fibre. Strategies include improving its transparency by eliminating NIR absorbing species such as adventitious $H_2O$ molecules[4], using the nonlinear optical (NLO) properties of $SiO_2$ to prevent pulse dispersion and thus signal loss[5] and applying dense wavelength division multiplexing (DWDM) technology[6], where up to 40 narrowly resolved wavelengths of light (each with Gigabit/s data rates) may simultaneously travel in a single fibre. Collectively, these efforts over the past three decades have elevated data rates in $SiO_2$ fibres to Terabits/s.

## 1.2 PHOTONIC MATERIALS

The ultimate goal of photonics is to extend the functionality of optical systems from simple data transmission to data processing, "smart" functions that are currently performed by electronic systems. Inspired by the success of microelectronics, photonics technology is now poised for the all-optical circuit - a single chip densely packed with active, micro-optical devices interconnected with passive waveguides - systems that are designed to harness and assign specific tasks to photons. The creation of such active devices demands materials that respond intelligently to light, are processable into miniaturised device platforms and optically compatible with existing $SiO_2$-based fibre systems.

### 1.2.1 Silica

Silica itself, in addition to its transparency to NIR light, has a selection of optical properties that may be used to create devices. For example, the glass undergoes a change in its refractive index (Δn) when exposed to visible[7] or UV light[8]. Indeed Bragg gratings, which are key elements in telecommunications systems[9], consist of a periodic modulation of $\Delta n$ photo-inscribed in $SiO_2$ optical fibres. Furthermore, the material is sensitive to the polarisation of the incident light. There have been several reports of optical anisotropy (birefringence) induced by linearly polarised laser beams in $SiO_2$, an amorphous material that initially has an isotropic refractive index[10]. This property has enabled the fabrication of polarisation sensitive micro-optical elements such as rocking filters[11].

Another useful property of $SiO_2$ is its nonlinear optical response (NLO) to high laser intensities, where it undergoes a refractive index change that is proportional to the intensity of the actinic light. This forms the basis of interferometric devices that are used as switches or modulators of light signals[12]. This form of NLO response also supports temporal[5] and spatial solitons[13], robust wavepackets of light, which do not suffer diffraction or dispersion as they propagate along the $SiO_2$ fibres.

### 1.2.2 Organic molecules and macromolecules

An impressive array of active micro-optical elements has been built from organic molecules and polymers. Light-emitting diodes, photodiodes, lasers[14], light amplifiers[15], field effect transistors[16] and solar cells (photovoltaic diodes)[17] have all been crafted from thin slices of organic semiconductors. Polarisation selectivity, crucial to flat panel display technology, is now possible in polymer sheets that are photoluminescent[18], doped with luminophores[19] or derivatised with liquid crystalline monolayers[20]. Carefully stacked polymer films with well-characterised refractive index profiles[21] form efficient and omnidirectional mirrors while antireflection coatings have been cast from nanoporous polymer (low-$k$) networks[22]. These devices take advantage of the rich assortment of molecular properties such as delocalised electronic structures, dipole-dipole orientation, amphiphilic interactions and polarisation sensitivity that are only available to organic molecules and macromolecules.

### 1.2.3 Hybrid silica-organic nanocomposites

Considerable attention has also been placed on silica-organic nano-composites. These hybrid materials are created through sol-gel processing, which consists of the hydrolysis and poly-condensation reactions of alkoxysilanes carried out in the presence of organic molecules (*vide infra*). The resulting hybrid organic-inorganic systems are attractive candidates for optical applications as they combine the desirable physical properties of silica, such as refractive index and transparency to NIR light, with the diverse functionalities that are available to organic molecules. However, it is important to note that these materials are not simply organosilica amalgams that display both sets of properties belonging to the organic and the silica components. By contrast, the co-existence of organic and inorganic phases at the molecular level, often imparts unique structural and optical properties to these hybrid networks.

## 1.3 SOL-GEL PROCESSING OF HYBRID ORGANIC-SILICA COMPOSITES

Conventionally glass is formed by heating sand or metal oxides at high temperatures. One and a half centuries ago, Ebelman[23] observed that amorphous silica could be formed at room temperature, through the hydrolysis and condensation reactions of silicic acid esters. The hydrolysis of silicon alkoxides leads to silicic acids (equation [1.1]), which undergo condensation reactions between themselves (equation [1.3]) or other alkoxide groups (equation [1.2]) to form siloxane bonds.

$$\mathrm{Si(OR)_4 + H_2O \rightleftharpoons Si(OR)_3OH + ROH} \qquad [1.1]$$

$$\mathrm{Si(OR)_3OH + Si(OR)_4 \rightleftharpoons (OR)_3Si\text{-}O\text{-}Si(OR)_3} \qquad [1.2]$$

$$\mathrm{Si(OR)_3OH + Si(OR)_3(OH) \rightleftharpoons H_2O\ (OR)_3Si\text{-}O\text{-}Si(OR)_3} \qquad [1.3]$$

As schematised in Figure 1.2[24], the resulting silicate oligomers dispersed in the solvent (as a sol) aggregate with time into a continuous network (or a gel). Sol-gel processing consists of guiding the structure and evolution of these polysilicate species into desired morphologies through reaction parameters such as temperature, reagent compositions, drying conditions and especially pH. For example, acid catalysis of the leads to minimally condensed, weakly branched polymeric silicates that undergo cluster-cluster aggregation to form a gel (A); an extended, solvent encapsulating silica-network that spans the reaction vessel. At the other extreme, charge stabilised particulate colloids are obtained when the same reactions are catalysed with bases (B). Xerogels formed upon further condensation and evaporation of solvent in the gel networks (D), can be consolidated into dense ceramics at high temperatures (E). Aerogels with remarkably low densities result from the rapid extraction of solvent from gels (C). Solvent evaporation is accelerated when sols are spin, dip or doctor-blade coated onto substrates. Condensation reactions also take place, leading to premature gellation in the films, which can be further densified with thermal treatment (G).

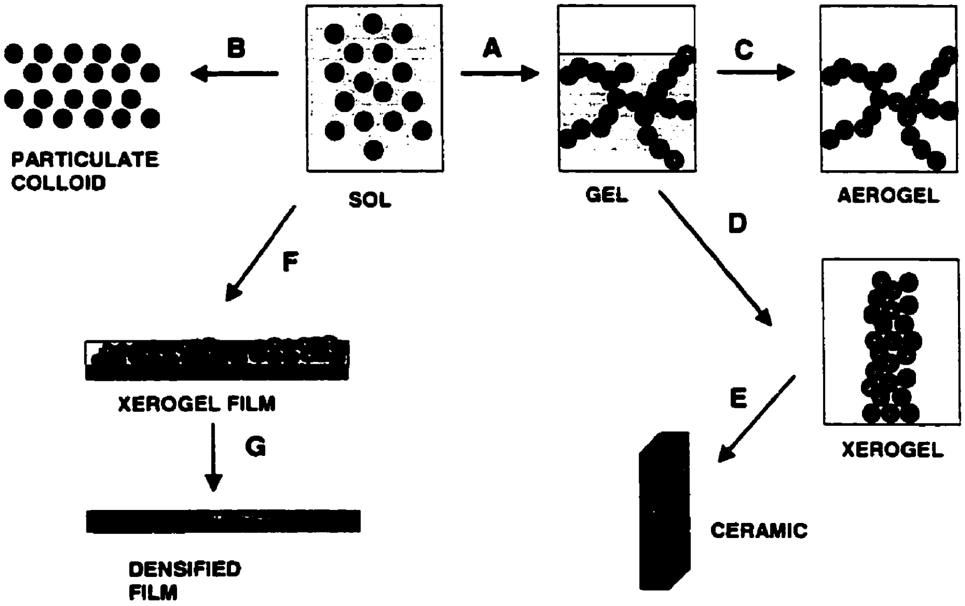

**Figure 1. 2** Various morphologies of silica obtained through sol-gel processing of alkoxysilanes

### 1.3.1 Incorporation of an organic component in the silica network

Organic molecules introduced at the early stages of sol-gel reactions are incorporated in the evolving inorganic network, leading to composites that consist of both a silica and an organic component. Such hybrid organic-inorganic glasses may be categorised into two classes[25]. In the first, silica glasses are doped with organic molecules, macromolecules and polymers. Coexistence of the two phases is mediated by weaker (van der Waals, hydrogen bonding, electrostatic) forces. A classic example is the hydrogen bonding between carbonyl and silanol groups, that prevent macroscopic phase separation in poly (methylmethacrylate) doped glass. In the second case, the organic component is introduced as a substituent on the alkoxysilane precursor. The Si-C bonds are non-hydrolysable and survive the inorganic polymerisation reactions. Ligands bound to their silicon centres are thus homogeneously distributed in the final silica gel. This ability to modify and functionalise silica has led to creative and significant advances in biomedical/chemical sensing, porous supports in catalysis, adhesive materials and resistive coatings[26a-d].

### 1.3.2 Optical properties of composites derived from organo-substituted alkoxysilanes

Few studies have been conducted of the optical properties organosilica composites belonging to the second class of hybrid composites. In the majority of cases, sol-gel glasses for optical applications have been derived from simple precursors such as tetramethoxysilane, tetraethoxysilane and methyl trimethoxysilane, which have served as passive hosts for active organic species[27].

However, several optical parameters of the final composite may be varied, controlled and enhanced by careful choice of a organo-substituted trialkoxysilane precursor. For example, glasses derived from organosubstituted alkoxysilanes are less porous and more homogenous than purely inorganic sol-gel derived silica networks. The organic substituent reduces the number of polymerisable alkoxides to three, and thus disrupts the three-dimensional silica structure. In effect, the ligand imparts flexibility to the network, which can undergo relaxation and rearrangements to counter the high capillary pressures that arise during drying processes. Consequently, light-scattering sites due to air holes or inhomogeneities in the material refractive index (*n*) are reduced in these organic-inorganic systems, which remain largely transparent in the visible and infrared spectral regions. Furthermore, the strong covalent bonds linking the organic and the inorganic components prevent macroscopic phase separation between the two phases. The interfacial zone between the organic and the inorganic components can be blurred even further by encouraging interactions between the organic group and its silica host. Hydrogen bonding between the lone pairs of carbonyl groups (C=O) and silanol (Si-OH) groups in the silica matrix has long been confirmed[28]. Similarly, electron-donating interactions can be encouraged through amino ($NH_2$) groups. Substituents may also be used to tune the refractive index of the composite.

The Clausius-Mossotti equation traces the microscopic origins of the refractive index ($n$) to the polarisability of molecules ($\alpha$). Substituents such as the polarisable phenyl functional groups could be used to increase the refractive index of hybrid glasses. A range of long-alkyl chain substituted trialkoxysilanes are commercially available. Microphase separation and orientation between the organic and the inorganic phases in may lead to long-range organisation and thus optical anisotropy or birefringence in the final composites. Materials obtained from trialkoxysilanes with vinyl substituents are especially attractive because the organic ligands transfer their photosensitivity to the composite. Once the silica network is formed, free-radical polymerisation of the vinyl groups can be initiated with light. This property may be used to photo-inscribe micrometric glass devices with lithographic techniques.

## 1.4 LIGHT-MATTER INTERACTIONS IN SILICA-METHACRYLATE COMPOSITES

The research presented in this thesis focuses on a class of photosensitive composites derived from methacrylate-substituted trialkoxysilanes. Initially pioneered by Schmidt and co-workers, these materials belong to the category of glasses, known as "ormocers", "ormosils", "ceramers", "polycerams", or simply hybrid sol-gel glasses (HSGGs)[29, 30]. Several research groups including our own, have adopted these hybrid systems for the photolithography of integrated optics devices. A wide range of micro-optical elements has been created on these photosensitive substrates including waveguides[31], directional couplers[32, 33], beam splitters and high reflectivity Bragg gratings on ridge waveguides[34]. In most of these cases, the devices have been fabricated through lithographic techniques borrowed from the microelectronics industry. Although such processes have paid careful attention[35] to the evolution of the refractive index profiles in the materials, fundamental questions regarding the molecular level photochemistry, the structural character, the form of co-existence between the organic and the inorganic components of the composites have remained, until now, mostly unanswered.

Our first objective was to gain a molecular-level understanding of photo-initiated processes in the hybrid silica-methacrylate matrix. In particular, we examined the light induced structural changes that led to refractive index increases in the material, a property that is used for the photolithography of micro-optical elements. Silica-methacrylate planar waveguides support transverse electric (TE) and transverse magnetic (TM) optical modes at both visible and infrared wavelengths. This property was used to initiate free-radical reactions in thin film silica-methacrylate material with guided optical modes of a visible $Ar^+$ laser. As polymer growth takes place, the laser beam propagates in a reaction medium with a continuously changing refractive index profile. We investigate if such a temporally and spatially transient refractive index leads to self-focusing of the c.w. laser beam. Our strategy of guided wave polymerisation enables us to carry out polymer growth under the highly anisotropic reaction field of a linearly polarised, optical field. We examine the effects of polarised guided optical waves and their ability to carry out photo-oriented polymerisation in the hybrid network. Our sol-gel derived nanocomposite consists of closely co-existing organic and inorganic components. We seek an understanding of amphiphilic interactions between these conventionally immiscible phases. We report the discovery of long-range, three-dimensional, periodic self-organisation in the methacrylate rich silica networks, which have until now been considered amorphous glasses. We describe how the sub-micrometric, organisation in the silica-methacrylate composites can be permanently captured in both thin film and monolithic form, through the polymerisation of the methacrylate functionalities.

The studies presented here combine the light-initiated growth of organic polymer chains in a sol-gel derived silica host with various forms of light-matter interactions that are of interest to photonics systems. These include processes such as the photolithography of integrated-optics (IO) devices, the self-focusing of laser beams in nonlinear optical media, laser-induced anisotropy and light diffraction that takes place in structures with periodically modulated refractive index changes. In turn, these optical processes provide unusual opportunities to examine polymer growth in the sol-gel derived composite.

The purpose of the following Sections is to briefly acquaint the reader with the concepts being examined in this thesis and to place our research objectives in the context of the broad fields of a) photolithography of micro-optical elements, b) nonlinear optical self-focusing phenomena, c) self-organisation in hybrid organic-inorganic systems, d) photonic crystals and e) laser induced birefringence. Detailed literature reviews and when necessary, theoretical overviews are provided in the introductory sections of each Chapter.

## 1.5 PHOTOLITHOGRAPHY OF INTEGRATED OPTICS (I-O) DEVICES ON PLANAR SUBSTRATES

This year Jack Kilby shared the Nobel Prize in physics for creating the first integrated micro-electronic circuit in 1958; a series of micron-scale transistors assembled on a single substrate. One of his key tools in constructing this device was photolithography, which enabled the precise positioning of the transistors and interconnecting Cu wiring onto a single silicon chip. The explosive growth of microelectronics and the ever-increasing power of microprocessors since then, are direct consequences of the advances made in optical lithographic techniques, specifically in increasing the resolution of photo-inscribed features. As predicted by Moore's law[36], the number of transistors supported on a single chip has increased by 400 fold in the past four decades[37]. Currently up to 16 million[38] transistors, features of less than 250 nm interconnected by kilometres of Cu wiring[39], may be densely packed onto a single computer memory chip that is no wider than a thumbnail.

### 1.5.1 Experimental set-up

A typical system for photolithography is schematised in Figure 1.3. The set-up consists of a light source, generally an ultraviolet (UV) lamp or laser, a photo-mask with a quartz engraving of the microelectronic circuit design and a Si wafer coated with a film of photoresist. UV light passed through the mask imprints the circuit pattern on the resist in a process that may be likened to print photography, where the mask functions as the photographic negative and the photoresist, as the photographic emulsion[40]. In subsequent processing steps, exposed or unexposed regions of the resist and sections of the underlying Si may be selectively etched to fabricate the microelectronic circuit.

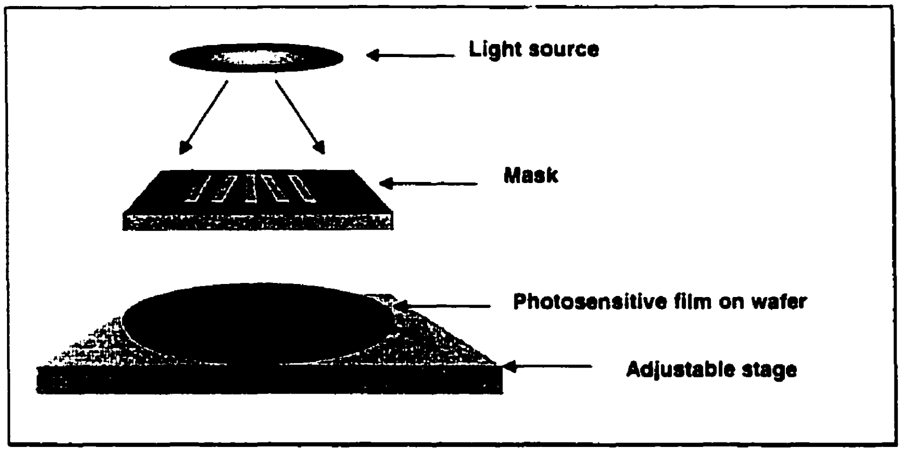

**Figure 1. 3** Set-up for the photolithography of micro-elements on photosensitive thin films

### 1.5.2 Photo-inscription of integrated-optics devices

In creating *photonic* chips, micro-optical elements must be integrated on a common substrate. Early efforts to construct such systems have simply borrowed from the sophisticated photolithographic tools developed by the semiconductor industry. For example, the sub-micrometric features corresponding to a range of I-O devices such as channel, ridge and array waveguides, gratings, mirrors, beam-splitters and couplers may all be patterned onto photosensitive substrates using the set-up shown in Figure 1.3. However, the crucial parameter in fabricating passive optical devices is the refractive index ($n$) profile of the final structure. For example, a channel waveguide is essentially a rectangular strip, a few microns wide and several centimetres long, which has a greater refractive index relative to its surrounding medium. The magnitude of its $n$ determines the wavelengths of light as well as the number of optical modes that the waveguide can support. On the other hand, surface-relief or Bragg gratings consist of a long-range, periodic variation in the refractive index ($\Delta n$). The periodicity and the magnitude of $\Delta$n determine the wavelength of the diffracted light and the diffraction efficiency respectively. Thus, once the device-pattern has been lithographically stencilled onto the substrate, subsequent steps generally involve the selective modification of n in the exposed or the unexposed regions through ion exchange[41] or thermal densification[42] processes.

### 1.5.3 Photo-induced refractive index changes

In some materials including our silica-methacrylate composites, an increase in the refractive index ($\Delta n$) may be induced by light itself, eliminating the need for such post-processing steps. For example, $\Delta n$ may be induced in germanium doped $SiO_2$ with either visible (514.5 nm)[7] or UV (248 nm) light[43]. Thus an optical interference pattern created by UV light in conjunction with photo or phase masks or even by counter-propagating laser beams, induces a periodic modulation of $\Delta n$ in the material, *i.e.* a grating. This serendipitous discovery made at the Communication Research Center of Canada[7] has triggered extensive research and industrial activity in the photolithography of Bragg gratings, a key element in telecommunication networks[44]. Light induced refractive index changes are also observed in organic systems such as photopolymers and polymers with multi-acrylate functionalities[47]. In these materials, the photo-initiated, free-radical polymerisation of organic monomers creates the required $\Delta n$. Several optical elements including gratings[45], waveguides, splitters and V-grooves have been successfully inscribed on these polymeric materials with one-step photolithographic techniques.

A refractive index increase may also be photoinduced in thin films cast from sol-gel derived silica-methacrylate composites. As mentioned earlier, several research groups including our own have applied this property to fabricate a suite of passive, I-O devices from these hybrid materials. Here too, the principal fabrication technique has been photolithography, where UV light passed through quartz opening in photo and phase masks defines the sub-micrometric features on the thin films.

### 1.5.4 Molecular origins of photosensitivity in silica-methacrylate composites

Our interest was in understanding the molecular-level photo-mechanisms that led to refractive index changes in the hybrid materials, *i.e.* the origins of its photosensitivity. In the parlance of physicists and optical engineers, the term photosensitivity refers simply to a light-induced change in the refractive index ($\Delta n$) and is applied indiscriminately over the wide range of materials used for photolithography. Unfortunately, this generalisation often overlooks the rich and varied molecular scale photochemistry that underlies ($\Delta n$) in these vastly different chemical systems. For example, although still incompletely understood, the photosensitivity of germanosilicates is attributed to the presence of oxygen deficient centres (ODCs), which are ionised upon irradiation[46]. The subsequent creation of colour centres leads to changes in the absorption spectrum of the material and consequently, its refractive index. At the other extreme, the $\Delta n$ in photopolymer formulations is due to the photoinitiated free-radical polymerisation of monomers incorporated in an inert plasticiser[47]. Polymer formation leads to local volume contraction and densification, which are observed as an increase in the refractive index.

Although the photosensitive silica-methacrylate composites have used in the fabrication of optical devices, detailed studies into light induced transformations in this hybrid matrix have until now, remained largely unexplored. Our initial objective was to parallel the device fabrication efforts with investigations into the photochemistry of this material. A correlation between changes at the molecular scale and those at the bulk level, such as refractive index and thickness, would be valuable in the photolithographic process.

Indeed, the composite merits investigation based solely on its interesting hybrid polymeric nature. It consists of a pre-formed, hydrophilic inorganic network coexisting with photosensitive propyl methacrylate substituents, which form a secondary organic polymer in a subsequent irradiation step. It is evident that exposure of the composite to UV light will initiate the free-radical polymerisation of methacrylate functionalities. However, unlike conventional bulk free-radical polymerisation processes, these reactions are hosted in the metastable environs of a sol-gel derived silica network. Furthermore, the photosensitive units are covalently grafted to Si centres, which in turn bear residual, reactive silanol and silicon methoxide functionalities. In addition, each Si centre is part of an extended, three-dimensional inorganic polymer network, which must impose severe steric constraints on the free-radical reactions.

Our goal was to monitor the photo-initiated organic polymerisation reactions in thin films of the composite, through a variety of techniques including infrared, $^{29}$Si NMR, waveguide Raman spectroscopy (WRS) and scanning electron microscopy and to examine their effects on the structure of the composite. Emphasis was placed on relating these observations to the evolution of the refractive index and film-thickness, and the consequent implications for the device-fabrication protocol.

## 1.6 NONLINEAR OPTICAL (NLO) RESPONSES OF MATERIALS

Like optical fibres, most of the I-O devices that have been fabricated through photolithography are passive elements. These are necessary building blocks for I-O systems but used only to direct light from one location to the next through rudimentary functions such as waveguiding, reflection, splitting, coupling and diffraction. The ultimate goal of miniaturised, integrated-optical systems is not only to serve as transmitters of light signals but also to perform specific functions. For example, the switching and routing of data packets in communications networks is currently carried out by electronic systems[12]. These will severely reduce the speed at which data is processed as the bandwidth of fibre-networks increases. Considerable research is aimed towards avoiding such electronic bottlenecks by creating "all-optical" networks, in which both data transmission and processing are light-based. Realistically such an ideal, which combines the speed of photons with the functionality of microelectronics, may only be approached if strategies are devised to elicit "intelligent responses" from photons.

### 1.6.1 Controlling light with NLO responses

Electrons are easily manipulated in microelectronic circuitry as they possess charge and may be controlled with a voltage. Photons on the other hand, are proving much more difficult to harness. Although waveguiding has proved to be an efficient means of transmitting light over long distances, signal loss may still be caused by the diffraction and dispersion of laser beams and pulses respectively. In addition, the scattering of light-waves at curves and sharp corners severely limits the miniaturisation and integration of waveguide devices on micron-scale platforms.

The key parameter that mediates the interaction between an optical wave and its medium is the refractive index ($n$) and it is through this physical property that the behaviour of light may ultimately be controlled. In most transparent dielectric media, light-matter interaction is a linear phenomenon in which neither $n$ nor the electromagnetic wave is altered. This is not the case in the realm of nonlinear optics (NLO). A specific form of NLO response is the Kerr effect, where at high laser intensities (I) the refractive index of a dielectric material may be described by:

$$\Delta n = n_2 I \qquad [1.1]$$

This equation in fact, represents a form of "dialogue" between the electromagnetic wave and its medium, the stimulus being the intensity (I) of the laser beam and the response, an increase in the refractive index ($\Delta n$) of the material. ($n_2$ is the nonlinear refraction coefficient). In turn, $\Delta n$ may be used to redefine (and thus control) the propagation conditions of the beam. The Kerr effect is already being used to create "smart" photonic devices such as switches based on nonlinear optical interferometers[12]. Here an intense light pulse induces $\Delta n$ in one arm of the interferometer, such that the relative phase shift introduced between the two arms causes the input signal to switch ports. A particularly interesting form of NLO based, self-action of laser light occurs in optical fibres. The NIR pulses used for telecommunications are intense enough to induce $\Delta n$ changes in $SiO_2$ fibres, according to Equation [1.1]. When this photoinduced $\Delta n$ exactly counterbalances the pulse-dispersion that would occur in a linear medium, the optical wavepackets propagate over long distances without broadening and retaining their initial profiles. Such unperturbed pulses are referred to as temporal solitons, which are actively used in telecommunications systems to reduce signal loss and improve data rates[5].

### 1.6.2. Self-focusing of light in silica-methacrylate composite

We are interested in the spatial analogue of temporal solitons. When a Gaussian shaped laser beam propagates in a medium that obeys equation 1.1, it induces a refractive index change that mirrors its own profile, *i.e.* a maximum at the most intense axial region with a circularly symmetric, exponential decay from this point. Note that this is essentially a self-induced, positive lens. The beam now focuses itself through this lens along its propagation axis (Figure 1.3a). The reciprocal action of self-focusing and lens-formation allows the beam to traverse the NLO material without diffracting or broadening as it would in a linear medium (Figure 1.3b). When the self-focusing action precisely balances diffraction, the beam retains its initial spatial (Gaussian) profile throughout its path. This is a spatial soliton.

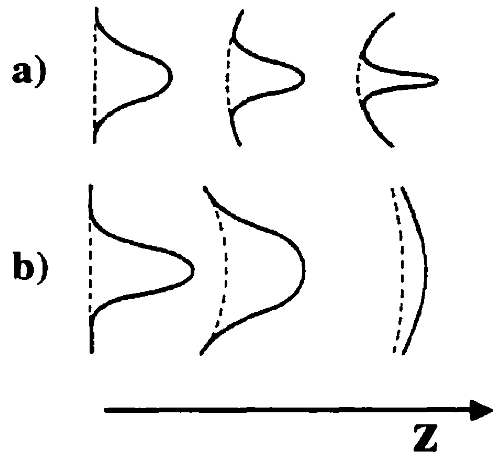

**Figure 1. 4 a)** self-focusing and **b)** diffraction of a laser beam along its propagation axis, *z*.

In the classical NLO response described by equation 1.1, Δn is due to contributions from the higher order electronic polarisability terms, which arise at high laser intensities (typically megawatts). However, it is important to note that the self-focusing phenomenon itself is insensitive to the molecular origins of Δn. The prerequisite for self-focusing, *i.e.* the formation of a lens along the propagation axis of the beam, simply requires a spatially localised and intensity dependent Δn. This condition is in fact, satisfied by the photo-responses of our silica-methacrylate composites. As mentioned in the previous Section, it is this very property that enables sub-micrometric optical devices to be photo-inscribed on thin films of the hybrid materials.

Our objective was to apply our knowledge of photoinitiated polymerisation reactions and the consequent evolution of Δn in the composites, to examine the self-focusing of a continuous wave (c.w.), visible laser beam in silica-methacrylate thin films. We reasoned that the propagating beam would initiate the free-radical polymerisation of methacrylate groups and simultaneously induce a localised refractive index that would maximise at the most intense, axial regions of the beam. Therefore a lens would be created in the path of the beam, causing it to self-focus and propagate through the waveguide without suffering diffraction.

The observation of self-focusing in this photochemical system would present a new perspective to a field that is dominated by physical mechanisms, such as the Kerr effect. Conversely, it would provide the unique opportunity of conducting a free-radical polymerisation reaction in the highly nonlinear environment of a self-focusing laser beam. In Kerr media, all traces of the photoinduced Δn disappear once the laser beam has been removed. In our system, the Δn due to the polymerisation reactions is permanent. This presents the exciting possibility of "fossilising" or permanently capturing the light-matter interactions that take place during the self-focusing process.

## 1.7 PHOTONIC CRYSTALS AND SELF-ORGANISATION

The temporal evolution of the refractive index in a medium is critical to the self-focusing phenomenon described in the previous section. Photonic band gap (PBG) materials rely on the spatial modulation of the refractive index to control the diffraction of light. Exciting photonic device principles have been identified that exploit the control over the dispersion of light provided by PBG materials or photonic crystals (PCs). As schematised in Figure 1.5, these are dielectric structures with a three-dimensional (3-D), periodic, nanoscale variation in the refractive index (*n*). Multiple interference between optical waves diffracted from the structure may open a photonic band gap (PBG)[48] analogous to the electronic band gaps of semiconductors. Wavelengths that fall within the PBG, incident from any angle will be totally reflected from and forbidden to propagate in the structure. However, light can be trapped[49], guided[50] or reflected[51] by defects or lapses in lattice periodicity.

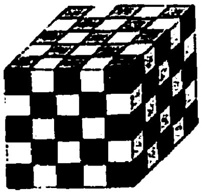

**Figure 1. 5** Schematic of a photonic band gap material

The fabrication of three-dimensional (3-D) dielectric crystals possessing complete (ominidirectional) band gaps presents a considerable challenge. The first example of a photonic crystal, the Yablonovite[52], was made by drilling through triangular arrays of holes in a mask placed over a dielectric slab. This time demanding and resolution-limited, element-to-element construction has also been the basis of recent methods including laser beam initiated chemical vapour deposition[53] and two-photon photo-polymerisation[54].

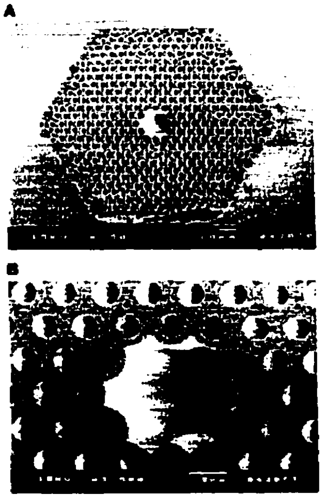

**Figure 1. 6** Example of a $SiO_2$/air photonic band gap material

Semiconductor micro-fabrication[55a-c] has the required resolution but creates structures only a few unit cells deep. A recent article[56] described a promising technique, holographic lithography, which creates submicron scale structures with long-range 3-D periodicity. An interesting example of a PBG material is shown in Figure 1.6[57]

This silica structure was constructed by drawing a thin fibre from a fused bundle of glass capillary tubes. The cross-section of the structure retains the resulting honeycomb arrangement of the glass tubes. The periodic $SiO_2$/air modulation due to this arrangement opens a PBG for specific wavelengths of visible light, depending on the overall size of the fibre.

### 1.7.1 Self-organisation of molecules and macromolecules

The quest for PBG materials coincides with the increasing attention being placed on chemistry at the mesoscale; a length scale (10 – 100 nm) that straddles the world of atoms and molecules and the macroscopic domain of bulk materials. The strategy of linking atoms with covalent bonds to form molecules, ubiquitous in traditional synthetic chemistry, is inefficient in this regime where structural order must be maintained over tens of nanometers. Self-organisation at these length scales is achieved by harnessing *inter*molecular forces such as amphiphilic effects, Coulombic and van der Waals forces and hydrogen bonding[58] to elicit the spontaneous self-assembly of molecules and macromolecules into thermodynamically stable, three-dimensional structures with well-defined geometries.

### 1.7.1.1 Templated growth of ordered inorganic structures

In bio-mineralisation processes, organic templates impart long-range order to inorganic materials in structures as varied as teeth, bone, leaves[59], shells[60], spider silk, the walls of diatoms[61] and the wings of butterflies. Inspired by the strength, functionality and exquisite morphologies of these hybrid structures, chemists are investing considerable effort in using self-organised organic systems to introduce order in inorganic structures. A particularly successful method is the use of the liquid crystalline (LC) mesophases of surfactant molecules or block copolymers to guide the growth of sol-gel derived inorganic structures[62]. The hydrolysis and condensation of silicon and metal alkoxides, restricted to the aqueous regions of the amphiphilic systems, form an amorphous inorganic structure that is actually the inverse replica of the organic phase. Once the organic component is removed by heating or chemical extraction, the inorganic shell that is cast behind bears voids or air holes that are often arranged in HCP, cubic and lamellar arrangements with long-range periodicity (Figure 1.7[62]).

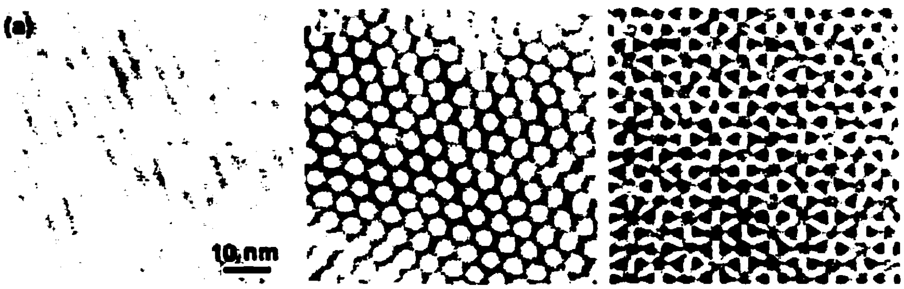

**Figure 1. 7** Surfactant-templated silica mesostructures with a) lamellar b) hexagonal close packed and c) cubic organisation.

These dielectric structures often have the strict, three-dimensional periodic variation of refractive index (through the alternating $SiO_2$/air arrangement) and may be valuable candidates as PBG materials. Notice for example, the striking similarity between the honeycomb arrangement of the air channels in the silica-based PBG structure shown in Figure 1.6, and the HCP organisation observed in the LC-templated silica structure shown in Figure 1.7b. Self-organised PCs would shift the burden of creating order from lithography and micro-machining techniques to the spontaneous self-assembly that is inherent to these amphiphilic systems. Indeed, the opal consists of a periodic arrangement of silica spheres with sub-micrometric lattice periodicities, which cause the Bragg diffraction of visible wavelengths. Unfortunately, the dimensions of the LC-templated structures are generally in the mesoscale (< 50 nm) whereas periodicities of hundreds of nanometres are necessary for the diffraction of optical and IR waves. Lattices formed by templating with assemblies of colloidal particles[63a-d] are restricted to a spherical geometry. In fact, the only self-organised PBG structure to date is an inverse replica in silicon of a self-assembled, face centred cubic (FCC) structure of colloidal spheres[64].

### 1.7.2 Amphiphilic interactions and their effect on the structural organisation in silica-methacrylate composites

In several examples of template-guided growth of inorganic structures, especially in the case of neutral surfactants and block polymer systems, sol-gel processing plays a passive role, *i.e.* it does not participate in the order creating process but rather builds a dense amorphous network around a pre-organised structure. In most of these systems, simple tetraalkoxysilane precursors, such as tetraethoxysilane and tetramethoxysilane are used to construct the silica network. Little attention has been paid to the microstructure of composites derived from trialkoxysilanes with long-chain organic substituents. It is important to note, that once hydrolysed such molecules with hydrophilic silanol containing head groups and hydrophobic organic tails may themselves exhibit amphiphilic character.

In Chapter five of this thesis, we describe how such amphiphilic interactions of 3-methacryloxypropyltrimethoxysilane (MAPTMS) lead to long-range, three-dimensional order in ol-gel derived silica-methacrylate composites. This is to our knowledge the first report of self-organisation in a sol-gel derived silica system formed in the absence of external templates. Significantly, the length scale of organisation here is on the order of 250 nm, which approaches the visible optical wavelengths and exceeds those obtained in LC-templated systems. The hybrid structures consist of a three-dimensional, periodic interdigitated arrangement of inorganic domains, each surface-derivatised with photosensitive methacrylate groups. The presence of sub-micrometric organisation in these silica based systems, together with the ability to capture this order through the polymerisation reactions of the methacrylate groups may be valuable properties for several photonic applications, including PBG materials.

## 1.8 PHOTO-INDUCED ANISOTROPY IN SILICA-METHACRYLATE WAVEGUIDES

Linearly polarised laser beams can often induce a net orientation in initially amorphous systems. The electric fields of laser beams often introduce an anisotropy in the refractive index (birefringence) of initially amorphous materials. As mentioned earlier, linearly polarised visible or UV laser beams can induce birefringence in $SiO_2$ fibres. Similarly, laser beams induced optical anisotropy in a variety of systems, including azo-dye doped systems, chalcogenide glasses and semiconductors[65]. Characterisation of optical anisotropy in turn, gives information about molecular-level anisotropy in the material. For example, birefringence in polymer systems often arises from chain orientation. Methods for orienting macromolecules include extrusion, injection moulding, melt and solution spinning and film production. In Chapter 6, we describe how orientation in hybrid silica-methacrylate composites may be introduced with self-focusing, linearly polarised light. We identify photo-induced orientation by characterising the associated birefringence with polarised light techniques.

### 1.8.1 Laser induced orientation in sol-gel derived silica-methacrylate planar waveguides

Our technique of guided-wave polymerisation provides the opportunity to study light-induced growth, orientation and micro-dynamics of organic chains in silica hosts. In Chapter six, we examine the effects of linearly polarised, waveguided light on free-radical polymerisation of methacrylate substituents hosted in a sol-gel derived silica network. We investigate the effects of the plane of polarisation on the photo-orientation process and characterise the laser-induced structural anisotropy in the material through polarised waveguide Raman spectroscopic and optical birefringence measurements.

## 1.9 SUMMARY OF RESEARCH OBJECTIVES

To summarise, the objectives of the research presented in this thesis are to:

1. Gain a molecular-level understanding of the photochemical reactions that underlie refractive index changes in sol-gel derived silica-methacrylate composites, especially in the context of the photolithography of I-O devices.
2. Apply the understanding gained in (1) to probe for and identify the self-focusing of a c.w. visible laser beam in a silica-methacrylate planar waveguide.
3. Understand the amphiphilic interactions between organic and inorganic components, and examine their influence on the sub-micrometric scale structure of the composite.
4. Examine the effect of linearly polarised guided optical waves on the free-radical polymerisation reactions in silica-methacrylate waveguides. Characterise the photo-orientation in the waveguides through polarised WRS and birefringence measurements.

## 1.10 ORGANISATION OF THESIS

Spectroscopic investigations of photo-induced transformations in the silica-methacrylate thin films are presented in the following Chapter. An *in situ* waveguide Raman study of UV induced reactions within a silica-methacrylate waveguide is presented in Chapter 3. In Chapter 4, our investigations into the self- focusing of a visible laser beam in the hybrid material are discussed. This Chapter culminates in the discovery of structural organisation, at the sub-micrometric scale, in the composite. The sequence of studies that led to the recognition of self-assembly in the sol-gel derived composites as well as further characterisation of this unexpected feature is presented in Chapter 5. Studies of photoinduced anisotropy in silica-methacrylate waveguides through polarised WRS and birefringence measurements form the subject of Chapter 6. The concluding Chapter contains a summary of the results presented in this work, the contributions made to original knowledge as well as suggestions for future research.

---

1. *Harnessing Light; Optical Science and Engineering for the 21st Century*, (National Research Council, National Academy Press, Washington D.C. 1998).
2. R. D. Maurer, *Proc. IEEE*, **61**, 452 (1973).
3. D. Jones, *Nature*, **396**, 117 (1998).
4. G. A. Thomas, B. I. Shraiman, P. F. Glodis and M. J. Stephen. *Nature*, **404**, 262 (2000).
5. F. Mollenhauer, R. H. Stolen and J. P. Gordon, *Phys. Rev. Lett.* **45**, 1095 (1980).
6. D. Clark, *Science*, **285**, 353, (1999).
7. K. O. Hill, Y. Fujji, D. J. Johnson and B. S. Kawasaki. *Appl. Phys. Lett.* **32**, 647 (1978).
8. T. Meyer, P. A. Nicati, P. A. Robert, D. Varelas, H. G. Limberger and R. P. Salathé *Opt. Lett.* **21**, 1661 (1996),
9. T. Tamir, *Guided-Wave Optoelectronics*, (Springer-Verlag, Heidelberg, Germany. 1988).
10. A. Kamal and P. St. J. Rusell, *J. Opt. Soc. Am. B*, **11**, 1576 (1994).
11. P. St. Russell and D. P. Hand, *Electron. Lett.* **26**, 1848 (1990).
12. D. Cotter, R. J. Manning, K. J. Blow, A. D. Ellis, A. E. Kelly, D. Nesset, I. D. Phillips, A, J, Poustie and D. C. Rogers, *Science*, **286**, 1523 (1999).
13. J. S. Aitchinson, A. M. Weiner, Y. Silberberg, M. K. Oliver, J. L. Jackel, D. E. Leaird, E. M. Vogel and P. W. E. Smith, *Opt. Lett.* **15**, 471 (1990).
14. V. G. Kozlov, V. Bulović, P. E. Burrows and S. R. Forrest, *Nature*, **389,** 362
15. M. Berggren, A. Dodabalapur, R. E. Slusher and Z. Bao. *Nature*, **389**, 466 (1997).
16. C. R. Kagan, D. B. Mitzi and C. D. Dimitrakapoulos, *Science*, **286**, 945 (1999).
17. J. H. Schön, Ch. Kloc, E. Bucher and B. Batlogg, *Nature*, **403**, 408 (2000).
18. C. Weder, C. Sarwa, A. Montalli, C. Bastiaansen and P. Smith, *Science*, **279**, 835 (1998).
19. S. H. Chen, D. Katsis, A. W. Schmid, J. C. Mastrangelos, T. Tsutsui, T. N. Blanton, *Nature*, **397**, 506 (1998).
20. V. K. Gupta and N. L. Abbott, *Science*, **276**, 1533 (1997).
21. M. F. Weber, C. A. Stover, L. R. Gilbert, T. J. Nevitt, A. J. Ouderkirk, *Science*, **287**, 2451 (2000).

---

22. S. Walheim, E. Schäffer, Jürgen Mlynek, Ullrich Steiner, *Science*, **283**, 520 (1999).

23. M. Ebelman, *Ann. Chim. Phys.* **16**, 319 (1845) as referenced in 24.

24. C. J. Brinker and G. W. Scherer, *Sol-gel Science, The Physics and Chemistry of Sol-Gel Processing*, (Academic Press Inc. San Diego, 1990).

25. P. Judenstein and C. Sanchez. *J. Mater. Chem.* **6**, 511 (1996).

26. For reviews see a) B. M. Novak. *Adv. Mater.* **5**, 422 (1993), b) J. Wen and G. L. Wilkes. *Chem. Mater.* **8**, 1667 (1996), c) U. Schubert, N. Husing and A. Lorenz. *Chem. Mater.* **7**, 2010 (1995), d) F. Ribot and C. Sanchez. *Inorg. Chem.* **20**, 327 (1997).

27. See for example, R. Gvishi, U. Narang, G. Ruland, D. N. Kumar and P. N. Prasad. *Appl. Organometallic Chem.* **11**, 107 (1997).

28 . P. A. Leermakers and H. T. Thomas, *J. Am. Chem. Soc.* **87**, 1621 (1965).

31. M. P. Andrews and S. I. Najafi, *Proc. SPIE Opt. Eng.* **2998**, 293 (1997).

32. (a) B. Novak. *Adv. Mater.* **5**, 422 (1993), (b) P. Judenstein and C Sanchez. *J. Mater, Chem*, **6**, 511 (1996), (c) U. Schubert, N. Husing and A. Lorenz. *Chem. Mater.* **7**, 2010 (1995).

31. P. Coudray, J. Chisham, M. P. Andrews, A. Malek-Tabrizi, C.-Y. Li, S. I. Najafi. *Opt. Commun.* **128**, 19 (1996).

32. C.-Y. Li, J. Chisham, M. P. Andrews, S. I. Najafi, J. D. Mackenzie, N. Peyghambarian. *Electron. Lett.* **31**, 271 (1995).

33. P. Coudray, J. Chisham, M. P. Andrews and S. I. Najafi. *Opt. Eng.* **36**, 1234 (1997).

34. M. A. Fardad, T. Touam, P. Meshkinfam, R. Sara, X. M. Du, M. P. Andrews and S. I. Najafi. *Electron. Lett.* **33**, 1069 (1997).

35. T. Touam, G. Milova, Z. Saddiki, M. A. Fardad, M. P. Andrews, J. Chrostowski and S. I. Najafi, *Thin Solid Films*, **203**, 307 (1997)

36. R. Lucky, *Science*, **289**, 259 (2000).

37. R. F. Service, *Science*, **278**, 383 (1997).

38. R. F. Service, *Science*, **274**, 1834 (1996).

39. R. D. Miller, *Science*, **286**, 421 (1999).

40. T. Ito and S. Okazaki, *Nature*, **406**, 1027 (2000).

41. S. I. Najafi, *Introduction to Glass Integrated Optics*, (Artech House, Boston. 1992).

42. G. W. Scherer, *J. Sol-Gel Sci. Technol.* **8**, 353 (1997).

43. D. P. Hand and P. St. J. Rusell, *Opt. Lett.* **15**, 102 (1990)

44. T. Tamir, *Guided-Wave Optoelectronics*, (Springer-Verlag, Heidelberg, Germany. 1988).

45. L. Eldada and J. T. Yardley, *Proc. SPIE Int. Soc. Opt. Eng.* **3289**, 122 (1998).

50. J. Albert, B. Malo, D. C. Johnson, F. Bilodeau, K. O. Hill, J. L. Brebner and G. Kajrys, *Opt. Lett.* **18**, 1126 (1993).

47. J. G. Kloosterboer, G. M. M. van de Hei, R. G. Gossink and G. C. M. Dortant, *Polymer Commun.* **25**, 322, (1984).

48. E. Yablonovitch, *Phys. Rev. Lett.* **58**, 2059 (1987).

49. J. S. Foresi, P. R. Villeneuve, J. Ferrera, E. R. Thoen, G. Steinmeyer, S. Fan, J. D. Joannopoulos, L. C. Kimerling, H. I. Smith and E. P. Ippen, *Nature*, **390**, 143 (1997).

50. S. Lin, E. Chow, V. Hietala, P. R. Villeneuve and J. D. Joannopoulos. *Science*. **282**, 274 (1998).

51. J. D. Joannopoulos, P. R. Villeneuve and S. Fan, *Nature*, **386**, 143 (1997).

52. E. Yablonovitch, T. Gmitter and K. Leung, *Phys. Rev. Lett.* **67**, 2295 (1991).

53. M. C. Wanke, O. Lehmann, K. Müller, Q. Z. Wen, and M. Stuke, *Science*, **275**, 1284 (1997).

54. B. H. Cumpston *et al. Nature*, **398**, 51 (1999).

55. a) C. C. Cheng *et al. J. Vac. Sci. Technol. B*, **15**, 2764 (1997), b) S. Noda, N. Yamamoto and A. Sasaki. *Jpn. J. Appl. Phys.* **35**, L909 (1996), c) J. G. Fleming and S-Y Lin, *Optics Lett.* **24**, 49 (1999).

56. M. Campbell, D. N. Sharp, M. T. Harrison, R. G. Denning and A. J. Turberfield, *Nature*, **404**, 53 (2000).

57. R. F. Cregan, B. J. Managan, J. C. Knight, T. A. Birks, P. St. Russell, P. J. Roberts and D. C. Allan, *Science*, **285**, 1537 (1999).

---

58. See for example, M. Muthukumar, C. K. Ober and E. L. Thomas, *Science*, **277**, 1225 (1997).
59. P. Szuromi. *Science*. **277** 1997 1183
60. S. I. Stupp and P. V. Braun. *Science*. **277** 1997 1242
61. N. Kröger, R. Deutzman and M. Sumper. Science 286 1999 1129
62. D. M. Dabbs and I. A. Aksay, *Annu. Rev. Phys.* Chem. **51**, 601 (2000).
63. a) A. van Blaaderen, R. Ruel and P. Wiltzius, *Nature*, **385**, 321 (1997), b) A. A. Zakhidov, R. H. Baughman, Z. Iqbal, C. Cui, I. Khayrullin, S. O. Dantas, J. Marti, V. C. Ralchenko, *Science*, **282**, 897 (1998), c) J. E. G. J. Winjnhoven, W. L. Vos, **281**, 802 (1998), d) S. A. Johnson, P. J. Ollivier, T. E. Mallouk, *Science*, **283**, 963 (1999).
64. A. Blanco, E. Chomski, S. Grabtchak, M. Ibistate, S. John, S. W. Leonard, C. Lopez, F. Meseguer, H. Miguez, J. P. Mondia, G. A. Ozin, O. Toader and H. M. van Driel, *Nature*, **405**, 437 (2000).
65. For example, a) P. A. Blanche, Ph. C. Lemaire, C. Maertens, P. Dubois and R. Jérôme, *Opt. Comm.* **139**, 92 (1997), b) P. Krecmer, A. M. Moulin, R. J. Stephenson, T. Rayment, M. E. Welland and S. R. Elliot, *Science* **277**, 1799 (1997)

# 2. PHOTO-INDUCED STRUCTURAL TRANSFORMATIONS IN SOL-GEL DERIVED COMPOSITE THIN FILMS - IMPLICATIONS FOR INTEGRATED-OPTICS DEVICE FABRICATION

## 2.1 INTRODUCTION

Photonics is concerned with optical input/output processes mediated primarily by light, rather than electrons. The chemistry of photonic materials is concerned among other things with articulating the molecular point of view on how matter acquires its suite of functional optical properties. In photonics, these properties include spatial confinement of the electromagnetic field, birefringence, photorefraction, Kerr and other nonlinear responses. In turn, these properties are of significant technological and scientific interest[1, 2], which is incentive to understand how to control bulk optical properties at the molecular level. The properties of micro-optical components like silica glass waveguides and Bragg gratings are manifestations of their ramifying molecular networks. The refractive index of silica-based glasses plays a key role in defining the boundary conditions for light propagation in integrated optics components, devices and circuits[3,4,5,6,7.] Accordingly, the refractive index emerges as a fundamental device performance material parameter. In this regard, network relaxations that lead to densification of glass are important because the local micro-structural rearrangements are often accompanied by increases in the refractive index that can be useful for fabricating optical devices. Douay and co-workers have cogently argued this point[8].

Inorganic glasses can be densified not only by thermal sintering, but also by irradiation with electron beams [9, 10, 11, 12, 13, 14, 15] neutrons[16, 17, 18] ions[19], X-rays $\gamma$-rays[11, 12, 13, 14, 15, 16], or ultra-violet (UV) light[20, 21, 22.] UV induced densification has also been studied for its relevance to optical damage in silicate glasses[20], where it has been observed that two-photon events induce elastic and inelastic densification of the structural framework. While most studies have focused on glasses derived from more or less traditional methods of high temperature processing, a low temperature route to glasses is attracting adherents [23]. It is well known that inorganic glasses can be prepared near room temperature by solution sol-gel processing. This method can produce very pure materials by acid or base-catalyzed hydrolysis and poly-condensation of main group and transition metal alkoxides. A high temperature post-consolidation step is usually required to collapse the pore structure of the gel phase material. Reductions in porosity (internal surface area) in this case are driven by gradients in curvature. Viscous flow, surface diffusion and evaporation/condensation usually conjoin to reduce the surface area that leads to densification in thin films[24].

High temperature densification is a drawback if the glass must be deposited onto substrates that would be damaged above 500 °C. Some effort has therefore gone into identifying methods to lower the post-process densification temperature so that gel films might be deposited onto more fragile substrates like organic polymers, or semiconductor integrated circuits. To some extent, densification at lower temperatures can be achieved by photons having energies greater than the band gap of the oxide (though this approach is problematic for photosensitive semiconductors and organic compounds). For example, Imai and co-workers[22] examined the structural changes induced when sol-gel derived silica was exposed to 9-18 eV vacuum UV (VUV) radiation. Compaction and dehydration of $SiO_2$ occurred to an extent similar to what was observed when gel films were sintered at 1000 °C. The authors suggested that bond cleavage/formation pathways, and light-enhanced poly-condensation steps were responsible for consumption of silanol Si-OH species leading to densification of the sol-gel glass. The findings of Imai *et al.* are significant for the present study. In the research described below we propose a different mechanism based on UV light initiated free radical polymerisation of an acrylate monomer and collateral network densification in a hybrid organic-inorganic composite.

In general, sol-gel processing of silica glass has been far less attractive as a route to integrated optics structures because high temperature consolidation also carries the disadvantage of compressive interfacial stresses that cause cracking and optical device failure. More significant perhaps is the fact that high temperature glass integrated optics is excluded from the opportunities created by organic chemistry; and this means the exciting advances in organic small molecule and polymer optical nonlinearities. A hybrid sol-gel glass, with an appetite for both organic and inorganic phases, can rationalize the attractive features of both material regimes.

As an alternative to high temperature gel phase densification, we have been exploring organically modified low temperature sol-gel glass fabrics to prepare micro-optical components and devices, including waveguides[25], directional couplers[26], [27], beam splitters and high reflectivity Bragg gratings on ridge waveguides[28]. The introduction of organic character into the silicate network offers exciting potential for the new materials field of hybrid glasses for photonics. Our materials belong to the category of glasses, variously known as "ormocers", "ormosils", "ceramers", "polycerams", or simply hybrid sol-gel glasses (HSGGs)[29, 30]. These are usually formed by acid or based-catalyzed reactions of mixtures of organosiloxanes with tetrafunctional silicon alkoxides. The covalently bonded organic group does not normally undergo hydrolysis, and so imparts organic character to the composite. The properties of HSGGs can therefore be varied at the molecular level between those of the parent organic polymer, and those of the homogeneous inorganic glass. This is accomplished by introducing the organic component as a pendant, bridging or polymerisable group. The latter can be polymerised sequentially or simultaneously with poly-condensation of the inorganic component to provide a mutually interpenetrating network. A principal advantage of a hybrid glass is that it admits elaborate molecular level control over macroscopic expressions of physical and chemical properties that are important for photonic devices. This gives the device designer an attractive generic silica-based medium (*i.e.*, refractive index matched to optical fibre) that allows rapid prototyping of devices and assessment of material reliability. On the other hand, complex permutations of compositional and processing variables demand that researchers understand molecular structure and correlations with intended optical and physical properties. To this end, we have undertaken a series of spectroscopic studies to formulate a picture of how changes in the organic and inorganic network of one particular HSGG can be used to advantage to design and fabricate functional photonic devices.

Methacryloxypropyltrimethoxysilane (MAPTMS) and methacrylic acid were selected as the photo-polymerisable components in our composites. Choice of the trifunctional $R\text{-}Si(OCH_3)_3$ is significant for the present work because R-group substitution at silicon reduces glass network connectivity and mechanical stiffness. Reduction in the mechanical stiffness of the network promotes capillary stress-induced collapse of the gel network during drying. This is reflected in enhanced relaxation rates and lower densification temperatures for the glasses. Choice of the vinyl ester functionality was also motivated by the large literature that has accumulated on acrylate photochemistry and photolithographic applications[31]. For acrylate hybrid glasses, UV light intervenes at the molecular level to modify the structure of the overall network, hence the refractive index, in ways that are not trivially related to radical polymerisation of the organic monomer component alone. Increases in the refractive index appear to be linked both to volume compaction due to organic chain growth, and to the simultaneous onset of local relaxations and chemical condensation of siloxy species in the metastable silica network. The following is an account of our understanding of these events.

## 2.2 EXPERIMENTAL

### 2.2.1 Sol - gel processing of silica-methacrylate colloids

#### A. Zirconia doped Silica-methacrylate

An adaptation of the procedure developed by Schmidt and co-workers [32] was followed. Precursors were 3-methacryloxypropyltrimethoxysilane (MAPTMS): zirconium(IV)-*n*-propoxide ($Zr(OC_3H_7)_4$): methacrylic acid (MAA) in a 10:4:4 molar ratio. MAA (1.39 g, 0.016 mol) was slowly added to $Zr(OC_3H_7)_4$ (7.49g of 70 % w/w in *n*-propanol, 0.016 mol). The exothermic reaction gave a clear-yellow, stable sol (i). Separately, 0.05M HCl (0.54g, 0.030 mol[1]) was added to MAPTMS (10.14 g, 0.040 mol). Within a few minutes of stirring, this initially phase separated system (ii) suddenly cleared. After an hour, ii was added drop wise to i, followed by distilled $H_2O$ (0.97 g, 0.054 mol). The clear, pale-yellow sol was stirred in a capped phial for 16 hours.

#### B. Zirconia doped Silicate-Acetate

Isobutyric acid (IBA) (1.42 g, 0.016 mol) was added to $Zr(OC_3H_7)_4$ (7.49 g of 70 % w/w in *n*-propanol, 0.016 mol) yielding a clear, colourless liquid (iii). 0.05 M HCl (0.54 g, 0.030 mol) was added to 3-acetoxypropyltrimethoxysilane (APTMS) (8.89 g, 0.040 mol). This mixture (iv) (a suspension of aqueous droplets in the organic liquid) was stirred vigorously for an hour. A transparent liquid was obtained when iv was slowly added to iii. After the addition of $H_2O$ (0.97 g, 0.054 mol), the sol was left stirring for 16 hours.

---

[1] According to sol-gel processing terminology, the r value is the molar ratio of [H2O]/[alkoxide functionalities]. In our case, R = 1.5 was used.

### C. Titania doped Silica-methacrylate

The procedure outlined for colloid A was followed with the Zr alkoxide substituted with molar equivalents of Ti(*iso*-OPr)$_4$ in distilled *iso*propanol. The complexation of the titanium precursor to MAA was carried out in an ice bath, to prevent precipitation. The final sol was orange in colour.

### Photosensitisation

1.5 % w/w 1-hydroxycyclohexyl-1-phenylketone ($\lambda_{max}$: 240-250 and 325-330 nm, Irgacure® 184) was added to all three sols. They were then passed through a 0.2 μm PTFE filter before storage in the dark.

### Materials

MAPTMS (98 %), MAA (99 %), IBA (99 %) and Ti(*iso*-OPr)$_4$ (97 %) were purchased from the Aldrich Chemical Company, Milwaukee, WI, USA. $Zr(OC_3H_7)_4$ was bought from Alfa-Aesar, Ward Hill, MA, USA. 0.05 M HCl was prepared from a standardised solution of 0.1036 N HCl from Aldrich. APTMS was purchased from Gelest Inc. Tullytown, PA, USA. All chemicals were used as purchased. MAPTMS and $Zr(OC_3H_7)_4$ were handled under $N_2$. Photoinitiators were provided by Ciba Specialty Chemicals Canada Inc. Missisauga, ON, Canada.

### 2.2.2 Preparation of thin films

Thin films from colloids A, B and C were cast on $SiO_2$ coated Si, Si or quartz substrates with a photoresist spinner (EC101D & PM101D series, Headway Research Inc. TX, USA). Film thickness of 3.7, 4.25, 4.50 and 5.00 μm were obtained at spin-casting speeds of 6000, 5500, 5000 and 3000 rpm, respectively. For cleaning, substrates were soaked consecutively in warm trichloroethylene, acetone and isopropanol, rinsed with distilled $H_2O$ and dried under flowing $N_2$.

### 2.2.3 Characterisation of the photo-initiated polymerisation process

#### 2.2.3.1 UV-Vis Absorption Spectroscopy

5 μm thick films from colloid A were cast onto 25 $cm^2$ quartz plates (Corning, NY, USA). Samples were dried at room temperature before being exposed to UV light from a Hg arc lamp (Oriel Corporation, CT. USA) with an emission maximum at 4.9 eV (over the range 2.5-5 eV) and irradiance of 14 $mW\text{-}cm^{-2}$. Exposure times ranged from 0 to 60 min. A Hewlett Packard 8452A spectrophotometer was used to acquire absorption spectra of the films over the 200 to 800 nm range.

#### 2.2.3.2 Fourier Transform Infrared (FT-IR) Spectroscopy

A 5 μm film from colloid A was spin-coated onto double-polished Si wafers (NOVA Electronic Materials, Richardson, TX, U.S.A). The film was dried at 100 °C for 30 minutes. The wafer was then cleaved into 2 x 1 $cm^2$ pieces before being irradiated. Three series of samples were prepared to cover various combinations of photon energy and irradiation times: 1) 2.5-5.0 eV irradiation over a period of 0 to 60 min; 2) 6.4 eV irradiation over a period of 15 to 300 s; 3) 0.5 min of 2.5-5.0 eV irradiation followed by 6.4 eV irradiation over a period of 0 to 180 s. The 6.4 eV light was provided by a pulsed ArF laser with a fluence of 20 $mJ/cm^2$ at a 30 Hz repetition rate. Infrared spectra were acquired over a range of 400 to 5000 $cm^{-1}$ with a Bruker IFS-48 Fourier transform infrared spectrometer. Series 1 was also prepared with colloids B and C.

#### 2.2.3.3 Solid-state $^{29}Si$ NMR

5 μm films were spin-coated onto micro-cover glasses from colloid A. Films were dried at 100 °C for 30 minutes before irradiation with 4.9 eV light. Samples were then crushed into fine pieces. Spectra were acquired on a 300 MHz Chemagnetics CMX300 spectrometer.

#### 2.2.3.4 Scanning Electron (SE) Microscopy

Irradiated and non-irradiated 5 μm films from colloid A cast on $SiO_2$-coated Si wafers were heated at 300 °C for 3 hours. A layer of Au/Pd was evaporated on the samples before they were characterised with a JEOL scanning electron microscope.

### 2.2.4 Photolithography of Integrated-Optics Devices

#### 2.2.4.1 Ridge Waveguides

A 5 μm film (colloid A) was spin-coated on a 2 x 1 $cm^2$ wafer fragment and dried in air at 100 °C for 30 minutes. Using a mask-aligner, the film was placed in direct contact with a photo-mask. The chrome-plated mask (QPS Technologies, Dorval, Quebec) was patterned with a set of rectangular quartz windows. The film was irradiated through the mask with UV (4.9 eV) light at 14 $mW\text{-}cm^{-2}$. Exposure times ranged from 5 to 60 seconds. The film was then washed with *iso*-propanol to remove the unexposed regions. The waveguides, now revealed as a series of fine lines on the substrate, were then heated at 120 °C for two hours.

#### 2.2.4.2 Bragg Gratings

An optical set-up designed for the fabrication of Bragg gratings in photosensitive optical fibres was modified for our purpose. Bragg gratings with $\lambda_B$ = 1.55 μm were inscribed on thin films and in ridge waveguides through phase masks. These are quartz gratings produced by reactive ion etching where the etch depth is optimised such that the plus/minus-first diffraction orders of an incident UV laser are maximised while the zero and higher orders are suppressed. As schematised in Figure 2. 1, interference from the diffracted first order beams produces a near-field fringe pattern on the photosensitive thin film placed under the phase mask. We used a mask with period size ($\Lambda$) = 1055 nm, where the zero order energy was minimised to < 1% at 193 nm, the laser line used to write the grating. $\lambda_B$ is related to $\Lambda$ through:

$$\lambda_b = n_{eff} \wedge \qquad [2.1]$$

where $n_{eff}$ is the effective index of the material.

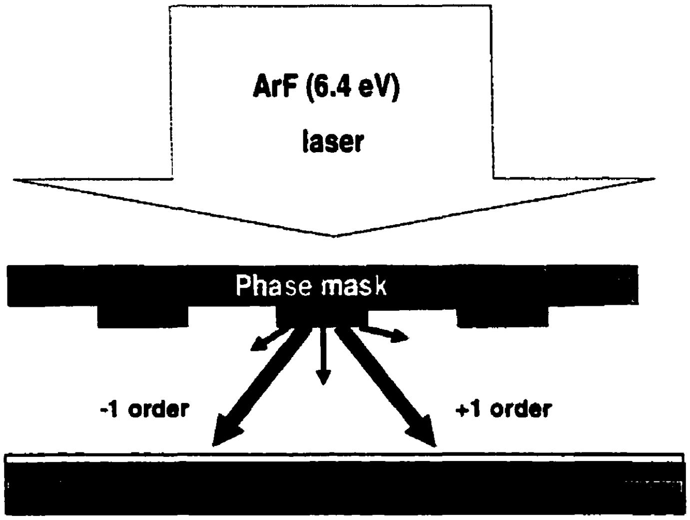

**Figure 2. 1** Experimental set-up for the photo-inscription of Bragg gratings

The ridge waveguide was placed in direct contact with the phase mask and aligned such that its long axis was normal to the grooves of the quartz grating. Samples were irradiated at a distance of 90 cm from the exit port of the raw ArF excimer laser (model AQX-150, MPB Technologies) beam. Exposure times ranged from 10 to 30 seconds with a fluence of 20 mJ-cm$^{-2}$ at a repetition rate of 30 Hz.

## 2.3 RESULTS AND DISCUSSION

### 2.3.1 Photo-initiated polymerisation in silica-methacrylate thin films

The photoinitiator present in the silica-methacrylate composite was 1-hydroxycyclohexyl-1-phenylketone. When exposed to UV light (4.9 eV), the molecule undergoes α-cleavage to produce benzoyl and 1-hydroxycyclohexyl free radicals. The former is primarily responsible for initiating free radical polymerisation of the propyl methacrylate and methacrylic acid groups although Phan[33] has provided evidence that the 1-hydroxycyclohexyl radical also initiates acrylate chain growth.

#### 2.3.1.1 UV-VIS Absorption spectroscopy of the polymerisation process

The series of spectra presented in Figure 2. 2 records changes in the silica-methacrylate films after 0, 5, 15, 30 and 60 minutes of irradiation with broadband UV light peaking at 4.9 eV. The spectral features are dominated by absorption bands of the methacrylate substituent, despite the presence of MAA complexed to Zr (IV) *n*-propoxide in the matrix. As confirmed by control experiments, the Zr (IV) *n*-propoxide: MAA complex contributes only a weak absorption band centred at 271 nm.

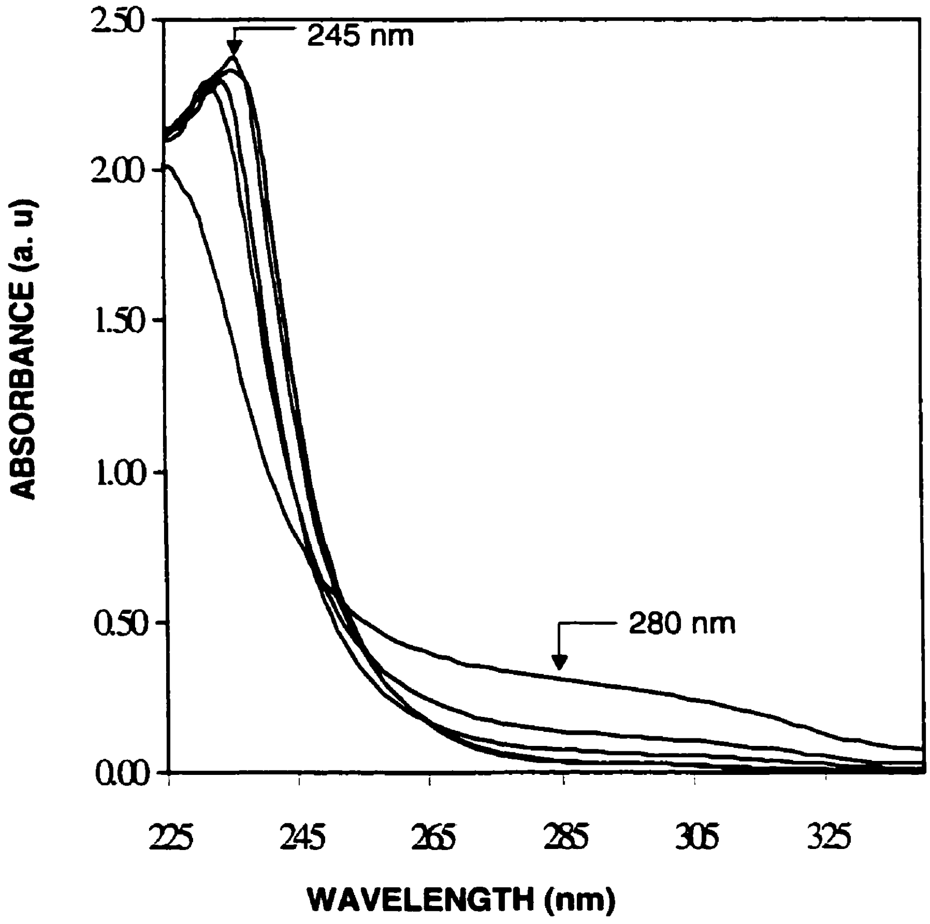

**Figure 2. 2** UV-vis absorption spectra of sol-gel derived films irradiated with 4.9 eV light at 0, 5, 15, 30 and 60 mins.

The spectrum of the non-irradiated film contains an absorption band peaking at 245 nm. This transition originates in the π → π* excitation of the conjugated ester carbonyl of MAPTMS[34, 35]. The band is blue-shifted from its peak maximum of 282 nm for MAPTMS dissolved in *iso*-propanol. A second high energy π → π* transition observed at 214 nm, is also blue shifted from its position at 242 nm in the MAPTMS/*iso*-propanol solution. The localised n → π* transition of the carbonyl group conjugated with the vinyl group occurs near 310 nm, but it is of very low intensity and is not visible on this scale. The n → π* transition undergoes a hypsochromic shift of about 10 nm in the film relative to MAPTMS in *iso*-propanol in the pseudo gel like medium. The shift to higher energy in the thin film suggests that the carbonyl moiety is hosted in a more polar (hydrogen bonding) environment, most likely containing water and silanol groups. This behaviour has been noted for carbonyl compounds in activated silica[36]. The blue-shift of the n → π* absorption band is caused by hydrogen bonding interactions of hydroxy moities with the ester carbonyl group[37]. Hydrogen bonding to the carbonyl is also evident in the IR as an absorption shoulder at 1700 $cm^{-1}$ adjacent to the 1722 $cm^{-1}$ band belonging to the carbonyl stretching-mode. This spectral feature will be discussed in Section 2.3.1.2.2.

With increasing UV irradiation, the 240 nm band was gradually depleted signifying the saturation of the C=C bond. At the same time, a broad band, peaking at approximately 280 nm, appeared. The latter is too intense to be associated solely with the carbonyl group's n → π* transition in polymerised methacrylate. Photolysis of side-chain ester groups in polymers is widely documented[38] and it is known that polyacrylates undergo main and side-chain scissions to give ketones and aldheydes, which characteristically absorb light from 280 - 300 nm[39, 40]. Extensive irradiation could cause similar degradation of the growing methacrylate chains in the silica-methacrylate composite. It is probable that the growing 280 nm absorption-band in Figure 2. 2 contains contributions from these photolysis products. Infrared spectroscopic evidence of the free-radical polymerisation process is presented in the following section.

#### 2.3.1.2 FT-IR study of the polymerisation process

Infrared spectra of silica-methacrylate films acquired prior to and after UV irradiation are presented in Figure 2. 3. Band assignments[41a-f] are collected in Table 2. 1. The bottom spectrum emphasises the significant changes that have taken place in the composite following the free-radical polymerisation of the methacrylate functionalities. Indeed, the gross features of the spectrum belonging to the irradiated film are similar to those of poly (methyl methacrylate) in sol-gel derived silica hosts[42]. Most significantly however, the spectroscopic study revealed that the free-radical polymerisation of organic substituents is not an insulated event in the composite. As will be detailed in the following sections, the IR spectra show that UV irradiation triggered two events in the silica-methacrylate composite: i) the expected polymerisation of the methacrylate substituents and consequently ii) further condensation reactions between residual silanol and silicon methoxide functional groups. The latter led to the densification of the sol-gel derived silica host, at the relatively low energies corresponding to the UV light (4.9 eV).

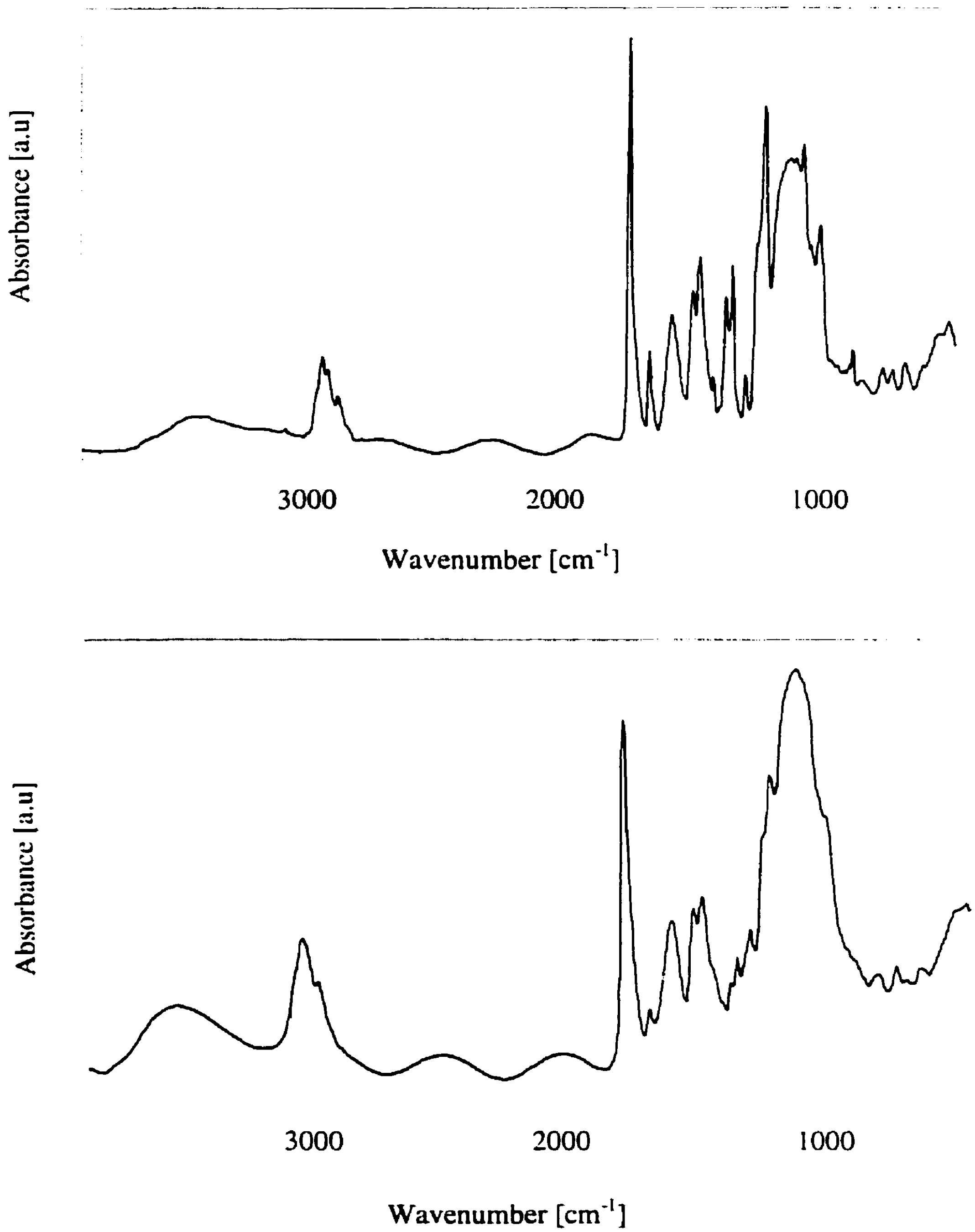

**Figure 2. 3** FT-IR spectrum of the silica-methacrylate thin film prior to (top) and after 25 min. of irradiation (bottom).

| Wavenumber ($cm^{-1}$) | Assignment |
|---|---|
| A. Methacryloxypropyl group | |
| 980 | $CH_2$ wag of = $CH_2$ |
| 1012 | trans (oop) C-H wag of =$CH_2$ |
| 1296 | -CH bending in vinyl |
| 1638 | $\nu(C=C)$ |
| 1720 | $\nu(C=O)$ of hydrogen bonded carbonyl group |
| 1722 | $\nu(C=O)$ |
| 2890 | $\nu_s(CH_3)$ |
| 2930 | $\nu_s(CH)$ of terminal methylene in =$CH_2$ |
| 3100 | $\nu_{as}(CH_2)$ of terminal methylene |
| B. Silica and Zirconia network | |
| 430 | $\delta_{as}(Si\text{-}O\text{-}Si)$ |
| 760 | $\nu_s(Si\text{-}O\text{-}Si)$ |
| 1060 | $\nu_{as}(Si\text{-}O\text{-}Si)$ |
| 1546 | $\nu(C=O)$ of zirconium-methacrylic acid complex |
| C. Alkoxy and silanol groups | |
| 472 | $\delta_{as}$Si-O-C of two or more $-OCH_3$ groups attached to Si |
| 816 | $\nu_s(Si\text{-}O\text{-}C)$ stretch |
| 944 | $\nu(Si\text{-}OH)$ |
| 1168 | $-CH_3$ rock of Si-$OCH_3$ |
| 2844 | $\nu_s(CH_3)$ of Si-$OCH_3$ |
| 2960 | $\nu_{as}(CH)$ of Si-$OCH_3$ |
| 3436 | $\nu(OH)$ Broad low band H-bonded molecular $H_2O$ |
| 3648 | $\nu(OH)$ of hydrogen bonded internal Si-OH |

**Table 2. 1** Vibrational frequency assignments for sol-gel derived silica-methacrylate thin films

### 2.3.1.2.1 Photo-initiated free-radical polymerisation of methacrylate substituents

Polymerisation reactions were followed by the loss of intensity of appropriate bands in the mid-infrared region. We focus on the vinyl group ν(C=C) mode at 1638 $cm^{-1}$, the $CH_2$ wag and *trans* (out-of-plane, o.o.p) C-H wag at 1012 and 980 $cm^{-1}$ respectively, and higher energy modes belonging to C-H symmetric (2930 $cm^{-1}$) and antisymmetric (3100 $cm^{-1}$) stretches.

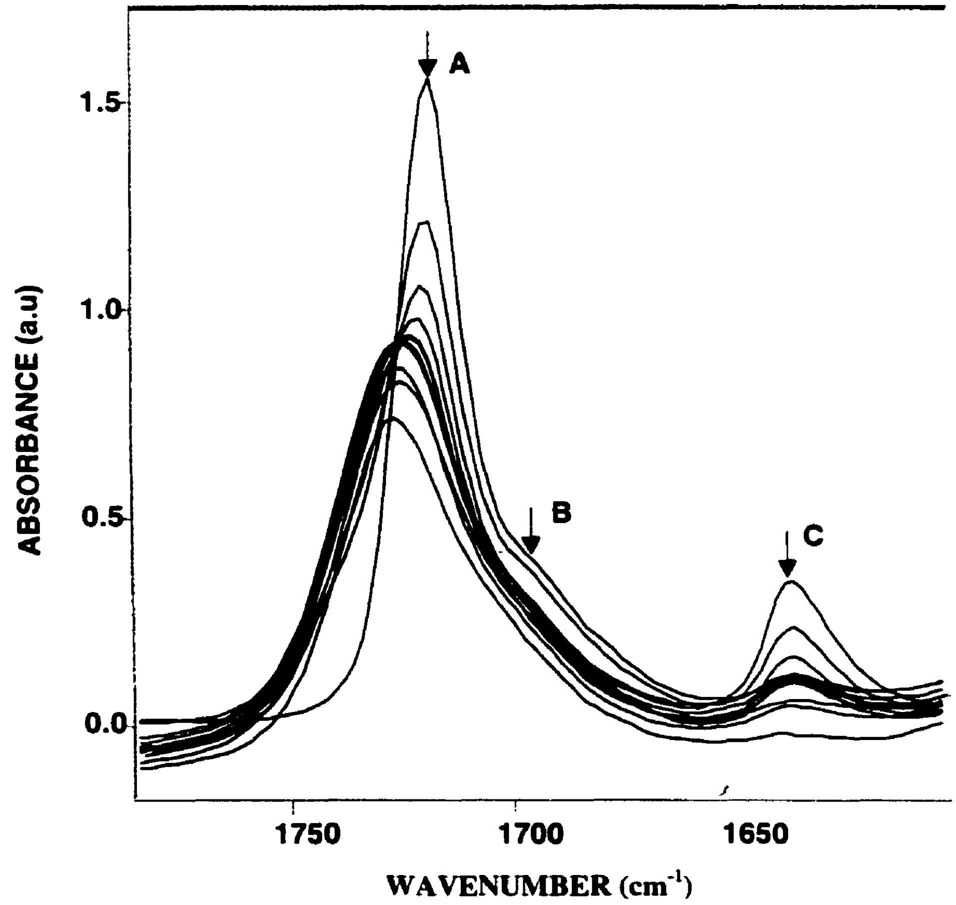

**Figure 2. 4** FT-IR spectra of thin films irradiated with 4.9 eV UV light at 0, 0.5, 2, 5, 10, 15, 20 , 25, 30, 35, 45, and 60 min where (A) ν(C=O) at 1718 $cm^{-1}$; (B) ν(C=O-H) at 1720 $cm^{-1}$ and (C) ν(C=C) at 1638 $cm^{-1}$.

Consumption of the ν(C=C) 1638 $cm^{-1}$ band (peak C, Figure 2. 4) is accompanied by a shift of the carbonyl ν(C=O) stretching mode from 1718 $cm^{-1}$ (peak A) to higher energy at 1724 $cm^{-1}$. The shift is typical for an ester carbonyl that is no longer conjugated with a vinyl substituent. Polymerisation is indicated, since the two events are related through an isosbestic point. Note however, that even after 60 minutes of irradiation, that not all the methacrylate substituents have been consumed. The residual intensity at 1630 cm$^{-1}$ and 1718 cm$^{-1}$, which belong to the ν(C=C) and ν(C=O) modes respectively, indicates the presence of unsaturated methacrylate species that remain in the network. This may be due to the three-dimensional, cross-linked silica host, which must impose a significant steric barrier to the propagation of the free-radical reactions and thus prevent the consumption of all monomeric units.

Additional photochemistry does occur in the silica-methacrylate film at longer irradiation times. This is indicated by the loss of the isosbestic point at 30 minutes of irradiation, the diminishing intensities of both the ν(C=O) and ν(C=C) bands, as well as a shift in the peak position of the ν(C=O) towards higher energy. This feature may correspond to the degradation due to photolysis of the methacrylate polymer upon extensive irradiation, also noted in the UV-Vis spectroscopic study of these reactions (Section2.3.1.1).

#### 2.3.1.2.2 Hydrogen bonding between carbonyl groups of the methacrylate substituents and silanol groups

The shoulder at position B (1700 cm$^{-1}$) in Figure 2. 4 may be assigned to the ν (C=O) mode of carbonyl groups that are hydrogen bonded to Si-OH groups[43a-c]. These interactions arise when the Si-OCH$_3$ groups of MAPTMS are hydrolysed to Si-OH during the sol-gel process. Figures 2.5 and 2.6 show different IR absorption regions of MAPTMS in the a) neat form and b) 60 minutes after hydrolysis had been initiated. The hydrolysis of the alkoxy functionalities is signified by the decrease in intensity of its absorption band $\nu_s$ (CH$_3$) at 2844 cm$^{-1}$ (Band A in Figure 2.5). This is accompanied by the growth of a broad band centred at 3436 cm$^{-1}$ (B), which may be assigned to the ν(OH) modes of both newly formed Si-OH and H$_2$O released during subsequent condensation reactions.

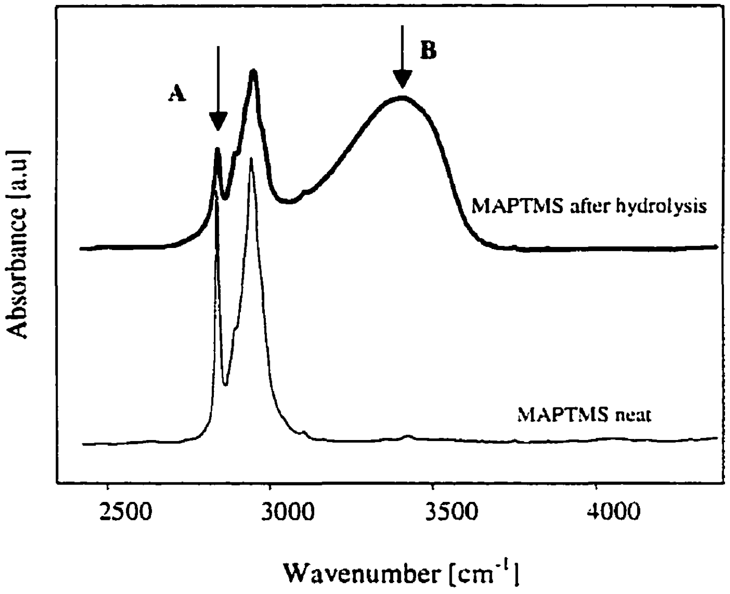

**Figure 2. 5** IR spectroscopic changes upon the hydrolysis of MAPTMS

During the same process, the decrease in the population of free C=O moieties (indicated by peak C in Figure 2.6) is accompanied by an increase in the absorption band at 1700 cm$^{-1}$ (peak D), as hydrogen bonding between the carbonyls and the newly formed Si-OH groups take place.

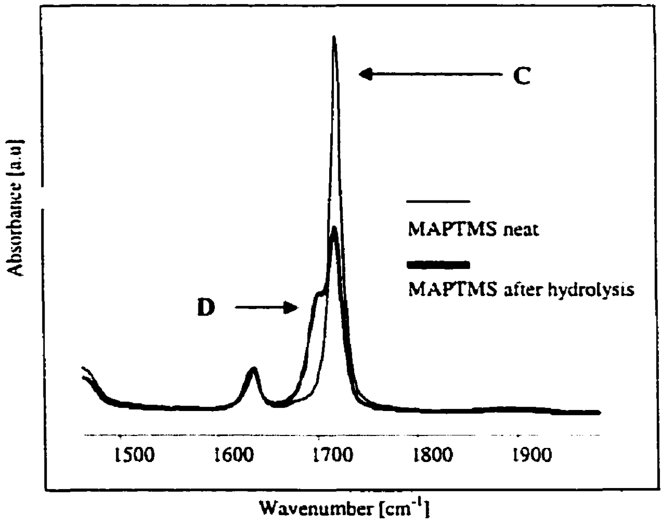

**Figure 2. 6** Spectroscopic evidence of H-bonding between carbonyl and silanol groups, upon hydrolysis of MAPTMS

Careful examination of Figure 2. 4 shows that the absorption band at 1700 cm$^{-1}$ (Band B) decreases in intensity with irradiation. This feature is associated with changes that take place in the silicate matrix during polymerisation of the organic groups and will be discussed in a later section.

### 2.3.1.2.3 Polymerisation of MAA complexed to zirconia clusters

Recall that the silica-methacrylate composite is doped with zirconia clusters complexed to methacrylic acid units. The large, polarisable transition metal elements are introduced to increase the refractive index (n) of sol-gel derived silica composites. In our case, the addition of the zirconia clusters increases the refractive index of the composite to 1.52, relative to that of pure sol-gel derived silica, which is generally in the range of 1.47.

In the preparation of our composite, the zirconium *n*-propoxide precursor was complexed in a 1:1 ratio with methacrylic acid before being added to the MAPTMS/acidified $H_2O$ reaction mixture. Transition metal alkoxides, due to the ability to increase their coordination numbers, have much greater reactivities than silicon alkoxides[44]. In mixed reaction systems containing both metal and silicon alkoxides, the rapid hydrolysis and condensation reactions of the former lead to the precipitation of metal oxo polymers and thus phase separation from the silica system. The reactivities of transition metal alkoxides may be controlled by complexation to strong ligands such as β-diketones, carboxylic acids and polyhydroxylated ligands. The ligands displace alkoxy functionalities and remain bound to the metal centres during the sol-gel process. When added to the MAPTMS/$H_2O$ system, the hydrolysis and condensation reactions of these complexes lead to MAA derivatised zirconia clusters, which are approximately 40 nm in size[32]. There is no concrete evidence of cross condensation reactions between the residual zirconium *n*-propoxide and silicon methoxide groups to form Si-O-Zr linkages. Schmidt has proposed that the zirconia clusters are uniformly distributed in the silica-methacrylate composite[32].

The MAA ligands are not affected during the condensation reactions and remain attached to the Zr centres in the final composite. In the IR spectrum of the material, this is confirmed by the band (M) at 1546 cm$^{-1}$ (Figure 2. 7), which may be assigned to the ν(C=O) stretching mode of the MAA ligands. The IR spectra also indicate that these ligands undergo polymerisation, when exposed to UV light. As shown in Figure 2. 7, band M migrates to higher energies 1560 cm$^{-1}$, as polymerisation proceeds and conjugation of the carbonyl unit with the vinyl group is lost. This region of the infrared spectrum also contains the decreasing intensity of bands at 1428 cm$^{-1}$, at 1322 cm$^{-1}$ and 1298 cm$^{-1}$.

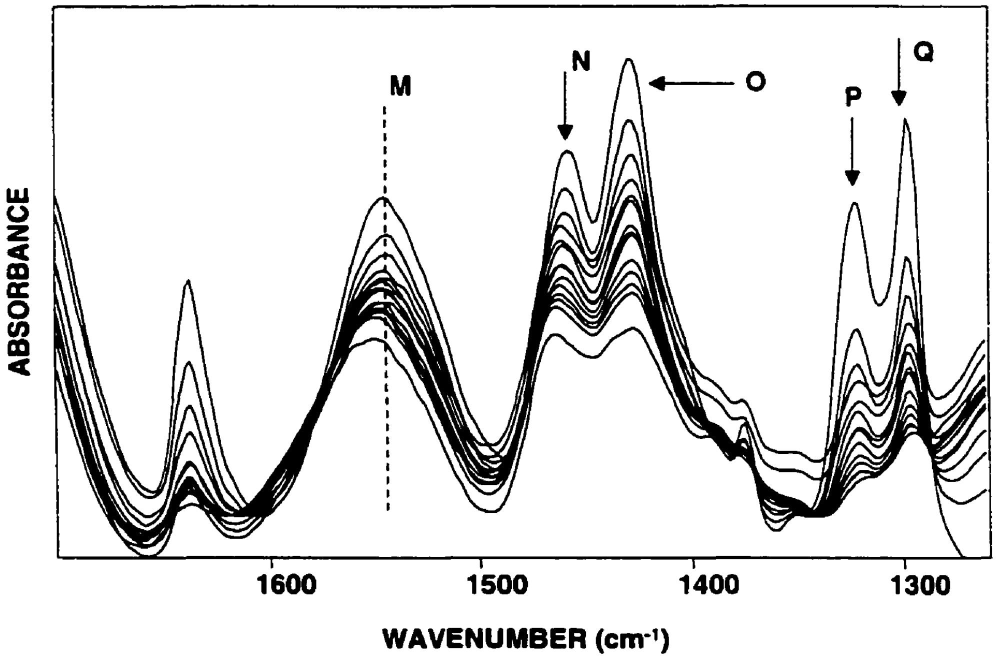

**Figure 2. 7** IR spectroscopic evidence of the polymerisation of MAA ligands upon UV irradiation

### 2.3.2 Photoinduced refractive index changes in the silica-methacrylate thin films

At the macroscopic level, the photo-initiated polymerisation reactions cause an increase in the refractive index of the silica-methacrylate composite. Qualitative similarities may be drawn between the conversion curve of the free-radical polymerisation process and the photoinduced increase of the refractive index ($\Delta n$) in the thin films. The relative intensities of the methacrylate ν(C=O) 1718 cm$^{-1}$ and ν(C=C) 1638 cm$^{-1}$ bands are plotted as a function of UV irradiation time in Figure 2. 8. The curves of both bands show the same trend, with polymerisation being most rapid within the first 10 minutes of irradiation. The curves for these modes then flatten out and there is negligible change in the intensity of ν(C=O) and ν(C=C) bands beyond 30 minutes of irradiation.

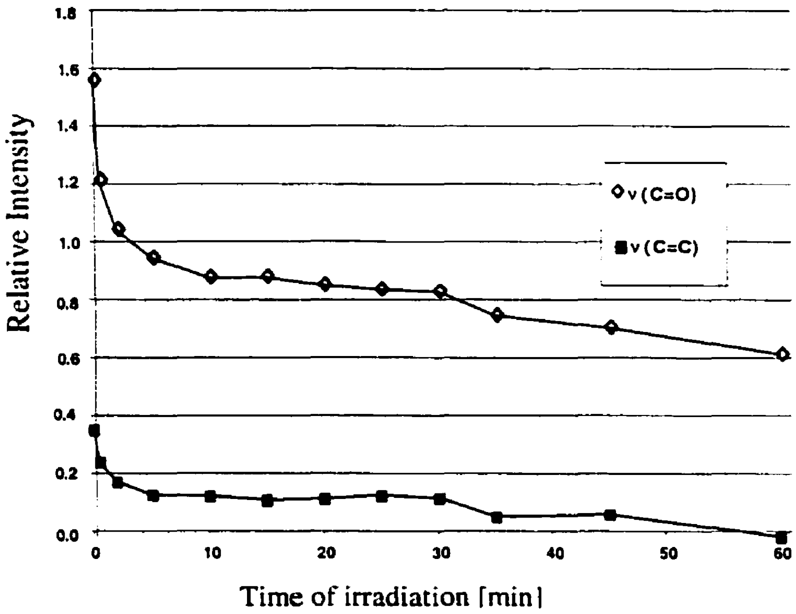

**Figure 2. 8** Intensity of ν(C=C) and ν(C=O) at 1638 $cm^{-1}$ and 1718 $cm^{-1}$ respectively vs. time of UV irradiation.

Figure 2. 9 graphs *n* (measured with both transverse electric (TE) and transverse magnetic (TM) polarisations of a 632.8 nm laser beam) films at increasing times of irradiation. The temporal profile of the refractive index change ($\Delta n$) for both $n_{TE}$ and $n_{TM}$ closely correlates to the conversion curve (Figure 2. 8) of the polymerisation process. After 60 minutes of irradiation, there is a maximum change in the refractive index of 0.015 from the initial values of $n_{TE}$ = 1.512 and $n_{TM}$ = 1.512. The maximum change of 0.012 occurs within the first 10 minutes. As observed in Figure 2.8, the greatest rate of polymerisation also occurs within this time period.

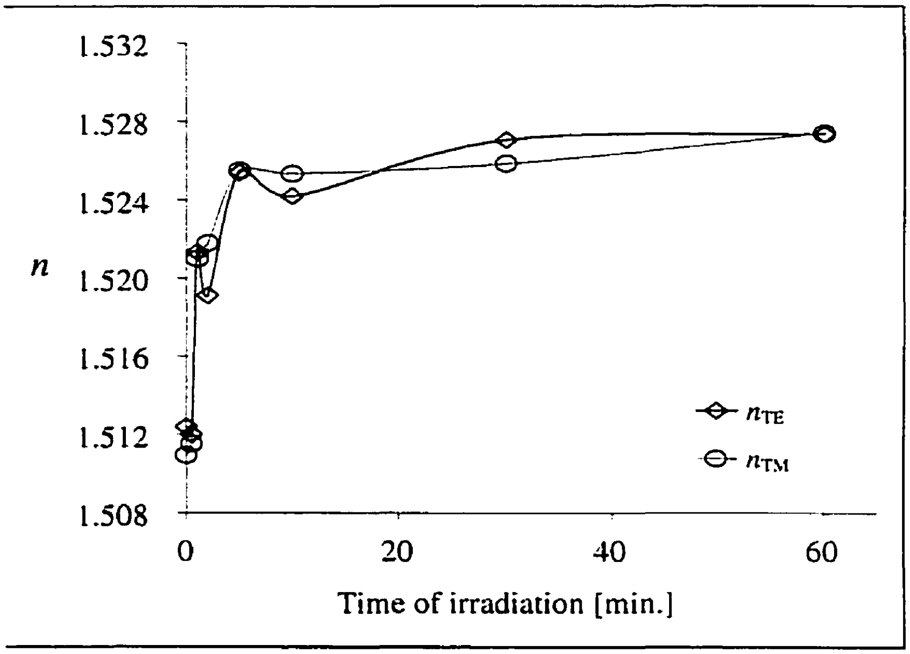

**Figure 2. 9** Photoinduced refractive index changes ($\Delta n_{TE}$ and $\Delta n_{TM}$) in a silica-methacrylate thin film.

Both the polymerisation process and the refractive index changes are accompanied by a significant decrease in the thickness (*d*) of the filmFigure 2. 10 shows the gradual decrease of *d* from 5.60 μm to 4.43 μm over 60 minutes of irradiation.

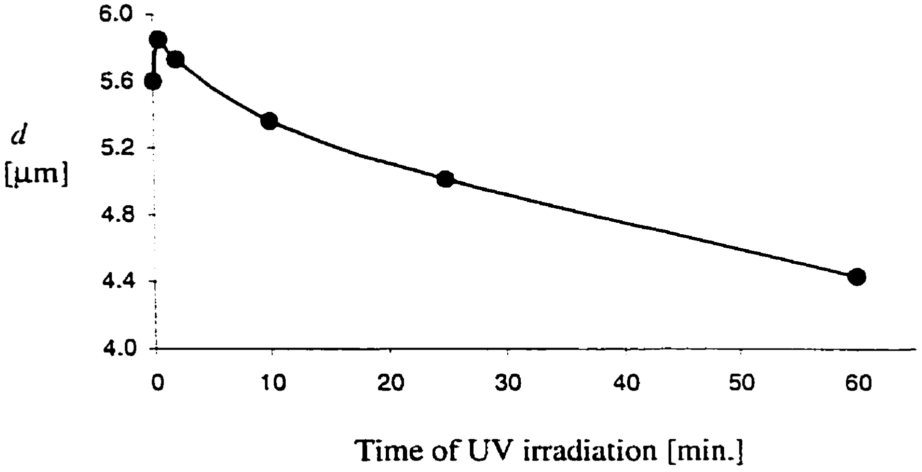

**Figure 2. 10** Change in thickness (*d*) of a silica-methacrylate thin film with increasing time of UV irradiation.

Collectively, these features paint a relatively simple picture of the photo-responses of the silica-methacrylate matrix. The sequence of IR spectra confirms that UV light initiates the free-radical polymerisation of the methacrylate moieties in the composite. It may then be argued that as polymerisation proceeds, the organic substituents, previously separated by van der Waals distances, are now brought closer together by covalent bonds[32]. The cumulative effect of these molecular-level changes would be the compaction or densification of the matrix, as confirmed by the decrease in the film's thickness *d*, and an associated increase in *n*. In this case, the photo-response of the silica-methacrylate composite may be likened to those of photopolymers, which consist of inert plasticisers doped with polymerisable monomers. Upon irradiation, polymerisation of the monomers leads to an overall volume compaction and a corresponding increase in n.

A closer examination of the spectroscopic evidence gathered in our study reveals that the structural changes in the silica-methacrylate composite do not arise from the free-radical reactions alone. In the following Sections, we will describe the spectroscopic features, which implicate that organic polymerisation process in triggering further condensation reactions between Si-OH and Si-$OCH_3$ groups in the matrix. These reactions contribute to the growth and densification of the sol-gel derived silica network. These finding emphasise that the polymerisation of the methacrylate substituents is not an insulated event and draws attention to the fact that it is not hosted in an inert matrix but in a metastable sol-gel derived silica matrix.

### 2.3.3 Co-densification of silica matrix

#### 2.3.3.1 FT-IR evidence

Close examination of spectral features in Figure 2. 4, Figure 2. 11 and Figure 2. 12 indicates that the photo-induced radical polymerisation indeed causes a cascade of chemical reactions and structural relaxation in the matrix. Observe in the Figures that there is a significant amount of residual Si-OH and alkoxy (Si-$OCH_3$) groups present within the film prior to photolysis. Band assignments are given in the Figure captions and marked by letters on the corresponding spectra. Hydrogen bonding between the methacrylate carbonyl and acidic silanol groups is indicated in Figure 2. 4 by the shoulder located at approximately 1700 $cm^{-1}$, at slightly lower energy with respect to the major ν(C=O) peak. Hydrogen bonding between silanol and the carbonyl oxygen of PMMA is well established[45], and it has been argued that such interactions may be essential to control phase separation to give transparent organosilicate composites that are homogeneous on a nanometre scale (nanocomposites)[46]. Figure 2. 4 shows that these hydrogen-bonded interactions are disrupted when samples containing MAPTMS are irradiated with 4.9 eV photons. Moreover, as the monomer polymerises, the silicate network is simultaneously elaborated through further hydrolysis and poly-condensation: both silanol and methoxide groups are consumed, and there is growth in the numbers of Si-O-Si linkages. These events are indicated in Figure 2. 11 by reductions in intensity of $Si\text{-}OCH_3$ and Si-OH group bands located at positions A ($CH_3$ rock of $Si\text{-}OCH_3$, 1638 $cm^{-1}$), D (ν(Si-OH) 944 $cm^{-1}$), and E (ν(Si-O-C) at 816 $cm^{-1}$). The decrease in absorption of the 944 $cm^{-1}$ peak of silanol indicates loss of hydroxyl groups upon irradiation; however, the effect cannot be due to excitation of the Si-OH hydroxyl because this requires 8 eV photons[54, 56].

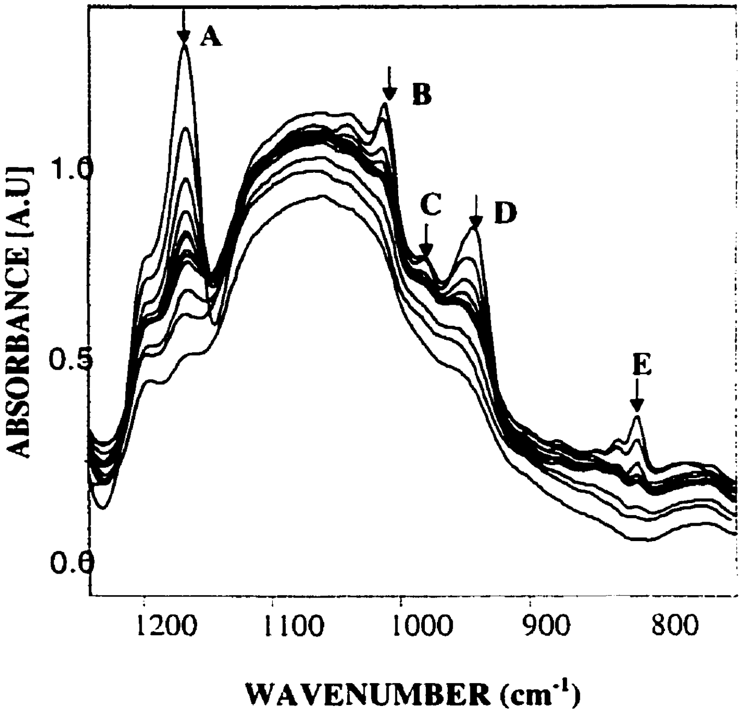

**Figure 2. 11** Changes in the IR spectral features of thin-film silica-methacrylate composite with increasing time of 4.9 eV irradiation where (A) –$CH_3$ rock of Si-$OCH_3$ at 1168 cm$^{-1}$; (B) and (C) trans (oop) CH wag and $CH_2$ wag of =$CH_2$ at 1012 and 980 cm$^{-1}$; (D) ν(Si-OH) at 944 cm$^{-1}$; (E) ν(Si-O-C) at 816 cm$^{-1}$. Time of irradiation (min): 0, 0.5, 2, 5, 10, 15, 20, 25, 30, 35, 45, 60.

Figure 2. 12 documents the condensation of ≡Si-$OCH_3$ by loss of methanol. This is evidenced through loss of intensity in the $\nu_s(CH_3)$ mode of Si-$OCH_3$ at 2844 cm$^{-1}$ and its asymmetric mode partner $\nu_{as}(CH_3)$ at 2960 cm$^{-1}$. The tell-tale band for the methanol product was detected through its Raman vibration at ~ 1029 cm$^{-1}$ (mixed $\nu_a$(C-O) + δ(COH)). This was obtained by launching 514.5 nm TE polarized laser light into a slab waveguide of the hybrid glass supported in a custom built precision integrated optics spectrometer equipped with a fast imaging spectrograph and charge coupled device detector[47]. The spectral data were acquired in real-time while the film was irradiated with UV light. This strategy allowed us to capture the spectrum of the methanol before the molecule diffused out of the film. Detailed results of the Raman experiments will be reported in Chapter 3.

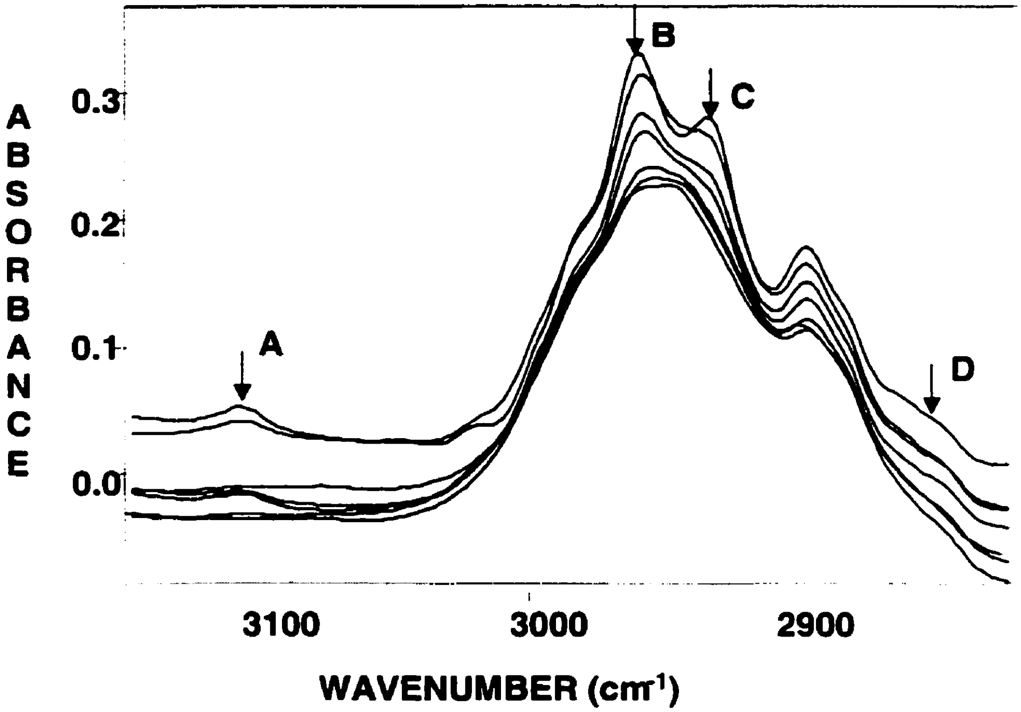

**Figure 2. 12** Diminishing intensities of (A) $\nu_{as}(CH_2)$ of $=CH_2$ at 3100 cm$^{-1}$; (B) $\nu_{as}(CH)$ of Si-OCH3 at 2960 cm$^{-1}$; (C) $\nu_s(CH)$ of $=CH_2$ at 2930 cm$^{-1}$; (D) $\nu_s(CH_3)$ of Si-OCH$_3$ at 2844 cm$^{-1}$ at increasing periods of UV (4.9 eV) irradiation. Time of irradiation (min): 0. 0.5, 2, 5, 10, 15, 20, 25, 30, 35, 45, 60.

From the above account, we can speculate on the origin of the increase in the refractive index of this type of hybrid network. Clearly, polymerisation of the organic unit does not proceed in isolation in the hybrid matrix. The film is metastable with respect to further poly-condensation reactions in the silica network, which continue in concert with the free-radical polymerisation reactions. Figure 2. 13 suggests a possible model for the photoinduced reactions in the composite.

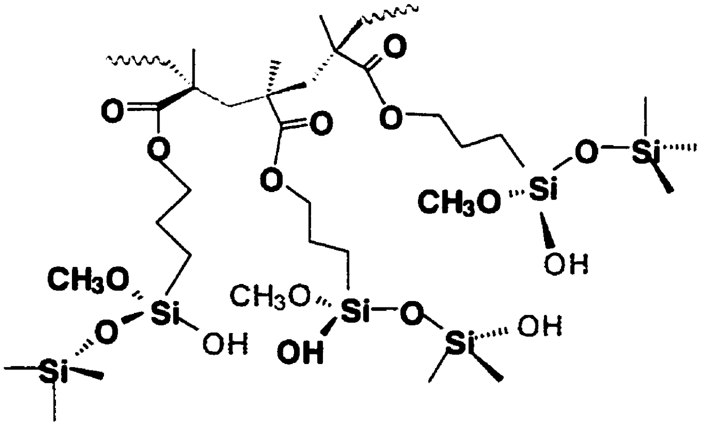

**Figure 2. 13** A possible model for the photo-induced densification of the silica-methacrylate composite

The carbon-carbon bonds formed between methacrylate units during the polymerisation process may bring their Si centres closer to each other, such that condensation reactions take place between their alkoxy and hydroxy substituents. We suggest that a form of "photo-induced sintering" takes place in the thin film. In this view, volume compaction is initiated by molecular rearrangements associated with methacrylate polymerisation and the consequent growth and densification of the silica matrix. As mentioned earlier, the former is a standard way of increasing both the density and refractive index of polymer materials, which are linearly correlated[48]. Network contraction during polymerisation is caused by conversion of non-bonded distances between monomers to shorter bonding distances in polymers[49]. In our case, this is accompanied by the densification of silica.

UV irradiation leads to densification in the silica-methacrylate films that is accompanied by a loss of hydroxyl groups in a manner that superficially resembles high temperature annealing. A notable difference is that heat treatment of silica at 1000 °C shifts the position of the $SiO_2$ $\omega_4$-transverse optical phonon mode[50] to 1080 $cm^{-1}$ [51]. In our films this mode is peaked at 1060 $cm^{-1}$, with a slight shift to lower wavenumber after photolysis.

The position of this stretching mode depends primarily on the average Si-O-Si bond angle, $\theta_{Si-O-Si}$. The decrease in energy of the peak position in our case is caused by a decrease in $\theta_{Si\text{-}O\text{-}Si}$. A shift in the IR band to lower frequency has been noted for silica films thermally grown on silicon[52]. The shift to lower energy in the vibrational peak corresponded to increasing biaxial compressive stress in the thin film. In fact, increases in fictive temperature, hydrostatic pressure or compressive stress, all cause $\theta_{Si\text{-}O\text{-}Si}$ to decrease, and the peak maximum of the mode to shift to lower wavenumber[53]. We conclude that the 1060 $cm^{-1}$ peak position of the $\nu_{as}$(Si-O-Si) mode in the HSGG film also indicates an increase in density of the matrix.

In closing this section, we point out that the photo-induced densification process we have observed in the hybrid material is achieved at considerably lower energy than what is required to densify purely inorganic sol-gel derived silica[54, 55]. In this case, a high energy photon (> 8 eV) is involved in direct electronic excitation either of Si-OH and/or to the conduction band of $SiO_2$. Bond rupture to create defects, and re-assembly could then lead to permanent atomic displacements consistent with network restructuring in $SiO_2$, densification and an increase in refractive index. In contrast, the principal role of the photon in the *hybrid* glass is to decompose the photo-initiator, which in turn generates methacrylate monomer free radicals. We surmise that the polymerisation step precipitates the chemical and skeletal changes in the inorganic host, which contribute to the photo-induced increase in the refractive index.

### 2.3.3.2 $^{29}$Si NMR evidence of silica growth

Further evidence of silica-growth during the free-radical polymerisation process in the hybrid networks was obtained through solid-state $^{29}$Si NMR spectroscopy of the composite films. Spectra of an unexposed film and one that had been irradiated for 60 minutes are presented in Figure 2. 14. In the non-irradiated matrix, peaks corresponding to three types of Si centres may be identified at -48, -59 and -68 ppm. These correspond to hydrolysed Si centres with 1, 2 and 3 siloxane (-O-Si) linkages respectively[56], labelled $T_1$, $T_2$, and $T_3$ according to convention[57]. Upon UV irradiation, there is a significant increase in the population of the $T_2$ species, accompanied by the decrease in intensity of the shoulder corresponding to the $T_1$ species. This indicates that condensation reactions that lead to the formation of additional siloxane bonds in the silica host, do accompany the UV initiated free-radical polymerisation reactions.

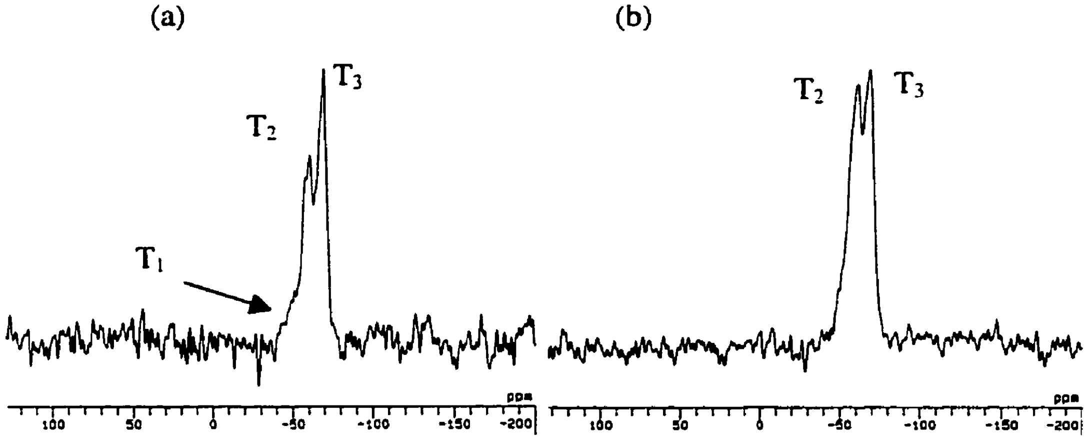

**Figure 2. 14** Solid state $^{29}$Si NMR spectra of (a) non-irradiated and (b) irradiated silica-methacrylate thin films

Note that there is no significant change in the band that corresponds to the $T_3$ species. This implies that silica-growth occurs mainly through the condensation reactions of $T_1$ species. It is possible that the $T_1$ species, with only one siloxane bond, is the most flexible Si centre and the least steric hindrance. In addition, it has the largest number (2) of unreacted silanol functionalies and thus the highest statistical probability to create additional Si-O-Si bonds.

### 2.3.4 The role of the methacrylate polymerisation – control experiment Saturated Glass

The studies presented in the previous Sections all indicate that silica densification occurs as a direct consequence of photo-initiated polymerisation of the organic component in the composite. To further test this model, a control experiment was designed with a hybrid silica-acetate composite. The material was prepared from 3-acetoxypropyltrimethoxysilane (APTMS) under the same conditions as the silica-methacrylate composite. The two alkoxysilane precursors MAPTMS and APTMS, have several similar features including the size of the organic substituents and the H-bonding between the C=O and the silanol groups (see peak F, Figure 2.16). In addition, both substituents impose similar steric and inductive effects on the hydrolysis and poly-condensation reactions of the trimethoxysilane precursors. Thus, it may be expected that their sol-gel reactions, carried out identical conditions, lead to similar silica networks.

Furthermore, zirconium *n*-propoxide was complexed with isobutyric acid, the saturated version of methacrylic acid, before being incorporated into the APTMS system. The major difference between the two materials then is the absence of a polymerisable vinyl group in the APTMS composite, *i.e.* a secondary organic polymer cannot be formed in the silica-acetate material. By subjecting this "saturated" composite to UV light, the behaviour of the silica host in the absence of free-radical polymerisation reactions could be selectively examined.

Thin films prepared from the saturated composite were exposed to UV light in the same sequence of irradiation times used to monitor the polymerisation in silicate-methacrylate thin films (Figure 2. 4). FT-IR spectra monitoring the UV irradiation of the saturated composites are presented in Figures 2.15 and 2.16. The spectra clearly indicate that the APTMS composite is insensitive to the low energy UV irradiation (4.9 eV). The absence of photo-induced structural transformations in the silica component is evident in Figure 2. 15, where during irradiation peaks A, B and D at 1198, 1045 and 970 $cm^{-1}$, corresponding to the $\nu$(Si-$OCH_3$), $\nu$(Si-O-Si) and $\nu$(Si-O(H)) respectively, remain unchanged. This indicates that condensation reactions between residual alkoxy and silanol groups in the silica component do not take place in the absence of free-radical reactions. The control experiment also validates our view that the free-radical polymerisation of the methacrylate groups is an *indirect* means of achieving additional growth and densification of the inorganic network, which by itself is insensitive to UV light.

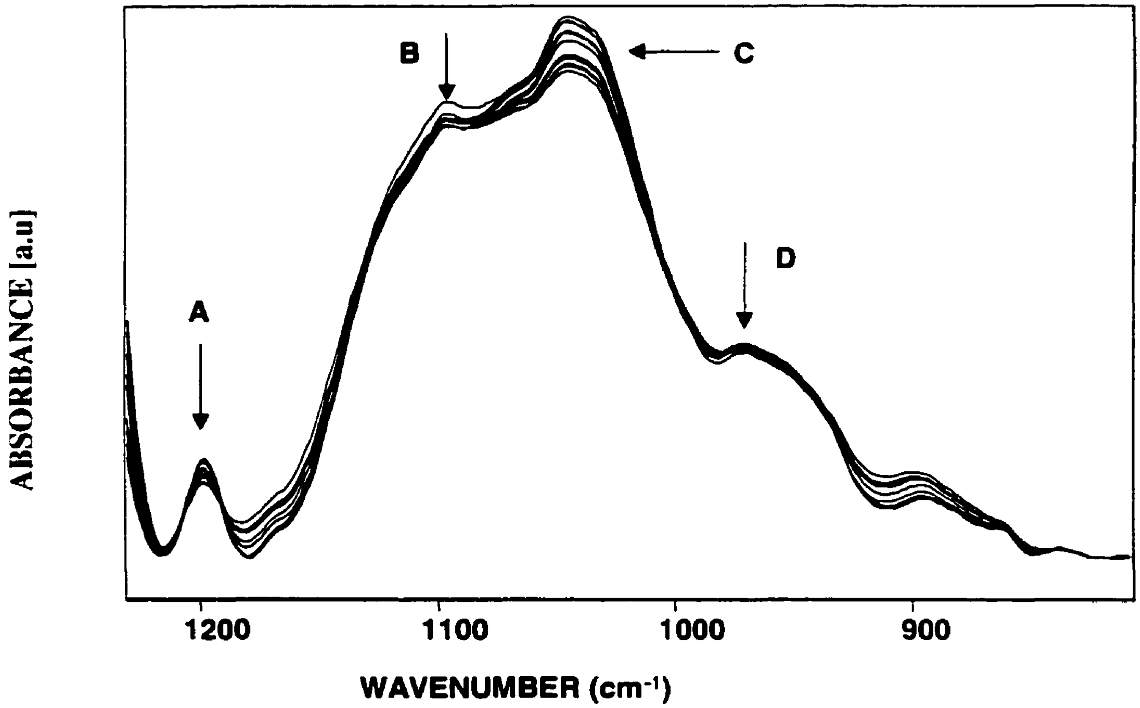

**Figure 2. 15** Effect of UV irradiation on thin films of APTMS-derived composites

Additional features were also noted in the FT-IR study presented here. As in the case of the silica-methacrylate matrix, the carbonyl groups in the saturated composite engage in hydrogen bonding with silanol groups. In Section 2.3.1.2.2, we observed that such hydrogen-bonded interactions were disrupted as polymerisation of the organic groups took place. The reverse occurs in the saturated composite. In Figure 2. 16, peaks E and F are correspond to the ν(C=O) modes of the "free" and the hydrogen bonded carbonyl species, respectively. With increasing irradiation time, there is a gradual decrease in intensity of peak E, suggesting that some form of photo-degradation of the ester was taking place. Interestingly, peak F remains unchanged indicating that the hydrogen bonded species are not depleted in the same way. Peak G at 1560 cm$^{-1}$ corresponds to the ν(C=O) stretching mode of the isobutyric acid ligands of the zirconia clusters. These too, remain unchanged upon irradiation.

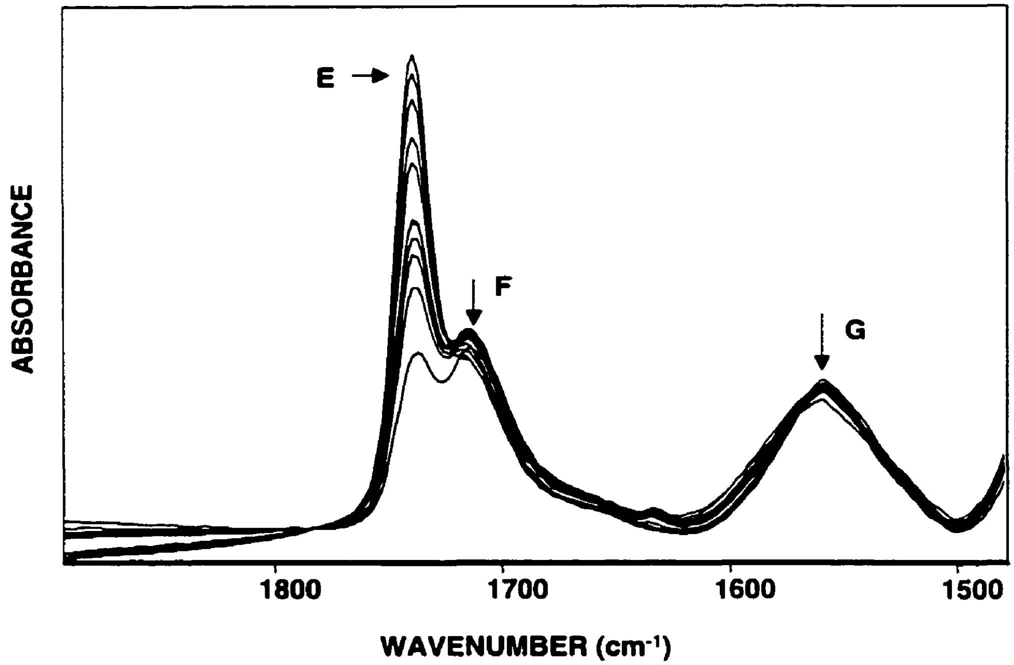

**Figure 2. 16** FT-IR spectra of thin films of silica-acetate composites with increasing times of UV irradiation

### 2.3.5 Titania doped silica-methacrylate composites

Growth of the silica matrix achieved through the photo-initiated polymerisation of methacrylate substituents was also observed in titania doped silica-methacrylate composites. FT-Ir spectra of unexposed and irradiated thin films of this composite are shown in Figure 2.17. Organic polymerisation is clearly evidenced in the mid-IR absorption spectra by loss of intensity of the vinyl group ν(C=C) stretching mode (B) at 1638 cm$^{-1}$, accompanied by the characteristic shift of the carbonyl stretching mode (A) ν(C=O) from 1717 cm$^{-1}$ to 1728 cm$^{-1}$. The concurrent condensation reactions between silanol and alkoxide groups in the metastable silica network are indicated by the diminishing intensities of ν(Si-O(H)) at 944 cm$^{-1}$ (G) and the –$OCH_3$ rock at 1166 cm$^{-1}$ (E). An increase in the distribution of the siloxane bond angles and the overall decrease in the Si-O-Si bond angle are indicated by the significant broadening of the $\nu_{as}$(Si-O-Si) and by its shift to lower wavenumber (1120 $cm^{-1}$ to 1110 $cm^{-1}$) respectively. The band at 920 $cm^{-1}$ (H) indicates the presence of Si-O-Ti bonds in the matrix.

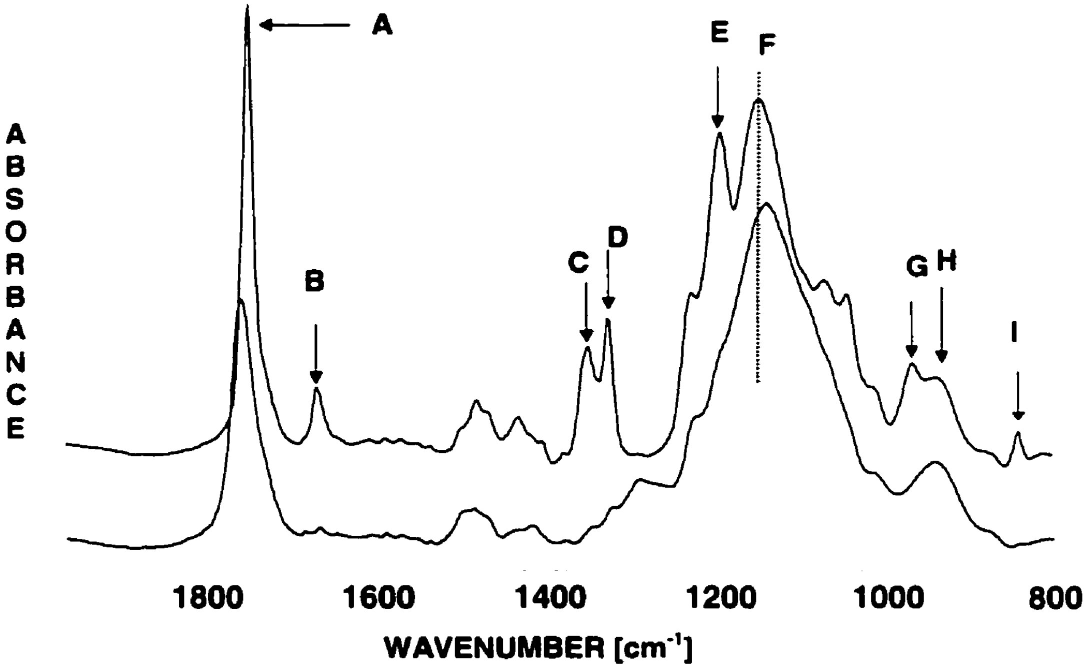

**Figure 2. 17** FT-IR spectra of (i) non-irradiated and (ii) irradiated titania doped silica-methacrylate thin films

### 2.3.6 Thermal densification of silica-methacrylate thin films

Densification of sol-gel derived silica composites may also be achieved with heat. Thermally induced condensation reactions between remnant alkoxide and silanol groups lead to additional siloxane bonds, growth and densification of the inorganic network. SE micrographs of thermally treated silica-methacrylate films are shown in Figure 2.18. Film (a) and (b) were irradiated for 15 and 30 minutes, respectively before being gradually heated to 300° C. Stress-induced cracking of the film takes place during thermal treatment. However, the gaps between the film fragments suggest that the extent of shrinkage is greater in the sample that had been irradiated for a shorter period of time. This is an interesting but qualitative observation, which implies that the condensation and thus the number of non-reacted alkoxide and silanol functionalities are greater in the less exposed film. We also note here that the unusually curved, scalloped edges of the film fragments were one of the earliest indications of organisation present within the silica-methacrylate composites. This feature will be discussed in detail in Chapter 5.

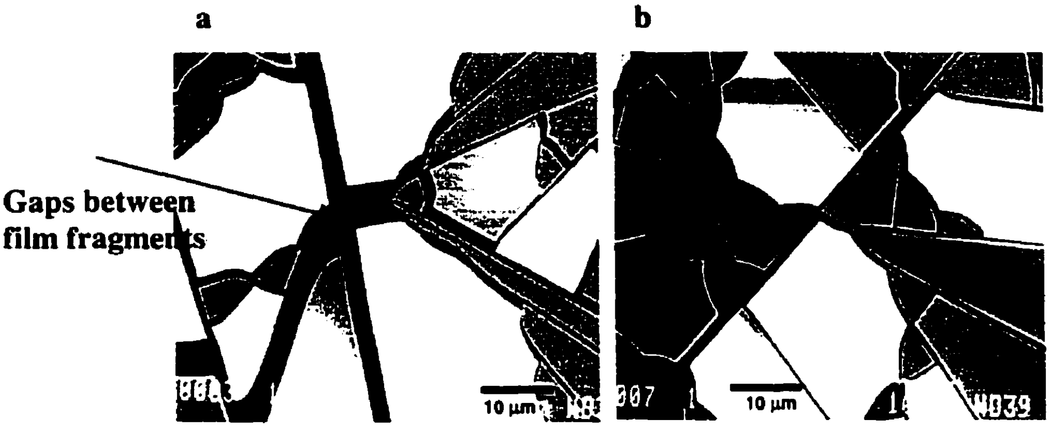

**Figure 2. 18** SE micrographs of thermally treated silica-methacrylate thin films, where film (a) was irradiated for 15 and (b) for 30 minutes

### 2.3.7 Spatial localisation – importance in resolution of integrated optics devices

The ability to induce a refractive index change in a material with light is one of the basic requirements in the photolithography of integrated-optics (IO) devices. Micron-scale regions of enhanced refractive index may be patterned on the photosensitive silica-methacrylate films with UV light passed through photo-masks. The photo-inscribed features with enhanced *n* values relative to the non-exposed regions of the film serve as micrometric optical devices, which guide, diffract, divide and reflect laser beams. As mentioned in the Introduction, a range of passive optical devices has already been constructed on silica-methacrylate thin films[58, 59] in which refractive index changes of up to 0.008 may be induced with UV light (Figure 2. 9).. The composites are suitable for this purpose as their base refractive index of 1.517 is compatible with that (1.469) of existing silica based optical-fibre systems. In addition, they are transparent at the 1.55 and 1.3 µm working wavelengths of telecommunications systems.

Figure 2. 19 shows SE micrographs of three types of I-O devices fabricated on silica-methacrylate films. Figure 2. 19a is a set of ridge waveguides, approximately 10 microns wide. A surface grating is shown in Figure 2. 19b was fabricated by the interference pattern produced by a phase mask on a thin silica-methacrylate film. A Bragg

grating deposited on a ridge waveguide is shown in Figure 2. 19c. The refractive index modulation associated with this device is seen as a series of alternating dark and light lines on the surface of the waveguide.

One of the most striking features in the series of micrographs is the resolution of the photoinduced structures. For example, the Bragg grating contains a strictly periodic, sub-micrometric (500 nm) modulation in the refractive index. This indicates that the photoinitiated free-radical polymerisation reactions in the silica-methacrylate network may be confined or spatially localised to within a few hundreds of nanometres.

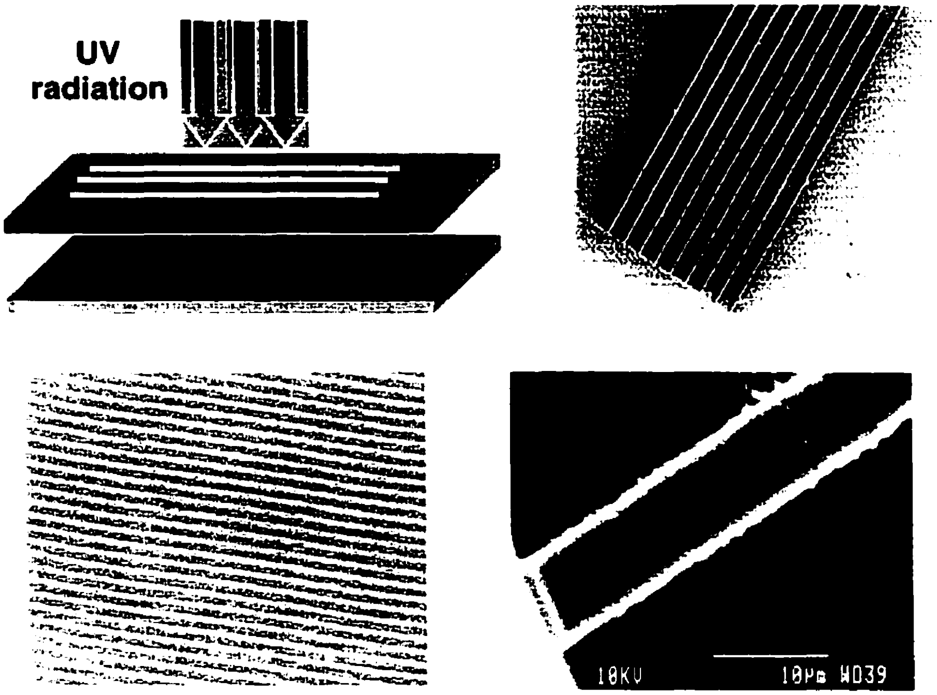

**Figure 2. 19** Selection of micro-optical elements photo-inscribed on silica-methacrylate thin films: (a) set of ridge waveguides; (b) surface-relief gratings: (c) Bragg grating in ridge waveguide

The propagation of free radical polymerisation reactions is diffusion limited. In bulk monomer solutions, the rate of polymerisation decreases with time as the growing polymer chains gradually increase the viscosity of the reaction medium. This effect is amplified in the gel-like media of thin films, which in general strongly suppress mass transport. Accordingly, in our silica-methacrylate films free-radical reactions do not go to completion, even when the film is exhaustively irradiated with UV light. This is evident in Figure 2. 4, which shows that unpolymerised methacrylate substituents (ν(C=C) 1638 $cm^{-1}$ and ν(C=O) 1718 $cm^{-1}$) are present in the matrix even after an exposure time of 1 hour.

In addition to the viscosity of the thin film medium, a feature that is unique to the silica-methacrylate composite also contributes to the steric hindrance imposed on free-radical reactions. Recall that the reactive methacrylate substituents are covalently grafted to Si and Zr centres, which are members of an extended, cross-linked inorganic network. This raises an additional and significant steric barrier against the diffusion of methacrylate radicals in the matrix. Figure 2. 8 indicated that the greatest extent of polymerisation occurred within the first 10 minutes of irradiation and it is possible that this time signifies reactions between methacrylate groups that are sufficiently close to each other. As described above, this time span coincides with the largest photoinduced refractive index change in the medium. In the context of photolithography, the sterically hindered free-radical reactions will be spatially constrained to illuminated regions. In this way, the refractive index change will strictly follow the patterns and dimensions defined by the photo-mask.

### 2.3.8 Effect of 6.4 eV ArF Excimer Laser Radiation

Bragg gratings are key building blocks of integrated optic devices[60]. They are used in distributed feedback lasers, in optical fibre amplifiers for gain flattening, and in wavelength division multiplexing (WDM). Bragg gratings can be used as mirrors to transmit light in free-space or waveguide interconnects between optical planes of photonic integrated circuits, and they have significant potential as heat/strain sensing elements. Glass optical fibre Bragg gratings have seen explosive development since the serendipitous discovery[61] that periodic refractive index modulations could be written by the constructive interference of counter-propagating visible, continuous wave (c.w) laser beams. It was this photo-response of optical fibre that has stimulated so much recent activity into the research and technology of the photoresponses of glass[62, 63, 64, 65, 66]. The origin of the isotropic index changes in optical fibres is still not fully understood, but it is clear that several light-activated mechanisms are involved[67, 68, 69, 70, 71], and light-induced densification figures prominently among them[72]. Unfortunately, the UV induced refractive index change in glass fibre is too small to be of practical use for making optical devices. Among other things, this is because fibre gratings must typically be ≥ 1.5 cm to achieve 100% reflectivity. Recently, Bragg gratings that were only 1.5 mm long were inscribed with an ArF laser in hybrid silica-methacrylate ridge waveguides[28]. The grating is a factor of 10 smaller than state-of-the-art fibre gratings, and achieves nearly 100 % reflectivity for both TE and TM light. Given the importance of the Bragg grating as a micro-optical element, we chose to compare the effects of 4.9 eV irradiation with those of 6.4 eV irradiation from the ArF laser.

We observed that pulsed 6.4 eV light polymerised the acrylate component of the hybrid glass within a few seconds. Changes in the electronic absorption spectra (not shown) were indistinguishable from those caused by 4.9 eV photons, except that the changes occurred in a matter of seconds. Polymerisation is confirmed in Figure 2. 20 by the infrared spectra acquired from the thin films exposed to 6.4 eV light for various times. There is loss of v(C=C) intensity at 1638 $cm^{-1}$, while the v(C=O) mode shifts from 1718 to 1720 $cm^{-1}$ as conjugation with the vinyl group is relieved.

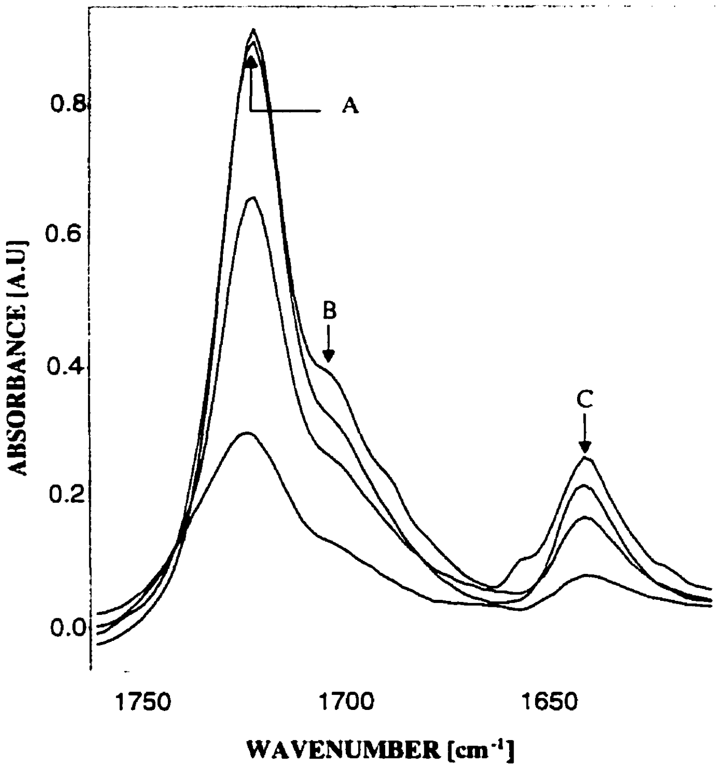

**Figure 2. 20** Changes in the ν(C=O) and ν(C=C) bands in thin-film composite upon ArF (6.4 eV) laser irradiation. Time of irradiation (30 Hz ·· 20 mJ-cm$^{-2}$): 15, 20, 60, 300 secs.

The accompanying silica network poly-condensation reactions are also recorded in the diminishing intensities of the Si-OCH$_3$ and Si-OH bands (Figure 2. 21). Note that the film was not exposed to 4.9 eV light at any stage of this experiment. Figure 2. 21 shows that the $\nu_{as}$(Si-O-Si) stretch shifts from 1090 cm$^{-1}$ to 1048 cm$^{-1}$ and broadens. By comparison, only a small shift was recorded for films irradiated with the lower energy UV lamp alone. In all other respects, the spectra show the same trends elicited by radiation from the 4.9 eV light source. This implies that densification of the silica matrix is triggered by the ArF laser as well.

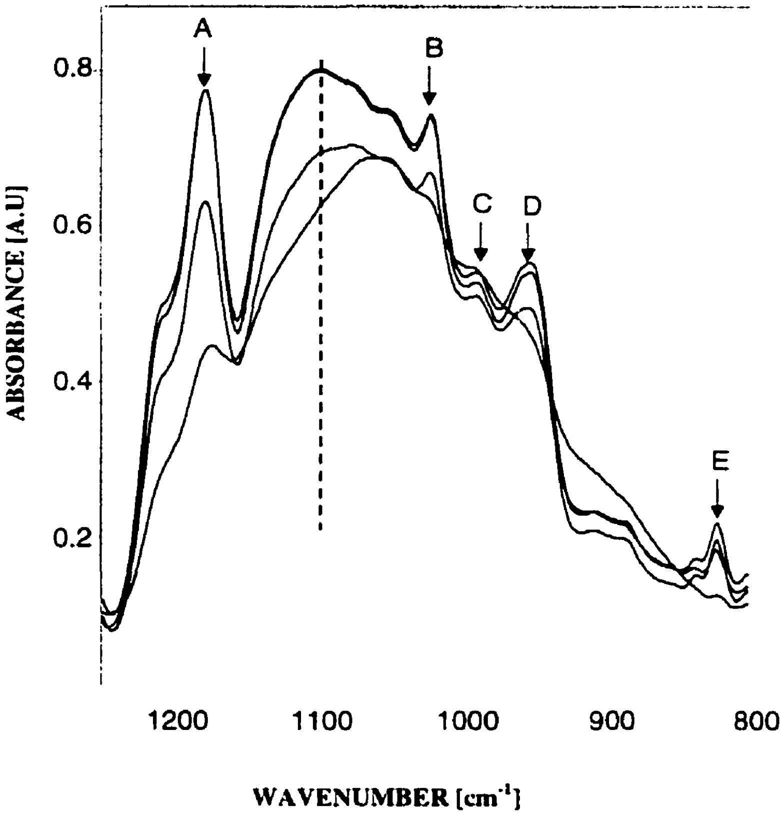

**Figure 2. 21** Changes in the spectral features of thin films upon 6.4 eV irradiation. The line is a guide to the shifting of $\nu_{as}$(Si-O-Si) from 1090 $cm^{-1}$ to 1048 $cm^{-1}$. The arrows mark the spectrum prior to photolysis.

### 2.3.8.1 Role of Photosensitivity in Bragg Grating Fabrication

The fabrication of ridge waveguides equipped with Bragg gratings is a multi-step process that includes two different UV radiation interventions. The waveguide is first defined as a channel by 4.9 eV UV illumination through a photo-mask. A propanol wet-etch step is then used to remove hybrid glass from regions of the silicon wafer not exposed to the light source. Smooth walled, rectangular ridge waveguides are produced by limiting the UV exposure time to 30 seconds. A SE micrograph of a typical ridge waveguide is shown in Figure 2. 19a. A Bragg grating was inscribed as a volume element by generating a plus/minus first order 6.4 eV interference pattern in the target ridge waveguide by excimer laser illumination through a precision phase mask. 193 nm light from an ArF laser was used to deposit the grating in the waveguide in 60 sec. A SE micrograph of a grating is also shown in Figure 2. 19. The periodic modulation of the grating is clearly seen at the surface of the ridge waveguide as alternating dark and light striations. This indicates that the interference pattern of the laser beam actually induces a corrugation on the surface of the waveguide, corresponding to densified (irradiated) and non-irradiated regions.

As the ridge waveguide/Bragg grating construction is made with two different UV energies, we chose to simulate the procedure by irradiating silica-methacrylate thin films on thermal oxide-on-silicon substrates under the same conditions used to make the Bragg device. The response of the hybrid glass to this radiation sequence was then monitored by infrared spectroscopy. Spectra of thin gel films exposed to 0.5 minutes of 4.9 eV radiation followed by periods of 6.4 eV radiation were acquired (Figure 2. 22Figure 2. 23).

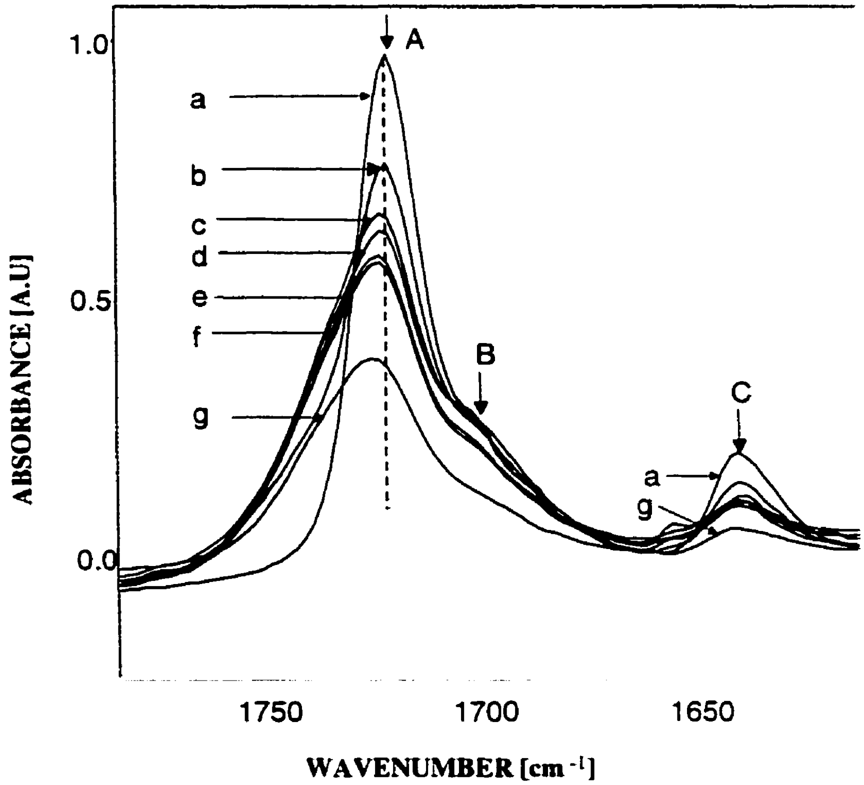

**Figure 2. 22** FT-IR spectra showing the effects of 0.5 min of 2.5-5.0 eV irradiation followed by 6.4 eV exposure. Spectra going down are (a) non-irradiated; (b-g) 0.5 min of 2.5-5.0 eV irradiated samples exposed to 6.4 eV irradiation for 0, 5, 10, 45, 60 and 180 secs.

Spectrum (b) in Figure 2. 22 was acquired after 30 sec of UV radiation from the 4.9 eV source. The film was not exposed to radiation from the excimer laser. The curve reveals, as expected, that the initial phase of irradiation to define the channel guide through the photo-mask stimulates radical polymerisation in the matrix. Spectra (c-g) record the outcome of successive treatments with the ArF laser. Polymerisation is indicated by the gradual loss of intensity in the1638 $cm^{-1}$ $\nu$(C=C) band (position C). Clearly, the conversion of vinyl substituents occurs much more rapidly (within 3 min) under the 6.4 eV source. Comparison of Figure 2. 4, Figure 2. 20 and Figure 2. 22 shows that the $\nu$(C=O) stretch near 1722 $cm^{-1}$ undergoes the same qualitative shift to higher wavenumber, regardless of the photon energy or sequence of irradiation. There is no clear isosbestic point in either of Figure 2. 20Figure 2. 22. This suggests that 6.4 eV photons open up additional photochemical channels in the hybrid glass. Indeed, the same results are obtained when the 1-hydroxycyclohexyl-1-phenylketone photoinitiator is omitted from the glass composition. By comparing Figures 2.11 and Figure 2. 23 (c-g) we confirm that polymerisation of the methacryloxypropyl groups at 193 nm elicits the same kind of activity from the silicon network: there is simultaneous poly-condensation of residual silanol and alkoxy groups. These events are indicated in Figure 2. 23 by reductions in intensity of Si-$OCH_3$ and Si-OH group bands (labelled A through E) in the same manner as discussed above for ~5 eV radiation.

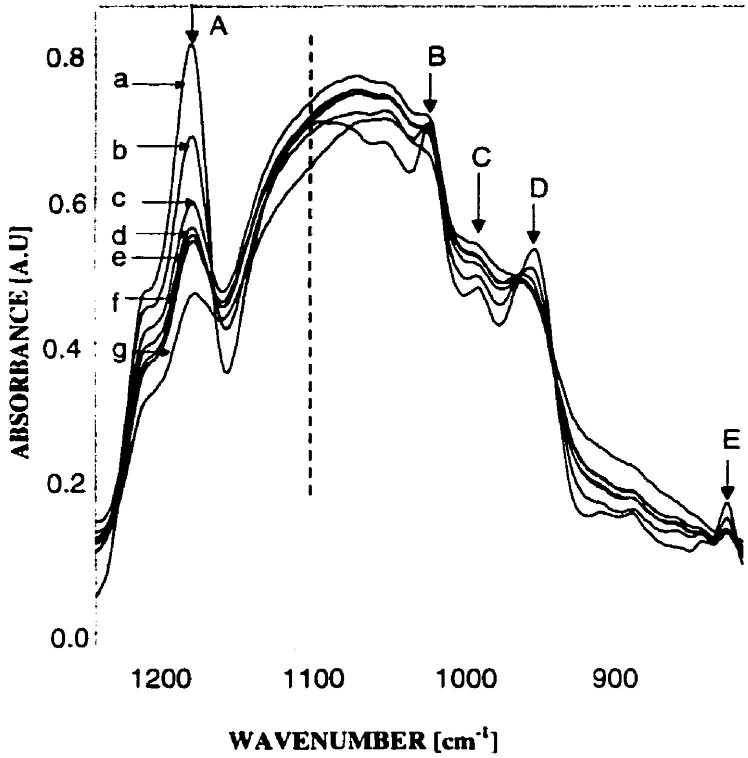

**Figure 2. 23** FT-IR spectra showing the effects of 0.5 min of 2.5-5.0 eV irradiation followed by 6.4 eV exposure. Spectra going down are (a) non-irradiated; (b-g) 0.5 min of 2.5-5.0 eV irradiated samples exposed to 6.4 eV irradiation for 0, 5, 10, 45, 60 and 180 secs.

It is tempting to attribute the refractive index modulation in the grating to densification of the hybrid glass, although additional experiments must be performed at 6.4 eV to evaluate this notion. The mechanism of Bragg grating formation in our samples is a subject for further inquiry. The change in the refractive index of an isotropic substance undergoing densification can be associated with a change in the number of oscillators per unit volume, anisotropy in the Lorentz-Lorenz polarization under stress, and variations in atomic polarisibilities with interatomic distance. Through compaction, a fractional increase in the refractive index may be viewed as the product of reorganization of existing bond structure coupled with bond formation. There can also be contributions to the refractive index through the products of bond scission and defect formation. Schenker[20] has reported that two 6.4 eV photons densify fused silica. He concludes, nevertheless, that there is no compelling evidence that bond rupture or defect formation is associated with densification. Although defect formation is possible in our hybrid glass composites, we believe that, should they exist, their contributions to the refractive index are small compared with the collateral densification that we observe.

## 2.4 CONCLUSIONS

New insight was provided into how I-O devices like ridge waveguides and Bragg gratings are inscribed by photolithography in methacrylate-rich hybrid sol-gel silica films on silicon substrates. Arguments were advanced linking the changes in the refractive index of the composites to chemical transformations and structural relaxation leading to densification. Electronic absorption spectroscopy indicated that the acrylate species underwent polymerisation when irradiated with 4.9 eV photons. Prolonged irradiation appeared to lead to secondary photochemistry that may involve polymer chain scission. Infrared spectroscopy confirmed that photo-initiated polymerisation occurs in the glass. Scrutiny of the time evolution of the IR absorption bands indicated that free radical polymerisation was accompanied by additional simultaneous poly-condensation in the silica matrix. Free silanol and unreacted methoxysilane were consumed in the process. Matrix densification was indicated by shifts in the transverse optical phonon mode associated with decreases in the Si-O-Si bond angle of the antisymmetric stretching vibration. Substantial growth in the Si-O-Si framework was observed through increased intensity in this IR absorption. Similar behaviour was observed for films irradiated with 6.4 eV light from an excimer laser. A phase mask in combination with pulsed 6.4 eV light was used to write a 1.5 mm, polarization independent high reflectivity Bragg grating into a ridge waveguide. The high reflectivity was rationalized by postulating a periodic modulation of the volume compaction of the matrix. Overall, the organic component of the glass conferred unique properties on the material that allowed it to be densified even with 4.9 eV light. By comparison, sol-gel silica with no organic component must be densified at nearly twice the photon energy.

---

1. M. C. Goopta, Ed., *Handbook of photonics*. (CRC Press, Boca Raton, Florida. 1996).
2. M. P. Andrews and S. I. Najafi, Eds. *Sol-gel and polymer photonic devices, Critical Reviews of Optical Science and Technology, Vol. CR68* (SPIE Opt. Eng. Press, Bellingham, WA. 1997).
3. M. P. Andrews and S. I. Najafi,.*Sol-gel and polymer photonic devices, Critical Reviews of Optical Science and Technology, Vol. CR68,* M. P. Andrews and S. I. Najafi, Eds., (SPIE Opt. Eng. Press, Bellingham, WA. 1997), p. 253-285.
4. M. P. Andrews. *Proc. SPIE, Opt. Soc. Eng.*, **2997**, 48 (1997).
5. S. I. Najafi, *Introduction to Glass Integrated Optics*, (Artech House, Boston. 1992).
6. R. R. A. Syms, W. Huang, and V. M. Schneider. *Electron. Lett.* **32**, 1233 (1996).
7. P. Coudray, J. Chisham, M. P. Andrews and S. I. Najafi. *Opt. Eng.* **36**, 1234 (1997).
8. M. Douay, W. X. Xie, T. Taunay, P. Bernage, P. Niay, P. Cordier, B. Poumellec, L. Dong, J. F. Bayon, H. Poignant, and E. Delevaque. *J. Lightwave Tech.* **15**, 1329 (1997).
9. (a) W. Primak and R. Kampwirth. *J. Appl. Phys.* **39**, 5651 (1968), (b) Primak and . Kampwirth. *J. Appl. Phys.* **39**, 6010 (1968).
10. P. L. Higby, E. J. Friebele, C. M. Shaw, M. Rajaram, E. K. Graham, D. L. Kinser and E. G. Wolf. *J. Am. Ceram. Soc.* **71**, 796 (1988).
11. E. J. Friebele and P. L. Higby, *Laser induced damage in optical materials*, H. H. Bennett, A. H. Guenther, D. Milam, B. E. Newman and M. J. Soileau Eds. (NIST Spec. Publ. 756, 1987, NIST, Boulder CO. 1988), p 89.
12. M. Rajaram, T. Tsai, and E. J. Friebele. *Adv. Cer. Mater.* **3**, 598 (1988).
13. C. I. Merzbacher, E. J. Friebele, J. A. Ruller, and P. Matic. *Proc. SPIE Opt. Eng.* **1533**, 222 (1991).
14. T. A. Dellin, D. A. Tichenor, and E. H. Barsis. *J. Appl. Phys.* **48**, 1131 (1977).
15. C. B. Norris, and E. P. EerNisse. *J. Appl. Phys.* **45**, 3876 (1974).
16. J. S. Lukesh. *Phys. Rev.* **97**, 345 (1955).
17. W. Primak. *Phys. Rev.* **110**, 1240 (1958).

18. J. B. Bates, R. W. Hendricks and L. B. Schaffer, *J. Chem. Phys.* **61**, 4163 (1974).

19. J. L. Brebner, L. B. Allard, M. Verhaegen, M. Essed, J. Albert, P. Simpson and A. Knights, *Proc. SPIE Opt. Soc. Eng.* **2998**, 122 (1997).

20. R. E. Schenker and W. G. Oldham, *J. Appl. Phys.* **82**, 1065 (1997).

21. D. C. Allan, C. Smith, N. F. Borelli, and T. P. Seward, III. *Opt. Lett.* **21**,1960 (1996).

22. H. Imai, K. Awazu, M. Yasumori, H. Onuki, and H. Hirashima, *J. Sol-Gel. Sci. Technol.* **8**, 365 (1997).

23. (a) C. J. Brinker and G. W. Scherer, *Sol-gel science*, (Academic Press, New York. 1990), (b) R.R. Reisfeld and C.K. Jørgenson, Eds., *Chemistry, spectroscopy and applications of sol-gel glasses*, (Springer-Verlag, Berlin. 1992); (c) L.C. Klein. *Annu. Rev. Mater. Sci.* **23**, 437 (1993).

24 . G. W. Scherer, *J. Sol-Gel Sci. Technol.* **8**, 353 (1997).

. P. Coudray, J. Chisham, M. P. Andrews, A. Malek-Tabrizi, C.-Y. Li, S. I. Najafi. *Opt. Commun.* **128**, 19 (1996).

26. C.-Y. Li, J. Chisham, M. P. Andrews, S. I. Najafi, J. D. Mackenzie, N. Peyghambarian, *Electron. Lett.* **31**, 271 (1995).

27. P. Coudray, J. Chisham, M. P. Andrews and S. I. Najafi, *Opt. Eng.* **36**, 1234 (1997).

28. M. A. Fardad, T. Touam, P. Meshkinfam, R. Sara, X. M. Du, M. P. Andrews and S. I. Najafi. *Electron. Lett.* **33**, 1069 (1997).

31. M. P. Andrews and S. I. Najafi, *Proc. SPIE Opt. Eng.* **2998**, 293 (1997).

32. (a) B. Novak, *Adv. Mater.* **5**, 422 (1993), (b) P. Judenstein and C Sanchez. *J. Mater, Chem.* **6**, 511 (1996), (c) U. Schubert, N. Husing and A. Lorenz. *Chem. Mater.* **7**, 2010 (1995).

31. J. F. Rabek, *Mechanisms of photophysical processes and photochemical reactions in polymers*, (Wiley. New York 1987).

32. H. Krug, F. Tiefensee, P. W. Oliviera and H. Schmidt, *Proc. SPIE Int. Opt. Eng.* **1758**, 448 (1992).

33. X. T. P. Phan, *J. Radiat. Curing*, **13**, 18 (1986).

34. C. N. R. Rao, *Ultra-violet and visible spectroscopy, chemical applications*, (Third

edition. Butterworths, London. 1974). p.42-47

35. J. G. Calvert and J. N. Pitts, *Photochemistry*, (Wiley, New York. 1966). p. 247-268.

36 . P. A. Leermakers and H. T. Thomas, *J. Am. Chem. Soc.* **87**, 1621 (1965).

37 . M. Ito, K. Inuzuka and S. Imanishi, *J. Am. Chem. Soc.* **82**, 1317 (1960).

38 Photolysis of side-chain ester groups

39. T.Mitsuoka, A. Torikai and K. Fuenki, *J. App. Polym. Sci.* **47**, 1027 (1993).

40. P. M.Fritz, Q. Q. Zhu, W. Schnabel, *Eur. Poly. J.* **30**, 1335 (1994).

41. a) D. L. Ou and A. B. Seddon, *J. Non-Cryst. Solid,*. **210**, 187 (1997), b) R. T. Conley, *Espectroscopia Infraroja*, (Alhambra, Madrid. 1979), p. 187-194. c) A. L. Smith, *Spectrochim. Acta.* **16**, 87 (1960), d) A. L. Smith, *Analysis of Silicones*, (Wiley, New York. 1974), p. 257-281, e) B. Stuart, *Modern Infrared Spectroscopy*, D. J. Ando, Ed. (Wiley, New York. 1996), f) K. Nakamoto, *Infrared and Raman Spectra of Inorganic and Coordination compounds*, (Fourth edition. Wiley, New York. 1986).

42. M. In, C. Gerardin, J. Lambard and C. Sanchez, *J. Sol-Gel Sci. Technol.* **5**, 101 (1995).

46. a) X. Li and T. A. King, *J. Non-Cryst. Solids*, **204**, 235 (1996), b) C. N. R. Rao, *Chemical applications of Infrared Spectroscopy*, (Academic Press. New York. 1963), p. 24, c) B. K. Coltrain, C. J. T. Landry, J. M. O'Reilly. A. M. Chamberlain, G. A. Rakes, J. S. Sedita, L. W. Kelts, M. R. Landry and V. K. Long. *Chem. Mater.* **5**, 1445 (1993).

44. See for example, D. C. Bradley, *Chem. Rev.* **89**, 1317 (1989).

55. C. J. T. Landry, B. K. Coltrain, J. A. Wesson, J. L. Lippert and N. Zumbulyadis, *Polymer*, **33**, 1496 (1992).

46 . N. K. Raman, M. T. Anderson and C. J. Brinker, *Chem. Mater.* **8**, 1682 (1996).

57. J. Baldwin, N. Schuhler, I. S. Butler and M. P. Andrews, *Langmuir*, **12**, 6389. (1996).

48. H. M. Cohen and R. Roy, *Phys. Chem. Glasses*, **6**, 149 (1965).

60. J. G. Kloosterboer, G. M. M. van de Hei, R. G. Gossink and G. C. M. Dortant, *Polymer Commun.* **25**, 322, (1984).

---

50 . F. L. Galeener, *Phys. Rev. B*, **19**, 4292 (1979).

62. R. M. Almeida, T. A. Guiton, and C. G. Patano, *J. Non-Cryst. Solids*, **121**, 193 (1990).

63. G. Lucovsky, J. T. Fitch, E. Kobeda and E. A. Irene, *The physics and chemistry of the $SiO_2$ and $Si$-$SiO_2$ interface*, C. R. Helms and B. E. Deal Eds., (Plenum Press. New York. 1988). p. 139.

53 . A. Agarwal and M. Tomozawa, *J. Non-Cryst. Solids*, 209, 166 (1997).

54. H. Imai, H. Hiroshima, K. Awazu and H. Onuki, *J. Ceram. Soc. Jpn.* **102**, 1092 (1994).

55. H.Himai, H. Hirashima, K. Awazu and H. Onuki, *Proc. SPIE. Soc. Opt. Eng.* **2288**, 71 (1994).

56. F. Babonneau, J. Maquet and J. Livage, *Chem. Mater.* **7**, 1050 (1995).

57. C. J. Brinker and G. W. Scherer, *Sol-gel Science The Physics and Chemistry of Sol-Gel Processing*, Chapter 3, (Academic Press, New York. 1990)

65. P.Coudray, J. Chisam, M. P. Andrews and S. I. Najafi, *Opt. Eng.* **36**, 1234 (1997).

59. (a) T. Touam, G. Milova, Z. Saddiki, M. A. Fardad, M. P. Andrews, J. Chrostowski and S. I. Najafi, *Thin Solid Films*, **203**, 307 (1997);
(b) T. Touam, G. Milova, Z. Saddiki, M. A. Fardad, M. P. Andrews, and S. I. Najafi, *Proc. SPIE Opt. Eng.* **2997**, 79 (1997).

67. T. Tamir, *Guided-Wave Optoelectronics*, (Springer-Verlag, Heidelberg, Germany. 1988).

68. K. O. Hill, Y. Fujii, D. J. Johnson and B. S. Kawasaki, *Appl. Phys. Lett.* **32**, 647 (1978).

62. G. Meltz, W. W. Morey, W. H. Glenn, *Opt. Lett.* **14**, 823 (1989).

63. D. P. Hand and P. St. J. Russell, *Seventh International Conference on Integrated Optics and Optical Communications*, IOOC '89, Kobe, Japan, paper 21C3-4. (1989).

64. J.-L Archambault, L. Reekie, and P. St. J. Russell, *Electron. Lett.* **26**, 453 (1993).

65. P. Simon, H. Gerhardt and S. Szatmari, *Opt. Lett.* **14**, 1207 (1989).

66. T. Tomie, I. Okuda and M. Yano, *Appl. Phys. Lett.* **55**, 325 (1989).

67. P. St. J Russell, L. J. Poyntz-Right and D. P. Hand. *Proc. SPIE Soc. Opt.*

*Eng.***1373**, 126 (1990).

75. *Photosensitivity and quadratic nonlinearity in glass waveguides: fundamentals and applications*, Technical Digest, Vol. 22, (Optical Society of America, Washington, D.C. 1995).

69. (a) K. O. Hill, B. Malo, F. Bilodeau and D. C. Johnson. *Annu. Rev. Mater. Sci.* **23**, 125 (1993), (b) M. G. Sceats, G. R. Atkins and S. B. Poole. *Annu. Rev. Mater. Sci.* **38**, 123 (1993).

70. D. P. Hand and P. St. J. Russell. *Opt. Lett.* **15**, 102 (1990).

71. D. Wong, S. B. Poole and M. G. Sceats. *Opt. Lett.* **17**, 1773 (1992).

72. J. P. Bernardin and N. H. Lawandy, *Opt. Commun.* **79**, 194 (1990).

# 3. *IN SITU* WAVEGUIDE RAMAN SPECTROSCOPY OF PHOTO-REACTIONS IN SOL-GEL DERIVED SILICA-METHACRYLATE THIN FILMS

## 3.1 INTRODUCTION

### 3.1.1 Thin film characterisation techniques

Thin film research is the study of atoms, molecules and macromolecules assembled onto quasi 2-dimensional platforms. The field thus relies heavily on characterisation techniques that distinguish thin films from bulk systems and are sensitive to their nano. meso and micro length scales, rich interfacial science, orientation, conformations, depth-dependence and phase changes. The sub-nanometric resolution of features on planar substrates became possible with the scanning tunnelling microscope (STM) and its derivative, the atomic force microscope (AFM). The chemical composition and thickness of films may be obtained through techniques such as X-ray photoelectron spectroscopy (XPS), secondary neutral mass and secondary ion mass spectrometric measurements (SNMS and SIMS, respectively). These methods generally identify the topography, chemical composition and thickness of the film.

Optical characterisation tools based on the total internal reflection (TIR) of light, apply the coherence, colour, intensity and polarisation of laser beams to probe features that are unique to thin films. As shown in Figure 3.1, when a beam of light incident from the higher refractive index layer ($n_h$) suffers TIR ($\theta > \theta_{critical}$) at a dielectric interface, its electric field decays exponentially into the lower refractive index layer ($n_l$) - the monolayer or thin film to be characterised. This evanescent wave (a function of the excitation beam's wavelength and therefore sensitive to nanometre length scales) excites optical phenomena such as infrared absorption, Raman scatter and fluorescence in the analyte layer, in a highly localised manner.

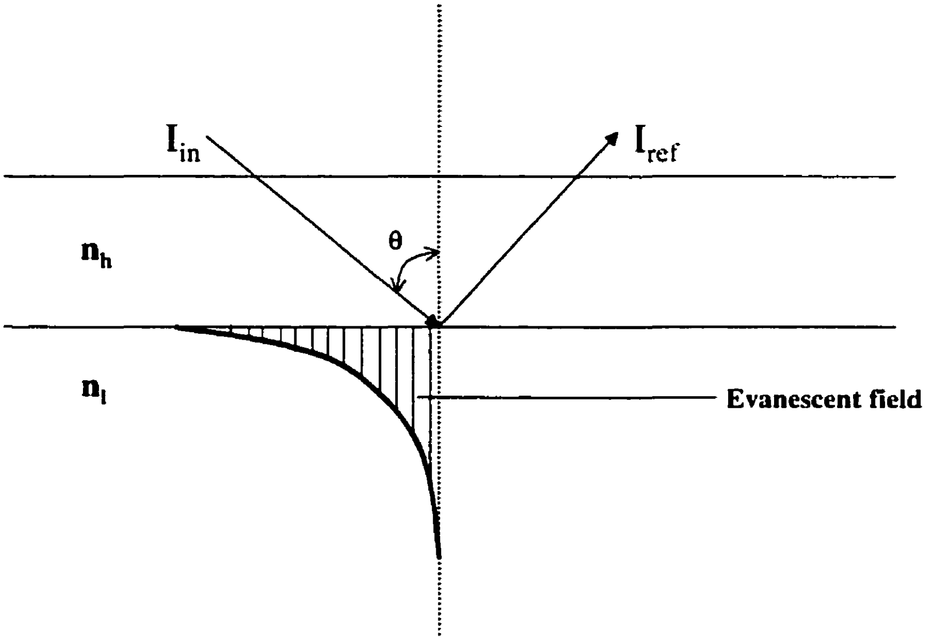

**Figure 3. 1** Total internal reflection (TIR) at a dielectric interface

Techniques such as attenuated total reflectance infrared spectroscopy (ATR IR), reflection absorption infrared spectroscopy (RAIRS), TIR Raman and TIR fluorescence are all based on this principle and collectively provide a wealth of spectroscopic information on thin film systems. Here, the angle of incidence and polarisation of excitation beams may be tuned to probe for orientation in thin films or monolayers. Furthermore, surface plasmon polaritons excited in noble metal layers placed at the interface can enhance signals from even nanomolar quantities of analyte.

### 3.1.2 Optical Waveguides

A special form of TIR occurs in an optical waveguide, the simplest element in integrated-optics (I-O) circuits. Simply, a laser beam injected into a planar (slab) waveguide suffers TIR at the upper and lower interfaces and travels in a zigzag path along the $z$-axis. As shown in Figure 3.2, an asymmetric slab waveguide is essentially a 1 – 10 μm thick dielectric film with a refractive index, $n_f$ (without an imaginary component) that is greater than those of its substrate $n_s$, and cladding, $n_c$. For a film of given $n$ and thickness d, waveguiding occurs only at specific values of θ, described by an eigenvalue equation..

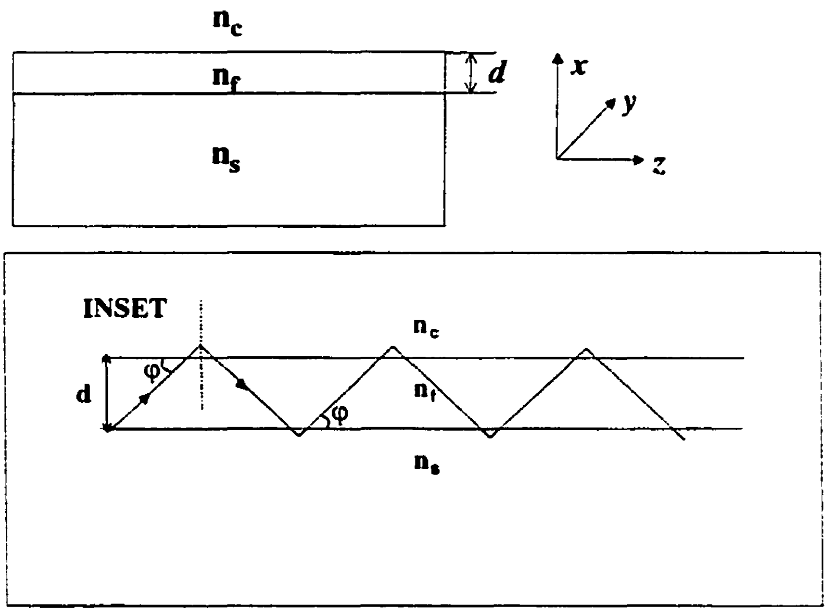

Figure 3. 2 Schematic of planar asymmetric waveguide

### 3.1.3 Fabrication of thin films for optical waveguides

I-O waveguides are essentially inorganic or organic thin films that are transparent to the excitation wavelength and have uniform thickness, good adhesion to the substrate and low scattering-defects. Inorganic thin films may be deposited on glass or plastic substrates through evaporation, sputtering and epitaxial growth techniques. On the other hand, organic polymer films may be cast from solutions or colloids through a variety of simple techniques. In the horizontal-flow method, the substrate is flooded with the solution or colloid and then simply stood upright to drain the excess liquid. In doctor blading, a flat knife spreads the precursor evenly across the substrate. Precise control over the thickness of the film may be obtained through spin-coating and dip-coating methods. In the former, the substrate is coated with the solution and spun at hundreds to thousands of rotations per minute. The liquid, driven by a centrifugal force followed by a rapid and uniform evaporation of solvent, is evenly coated over the substrate. In dip-coating, the substrate is withdrawn vertically from the precursor solution. Here, drainage of the precursor solution is followed by evaporation of the solvent lead to uniform films of controlled thickness. In all of these methods, the thickness of the film may also be varied through the concentration or viscosity of the precursor solution.

### 3.1.4 Thin film characterisation with guided optical waves

Waveguiding is an alternative to characterisation techniques such as ellipsometry and interferometry for determining the optical parameters of thin films such as the refractive index (*n*), birefringence, absorption, propagation-loss and film thickness from a range of polymer films. Vibrational spectroscopic data from polymer waveguides may be collected through waveguide Raman spectroscopy. In this experiment a streak of light containing Rayleigh and Raman scatter excited by the propagating beam, was visible at the surface of the polymer waveguide. This line of light was focussed into and analysed by a conventional Raman spectrometer. Further waveguide Raman spectroscopic experiments confirmed the general applicability of this technique to thin polymer films and over the past three decades, thin film I-O waveguiding has becomes an established spectroscopic technique.

Waveguide Raman spectroscopy boasts an approximate $10^4$ enhancement in the S/N ratio, compared to conventional Raman experiments with the 90° scattering geometry. This is due in part to an increase in the path length of the excitation beam (and hence in the scattering volume) as well as the enormous power densities created by confining the laser beam in a microscopic film. Two valuable features of this technique include polarised WRS and depth profiling. The former combines the linear polarisation of the laser beam's electric field with the anisotropic scattering properties of molecules, to detect orientation in thin films. The latter selectively excites modes (and thus electric field profiles) to elicit Raman signal from different sections of the thin film. The field profile of a bound mode includes an evanescent field that penetrates the substrate and the cladding, the decay being especially pronounced for higher order modes. Thin films or monolayers, unable to support modes by themselves, may be adsorbed onto the waveguide surface and examined with this interfacial electromagnetic tail.

### 3.1.5 WRS characterisation of sol-gel derived thin films

Limitations of WRS include its requirement of a strictly homogenous, transparent waveguide with a specific *n* and thickness (d). Sol-gel derived inorganic films often intended for optical applications, fulfil these criteria. In the past decade, WRS has characterised a variety of these materials such as silicate-titanate[1], zirconia[2, 3], $GeO_2$-silicate and aluminosilicate[4] thin films. In addition to the chemical composition, the Raman spectra provide information on the phase and structure of thin films. Recent publications report WRS investigations of CdS nanocrystals in zirconia films[5], the phase microstructure in lead titanate[6] matrices, the formation of Si-O-Ge linkages[7] and the photosensitivity of $Cerium^{3+}$ doped aluminosilicate networks[8].

Many of the waveguiding studies have been restricted to the purely inorganic sol-gel derived glasses. In this Chapter, we describe the characterisation of hybrid silica-methacrylate thin films through waveguide Raman spectroscopy.

### 3.1.6 WRS characterisation of photoreactions in silica-methacrylate films

Our intent is to understand the photochemical and physical mechanisms in silicate-methacrylate thin films, especially in the context of the photolithography of optical devices. Studies described in chapter two of this thesis indicated that the photo-induced polymerisation of methacrylate components were associated with the concurrent growth and densification of the silicate host; events that are responsible for volume compaction and hence, the refractive index increase in the material.

Here, we describe an *in situ* WRS study of photo-processes in these films. The thin films are planar waveguides that support visible and infrared light. Thus they are suitable for WRS where the excitation beam is coupled into the thin film. The technique provides a non-destructive, autoscopic probe of structural changes that take place in the thin film as it is irradiated with UV light. The Raman data collected here complemented the spectroscopic studies of the previous chapter. In addition, this study in WRS is (to our knowledge) the first to monitor reactions in thin films in real time and hints at the potential of WRS as an *in situ* probe to light induced reactions in thin films.

## 3.2 EXPERIMENTAL

### 3.2.1 Overview

As schematised in Figure 3.2, the waveguide Raman spectroscopic experiment described here was designed to monitor *in situ*, the photoinduced polymerisation reactions within a silicate-methacrylate thin film waveguide. The visible Raman excitation wavelength, the 514.5 nm line of an $Ar^+$ laser beam, was coupled into the waveguide through a high refractive index prism. As the guided optical mode propagated, its path was evident by a streak of scattered light at the waveguide surface. This line containing both Raman and Rayleigh scatter was focussed into the entrance slits of a spectrometer. To initiate photo-polymerisation, the photosensitive film's surface was irradiated with UV light passed through an optical fibre bundle. The polymerisation process within the film could be monitored over time by simultaneously collecting waveguide Raman spectra.

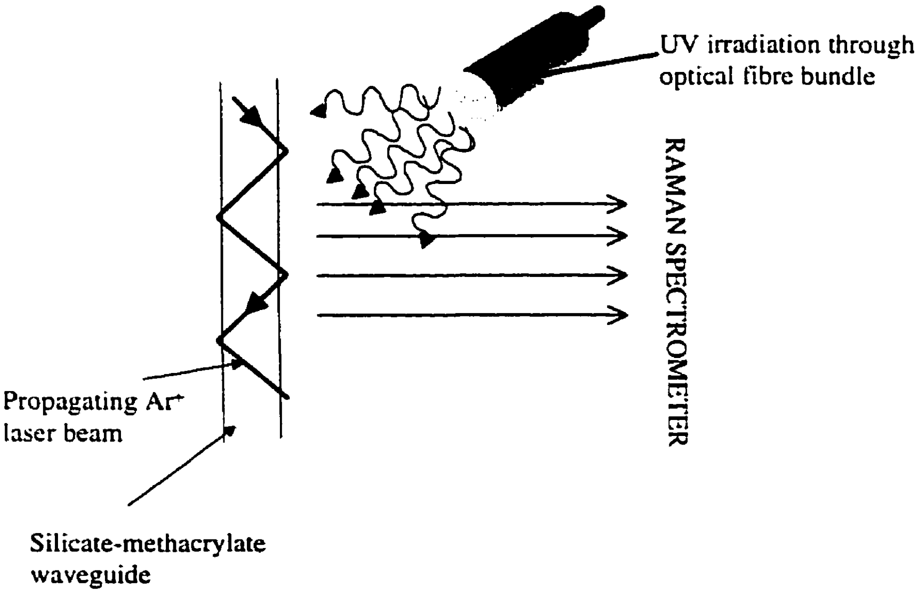

**Figure 3. 3** Schematic of *in situ* waveguide Raman spectroscopy experiment

### 3.2.2 Thin films of methacrylate-silicate

The procedure outlined in Section 2.2 of Chapter 2 was followed to fabricate thin methacrylate-silicate films. Films with d = 5.4 μm were spin-cast, then heated at 100 °C for 30 minutes. Samples that were smooth, homogenous and dust-free to the naked eye were chosen for the WRS experiment.

### 3.2.3 Waveguide Raman spectroscopy (WRS)

Waveguide Raman spectra of thin films were acquired with an Integrated Optics (IO) spectrometer[26] that combined a prism-coupled waveguide assembly with a fast multichannel Raman detection system. A schematic and photograph of the system are presented in Figures 3.5.

#### 3.2.3.1 Prism-coupling of excitation beam into the thin film

A LAFN-28 prism (P in Figure 3.4) with a 45°- 45°- 90° geometry and a 1.0 cm base (Precision Optical, Costa Mesa, CA, USA) was clamped onto the surface of a SAC-01 film (F in figure 3.5) with a height-adjustable horizontal, steel bar. The prism was truncated at the top for the application of pressure and at the base, for added strength. A stainless steel holder supported both the film and the prism. Under optimal coupling conditions, the interference pattern at the base of the prism (Newton fringe) would be a parallel set of lines.

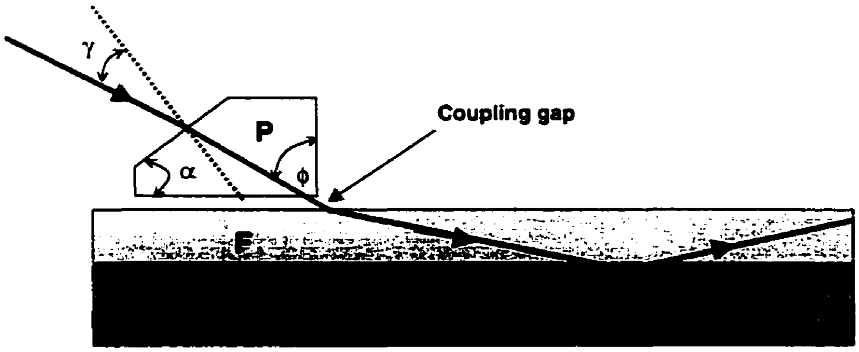

**Figure 3. 4** Prism-coupling laser beam into planar waveguide

Dust particles or random irregularities on the film create a small air gap (≈ 70-100 nm) between the prism base and the film's surface. When the laser beam ($Ar^+$) incident at the hypotenuse face suffers total internal reflection at the base of the prism, an evanescent tail decays through this coupling gap into the underlying film. When the wavevector ($k$) of this evanescent wave matches that of a mode supported by the waveguide, energy is transferred into the film, the mode is excited and guiding occurs. The high refractive index ($n$ = 1.78 at 514.5 nm) of the prism, allows a large range of $k$ values to be sampled with very small changes to the coupling angle, $\gamma$.

### 3.2.3.2 Optical Set-up

In this experimental design (see Figures 3.5 and 3.6), the waveguide in its holder was mounted on a 3-axis translation stage (TS) and remained fixed in space as the laser beam incident on the prism face, searched for in-coupling angles at which guidance occurred. The excitation source was the 514.5 nm emission line of an $Ar^+$ laser. The beam initially passed through a Pellin Broca pre-monochromator, collimating optics and a broadband polarisation rotator. It was then reflected by two 45° mirrors to the optical bench supporting the I-O spectrometer.

Here, as shown in Figure 3.5, it was guided through two pin-holes (P1 and P2) before entering a beam-steering assembly that consisted of three mirrors (M1, M2, M3) positioned at 90° angles to each other. A Glan-Thompson polarising cube (GT) was placed between the second and third mirrors and a half-wave retardation plate ($\lambda/2$) (Newport, model 05RP22-03), positioned after the plano-convex lens (L) that focussed the beam onto the hypotenuse face of the prism.

With the system properly aligned, the beam steering assembly could be rotated 360° about the axis (RA), which was collinear with the back edge of the prism. In this way,

the laser beam scanned the loci of angles about the coupling spot on the prism face, which remained stationary at least in the range of angles at which guiding occurred. The motion of the beam steering assembly was controlled by a motorised rotation stage, which in turn received commands from a P. C. The *y* and *x* axes of the translation stage were used to vary the position of the beam spot on the prism.

Once a mode was excited in the waveguide, a bright streak (initially orange due to fluorescence from impurities and green after 15 minutes of exposure to the 100 mW beam) was seen at the surface of the film. As the coupling angles were scanned, streaks belonging to the different modes in the waveguide could be resolved. In this case, streaks would flash on and off as the coupling angles were scanned. Modes were resolvable in films with $d \leq 5.4$ µm.

### 3.2.4 Raman spectroscopy

Streak intensities were maximized by iterative adjustments with the *x* and *z* axes of the stage. Raman spectra were collected from the mid-section of the streak (2 cm away from the coupling prism edge). This reduced interference from radiative modes and beam divergence[27]. Collection optics (C1 and C2) focussed this segment of the streak onto the spectrometer slits (2 cm x 300 µm). The Raman signal was maximised with real-time spectral acquisitions of the C-H stretching region while adjusting C1 and C2, mounted on translation stages, in the z and y directions.

The Raman spectrometer consisted of a Jobin Yvon THR640 monochromator, a liquid-$N_2$ cooled CCD detector. A holographic Supernotch™ filter (Kaiser Optical Systems, MI) was placed just before the monochromator slits for rejection of the Rayleigh line.

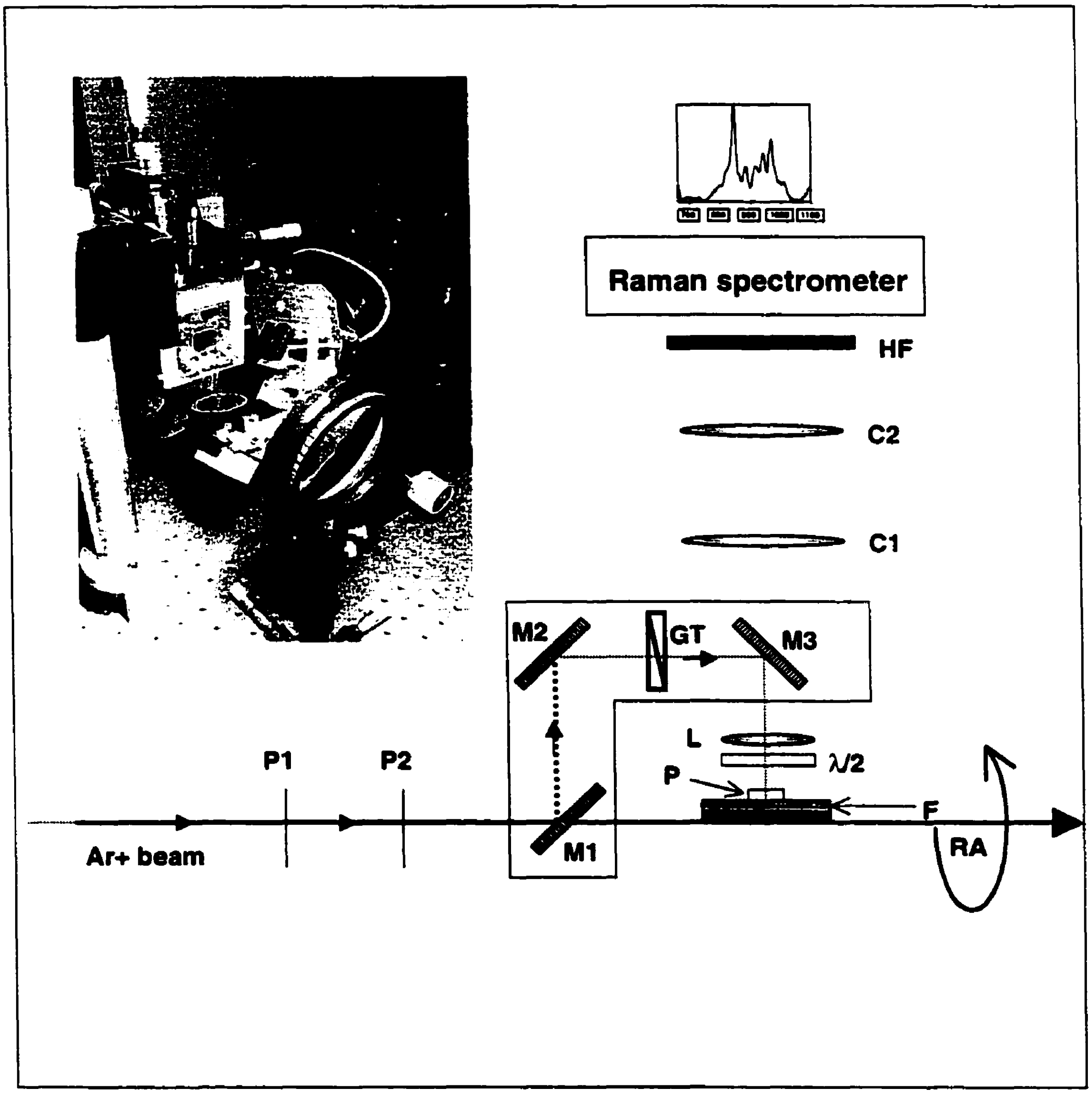

**Figure 3. 5** Schematic (and inset photograph showing first collection lens C1 and waveguide in holder) of waveguide Raman spectroscopic set-up

### 3.2.5 *In situ* study of UV induced reactions

Spectra were acquired from a 5.4 um thick silicate-methacrylate film, characteristic of films used for photolithography. In addition, the thicker film improved the S/N ratio of the experiment. Simulations calculate that the film supports 10 modes at 514.5 nm. Experimentally, this number of modes was difficult to resolve. The largest coupling angle relative to the prim-normal, corresponding to the fundamental mode, was used for Raman spectroscopy.

For *in situ* photolysis studies, the waveguide was irradiated with UV light from an optical fiber bundle (model 77403, Oriel, CT) that was connected to a 75 W Hg lamp ( Oriel, CT, USA). The power of 254 nm emission line of the lamp at the face of the film was measured to be 8 mW $cm^{-2}$.

### 3.2.6 Acquisition conditions

Spectra were acquired during irradiation of the silica-methacrylate thin film. Spectral windows that were 600 $cm^{-1}$ wide could be acquired at a time. Acquisition times ranged from 10-20 seconds for each window and 30 scans were averaged for each spectrum. Laser power was maintained at approximately 1.5 W (measured before the beam-steering optics) during acquisition. Raman spectra were acquired from the $TE_0$ mode excited in the waveguide. GRAMS/32 (version 4.01A, Galactic Industries, Salem. NH) software was used for spectral processing.

## 3.3 RESULTS AND DISCUSSION

**3.3.1 Waveguide Raman spectrum of silica-methacrylate waveguide** is presented in Figure 3.6. Assignments made from literature[28a-c] are listed in Table 3.1. The spectrum of the 5.4 μm thick film does not differ significantly from that of the bulk sol. Both are dominated by the vibrational bands of the propyl-methacrylate substituent. A noticeable difference is the ν(C-O) band belonging to methanol, which is present at 1032 $cm^{-1}$ in the bulk spectrum (not shown here). The band has negligible intensity in the spectrum of the non-irradiated film as much of the solvent evaporates from the composite during film-casting and the subsequent thermal treatment.

Complementary to the IR spectrum, the vibrational mode of the free carbonyl occurs at 1720 $cm^{-1}$. The absorption due to hydrogen-bonded carbonyl species is only faintly visible as a shoulder at the lower wavenumber side of the carbonyl stretch, which has an inherently weaker Raman activity. The weak band at 1600 $cm^{-1}$ is attributed to the carbonyl functional groups belonging to the methacrylic acid units complexed to zirconium centres.

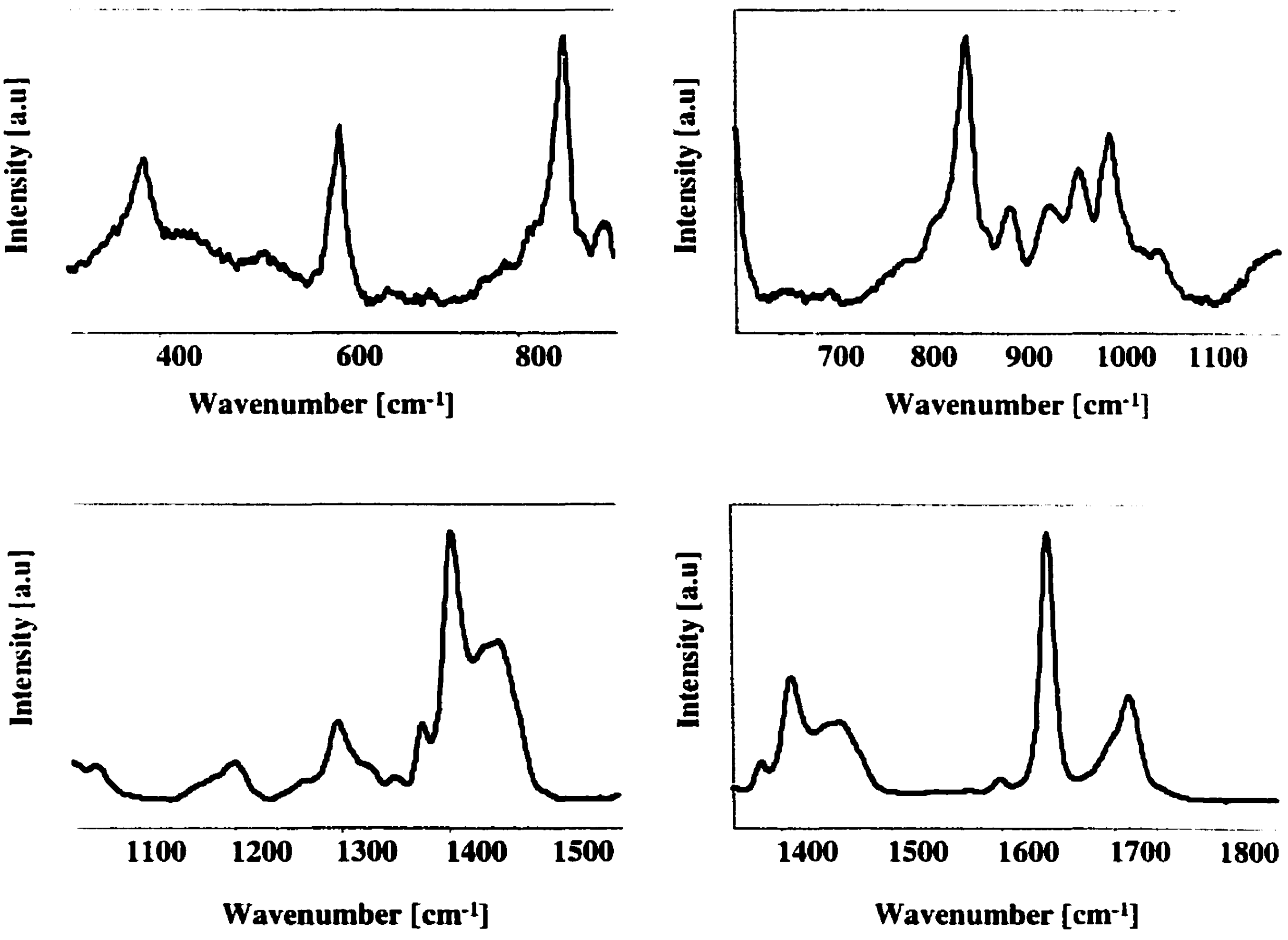

**Figure 3. 6** Waveguide Raman spectrum of silica-methacrylate film

**Table 3.1** Spectral assignments for silica-methacrylate waveguide

| **Wavenumber [cm$^{-1}$]** | **Assignment** |
|---|---|
| 818 (w, sh) | $\nu$(Si-O-C) |
| 854 (m) | $\delta$(=CH$_2$) o. o. p |
| 903 | |
| 952 (w) | $\nu$(Si-O-(H)) |
| 977 (m) | CH$_2$ wag of =CH$_2$ |
| 1012 (m) | Trans o. o. p C-H wag |
| 1066 (s) | $\nu_{as}$(Si-O-Si) |
| 1297 (m) | CH bend |
| 1348 | |
| 1381 (w, sh) | $\delta_s$CH$_3$ |
| 1408 (m) | $\delta$CH i. p of =CH$_2$ |
| 1450 (m) | $\delta_{as}$CH$_3$ |
| 1638 (s) | $\nu$(C=C) |
| 1712 (m) | $\nu$(C=O) (unsaturated ester) |
| 1738 (m, sh) | $\nu$(C=O) (saturated ester) |
| 2899 (s, sh) | $\nu_s$(CH$_3$) |
| 2929 (vs) | $\nu_s$(CH$_2$) of =CH$_2$ |
| 2958 (m, sh) | $\nu$as(CH) of Si-OCH$_3$ |
| 2996 (s) | $\nu_s$(CH) of =CH$_2$ |
| 3045 (w, sh) | |
| 3105 (w) | $\nu a_s$(CH$_2$) of =CH$_2$ |

### 3.3.2 *In situ* spectroscopy of UV initiated polymerisation

The free-radical polymerisation of methacrylate functionalities in the waveguide was initiated with UV light. The WR spectra following the reactions over time are presented in Figure 3.7.

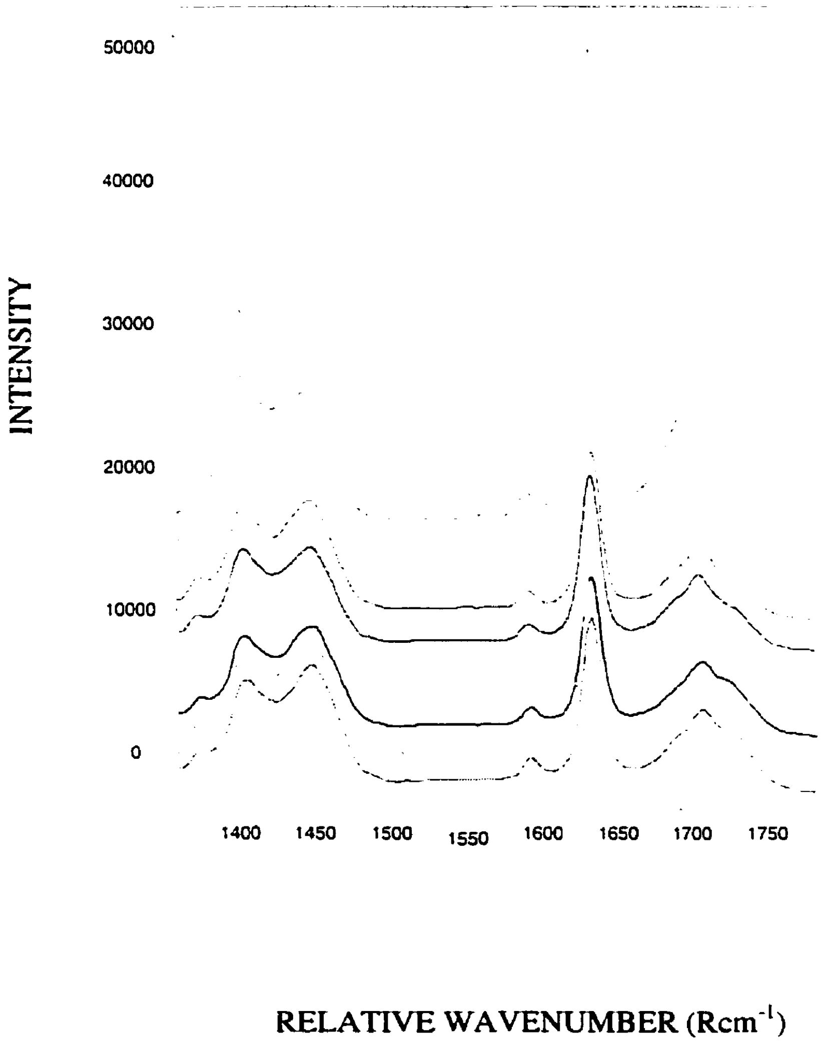

**Figure 3. 7** WR spectra monitoring UV-initiated reactions in silica-methacrylate waveguide, spectra are offset for clarity

This region of the spectrum is dominated by features characteristic of the polymerisation event. The ν(C=C) stretch (A) at 1638 cm$^{-1}$ and the carbonyl absorption ν(C=O) (B) centred at 1720 cm$^{-1}$ both decrease in intensity with increasing UV exposure time. Similar to the observations made in the infrared spectroscopic study in Section 2.3 of Chapter 2, the gradual broadening on the higher energy side of this band (C = 1738 cm$^{-1}$) indicated that a population of carbonyl groups emerged in a saturated oligomeric or polymeric environment, as conjugation with the vinyl groups is lost. The decreasing intensity of the weak band at 1600 cm$^{-1}$ (D) indicates that methacrylic acid moieties complexed to zirconium-oxo clusters also undergo free-radical polymerisation. Other features that indicate the saturation of the vinyl group, include the diminishing intensities of the C-H in-plane deformation mode at 1404 cm$^{-1}$ (E). At higher energies, the $CH_2$ wag and the *trans* out-of-plane wag of the vinyl group, the symmetric and asymmetric CH stretching modes of the methacrylate group at 2998 cm$^{-1}$ and 3100 cm$^{-1}$ respectively, and its symmetric $CH_2$ stretching mode at 2931 cm$^{-1}$ (Figure 3.8) all decreased in intensity, confirming that free-radical polymerisation of methacrylate substituents takes place in the waveguide.

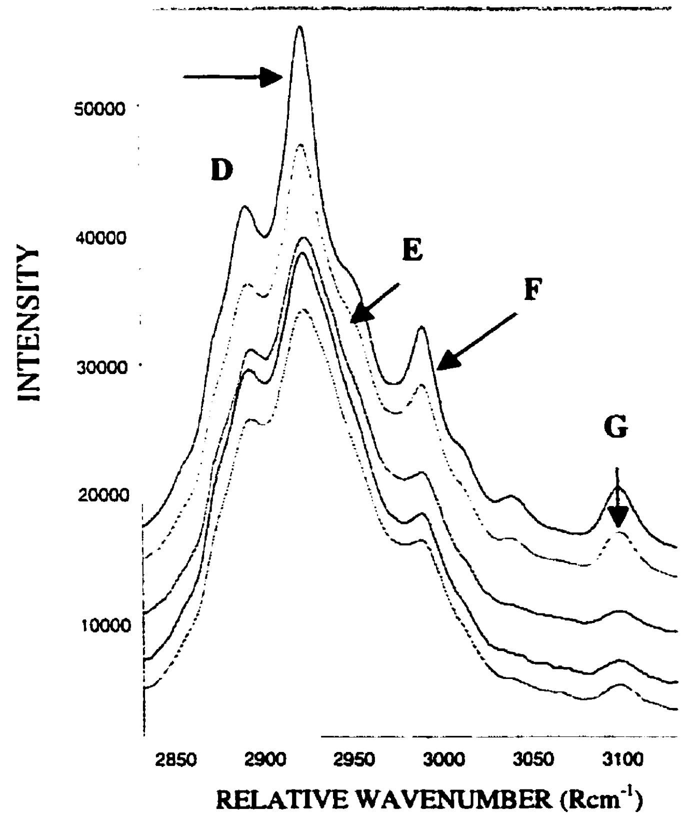

**Figure 3. 8** Details of the C-H region where (D) $\nu_s(CH_2)$ of $=CH_2$ at 2930 cm$^{-1}$, (E) $\nu_{as}(CH_3)$ of Si-$OCH_3$ at 2968 cm$^{-1}$, (F) $\nu_s(CH)$ and (G) $\nu_{as}(CH)$ of of $=CH_2$ at 2998 cm$^{-1}$ and 3100 cm$^{-1}$

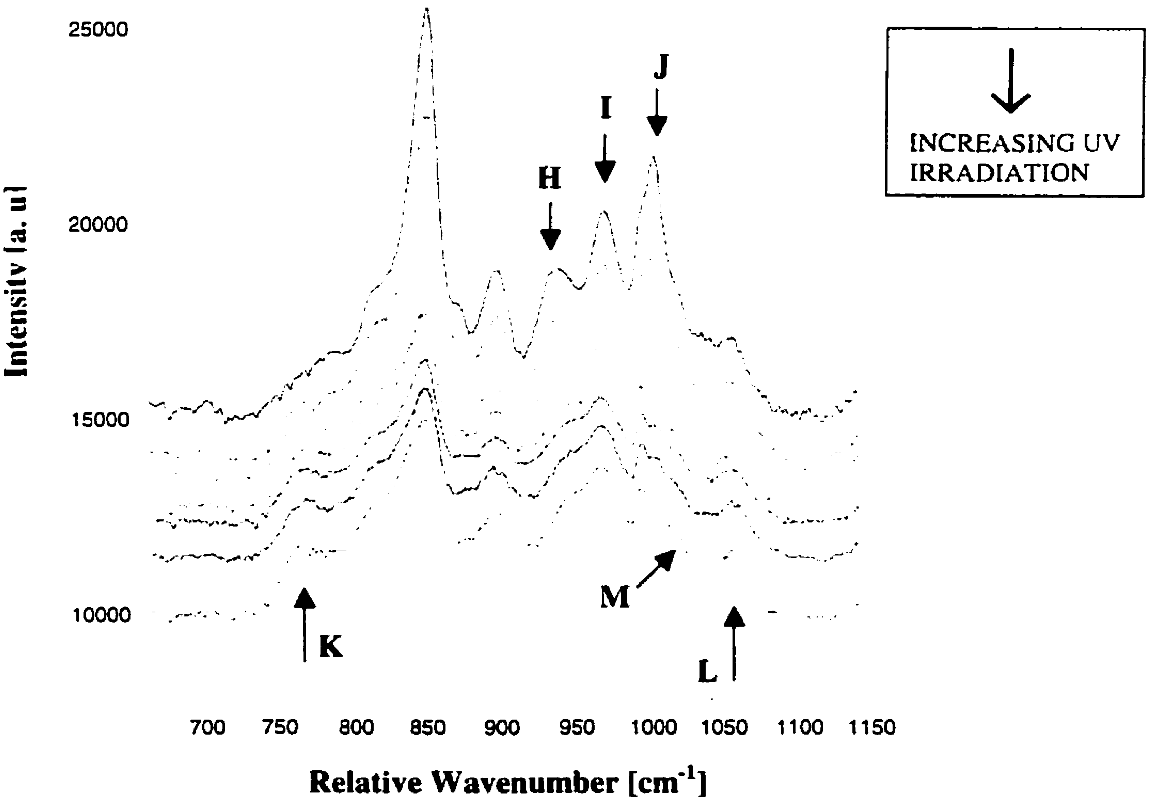

**Figure 3. 9.** Evolution of the waveguide Raman spectra of an HSGG thin film upon UV irradiation where (H) ν(Si-O(H)) at 952 cm$^{-1}$, (I) $CH_2$ wag and (J) trans o.o.p. C-H wag of =$CH_2$ at 978 cm$^{-1}$ and 1010 cm$^{-1}$ respectively, (K) $\nu_s$(Si-O-Si) at 796 cm$^{-1}$, (L) $\nu_{as}$(Si-O-Si) at 1066 cm$^{-1}$ and (M) is ν(C-O) of $CH_3OH$.

The Raman data support our contention[9] that polymerisation of the organic component is not an insulated event in the composite. The reduction in C-C bond distances (Van der Waals distances on the order of 3-4 Å reduce to about 1.54 Å C-C) during the linking of methacrylate groups brings Si centres closer together. Residual Si-OH and Si-$OCH_3$ can now react to form additional Si-O-Si bonds. The decreasing intensity in the shoulder at 2962 cm$^{-1}$ (the ν($CH_3$) band of the Si-$OCH_3$ group) is shown in Figure 3.8. This is accompanied by the depletion of Si-OH groups (Figure 3.9). The growth of a slight shoulder at 1030 cm$^{-1}$ is due to the ν(C-O) mode of $CH_3OH$, the by-product of the condensation reactions. Silicon-oxo bond formation in the network is indicated by the growth of bands at 795 and 1070 cm$^{-1}$, which are assigned to the symmetric and asymmetric stretches of Si-O-Si bonds.

Direct photolysis of the SiO-H bond cannot occur under our UV conditions, because bond cleavage would require at least 8 eV photons. These data complement our conclusions from the previous spectroscopic studies[8, 9] that photoinduced polymerisation activates polycondensation reactions between reactive Si-$OCH_3$ and Si-OH groups and growth in the silicate matrix. Collectively[8,9] our experiments confirm a facile photodensification ("glass photosensitivity") response of the silicate-methacrylate composite. Increases in refractive indices suitable for integrated optics device fabrication[8, 9] in thin films are achieved with lower energy 3-5 eV photon energies than must be used to define devices in glass fibre or high temperature process silica glass on silicon[12,13]. .

## 3.4 CONCLUSIONS

A WRS study of photoreactions in silica-acrylate planar waveguide was described. The Raman data collected here complement the studies described in Chapter 2 and reinforce our notion that poly-condensation reactions in the silica matrix are initiated by the organic free-radical polymerisation process. In addition, Raman bands provide direct evidence siloxane bond formation and the release of methanol from condensation reactions in the thin film. This *in situ* waveguide Raman spectroscopy has provided supplementary evidence that photo-inscription of optical devices in photosensitive methacrylate hybrid sol-gel films involves changes in the refractive index of the irradiated region that result from collateral densification caused by a photo-sintering effect in the film. Indeed, formation of covalent C-C bonds by polymerisation of olefinic moieties causes the glass network to draw closer together and promotes further polycondensation reactions in the medium.

---

1. N. Goutev, Zh. S. Nickolov, J. J. Ramsden, *J. Raman Spectrosc.* **27**, 897 (1996).
2. C. Urlacher, J. Dumas, J. Serughetti, J. Mugnier and M. Munoz, *J. Sol-Gel Sci. Technol.* **8**, 999 (1997).
3. C. Urlacher, C. Marco De Lucas, J. Mugnier, *Synth. Met.* **90**, 190 (1997).
4. J. M. Nedelec, M. Benatsou, C. Duverger, B. Capoen, M. Bouazaoui, S. Turrell, *Asian J. Phys.* **7**, 357 (1998).
5. I. Mikulskas, E. Bernstein, J. C. Plenet C. Bovier, R. Tomasiunas, V. Grivickas, J. V. Vaitkus, J. Mugnier and J. Dumas, *Mater. Sci. Eng. B*, **B69-70**, 418 (2000).
6. C. Urlacher, O. Marty, J. C. Plenet, J. Serughetti, J. Mugnier. *Thin Solid Films*, **349 (1,2)**, 61 (1999).
7. D-G Chen, B. G. Potter, J. H. Simmons, *J. Non-Cryst. Solids*, **178**, 135 (1994).

. J. M. Nedelec, J. Grimblot, S. Turrell and M. Bouazaoui. *J. Phys. Chem. B*, **104**, 926 (2000).

9. J. Baldwin, N. Schuler, I. S. Butler and M. P. Andrews, *Langmuir*, **12**, 6389 (1996).
10. J. T. Ives, W. M. Reichert, *J. Appl. Poly. Sci.* **36**, 429 (1988).
11. a) A. L. Smith, *Spectrochim. Acta.* **16**. 87. (1960), b) X. Li and T. A. J. King, *J. Non.Cryst. Sol.* **204**, 235. (1996), c) J. L. Lippert, S. B. Melpolder and L. M. Kelts, *J. Non-Cryst. Solids*, **104**, 139 (1988), d) T, W. Zerda and G. J. Hoang, G, *J. Non-Cryst. Solids*. **109**, 9 (1989), e) A. L. Smith. *Analysis of Silicones*. (Wiley, New York, 1974).
12. H. Imai, H. Hiroshima, K. Awazu and H. Onuki, *J. Ceram.Soc. Jpn.* **102**. 1094 (1994).
13. H. Himai, H. Hirashima, K. Awazu and H. Onuki, *Proc. SPIE.* **2288**. 71 (1994).

# 4. SELF-FOCUSING OF LIGHT IN HYBRID SILICA-METHACRYLATE NANOCOMPOSITES

## 4.1 Introduction

Diffraction of light is a naturally occurring event. As schematised in Figure 4.1a, a beam of light diverges or broadens in space as it propagates along a straight line. The opposite may occur in a medium that can undergo an intensity-dependent and spatially localised increase in its refractive index (Δn) in the presence of an optical field. In such materials, a laser beam is able to create a positive lens and continuously focus itself along the propagation axis. As the beam self-focuses in this manner, its diameter actually decreases with propagation distance (Figure 4.1b) and it is able to traverse the medium without suffering diffraction.

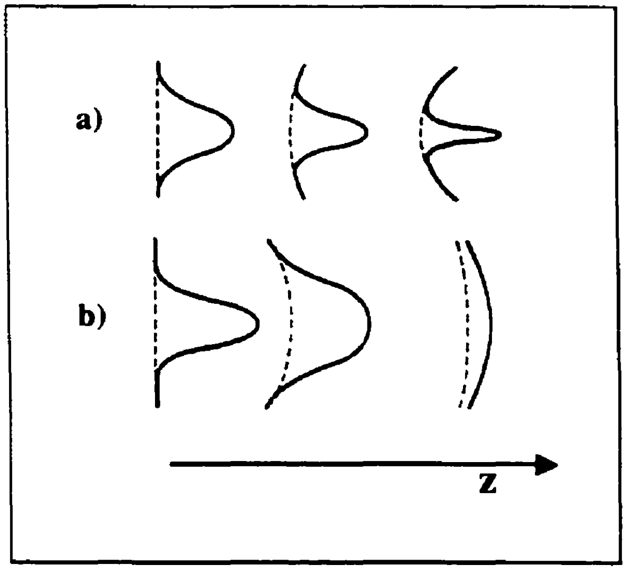

**Figure 4. 1 a)** self-focusing and **b)** diffraction of a laser beam along its propagation axis, $z$.

The self-focusing of a laser beam was first observed in a Kerr medium, where Δn originates from the nonlinear optical (NLO) polarisation response of the material to the intense electric field provided by a laser beam. Self-focusing was initially assigned to the group of classical nonlinear optical (NLO) phenomena such as second and third harmonic generation, sum and difference frequency generation and optical parametric oscillation, all of which depend on higher order, susceptibility coefficients that contribute to the NLO polarisation response of a medium. In this case, the Δn underlying self-focusing is strictly electronic in origin and can qualitatively be attributed to polarisation – or distortion - of electron density in the medium.

In this Chapter, we describe the self-focusing of a continuous wave (c.w.), visible laser beam through the change in refractive index ($\Delta n$) due to a photochemical reaction. In Chapters 2 and 3, we described the photo-responses of sol-gel derived silica-methacrylate films where photoinitiated free radical reactions lead to spatially localised, changes in the refractive index of the medium. Here, we demonstrate how these reactions can be initiated by the guided-optical modes of a 514.5 nm laser beam propagating in a silica-methacrylate planar waveguide. As it travels, the beam triggers free-radical polymerisation of methacrylate substituents distributed in the composite. Polymerisation is accompanied by a spatially localised $\Delta n$ in its propagation path and self-focuses in the nascent reaction medium.

Our demonstration of self-focusing through localised photo-polymerisation gives a chemical perspective to the study of nonlinear light-matter interactions, which are dominated by "physical" mechanisms such as electronic polarisation and resonant absorption. At the same time, the research presented here introduces an interesting method to conduct polymerisation reactions. Photoinitiated free-radical polymerisation itself is a well-established research and technological field. However, the ability to carry out polymerisation under the intense and continuously changing optical field of a self-focusing laser beam presents an unique opportunity to probe the nature of polymer growth in a highly nonlinear optical environment.

### 4.1.1 Dispersion and diffraction of light

A pulse or a beam of light will broaden as it travels in a transparent medium. This can be understood as follows: an optical pulse is composed of several frequency components that initially have a phase difference of zero, whereas a quasi-monochromatic laser beam may be represented by a coherent bundle of rays or a superposition of plane waves with the same wavenumber $k_0 = \frac{n\omega}{c}$. Each pulse component has a characteristic velocity and acquires a different phase as it propagates. This leads to dispersion in the wavelengths (chromatic dispersion). The pulse loses intensity and broadens in time. In a beam, each ray or plane wave travels at a slightly different angle (and a different phase velocity) to the propagation axis. Phase differences that arise between plane waves, cause beam broadening - diffraction - with distance.

### 4.1.2 Dispersion compensation through nonlinear optical responses

Both dispersion and diffraction can be undesirable in photonic applications. For example, in the optical-communications networks, which delivers information in the form of near infrared (NIR) pulses at billions (and in research labs trillions[1]) of binary digits per second, optical dispersion in a glass fibre severely distorts the transmitted signal. Much effort has gone into the development of zero dispersion fibre (ZDF) and dispersion compensation devices to overcome this effect.

Dispersion can be avoided in materials that are driven into a nonlinear optical (NLO) regime. In such media, electromagnetic waves induce a local and intensity dependent change in the refractive index. In turn, $\Delta n$ alters the propagation conditions for the optical waves. In 1973, Hasegawa and Tappert[2] recognised that the nonlinear increase in the refractive index of silica under intense laser light could compensate for accumulated phase differences in dispersing pulses. When this process, known as self-phase modulation, counterbalanced dispersion in a silica fibre, optical pulses could propagate over several hundreds of kilometres without perturbation. These robust wavepackets that travel without any changes to their initial profiles are called temporal solitons. They were first demonstrated by Molenhauer and coworkers[3]. Solitons are now actively used for data transmission[4] over transoceanic distances[5], recently at terabit rates[1].

#### 4.1.2.1 Intensity dependent refractive index changes – the Kerr effect

Self-induced phase modulation in glass fibre occurs through the (nonlinear) optical Kerr effect. Under intense electromagnetic radiation at nonresonant frequencies, the refractive index (*n*) of most dielectric materials increases according to:

$$n = n_o + n_2 I(\vec{r}, t) \qquad [4.1]$$

where $n_o$ is the linear refractive index (at weak intensity), $n_2$, the nonlinear refraction coefficient and $I(\vec{r}, t)$, the intensity of the optical field. $n_2$ is directly proportional to the material's third-order nonlinear susceptibility to polarisation, $\chi^{(3)}$. The Kerr effect, originating from the distortion of electron density, induces a refractive index change on the order of $10^{-16}$ at a laser intensity of 1 W-cm$^{-2}$. The delay between irradiation and $\Delta n$, *i. e.* the response time of the medium, is effectively zero ($10^{-15}$ s)[6].

The positive $\Delta n$ induced in a glass fibre, shifts the phase and the frequency of the various components of a pulse. When these changes cancel exactly those due to dispersion, the pulse propagates as a temporal soliton.

### 4.1.3 Diffraction compensation through nonlinear optical effects in the spatial domain

The previous Sections described how the NLO response of a material and the induced $\Delta n$ could prevent the divergence of an optical pulse over time. The research presented in this Chapter concerns NLO phenomena that oppose the spatial divergence of a "pulse in space"[7], *i.e.* a narrow beam of light.

The diffraction of a laser beam is proportional to $\frac{1}{k_0^2 a^2}$ where a is the beam radius and $k_0$, the free space wavenumber. In a Kerr medium, a process known as self-lensing or self-focusing of the beam can cancel this divergence. Consider a laser beam with a Gaussian beam profile

$$\mathcal{E}(x, y, t) = \mathcal{E}_0 e^{\frac{-(x^2+y^2)}{a^2}} \qquad [4.2]$$

propagating along the *z* axis in a Kerr medium. As mentioned in Section 4.1.2.1, the Kerr response described by equation 4.1 is virtually instantaneous. It is also critically sensitive to the intensity profile of the laser beam and $\Delta n = n_2I$ varies strictly according to the shape of the input beam. Thus, a Gaussian beam induces a $\Delta n$ profile that mirrors its own non-uniform shape, *i.e.* a maximum at the axial or the most intense region, with a radially symmetric decay from this point. Consequently, the central part of the beam experiences a greater n and travels with a decreased phase velocity relative to its edges. The wavefront of the beam that is initially equiphase, now develops depressions in the axial region where the intensity is greatest. This is similar to the distortions of a beam of light caused by a positive gradient index (GRIN) lens. It follows by Huygen's principle[8] that the rays at the beam edges move towards the axial region, causing the intensity there to further increase. If the induced $\Delta n$ lens is sufficient to counteract diffraction, the beam appears to self-focus along z. The continuous action between self-focusing and refractive index change creates a channel waveguide, which guides the beam across the medium without suffering diffraction. As indicated earlier, Figure 4.1 describes the effects of self-focusing (a) and diffraction (b) on a beam of light.

### 4.1.4 Theoretical treatment of self-focusing

Self-focusing of a laser beam in a Kerr medium may be described mathematically by both geometric and wave optics. Both are briefly described in the following Sections.

#### 4.1.4.1 Geometric optics

The ray-optics approach to self-focusing[9] considers Snell's law and the maximum diffraction angle of rays in a beam. The model assumes a flat-top intensity distribution of the laser beam, which induces a uniform, rectangular $\Delta n$ (Figure 4.2) profile resembling a channel waveguide in the medium.

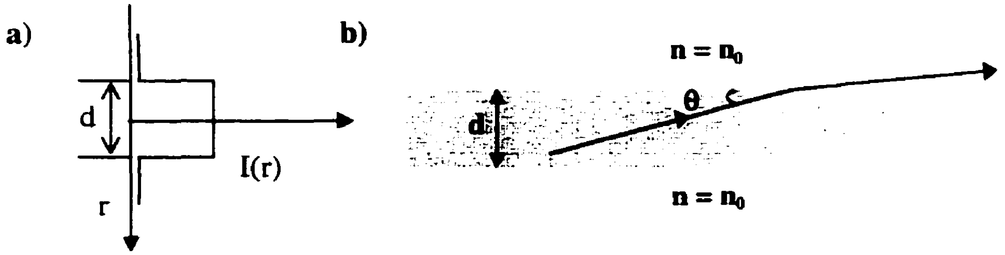

**Figure 4. 2** Rectangular channel waveguide **(b)** induced by a beam with a flat-top intensity profile **(a).**

A ray belonging to the propagating beam undergoes total internal reflection at $\theta < \theta_c$, the critical angle:

$$\cos\theta_c = \frac{n_0}{n_0 + \Delta n} \qquad [4.3]$$

Assuming $\Delta n << n$ then:

$$\theta_c = \left(\frac{2\Delta n}{n_0}\right)^{1/2} \qquad [4.4]$$

The maximum diffraction angle of rays contained in the beam of diameter a, is:

$$\theta_a = \frac{0.61\lambda}{n_0 a} \qquad [4.5]$$

If $\Delta n$ is such that $\theta_c = \theta_a$ then,

$$\Delta n' = \tfrac{1}{2} n_0 (0.61\lambda / a n_0)^2 \qquad [4.6]$$

If the photoinduced $\Delta n = \Delta n^*$ then the photoinduced refractive index change exactly counteracts the diffraction of the beam. This is referred to as the self-trapped condition, where all the rays in the beam, including the ones with the maximum diffraction angle $\theta_a$, undergo total internal reflection at both the upper and lower interfaces of the waveguide shown in Figure 4.2. Such rays propagate without diffraction in a self-inscribed waveguide. Self-focusing occurs for $\Delta n > \Delta n^*$. The critical beam power $P_{cr}$, at which this takes place may be calculated by substituting equation 4.1 into equation 4.6 to give:

$$a = 0.61\lambda(2n_0n_2I(\vec{r}))^{-1/2} \qquad [4.7]$$

$P_{cr}$ may now be determined from the diameter of the beam a:

$$P_{cr} = \frac{\pi}{4}a^2I = \frac{\pi(0.61)^2\lambda^2}{8n_0n_2} \qquad [4.8]$$

The self-trapping condition described by equation 4.6 occurs at $P = P_{cr}$. When $P > P_{cr}$, the photoinduced $\Delta n > \Delta n^*$ and self-focusing of the beam occurs. When $P < P_{cr}$, self-focusing of the propagating beam does not take place.

#### 4.1.4.2. Wave optics

Although the geometric optics approximation provides a qualitative description of self-focusing, it ceases to be valid when the beam-diameter approaches multiples of its wavelength (*i.e.* microns) and a more accurate description of self-focusing is obtained through wave optics[10]. In a NLO medium that is isotropic and has a refractive index according to equation 4.1, the propagation of an electromagnetic wave may be described by:

$$\nabla^2\vec{E}-\left(\frac{\partial^2}{c^2\partial t^2}\right)\left[(n_0+\Delta n)^2\vec{E}\right]=0 \qquad [4.9]$$

where $\Delta n$ and $n_0$ are real and positive and $\Delta n << 1$. The laser beam is linearly polarised with a frequency ω and propagates along z according to:

$$\vec{E}=\mathcal{E}\left(\vec{r},z,\xi\right)e^{i(kz-\omega t)} \qquad [4.10]$$

where $e^{i(kz-\omega t)}$ is the complex notation representing the time harmonic field (the propagating component of the wave) and $\mathcal{E}(r,z,\xi)$ is the slowly varying electric field envelope amplitude. The time dependence has been eliminated by introducing $\xi$, a reduced time variable that is defined as $\xi=t-\frac{z}{v_g}$ where $v_g$ is the group velocity. The Gaussian beam is assumed to be radially symmetric, with $\vec{r}$ being the radial coordinate. Substituting [4.10], equation [4.9] may now be rewritten as a first order partial differential equation that is formally equivalent to the Schrödinger equation:

$$ik_0n_0\frac{\partial\mathcal{E}}{\partial z}+\tfrac{1}{2}\nabla_\perp^2\mathcal{E}+k_0^2\frac{\Delta n}{n_0}\mathcal{E}=0 \qquad [4.11]$$

Note that this equation contains the opposing effects, diffraction of the beam in both the x and y directions (perpendicular to the propagation axis) represented by $\nabla_\perp^2=\frac{\partial^2}{\partial x^2}+\frac{\partial^2}{\partial y^2}$, and the nonlinear $\Delta n$ term that varies with intensity according to equation 4.1. The absolute amplitude A and the phase $\phi$ of the optical field are functions of r, z and $\xi$ and $\mathcal{E}$ may also be written as:

$$\mathcal{E}=Ae^{i\phi} \qquad [4.12]$$

Equation can now be written in terms of $A$ and $\phi$:

$$\frac{\partial}{\partial z}\phi+\frac{1}{2k}(\nabla_{\perp}\phi)^2-\frac{k}{2}\left(\frac{\nabla_{\perp}^2 A}{k^2 A}+2\frac{\Delta n}{n_0}\right)=0 \quad [4.13]$$

In Section 4.1.3, self-lensing of the laser beam was qualitatively described as a gradual distortion of the propagating beam wavefront. The relationship between the wavefront, represented by the phase function φ (r, z, ξ), the diffraction $\frac{\nabla_{\perp}^2 A}{k^2 A}$ and the self-focusing of the beam due to a photoinduced refractive index change $\frac{\Delta n}{n_0}$ is expressed by equation [4.13].

### 4.1.5 Physical description of self-focusing in Kerr media

In physical terms, equation 4.11 describes the reciprocal action between self-focusing and $\Delta n$, which creates a circular waveguide in the material: a localised region with a refractive index gradient where n is maximal at the axis and decays radially from this point. The beam is supported as an optical mode in its self-inscribed, channel waveguide and moves through the medium without suffering diffraction.

The self-focusing of laser light in Kerr media, predicted by R. Y. Chiao and co-workers[10], has been demonstrated in $CS_2$[11] and glass planar waveguides[12]. The propagation of optical modes in planar waveguides was described in Chapter 3. Briefly, in the planar or slab configuration, light propagates that along the z axis is confined by interfaces in the x direction. The beam is free to diffract (Figure 4.3a) and thus self-focus (Figure 4.3b) only in the *y* direction.

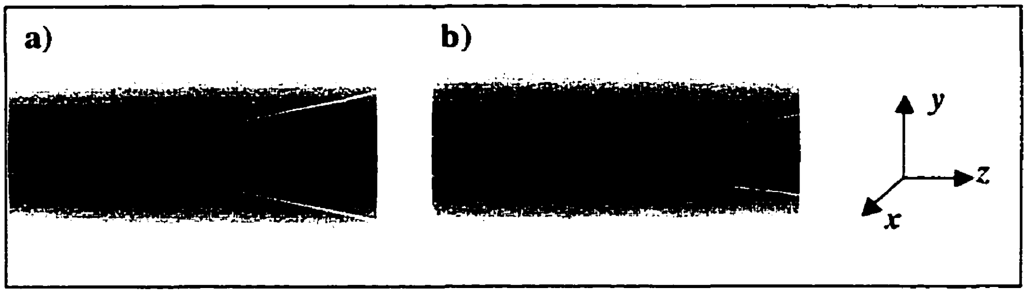

**Figure 4. 3a)** diffraction and **b)** self-focusing of a laser beam in a planar waveguide

Attempts to observe self-focusing in both the $x$ and $y$ directions, for example of a circular beam in bulk Kerr media, have always failed[7]. As the Kerr effect is highly localised in time and space, even slight fluctuations in the circular beam's intensity or shape may disrupt the self-focusing process. Furthermore, as seen in equation 4.1, $\Delta n$ in a Kerr medium may increase indefinitely with beam intensity. Initial self-focusing of the laser beam decreases its beam-width, thereby increasing its intensity. In turn, this induces an even greater $\Delta n$ and further self-focusing, which could lead to anomalously large intensities in the medium. This may lead to catastrophic self-focusing[8], where the beam breaks up into several separate filaments. Alternatively, the unregulated cycle is interrupted by some other nonlinear optical effect such as stimulated Raman, Brillouin scattering, two photon absorption or even permanent damage to the material[13].

### 4.1.6 Diverse photophysical mechanisms leading to laser self-focusing

Self-focusing is not restricted to Kerr media and may be observed in a wide range of materials. This is because photo-mechanisms that have remarkably diverse physical origins may all produce spatially localised, intensity-sensitive $\Delta n$ changes in materials and allow the self-focusing of light[14]. Indeed, the Kerr-effect's contribution to $\Delta n$ is not exclusively electronic in origin and may arise from electrostriction - optical field induced density changes - or molecular orientation where anisotropic molecules are aligned through their interaction with linearly polarised light[6].

### 4.1.6.1 Photomechanisms with saturable photo-responses ($\Delta n_{sat}$)

$\Delta n$ may also be induced at optical frequencies that are close to narrow absorption bands in the medium. At a transition frequency, the population-difference ($\Delta\rho$) created between the ground and excited states is directly proportional to the resonant susceptibility ($\chi_r$) and thus $\Delta n$. Resonant excitation at high laser intensities creates a significant population redistribution in the system, with $\Delta\rho$ monotonically decreasing at increasing beam intensities. This in-built saturability of the mechanism is reflected in the refractive index, which in sharp contrast to the Kerr effect, maximises ($\Delta n_{max}$) at high beam powers. $\Delta n$ values in this case are larger than those due to the Kerr effect and are on the order of $10^{-10}$ at an intensity of 1 W-cm$^{-2}$, with a response time of $10^{-8}$ seconds.

Although self-focusing of light does occur at resonance frequencies, it is arrested at high beam intensities once $\Delta n_{max}$ is reached. Above this threshold intensity, the beam continues to propagate without diffraction in its self-induced channel waveguide but cannot self-focus further. Consequently, the catastrophic self-focusing effects seen in Kerr media are avoided here and the inbuilt saturability of the mechanism protects the material from slight fluctuations in the beam parameters. The successful self-focusing of a circular beam (in both $x$ and $y$ directions) in a bulk medium was first observed in a resonant medium. Two-dimensional self-focusing of a continuous wave (c.w.) dye-laser beam with a frequency within Doppler widths to the alkali metal's D line transition, was first reported by Bjorkholm and Ashkin in Na atomic vapour in 1974[15]. The green beam self-focussed in both $x$ and $y$ directions and confined to a narrow cylindrical region, propagated across the medium without broadening.

Semiconductors can also support self-focusing[16]. Here, the self-focusing laser beam, which falls into the absorption band of the semiconductor, pumps electrons into the conduction band leaving holes in the valence band. The steady-state population distribution of the electrons and the holes is determined by the balance between optical pumping and electron-hole recombination. Population redistribution causes a change in the absorption spectrum of the material, which in turn is related to $\Delta n$.

An interesting example of saturable $\Delta n$ is found in poly(diacetylene para-toluene sulphonate) (PTS), which has the largest Kerr nonlinearity ($\Delta n = 10^{-3}$) measured in any material[17]. Efficient self-focusing of NIR light (1600 nm) has been observed in PTS. Although $\Delta n$ arises from the Kerr effect in this material, its saturability at high powers is due to a fifth order nonlinearity, which contributes a negative $\Delta n$ ($= -10^{-4}$).

### 4.1.6.2 Self-focusing in photorefractive crystals (PRCs)

The swift revival of interest in self-focusing phenomena is undoubtedly due to the sequence of careful studies on laser interactions in photorefractive crystal (PRCs)[14] over the past seven years. PRCs are non-centrosymmetric, inorganic crystals, conventionally used as recording media for volume holography, for optical data storage applications. When such a crystal is illuminated, the charge carriers that are released diffuse over a short distance (micrometer scale) in the crystal, leaving behind fixed, opposite charges. The resulting internal space charge field ($E_{sc}$), induces a $\Delta n$ in the material through the Pockel's electrooptic effect, which relates the two parameters through the second order nonlinearity of the crystal:

$$\Delta n(x) = -\tfrac{1}{2} n^3 r_{eff} E_{sc}(x) \qquad [4.\ 14]$$

where $n$ is the average refractive index of the material. The effective electro-optic coefficient $r_{eff}$, consists of different electro-optic tensor elements that may be related to the second order susceptibility $\chi^{(2)}$ of the medium.

Self-focusing in PRCs was proposed by Segev and co-workers in 1992[18] and was first identified in $Bi_{12}TiO_{20}$ planar waveguides by Iturbe-Castillo and colleagues in 1994[19]. Reports of two-dimensional self-focusing of visible laser beams in strontium barium niobate (SBN) soon followed[20]. PRCs also have a $\Delta n_{max}$, the saturability of this mechanism being due to the finite number of charge carriers present in the matrix. The response time in these systems ranges from milliseconds to seconds[20], several orders of magnitude larger than the response time of the previously discussed NLO mechanisms.

#### 4.1.6.2.1. Self-focusing in PRCs as a precursor to spatial solitons

Self-focusing in photorefractive media has been examined largely in the context of solitons, the spatial analogues of temporal solitons. The latter were described in

Section 4.1.2 as optical pulses that travel in Kerr media without suffering chromatic dispersion. Consequently, the pulses retain their temporal profiles over long propagation distances. Spatial solitons are solitary waves that propagate without changing shape in NLO media such as PRCs. From equation 4.13, spatial solitons form when diffraction is precisely balanced by the effects of self-focusing, *i.e.*:

$$2\frac{\Delta n}{n_0}+\frac{\nabla_\perp^2 A}{k^2 A}=0 \qquad [4.\ 15]$$

Under this condition, the beam retains both its phase $\left(\left(\partial\phi/\partial z=0\right)\right)$ and its amplitude $(\partial A/\partial z=0)$ and propagates across the medium without altering its transverse spatial profile.

There is also great interest in the interactions[7, 14] (collisions, repulsion and attraction) between such solitary waves, which have been likened to particle interactions. PRCs have proven to be ideal media in which to characterise the interactions of solitons with three-dimensional trajectories. Both "attractive" and "repulsive" forces have been identified between two solitons, and may be explained by considering their overlapping optical fields. For example the overlap between the fields of two coherent solitons that are in phase, always produces an increase in the electromagnetic field intensity, increasing n. Thus, the two solitons "gravitate" towards this region of relatively greater n and appear to be attracted to each other. On the other hand, if the beams are out of phase by π, their fields interfere destructively and the solitons seem to repel each other. Coherent interactions may only take place, if the phase difference between the two solitons remains constant over a period longer than the response time of the medium. This is often not the case in PRCs, where the phase changes of the light beams are much more rapid than the response times of the medium. The medium thus responds to a time-averaged intensity of the solitons. Here, overlapping optical fields always produce an increase in intensity and Δn and the "incoherent" solitons always seem to attract one another. In PRCs, solitons launched parallel to each other have been shown to fuse if their collision angle is less than their critical angle for total internal reflection (TIR). At angles that are larger than the

TIR, the solitons pass through each other unperturbed, both conserving their initial propagation velocities. It has also been predicted that a pair of solitons could produce a third one during collision (fission) or completely annihilate each other. Recently, the spiralling of two solitons about each other in a delicate interplay between centrifugal rotational and attractive forces was observed and raising questions whether the interacting solitons conserve angular momentum[21].

### 4.1.7 Common features of self-focusing

The self-focusing event is remarkably indifferent to the molecular mechanisms that give rise to it. As described in the previous Sections, this nonlinear behaviour of light may occur in materials with vastly different photophysical mechanisms and has been observed in materials as varied as liquid $CS_2$, glass, polymers, atomic vapours and semiconductors. In these cases, self-focusing occurs through "classical" nonlinear optical responses such as the Kerr effect and resonance excitation, where the photoinduced $\Delta n$ is due to a nonlinear polarisation response of the material. The universality[14] of self-focusing phenomena truly became evident during the studies conducted with PRCs, which respond in a significantly different manner to light. Indeed even within this class of materials, $\Delta n$ *is* induced through a variety of mechanisms such as photovoltaic, steady-state screening and quasi steady- state screening effects. In all of these cases, the photoinduced $\Delta n$ is due to the space charge field, $E_{sc}$ that results from the migration of charge carriers in the crystal.

The diversity of these photo-mechanisms reflects the fact that self-focusing is governed principally by the macroscopic response of the material. This is expressed by equation 4.9, which states the *general* requirement of i) an intensity-dependent and ii) spatially-localised $\Delta n$ for self-focusing to take place.

### 4.1.8 Self-focusing through localised photochemistry

We are interested in laser-initiated chemical reactions with macroscopic effects that satisfy equation 4.11. In such photochemical systems, the laser beam that is initiating the reaction may simultaneously self-focus in the reaction medium. We term this "self-focusing through localised photochemistry" as equation 4.11 requires a spatially restricted photo-response ($\Delta n$) from the medium.

The study of photon-matter interactions has been dominated by accounts of physical mechanisms, such as the ones described in the previous Sections. Chemical reactions carried out in intense optical fields can induce nonlinear responses, offering opportunities for new and exciting perspectives on this field of study.

There are few examples of self-focusing through laser-initiated chemistry. A recent publication reported the self-focusing of short laser pulses in air, describing these as "optical bullets" that were observed to propagate over several metres[22]. The authors theorised that this effect was due to a balance between self-focusing due to the Kerr effect and refractive index changes caused by the laser-induced ionisation of air.

Monro and co-workers[23] gave a theoretical account of the self-focusing of laser beams in photosensitive germanosilicate glasses. The sensitivity of Ge-doped silica to a 514.5 nm laser beam was serendipitously observed in optical fibres in 1977[24]. When irradiated with UV or visible laser light, the glass exhibits a highly localised, intensity-dependent perturbation of the refractive index:

$$\Delta n(\vec{r},t) \propto \int^{t} I^{2}(\vec{r},t')dt' \qquad [4.16]$$

where I, $(\vec{r},t')$ are intensity of the laser beam, position in the material and time respectively. This property is now widely used to create Bragg gratings in optical fibres[25]. The photo-mechanisms that underlie the permanently induced $\Delta n$ in germanosilicates glasses are not completely understood. Studies suggest that germanium dopants introduce oxygen deficient centres (ODCs) in the silica network[26]. Upon irradiation, these sites are consumed causing local matrix-rearrangement, compaction and a saturable, positive $\Delta n_{max}$ on the order of $10^{-3}$ at laser powers of 0.5 W. The response time for this material is on the order of hours, in sharp contrast to the photophysical mechanisms discussed in the previous Sections. Recently, this intensity-dependent, spatially localised $\Delta n$ was used to demonstrate the self-focusing of a 488 nm laser beam in a Ge-doped silica slab waveguide[27].

Self-focusing has also been identified in bulk samples[28] and slab waveguides of chalcogenide glasses[29]. In the former case, arsenic trisulphide ($As_2S_3$) was exposed to intense (10 $Wcm^{-2}$) 632.8 nm (2.0 eV) light. This wavelength falls in the absorption band ($\approx$ 2.4 eV) of the chalcogenide glass. Irradiation causes a bathochromic shift in the material's absorption band (photo-darkening), which creates a $\Delta n$ in the material. In the case of the planar waveguides, the authors demonstrated that $As_2S_3$ is sensitive to even lower optical energies (800 nm), well away from the bandgap. They suggested that this was caused by two-photon absorption. Thus, 800 nm pulses from a Ti:saphire laser were self-focussed in a $As_2S_3$ slab waveguide.

In 1999, the nonlinear propagation of a laser beam was observed in the thermodynamically metastable, paraelectric-ferroelectric transition state of a potassium lithium tantalum niobate (KLTN) crystal[30]. As it propagated, the 514.5 nm laser beam nucleated the crystalline ordering of ferroelectric clusters in its path, which led to its efficient self-trapping in the crystal.

Self-defocusing of light has been observed in photo-bleachable laser dye-doped materials. The photolysis of the dye changes the absorption spectrum of the material, with a corresponding negative $\Delta n$[31].

Yariv and co-workers[32] simulated and experimentally demonstrated the self-focusing of UV laser pulses in liquid acrylate monomer. The induced $\Delta n$ was caused by a free-radical polymerisation process that created dense polymeric filaments of uniform diameter in the liquid medium. In their report, 1 mW pulses of a 325 nm laser beam were used to create the polymeric filaments in cuvettes filled with the monomer solutions. The 10 μm diameter of the fibres was maintained over distances that were much longer than the confocal parameter of the Gaussian input beam and the authors considered this to be evidence of the non-diffracting path and thus the self-focusing of the laser beam in the medium. Similarly, Shoji and Kawata[33] reported the formation of "self-grown", polymerised fibres in liquid urethane acrylate monomers and oligomers.

The above account of self-focusing spans a rich collection of photochemical processes that lead to the self-focusing of light includes photoinduced matrix relaxation, colour change, optically seeded phase transition, photoinitiated free-radical polymerisation, photobleaching and the partial ionisation of a neutral gas. The survey of these types of laser-matter interactions allows us to bring out a common feature among them, namely the creation of a spatially localised, intensity-dependent $\Delta n$. As mentioned in Section 4.1.3, this property is characteristic of the classical NLO responses such as the Kerr effect, which allows a laser beam with a non-uniform intensity profile (e.g. Gaussian) to self-focus.

#### 4.1.8.1 Sol-gel derived hybrid silica-methacrylate composites as self-focusing media

In this Chapter, we identify and characterise the self-focusing of a visible, continuous-wave laser beam in a silica-methacrylate slab waveguide. As the beam propagates, it initiates the polymerisation of methacrylate groups in its path, inducing a refractive index change that enables it to self-focus in the nascent reaction medium. The evolution of intensity at the waveguide output is used to monitor the self-focusing of the beam and thus the refractive index changes in the slab. The dependence of laser power on the process is also studied.

Arguments are made to attribute the origins of self-focusing to photo-transformations that are unique to the hybrid silica-methacrylate class of composites. In addition to the optical characterisation of the process, we introduce the concept of inducing photochemical reactions and structuring materials in the presence of a self-focusing laser beam. Specifically, we report the first example (to our knowledge) of a circular-waveguide supported on a substrate, which was self-inscribed by the self-focusing beam. To explore the molecular origins of the self-focusing photo-response further, we prepared a series of new hybrid silica-acrylate composites to examine the impact of a) silica network connectivity, b) alkyl-chain lengths linking methacrylate units to Si centre, c) availability of free, polymerisable monomer molecules in a photo-inert silica matrix and d) the role of methacrylic acid units complexed to zirconia clusters.

We also present preliminary evidence for the self-focusing of incoherent white light in the silica-methacrylate colloidal medium; an exciting event, previously observed only in photorefractive crystals[34]. We show that this spatially and temporally incoherent wavepacket is captured and propagates without broadening in a self-inscribed waveguide. In addition, this Chapter describes the discovery of a remarkable degree of long range, sub-micrometric organisation in the composite. Until now, such materials have been considered amorphous. This self-organisation will be described more extensively in Chapter five of this thesis. We introduce it here, because it bears directly on our understanding of the structural origins of self-focusing.

## 4. 2 EXPERIMENTAL

### 4.2.1 Sol-gel derived composites : the SAC series

The main objective of the work presented in this Chapter was to detect self-focusing in the silicate-methacrylate composite, described in Chapters 2 and 3 of this thesis. Precursors to this sol-gel derived material are 3-methacryloxypropyl trimethoxysilane (MAPTMS), zirconium (IV) tetra *iso*-propoxide and methacrylic acid (MAA) in a 10:4:4 ratio. In order to understand the contributions of the various components in the composite – methacrylate substituent, methacrylic acid, silicate network - in the self-focusing phenomenon, we designed a series of silicate-acrylate composites based on precursors with slightly varying chemical structures. For all the composites, the same sol-gel processing conditions were maintained and the precursor composition was always retained at a 10:4:4 ratio between the organosubstituted alkoxysilane: zirconium (IV) tetrapropoxide: organic acid precursors.

We label this the SAC (Silica-Acrylate Composite) series. SAC includes the original silica-methacrylate composite (SAC-01) and its "saturated analogue" SAC-02 (see Chapter 2, Section 2.2), which is based on acetoxypropyl trimethoxysilane (APTMS) and isobutyric acid (IBA). New composites include SAC-03 and SAC-04. which selectively examine the photosensitivity of MAPTMS and MAA in the composite. SAC-05, SAC-06 and SAC-07 are poly (methylmethacrylate) (PMMA), methacrylic acid (MAA) and methyl methacrylate (MMA) doped saturated glasses (dopant quantities at a 1:1 ratio with the alkoxysilane precursor were added). In SAC-08, the propyl chain of the methacrylate substituent has been replaced by a methyl linker. SAC-09 is derived from a dimethoxysilane precursor.

**SAC-01** The procedure developed by Schmidt and co-workers was adapted[35]. Precursors to the composite were 3-methacryloxypropyltrimethoxysilane (MAPTMS): zirconium(IV)-*n*-propoxide ($Zr(OC_3H_7)_4$): methacrylic acid (MAA) in a 10:4:4 molar ratio. MAA (1.39g, 0.016 mol) was slowly added to $Zr(OC_3H_7)_4$ (7.49g of 70 % w/w in *n*-propanol, 0.016 mol). The exothermic reaction gave a clear, yellow and stable liquid (i). Separately, 0.05M HCl (0.54g, 0.030 mol[1]) was added to MAPTMS (10.14 g, 0.040 mol). Within a few minutes of stirring, this initially phase separated system (ii) suddenly cleared. After an hour, ii was added drop wise to i, followed by distilled $H_2O$ (0.97 g, 0.054 mol). The clear, pale-yellow sol was stirred in a capped phial for 16 hours.

**SAC-02** Isobutyric acid (IBA) (1.42 g, 0.016 mol) was added to $Zr(OC_3H_7)_4$ (7.49 g of 70 % w/w in *n*-propanol, 0.016 mol) yielding a clear, colourless liquid (iii). 0.05 M HCl (0.54 g, 0.030 mol) was added to 3-acetoxypropyltrimethoxysilane (APTMS) (8.89 g, 0.040 mol). This mixture (iv) (a suspension of aqueous droplets in the organic liquid) was stirred vigorously for an hour. A transparent liquid was obtained when iv was slowly added to iii. After the addition of $H_2O$ (0.97 g, 0.054 mol), the sol was left stirring for 16 hours.

**SAC-03** 0.05 M HCl (0.54 g, 0.030 mol) was added to APTMS (*cf.* iv). After stirring for an hour, the sol was slowly added to the preformed $Zr(OC_3H_7)_4$: MAA complex (*cf.* i). After addition of $H_2O$ (0.97 g, 0.054 mol), the sol was left stirring for 16 hours.

**SAC-04** 0.05 M HCl was added to MAPTMS (*cf.* ii). After an hour, it was added to the preformed $Zr(OC_3H_7)_4$: IBA complex (*cf.* iii). Distilled $H_2O$ (0.97 g, 0.054 mol) was added and the clear sol was stirred for 16 hours.

**SAC-05** SAC-02 was prepared. Immediately following the addition of $H_2O$, 5 % w/w of polymethyl methacrylate (PMMA, M. W. 93,300, M. N. 46, 400) was slowly stirred into the sol. The viscous mixture was left stirring for 16 hours.

**SAC-06** SAC-02 was prepared. MAA (4.87 g, 0.056 mol) was slowly added and the sol. stirred for 16 hours.

---

[1] According to sol-gel processing terminology, the r value is the molar ratio of [H2O]/[alkoxide groups present]. In our case, r = 1.5 was used taking into both the silicon and the zirconium alkoxide precursors.

**SAC-07** SAC-02 was prepared. Methyl methacrylate (MMA) (5.61 g, 0.056 mol) was slowly added and the sol, stirred for 16 hours.

**SAC-08** 0.05 M HCl (0.54 g, 0.030 mol) was added to 3-methacryloxymethyltriethoxysilane (MAMTES). After an hour, this clear liquid was slowly added to the $Zr(OC_3H_7)_4$: MAA complex (c.f. i). Distilled $H_2O$ (0.97 g, 0.054 mol) was added and the sol, stirred for 16 hours.

**SAC-09** 0.05 M HCl (0.36 g, 0.020 mol) was slowly added to 3-methacryloxypropylmethyldimethoxysilane (MAPDMS) (9.43 g, 0.040 mol). After the clear liquid was stirred vigorously for an hour, it was added to the $Zr(OC_3H_7)_4$: MAA complex (*c.f.* i). Distilled $H_2O$ (0.79 g, 0.044 mol) were added and the sol, left stirring for 16 hours.

### Photosensitisation

All sols were aged for 16 hours. 1.5 % w/w of Irgacure® 184 (1-hydroxy cyclohexyl phenyl ketone, $\lambda_{max}$: 240-250 and 325-330 nm), Irgacure® 819 (bis (2, 4, 6-trimethylbenzoyl)-phenyl phosphine oxide, $\lambda_{max}$: 270-320 and 360-420 nm) or Irgacure® 784 (bis ($\eta^5$ cyclopentadienyl) bis (2, 6-difluoro-3-(1H-pyrrol-1-yl)-phenyl) titanium, $\lambda_{max}$ : 400-530 nm) was stirred into the sols, which were then passed consecutively through 1 μm and 0.2 μm PTFE filters. Sols sensitised to visible light were stored in the dark and handled under red light.

### Thin film formation

Thin films were cast on Si wafers that had a thermally grown, 2 μm thick oxide layer. Samples for FT-IR were cast on Si wafers (transparent in the mid-IR) that were polished on both sides. Substrates were cleaned by soaking consecutively in warm trichloroethylene, acetone and isopropanol, rinsed with distilled $H_2O$ and dried under flowing $N_2$. Films were cast on a Headway photoresist spinner (EC101D & PM101D series). For SAC-01, thickness of 3.7, 4.25, 4.50, 5.00 μm were obtained at spin-casting speeds of 6000, 5500, 5000 and 3000 R.P.M respectively for 40 seconds. All other films for the self-focusing experiments were cast at 3000 R.P.M for 40 seconds.

### Materials

MAPTMS (98 %), MAA (99 %), MMA (99 %), ALDIOL (99 %), IBA (99 %), AA (97 %), PMMA, Ti(*iso*-OPr)$_4$ (97 %), VTMS (97 %) were purchased from the Aldrich Chemical Company, Milwaukee, WI, USA. $Zr(OC_3H_7)_4$ was acquired from Alfa-Aesar, Ward Hill, MA, USA. 0.05 M HCl was prepared from a standardised solution of 0.1036 N HCl from Aldrich. APTMS and MAMTES were purchased from Gelest Inc. Tullytown, PA, USA. MAPDMS was obtained from United Chemical Technologies Inc. Bristol, PA, USA. MAPTMS and $Zr(OC_3H_7)_4$ were handled under $N_2$. Photoinitiators were provided by Ciba Specialty Chemicals Canada Inc. Missisauga, ON, Canada. Si wafers were purchased from Nova Electronic Materials, Inc., Richardson, TX, USA.

### 4.2.2 Optical Set-Up

The prism-coupling waveguide assembly for waveguide Raman spectroscopy described in Chapter 2, was modified for this purpose.

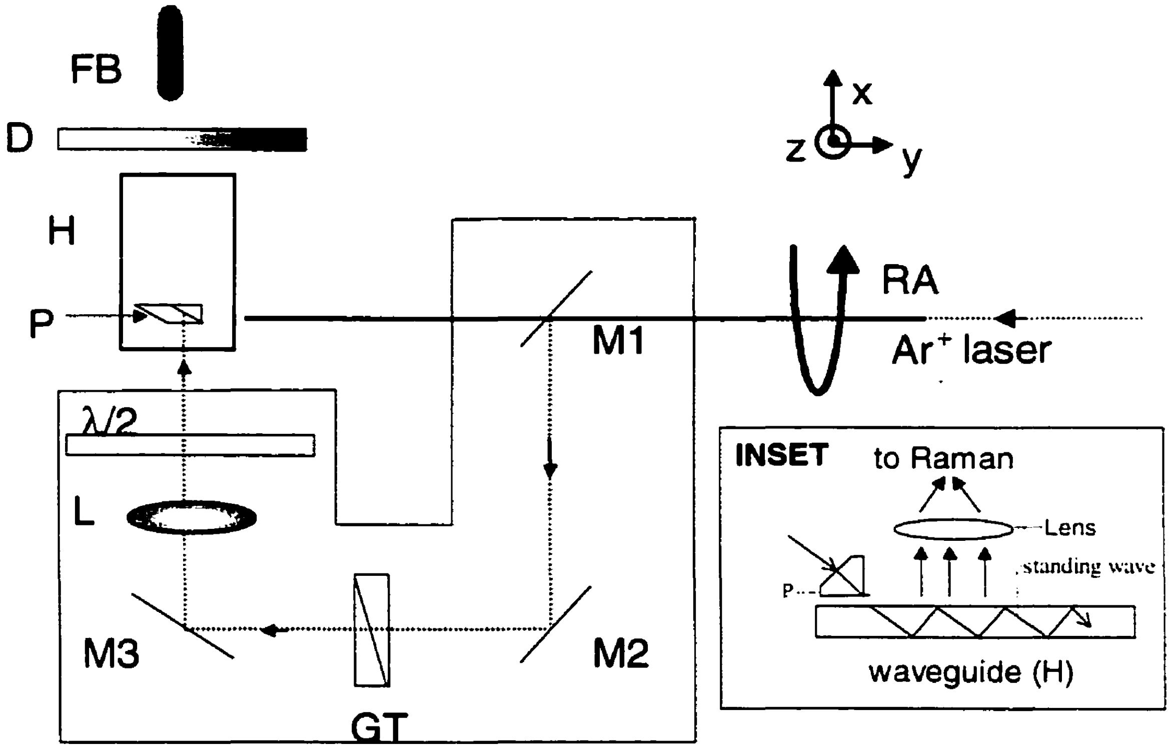

**Figure 4. 4** Optical set-up for self-focusing experiments

The 514. 5 nm line of an $Ar^+$ laser was coupled through a high refractive index (n=1.780 at 514.5 nm) prism [P] (Precision Optics) clamped onto the film surface (H). The computer-controlled beam steering assembly focussed (L) the beam after reflection through three mirrors (M1-3) onto the prism hypotenuse plane and scanned the coupling angles about a rotation axis (RA) until waveguiding was achieved. A half wave retardation plate ($\lambda/2$) in combination with a Glan Thompson polarizing cube (GT) specified the polarisation plane of the input light. The output light was collected through an optical fibre bundle (FB) (Oriel Corporation) and measured by a spectrograph (MultiSpec, Oriel Corporation, CT. USA) equipped with a photodiode charge coupled device (PCCD) detector (Lamda™ LS-2000 Series multichannel Optical Analyser. Optikon Corporation Ltd. Waterloo, ON, Canada).

### 4.2.3. Characterisation of the self-focusing of a c.w $Ar^+$ laser beam is SAC-01 planar waveguides

#### 4.2.3.1 Measurement of waveguide output-intensity evolution

Self-focusing experiments in SAC-01 slab waveguides were carried out at laser powers of 5, 25, 50, 100, 250, 500 mW (measured at the laser output). The beam's plane of polarisation was TE (0°, $y$ axis), TM (90°, $z$ axis) or TE+TM (45°). During the process, time-resolved measurements of the waveguide-output were automated with software provided with the PCCD instrument. Acquisition times were typically 0.05 seconds. The output intensity was measured every second for the first 100 seconds and then for every 10 seconds over the next 1200 seconds. Self-focusing in SAC-03, 04, 05, 07 and 08 slab waveguides were all carried out at 100 mW. To prevent detector saturation, output intensities were attenuated with neutral density filters (Oriel Corporation, CT. USA) that had optical densities (O.D) of 0.09, 0.20, 0.30, 0.41, 0.51 and 1.00 at 500-550 nm.

#### 4.2.3.2 Video-imaging of self-focusing process

During self-focusing experiments, the streak of light at the surface of the planar waveguide was monitored by a digital CCD video camera (Kodak DVC325 Digital). Snapshots of the film surface were taken (15 frames/sec) during the first five minutes after the laser beam was coupled into the waveguide. Photographs were taken at 5 minute intervals for a 90 minutes.

**4.2.3.3 *In situ* waveguide Raman spectroscopy** monitored polymerisation in the thin film. Raman intensity scattered normal to the waveguide was collected in real-time with diffraction-limited optics and focussed into a Raman spectrometer[36] (see Chapter 3, Section 3.2). Spectra over spectral windows ranging from 400 $cm^{-1}$ to 3500 $cm^{-1}$ were acquired. Laser power was maintained at 100 mW, with acquisition times ranging from 30 seconds to 60 seconds. An average of 20 scans was made for each spectrum.

#### 4.2.3.4 Wet-etching of self-focused regions in planar waveguides

After the optical measurements of self-focusing (output intensity, *in situ* waveguide Raman spectroscopy), the planar waveguide was dismounted from its holder. The film was immersed at once into a phial containing *iso*-propanol and placed in a sonicator for 30 to 60 seconds. The film was then gently dried under a $N_2$ stream. Typically, a narrow (microscopic) silvery line running along the long-axis of the film was visible at the surface of the wafer. A perpendicular line marking the back edge of the prism was also seen. Wafers were then cleaved for inspection under optical and scanning electron microscopes. When the films were dipped into *iso*-propanol for 30 seconds without sonication followed by drying, silvery regions developed on the films especially towards the output edges of the waveguide.

### 4.2.4 Scanning electron microscopy

A thin Au/Pd layer was evaporated onto thin films containing self-inscribed waveguides. Micrographs were acquired with a JEOL scanning electron microscope.

### 4.2.5 FT-IR Spectroscopy

Transmission IR spectra of thin films were acquired over a range of 400 to 5000 $cm^{-1}$ with a Bruker IFS-48 Fourier transform infrared spectrometer. Resolution of the acquisition was set at 4 $cm^{-1}$. Acquisition conditions and times were identical for a series of spectra of the same thin film composite.

### 4.2.6 Optical Microscopy

A Nikon OPTIPHOT microscope with the UFX-IIA photo-micrographic attachment was used. Photographs were taken with a Nikon F-301 camera.

## 4.3. RESULTS AND DISCUSSION

Our objective was to demonstrate the self-focusing of a c.w. $Ar^+$ laser beam (514.5 nm) in a SAC-01 slab (planar) waveguide. In this experiment, the laser beam propagates as an optical mode along the *z* axis of the waveguide and is confined by the (air/SAC-01 and SAC-01/$SiO_2$) interfaces in the $x$ direction (see Figure 4.5). A slab waveguide is assumed to extend infinitely long the $y$ axis[37] thus diffraction and the opposing self-focusing effect are observed only in this direction[38].

As detailed in Chapters 2 and 3, thin films cast from the SAC-01 colloid are efficient planar waveguides that support transverse magnetic (TM) and transverse electric (TE) guided optical modes at both 632.8 nm and 514.5 nm. For the self-focusing experiments, we chose a 5.4 μm thick film that was 4.5 cm long and supported on a $SiO_2$ ($d_s$ = 2.00 μm) coated Si wafer (Figure 4.5). Prior to irradiation, the slab had $n_f = 1.517$ at 514.5 nm.

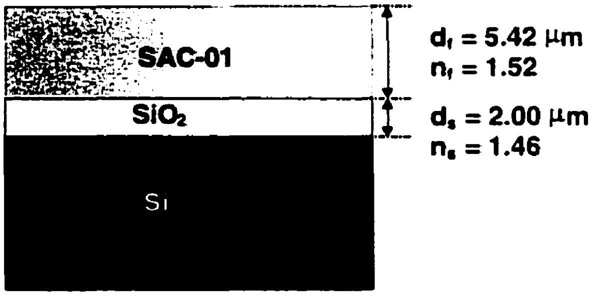

**Figure 4. 5** Trilayer SAC-01 planar waveguide

The SAC-01 material is transparent to most of the visible region (400 – 800 nm) of the electromagnetic spectrum (Chapter 2, Section 2.3) whereas a strong interaction between the 514.5 nm laser beam and the material is necessary for self-focusing to occur. As mentioned in the Introduction (Section 4.2.3) and expressed by Equation 4.11, a monochromatic beam can self-focus in a medium only if it induces a spatially localised refractive index change that opposes the beam diffraction. In SAC-01 thin films, $\Delta n$ changes up to 0.015 can be photoinduced through the free-radical polymerisation of methacrylate groups in the composite (Chapter 2, Section 2.3). For the current experiment, the SAC-01 planar waveguide was sensitised to green light with 0.8 % w/w of the free-radical photoinitiator bis($\eta^5$ cyclopentadienyl) bis(2, 6-difluoro-3-(1H-pyrrol-1-yl)-phenyl)titanium (Irgacure 784®), which absorbs from 400 - 530 nm.

### 4.3.1 Visible light photoinitiation of free-radical polymerisation

The titanocene photoinitiator used in this experiment belongs to a group of organometallic photosensitisers, developed specifically for the rapid, visible-light curing of thick polymer films. Its efficient photobleaching properties allow the incident light to penetrate up to 70 μm into films[39], much further than allowed by conventional photoinitiators. The titanocenes have also been shown to increase the rate of free-radical polymerisation reactions. For example, the curing rate of acrylate photoresists is increased three-fold when ketonic photoinitiators are replaced with the organometallic one. In addition, titanocene complexes with fluorinated aryl substituents are thermally and oxidatively more stable than their parent biphenyl titanocenes.

The initiation mechanism of this specific class of photoinitiators has been elucidated through flash photolysis studies[40]. Upon irradiation, the parent diphenyl titanocenes undergo homolytic σ bond cleavage to produce phenyl radicals, which initiate polymerisation. Indeed, these titanocenes are the only free-radical initiators that can be photolysed directly with visible light. By contrast, the fluorinated derivatives react differently to visible light and there is no evidence of phenyl radicals generation here. As schematised in Figure 4.6, when the molecule with a fluorinated phenyl group is irradiated with blue or green light, it undergoes an $\eta^5$ to $\eta^1$ haptotopic ring slippage and a transient isomer forms with unit quantum yield within 25 nanoseconds of absorption.

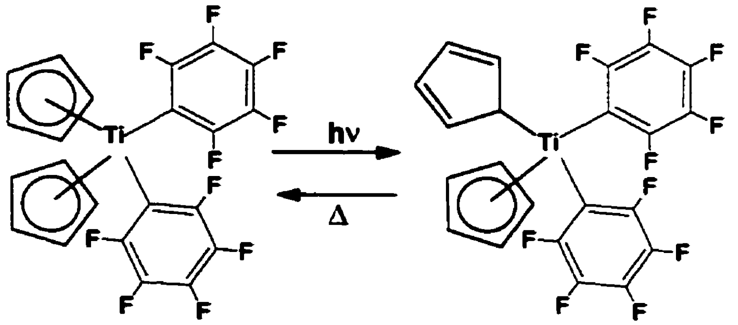

**Figure 4. 6** Photoisomerisation of the titanocene photoinitiator[40]

The coordinatively unsaturated Ti centre of the isomer shows enhanced electrophilicity and can bind two methacrylate groups with reductive elimination of (cyclopentadienyl) pentafluorostyrene[41]. This reactive biradical then initiates free radical polymerisation of methacrylate monomer.

### 4.3.2 Guided-wave initiated free-radical polymerisation

Free-radical polymerisation of methacrylate substituents may be initiated with visible light. The 514.5 nm line of the $Ar^+$ laser was coupled into the photo-initiator doped slab. The beam was introduced at the largest angle of coupling from the prism-normal, corresponding to the transverse electric (TE), fundamental mode ($m = 0$). Once coupled, an orange streak at the film's surface (laser-induced luminescence) in the material marked the beam's path within the slab. In Figure 4.7, photographs of the waveguide-surface captured within the first 5 minutes after in-coupling, follow the progress of the laser beam.

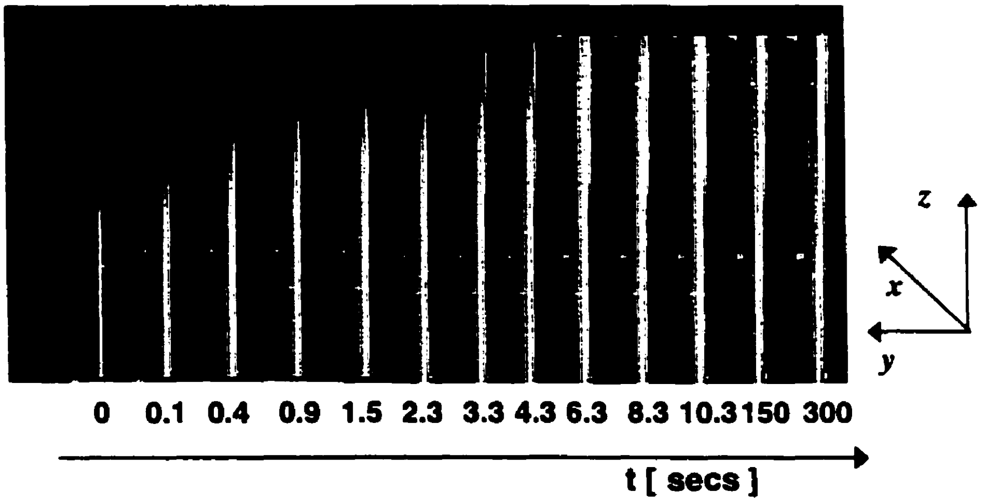

**Figure 4. 7** Propagation of 514.5 nm in a titanocene doped silica-methacrylate slab waveguide

As the light propagated in the SAC-01 waveguide, it activated the isomerisation of titanocene molecules and in turn the free-radical polymerisation of methacrylate groups in its path. Neither the transient photoisomer shown in Figure 4.6 ($\lambda$ = 580 nm[41]) nor the growing methacrylate polymer ($\lambda$ = 280-300 nm) absorb at 514.5 nm. As the beam consumed titanocene molecules, it created a less absorptive and thus a more transparent path for itself in the waveguide. As can be seen in the sequence of photographs presented in Figure 4.7, this photobleaching event required less than 6 seconds for the laser beam to propagate across the ≈ 40 mm length of the slab.

Note that mode propagation in the SAC-01 planar waveguide occurs in the $z$ direction (in laboratory frame). The optical mode is confined in the $x$ direction by the air/ $SiO_2$ interfaces and is free to diffract (and self-focus) in the $y$ direction. The initial divergence of the beam along the $y$ axis as it propagates away from the prism edge is evident in the final photograph (t = 300 sec.) of the series presented in Figure 4.7. At this time, the photoinduced $\Delta n$ in the SAC-01 planar waveguide is insufficient to counter diffraction of the laser beam.

### 4.3.3 Waveguide Raman Spectroscopy (WRS) of polymerisation reactions in the path of the laser beam

Over time, the visible laser initiated the free-radical polymerisation of methacrylate groups in the SAC-01 waveguide. These reactions were characterised by *in situ* waveguiding Raman spectroscopy (see Chapter 3, Section 3.2 for a description of this technique). Briefly, the streak of light containing both Raman and Rayleigh scatter at the film's surface was focussed into a Raman spectrometer. Spectra acquired over time from this guided wave were used to monitor the extent of polymerisation in its path.

Spectra collected during the self-focusing process are presented in Figure 4.8. The polymerisation of methacrylate groups with increasing exposure time is indicated by the decreasing intensities of bands corresponding to the olefinic components: $\nu(C{=}C)$ mode at 1638 $cm^{-1}$, in-plane C-H deformation of the vinyl group at 1408 $cm^{-1}$, the $\nu_s(CH_2)$ and $\nu_{as}(CH_2)$ of $=CH_2$ at 2929 $cm^{-1}$ and 3105 $cm^{-1}$, respectively. Depletion of the band at 1712 $cm^{-1}$ is accompanied by growth of one at 1738 $cm^{-1}$. The latter signifies that the ester carbonyl group is no longer conjugated with the vinyl group, *i.e.* that polymerisation has occurred. Simultaneous loss of intensity of the $\nu(Si\text{-}O(H))$ band at 954 $cm^{-1}$ and the $\nu_{as}(CH)$ of $Si\text{-}OCH_3$ at 2958 $cm^{-1}$, suggest polycondensation reactions have taken place between residual silanol and alkoxy groups in the silicate network coinciding with polymerisation of the organic monomer. (Codensification in the hybrid materials, was discussed in detail in Chapters 2 and 3).

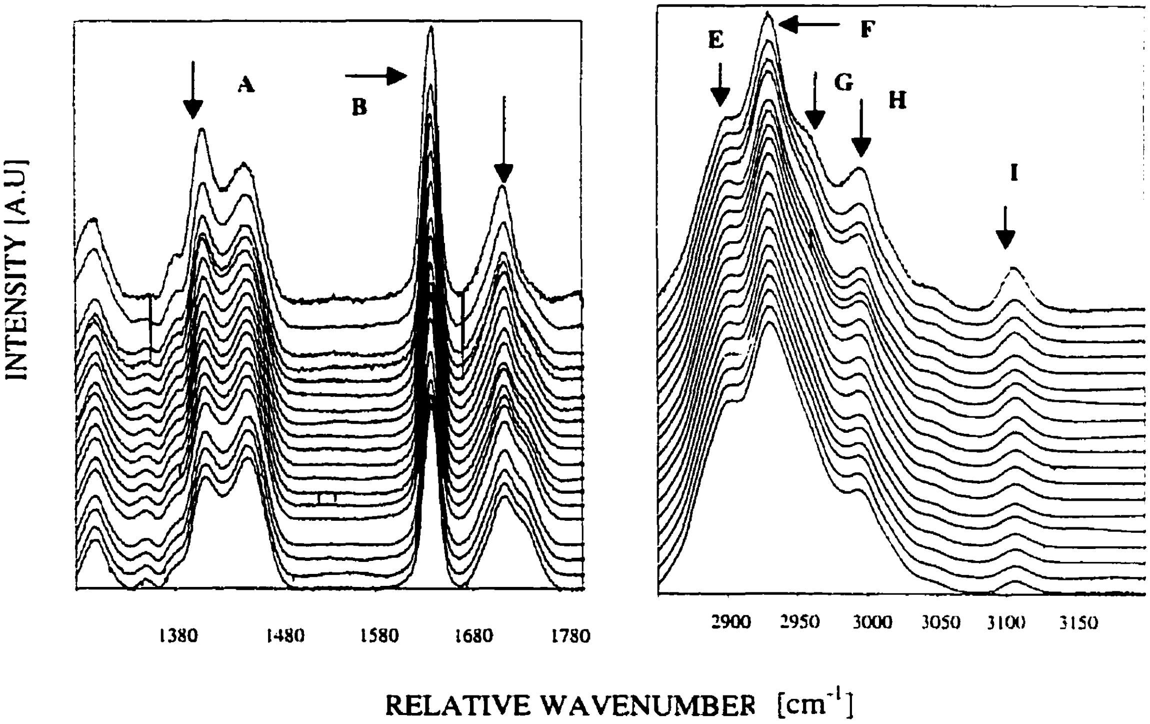

**Figure 4. 8** WR spectrum of laser initiated polymerisation in silica-methacrylate waveguide. (A) $\delta$ CH i.p. of $=CH_2$ at 1408cm$^{-1}$; (B) $\nu(C=C)$ at 1638 cm$^{-1}$; (C) $\nu(C=O)$ at 1712 cm$^{-1}$ (unsaturated ester) and (D) 1738 cm$^{-1}$ (saturated); (E) $\nu_s CH_3$at 2899 cm$^{-1}$; (F) $\nu_s(CH_2)$ of $=CH_2$ at 2929 cm$^{-1}$; (G) $\nu_{as}(CH)$ of Si-$OCH_3$ at 2958 cm$^{-1}$; (H) $\nu_s(CH)$ of $=CH_2$at 2996 cm$^{-1}$; (I) $\nu_{as}(CH)$ of $=CH_2$ at 3105 cm$^{-1}$. Spectra are offset for clarity.

Collectively, the spectra confirm that the propagating laser beam initiates the polymerisation of methacrylate groups in the waveguide. As an aside, we note that the above spectroscopic method may complement the conventional FT-IR based technique used to measure the kinetics of photoinitiated, free-radical polymerisation of vinyl monomers. Here, the polymerisation reactions are initiated (in liquid monomer or thin film form) with a laser beam or broadband UV light while vibrational spectra are acquired at regular intervals with a second laser beam. Typically, the rates of the reaction are measured by the decreasing intensity profiles of the ν(C=C) absorption band[42] that belongs to the vinyl monomer. For the *in situ* Raman study described above, a single laser beam both initiates and provides spectroscopic data about a free-radical polymerisation process. Currently, there is a trend towards visible light initiated polymerisation reactions[43] due to the efficiency and decreasing costs of visible lasers and the advances made in developing visible light activated photoinitiators. The technique described above may be a simple and valuable tool in characterising such reactions.

### 4.3.4 Self-focusing of light

The WRS study described in the previous Section confirmed that laser-induced free-radical polymerisation of methacrylate substituents indeed occurs within the SAC-01 planar waveguide. We describe this process as "guided-wave polymerisation" to signify that the free-radical reactions are initiated by the mode-selected optical field in a planar waveguide. The polymerisation of methacrylate substituents creates a positive refractive index change ($\Delta n$) in the SAC-01 thin film. Therefore as the free-radical reactions proceed in the waveguide there is an associated increase in $n$, along the path of the propagating beam. The experimental evidence presented in this Chapter confirms that this is in fact the chemical analogue of the Kerr response. In the classical NLO medium, an intense laser beam induces a $\Delta$n along its path due to the nonlinear polarization response of the material (see Section 4.1.2). In guided wave polymerisation, $\Delta$n originates from a photochemical reaction. In both of these systems the propagation conditions of the electromagnetic wave are continuously modified by the evolving refractive index profile. As described by equation [4.11], this may lead to the self-focusing of the laser beam.

### 4.3.4.1 Self-focusing in a planar waveguide

Recall that in the case of the SAC-01 planar waveguide, the laser beam excites an optical mode. The electric field of the guided wave may be represented by:

$$\vec{E}(x,y,z,t) = F(x)\mathcal{E}(y,z,t)e^{i(kz-\omega t)} \qquad [4.\ 17]$$

where the monochromatic laser beam with frequency ω, has the one-dimensional Gaussian profile[44]:

$$\mathcal{E}(y,z,t) = \mathcal{E}e^{-y^2/a^2} \qquad [4.\ 18]$$

The wavenumber is represented by $k = \frac{\omega}{c}n = \frac{2\pi\nu}{c}n$, where n is the refractive index of the non-irradiated waveguide and c, the speed of light. F(x) describes the modal profile, determined by the SAC-01/air and SAC-01/$SiO_2$ interfaces. The refractive index differences at these interfaces are 0.51 and 0.03 for SAC-01/air and SAC-01/$SiO_2$ respectively, whereas the maximum refractive index change induced in the SAC-01 composite is 0.015 (Chapter 2, Section 2.3). It may then be assumed that the transverse profile of the electric field in the *x* direction, remains unchanged by the refractive index changes induced in the SAC-01 waveguide[45]. Thus as mentioned earlier, a laser beam propagating in a planar waveguide diffracts only in the *y* direction and self-focusing may also occur only in this direction. In Equation 4.11, the diffraction term $\nabla_{\perp}^{2}$ simplifies to $\frac{\partial}{\partial y^2}$.

### 4.3.4.2 Material requirements

Not all photoreactions that lead to an increase in the refractive index allow the self-focusing of light. As mentioned in Section 4.1.3, equation [4.11] imposes certain conditions on the material's response to light. A laser beam can self-focus in a photo-responsive system if it induces a $\Delta n$ with the gradient-index (GRIN) profile of a positive lens *i.e.* a maximum *n* at the axial position with a radially symmetric decay from this point. This corresponds to the typically Gaussian intensity profile of the self-focusing laser beam. Two principal characteristics of lassical NLO responses (Kerr, resonant excitation) enable this lens to be created: i) the photoinduced $\Delta n$ is directly proportional to the intensity of the beam (by Equation 4.1) and ii) $\Delta n$ is highly localised in space. Consequently, the Gaussian profile of the laser beam is replicated in the $\Delta n$ that it induces in the nonlinear optical medium. This is effectively a lens through which the beam may focus further along its propagation axis. The sequential lensing and focusing action of the beam induces a channel waveguide in the medium. The laser beam is then supported as an optical mode in its self-inscribed waveguide and traverses the medium without suffering diffraction.

Such a lens may only be created in the SAC-01 waveguide if the photo-mechanisms underlying $\Delta$n follow i) and ii) as described above. As mentioned earlier, photoinduced $\Delta n$ values are proportional to the rates of photoinitiated polymerisation in the SAC-01 composite. Thus to satisfy condition i, these reaction rates must be directly proportional to the beam's intensity. Secondly the photoinduced free-radical reactions must be sufficiently localised in space, such that the transverse intensity profile of the beam is "captured" or reproduced in the photoinduced refractive index profile.

#### 4.3.4.3 Dependence of rates of polymerisation and Δn on beam intensity

It is well known that the rate of photoinitiated free-radical polymerisation is directly proportional to the intensity of the initiating light and the equations expressing this relationship follow. The rate of titanocene activation in the film may be represented by the equation for photoinitiator dissociation[46]:

$$R_d = \Phi I_a = \Phi I_0 \varepsilon c l \quad [4.19]$$

where $I_a$ is the absorbed intensity, $I_0$ is the intensity of the incident light and $\Phi$, the quantum yield of radical formation, [I] is the initiator concentration and $l$ the path length of light. Note that $R_d$ is proportional to $I(\vec{r})$ and at a given time, will vary according to the non-uniform profile of an input beam.

In addition, $R_d$ is path-length dependent due to the Beer-Lambert law:

$$R_d = \Phi I_a = \Phi I_0 (1 - e^{-\varepsilon [I] l}) \qquad [4.20]$$

Note that the greatest dissociation rate will initially be at the early sections of the beam's path, from the input side of the film, *i.e.* where $l$ is minimum. In the simplest case, the initiation rate $R_i$, of the free radical reaction is equal to $R_d$ and under the steady-state assumption, determines the propagation rate of the reaction:

$$R_p = k_p \left( \frac{I_0 \varepsilon l \Phi [I]}{k_t} \right)^{1/2} [M] \qquad [4.21]$$

Equation 4.21 shows that the rate of polymerisation $R_p$ and consequently the photoinduced $\Delta n$ is directly related to the intensity of the laser beam.

### 4.3.4.4 Spatial localisation of Δn in SAC-01

Condition *ii*, the spatial localisation of the photo-response, is atypical of free-radical polymerisation processes. In the laser-initiated polymerisation of bulk monomer liquids, free-radicals may diffuse over large volumes (on the order of $cm^3$) and are not necessarily constrained to the region of irradiation, *i.e.* the beam width. In this case, reaction rate is determined by the ***average*** intensity of the beam and thus is insensitive to the intensity variations within the micron-sized laser beam dimension. As a result, the polymer product does not retain any "memory" of the c.w. laser beam intensity profile and the GRIN lens necessary for self-focusing cannot be created in these systems. Furthermore, polymer chains created by free-radical reactions generally have large polydispersities, are inhomogeneous and as a result opaque or milky. A visible laser beam propagating in such a medium is likely to suffer severe attenuation due to scattering. In the conventional form, free radical polymerisation reactions are unsuitable for the self-focusing of monochromatic light.

Free-radical polymerisation reactions in the SAC-01 composite behave differently. The structural characteristics of this material and their effect on the photoinitiated polymerisation of methacrylate groups were detailed in the first two chapters of this thesis. A brief recapitulation is given here. In the SAC-01 composite, the polymerisable methacrylate units are substituents of Si centres that belong to an extended, sol-gel derived silica network. Thus once the polymerisation process is initiated, the reactive free radicals remain covalently bound to the network and consequently have decreased diffusion coefficients compared to the free monomer. Furthermore, these reactions are hosted in a preformed, three-dimensional inorganic matrix, which must impose severe steric and spatial constraints on free-radical propagation. In addition to these factors, our IR, Waveguide Raman and $^{29}$Si NMR spectroscopic studies (see Chapters 2 and 3) showed that polymerisation of the organic substituents triggers polycondensation reactions between remnant silanol and silicon methoxide groups in the sol-gel derived host medium. These introduce additional Si-O-Si bonds, which cause further growth and compaction of the silicate network (this was observed as the depletion of Si-OH and Si-OCH$_3$ bands in the WR spectra collected in this experiment, see Section 4.3.3). The above factors collectively raise a significant steric barrier against the propagation of the free-radical polymerisation reactions. As a result, they remain spatially constrained to the irradiated areas.

The spatial localisation of these reactions is most evident in the fabrication of micro-optical devices on SAC-01 thin films. A particularly striking example is the photo-inscription of Bragg gratings with the interference pattern produced by a UV laser beam (see Chapter 2, Section 2.3). Briefly, a 5 $\mu$m thick SAC-01 film is exposed to the interference pattern of a UV laser beam that has a 500 nm period ($\Lambda$). Scanning electron microscopy, optical microscopy and grating reflectivity measurements with an optical spectrum analyser all showed that the composite had accurately recorded the interference pattern and that the grating created in the SAC-01 film consisted of a periodic (500 nm) modulation of the photoinduced $\Delta n$. This demonstrated that the free-radical polymerisation reactions in the SAC-01 films could be confined to illuminated regions with sub-micrometric resolution.

We emphasise that the self-focusing phenomenon studied in this Chapter is very different to the photolithographic process described above. In the latter, UV light from a lamp or a laser beam is shone through photo or phase-masks onto the surface of the SAC-01 thin film. By contrast, self-focusing strictly involves the self-action of a c.w. laser beam propagating as an optical mode within the photosensitive slab waveguide. However, from the sub-micrometric resolution of $\Delta n$ observed in the photolithographic process, it is reasonable to expect the rates of polymerisation $R_p$, and the corresponding $\Delta n$ to be sensitive to the intensity variations (see Equation 4.18) within the 4000 nm wide beam used for self-focusing.

We expected $R_p$ (and $\Delta n$) to maximise at the axial region of the propagating beam and decay from this point, in the $y$ direction roughly following the intensity variation described by Equation 4.18. This carefully modulated photo-response would create the lens necessary for self-focusing to take place in the SAC-01 waveguide. It is also important to note that the SAC-01 composite retains its transparency to visible light even after the onset of polymerisation reactions. The electronic absorption spectroscopic study of the polymerisation process (Chapter 2, Section 2.3), showed that the changes to the absorbance spectrum of the composite occurred well below 400 nm. In the context of the self-focusing event, this ensures that the 514.5 nm laser beam continues to propagate without significant attenuation after the lens has been induced.

#### 4.3.4.5 Response time of the medium

The response time of a Kerr medium, defined as the interval between irradiation and the consequent $\Delta n$, is on the order of $10^{-15}$ s. Thus a laser beam of appropriate intensity appears to self-focus immediately in a Kerr medium because the sequence of events that lead to self-focusing, *i.e.* required $\Delta n$ corresponding to the GRIN lens and the channel waveguide are induced almost instantaneously. Therefore, in the mathematical description of the system, there is no time dependence associated with the photoinduced $\Delta n$ (see equation [4.11]).

By contrast, the response time in SAC-01 composites depends on the rate of a photochemical reaction, which underlies the photo-induced $\Delta n$. The reaction times of free-radical polymerisation typically vary from milliseconds at the initial stages to seconds, as the monomer source is rapidly depleted. In the case of the SAC-01 composites, this scale is increased further to seconds and minutes. The conversion curve plotted for the UV induced reactions (Section 2.3, Chapter 2), indicated that the extent of polymerisation (and $\Delta n$) was greatest only after 10 minutes of irradiation. Unlike Kerr media, the photoinduced $\Delta n$ in the SAC-01 system studied here is not an instantaneous event and has a time dependence that varies from seconds to minutes as the self-focusing event proceeds.

The time dependence of $\Delta n$ may be represented by the empirical model for free-radical polymerisation reactions[32]:

$$\frac{\partial \Delta n}{\partial t} = A[EE^{*}]\left(1 - \frac{\Delta n}{\Delta n_{sat}}\right) \quad [4.22]$$

$\Delta n$ (through $R_p$ in equation [4.21]) depends on the square of the electric field amplitude (E), *i.e.* its intensity. Equation 4.22 also states that photoinduced $\Delta n$ becomes 0 once $\Delta n_{sat}$ is reached. *i.e.* as expressed by Equation [4.21], once all the photosensitive monomer units [M], are consumed. The saturation of the polymerisation reactions and consequently, the refractive index of the silica-methacrylate thin films, were described in Section 2.3, Chapter 2. As mentioned previously, the saturability of the photo-induced $\Delta n$ in a material is a valuable feature that prevents the catastrophic self-focusing of light.

We summarise the self-focusing of a monochromatic c.w. laser beam in a slab silica-methacrylate waveguide by three equations: Equation [4.11] the modified Maxwell's equation that describes the propagation of an electromagnetic wave in a medium with an intensity-dependent refractive index change ($\Delta n$); Equation [4.22], which describes the time-dependence of the $\Delta n$ and Equation [4.17], which describes the electric field profile of the propagating laser beam in the waveguide.

There are no known exact solutions to this system of equations. A similar problem has been modelled by Monro and co-workers[23]. The predictions made by their model are summarised below:

Initially, the refractive index (n) of the planar waveguide is presumed to be isotropic. Over time, the Gaussian beam induces a GRIN lens that is able to counter the diffraction of the beam and focus it along the propagation axis further into the waveguide structure. This "focal point" of the beam corresponded to a maximum in the local intensity, referred to as a "primary eye". The eye induces a refractive index maximum (*i.e* another GRIN lens), which enables it to focus further and further along the propagation axis without suffering diffraction. In this way, the primary intensity eye creates primary eyes of refractive index as it travels in a straight line. Although the paths of both maxima are observed to be the same, they are separated by a time delay that corresponded to the non-instantaneous photo-response of the material. As in the case of self-focusing in classical NLO media, the reciprocal action between self-focusing and refractive index increase creates a channel waveguide in the slab. With increasing exposure time, $\Delta n_{sat}$ is reached and the self-inscribed waveguide is able to support the propagating beam as an optical mode. In this way, the beam is able to traverse the waveguide without diffracting.

For our purposes, the Monro model asserts that self-focusing of light may take place in a system that has a delayed photo-response, *i.e.* free-radical polymerisation. Self-focusing in such a medium would proceed through the same sequence of events as in saturable, NLO media. The important difference is the time delay associated with each step. This is a direct consequence of the time-delay between irradiation and the refractive index change (represented by equation [4.22]). *i.e.* the optical nonlinearity in these systems may be described as non-instantaneous. As will be described in the following Sections, several of these predictions were observed in the self-focusing of light in the SAC-01 planar waveguide.

### 4.3.5 Evidence of self-focusing in the SAC-01 planar waveguide

Recall that after the first few minutes of being coupled into the SAC-01 slab waveguide, divergence of the beam along the $y$ axis was observed (Figure 4.7). Over time, this streak of light at the surface of the film narrowed significantly in the $y$ direction. This was one of the first indications of self-focusing. As predicted theoretically[23], self-focusing of the laser beam gradually creates a narrow, channel waveguide within the planar waveguide. Light is now confined to this narrow region, which has an increased refractive ($n + \Delta n$) index relative to the non-irradiated regions ($n$) of the film. The formation of the channel waveguide and the subsequent capture of the beam within its walls, are seen as a significant narrowing of the scattered streak of light at the surface of the SAC-01 waveguide. Video clips of this behaviour are shown in Figure 4.9. At early times (8 minutes), the streak is relatively broad in the $y$ direction. It then narrows over 60 minutes, into a fine green line.

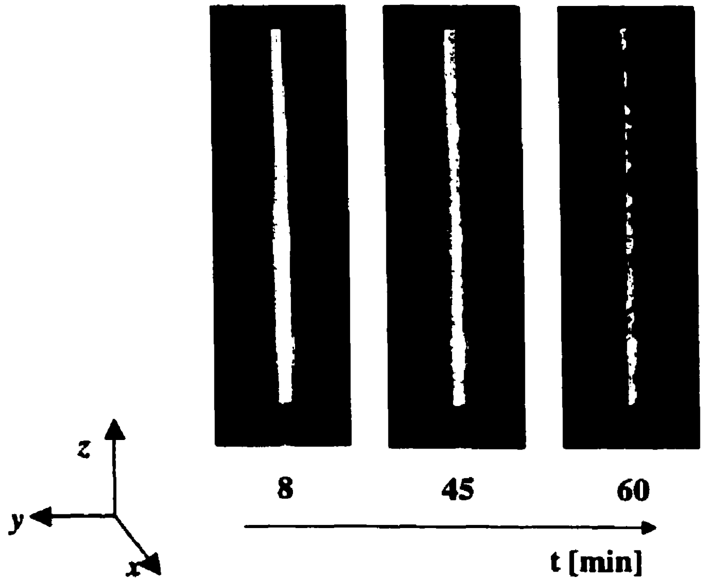

**Figure 4. 9** Evidence of self-focusing at the surface of the SAC-01 planar waveguide

In literature, the preliminary indication of self-focusing in planar waveguides and bulk media has often been the narrowing of scattered or luminescent light. Photographs by Segev and co-workers[47] dramatically contrasted scatter streaks from diffracting and self-trapped light in a strontium barium niobate (SBN) crystal. Red luminescence excited by the propagating 488 nm beam traced its self-focusing in a Ge-doped silica planar waveguide[27] whereas resonance fluorescence revealed the narrowing of a laser beam in Na vapour[48]. In all of these examples, this particular observation has been the most tangible evidence of the nonlinear optical event, in which an intense laser beam creates a transient cylindrical waveguide to counterbalance diffraction in a medium.

#### 4.3.5.1 Proof of self-focusing in SAC-01 planar waveguide

Quantitative evidence of self-focusing in the SAC-01 waveguide was obtained by monitoring the intensity of output-light as a function of time. The evolution of the output-intensity plotted in Figure 4.10 for a 100 mW beam, reveals the dynamics of photoinitiated polymerisation reactions, the associated refractive index change and the consequent self-focusing of light in the composite film.

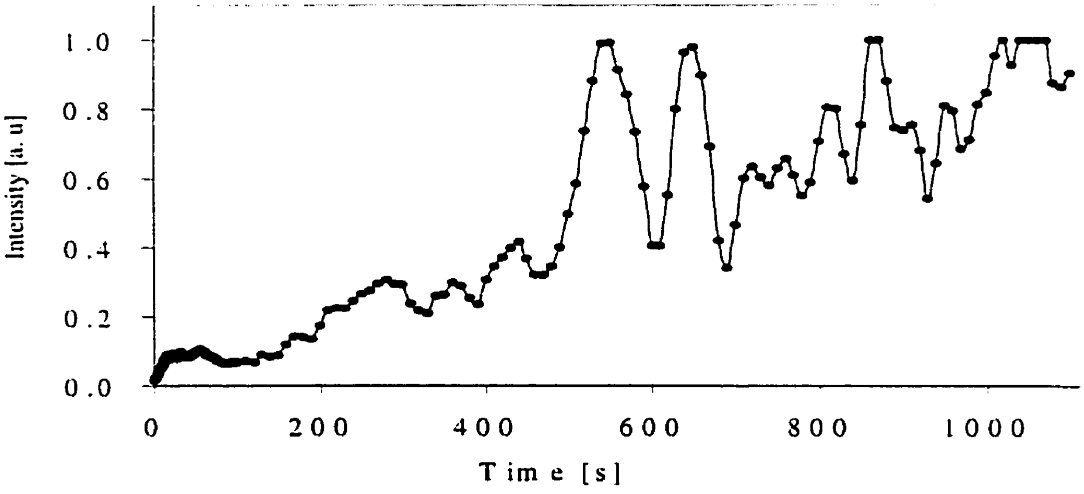

**Figure 4. 10** Evolution of output-intensity during self-focusing of the 514.5 nm laser beam in a SAC-01 planar waveguide.

Within the first 8 seconds there is a rapid increase of intensity as the laser beam photo-bleaches a path through the slab. This time-scale corresponds to the photographic sequence of the same event shown in Figure 4.7. The signal flattens briefly for 90 seconds and then increases four-fold after 440 seconds. At 540 seconds, the output-intensity increases ten-fold. This point marks self-focusing in the slab waveguide.

From Equation 4.21, dissociation of the photoinitiator is greatest where $I$ is minimum. Therefore, initially the rate of polymerisation ($R_p$) and the consequent $\Delta n$ are greatest at the early parts of the laser beam's path in the waveguide. The rates of the spatially localised reactions will be greatest at the most intense, axial regions of the beam and will decay in a symmetric manner from this point in the $y$ direction – essentially creating a GRIN lens in the waveguide. The beam then self-focuses through the lens and advances its intensity maximum (primary eye) along the propagation axis $z$. Here, it initiates additional polymerisation reactions and induces $\Delta n$, also in the form of a positive lens. The reactions in the earlier part of the waveguide terminate as $\Delta n_{sat}$ is reached. As the intensity maximum is focussed and advanced along the propagation axis, the path behind it approaches $\Delta n_{sat}$, ultimately yielding a channel waveguide with a uniform (step) refractive index profile. Light that was first diffracted now converges in the region of increased $n$ and confines itself within the walls of the self-inscribed waveguide. As light propagates in this newly created channel waveguide without divergence, there is a significant increase in the output intensity. The increased output-intensity seen in Figure 4.10 indicates that such a waveguide is being created in the SAC-01 slab. Similar behaviour has been observed during self-focusing events in both chalcogenide[29] and Ge-doped silica[27] planar waveguides.

### 4.3.5.2 Higher order modes – consequence of $\Delta n_{sat}$

The fundamental optical mode was used for self-focusing in the SAC-01 waveguide. The oscillations of the output signal that begin at 540 seconds in Figure 4.10, signify the presence of higher order, optical modes in the evolving channel waveguide. As the refractive index of the self-inscribed waveguide increases, it is permitted to host multiple modes at the self-focusing wavelength. These modes have different propagation constants $\beta_m$, which beat at a periodic length = $\frac{2\pi}{|\beta_{m1} - \beta_{m2}|}$. At the waveguide output, this is indicated as a periodic oscillation in intensity[44].

A second mode in a self-induced waveguide has been observed in both Ge-doped silica[27] and chalcogenide ($As_2S_3$)[29] waveguides, where a similar oscillation of the output intensity was observed. In both cases, only one additional mode was detected on a time scale comparable to the one in our experiment. The irregular intensity and frequency of oscillations in the SAC-01 waveguide (Figure 4.10) suggest that there are more than two modes propagating in the waveguide. Indeed at the output of the waveguide, several m-lines could be detected as self-focusing progressed in the waveguide. These correspond to the intensity maxima belonging to the fundamental and the higher order modes.

$\Delta n_{sat}$ recorded in the SAC-01 composite is at least an order of magnitude greater than that for germanosilicates and photosensitive chalcogenides. The rapid and significant change in refractive index may permit the self-inscribed waveguide in the SAC-01 waveguide to support more than two optical modes.

The theoretical analyses of Monro and co-workers[23] predict that higher order modes can be populated in a self-inscribed waveguide. In the mathematical models, the interference between the modes is evidenced by the appearance of local intensity maxima (secondary eyes) in the evolving waveguide. Physically, this may be understood by considering the saturability of the self-focusing medium. As mentioned earlier as demonstrated in the SAC-01 waveguide, self-focusing will occur in a medium with a saturable refractive index change ($\Delta n_{sat}$). However, when $\Delta n_{sat}$ is approached, a gradient in $n$ is no longer present and the self-inscribed waveguide evolves towards an uniform refractive index profile. In effect, the waveguide becomes "wider not stronger"[7], thereby increasing its numerical aperture ($N_A$) and it ability to populate higher order modes. This is also the reason why saturation of $\Delta n$ prevents the catastrophic self-focusing, which occurs in a non-saturable medium.

### 4.3.5.3 Time scale

Although the sequence of events associated with self-focusing – formation of GRIN lens, focusing of the beam, channel waveguide formation – is common to all media, the time-scale associated with each process depends on the physical or chemical mechanism that underlies $\Delta n$. Previously, a comparison was drawn between the response times of Kerr media and the SAC-01 composite. In the former, refractive index changes are induced within femtoseconds and self-focusing occurs almost instantaneously. By contrast, in the SAC-01 composite $\Delta n$ is determined by the rates of polymerisation reactions, which vary from seconds to minutes as the reactions proceed. Note that this correlates to the time scale of the self-focusing event recorded in Figure 4.10. As mentioned above, the initial increase in intensity corresponding to the formation of the "primary eye" occurs within 10 minutes. The addition of the higher-order modes that occur in the next few minutes, are also related to further increases of n in the waveguide.

It is interesting to contrast the photo-response time in SAC-01 waveguide with the time required for self-focusing in Ge-doped silica waveguides. In the latter, refractive index changes may be induced only after several hours of exposure. Accordingly, the time-scale associated with self-focusing in the germanosilicates is also on the order of 8 hours. Similarly in PRCs, the refractive index change induced by a 1-10 μW laser beam is on the order of 0.1 to 1 seconds. As expected, self-focusing and self-trapping of the beam in the crystal is achieved within this time-scale.

### 4.3.6 Permanent record of self-focusing behaviour

One of the most powerful consequences of self-focusing through localised photochemistry is that the $\Delta n$ changes induced during the nonlinear optical event are permanent. By contrast, photo-induced $\Delta n$ changes in Kerr, PRC, semiconductor, resonant media are temporary *i.e.* once the optical field is removed, the photophysical mechanism underlying the refractive index change relaxes; in Kerr media, the polarised electron density returns to equilibrium. In absorptive and semiconductor media. the population also equilibriates once the pump laser is removed. In PRCs the charge carriers recombine with the opposite charges (although in certain crystals, this may take years).

As discussed previously, theory predicts that the photoinduced $\Delta n$ changes during the self-focusing event create a channel waveguide in the medium, which subsequently guides the beam and suppresses diffraction. In the NLO materials described above, this is a transient event made evident only by the narrowing of the streak of light at the surface of the medium. Once the optical field is removed, no trace of this waveguide remains in the medium.

By contrast in the SAC-01 slab, $\Delta n$ changes during the self-focusing event occur through a polymerisation process, a chemical change in the material that persists even after the optical field that originally induced it is removed. The medium thus bears a "frozen" record of the light-matter interaction that took place during the self-focusing event. Photo-polymerised regions of the SAC-01 composite are insoluble in common organic solvents. $\Delta n$ patterns induced by the self-focusing beam, can therefore be visualised by etching the film in *iso*-propanol to remove the non-irradiated regions. Through this process, a long, narrow fibre-like structure was revealed on the Si substrate. This is the channel waveguide inscribed by the self-focusing laser beam.

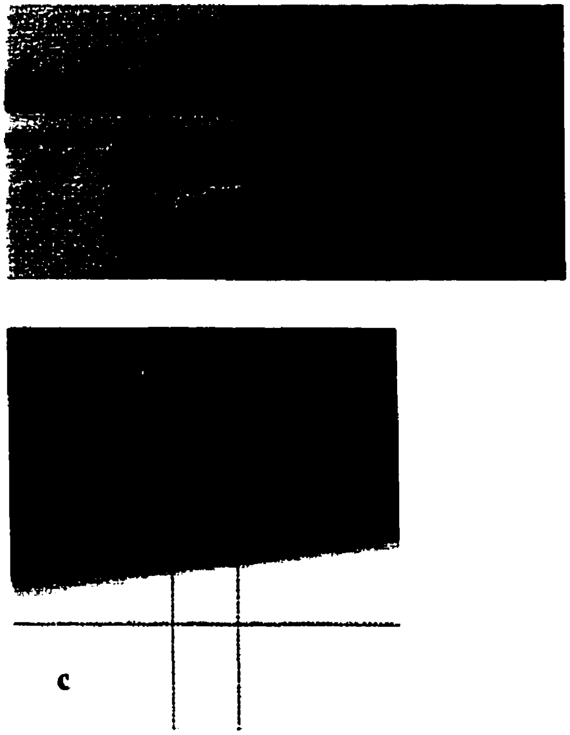

**Figure 4. 11(a-c)** Self-inscribed channel waveguide in SAC-01 medium showing a) scanning electron micrograph of non-etched b) optical micrograph of wet-etched and c) cross-section of the structure.

Figure 4.11a shows a partially wet-etched region of the SAC-01 slab, which reveals the narrow, densified channel waveguide buried within the non-irradiated regions of the film. Figure 4.11b features the completely wet-etched film supporting the roughly cylindrical waveguide. The optical micrograph in Figure 4.11c shows the elliptical cross-section of the waveguide, with a diameter (in the $y$ direction) of 10 µm.

The channel waveguide bears several imprints of the self-focusing event. Its walls are curved. Recall, that the intensity profile of the fundamental optical mode is circularly symmetric about the propagation axis. Polymerisation reactions are initiated within this circumference. Various sections of the structure, which run from the back edge of the coupling-prism to the output edge of the slab, were examined under the scanning electron microscope. The waveguide's width is approximately uniform along its entire length. This was a theoretically foreseen but until now unobserved feature[27]. According to the self-focusing model, once the refractive index maximum (GRIN lens) is formed and propagates along $z$, the region behind it approaches $\Delta n_{sat}$ and thus evolves into a particularly uniform channel waveguide. Although this feature should also have been observed in the other two cases of self-focusing through photochemistry, *i.e.* the Ge-doped silica and the chalcogenide glass, no efforts were made to physically characterise the self-written waveguides. As these materials themselves are difficult to treat and selective etching is difficult, the modified refractive index regions could have been identified with reflection or transmission optical microscopic techniques.

The self-inscribed waveguide in the SAC-01 slab is 40 mm long. We have observed channel waveguides as long as 120 mm in this composite medium. By contrast, the waveguides induced in germanosilicate and chalcogenide slabs, where self-focusing has been observed over only 11 mm and 4 to 5 mm, respectively. The relatively long distances over which self-focusing occurs in SAC-01 planar waveguides may also be traced to the mechanism of refractive index change. In photoinitiated free-radical polymerisation, both the laser beam and the initiator share the task of inducing $\Delta n$. The energy threshold in this photochemical reaction, determined only by the photoinitiator, is much lower than the two-photon process. In addition, the photoinitiation step (a one-photon process) has a considerably higher transition probability and unit quantum yield. Furthermore as the titanocene is the only absorbing species in the matrix, its consumption is marked by increasing transparency in the matrix. Therefore, the laser beam is able to propagate without significant attenuation, even as the refractive index of the medium evolves towards higher values.

The self-inscribed waveguide in Figure 4.11 indicates the significant degree of spatial localisation of free-radical reactions in the SAC-01 matrix. The curved walls of the feature as well as its uniform diameter, which remains constant over a longitudinal 40 mm imply that the free-radical reactions are localised to the path of the self-focusing beam in the waveguide. Unlike our finding, self-focusing of a UV (325 nm) beam in neat acrylate monomer liquid is difficult to achieve because the entire volume of monomer is readily polymerised due to diffusion of free-radicals[32]. To achieve self-focusing, polymerisation must be initiated with low intensity (5 mW) light pulses that were 1/16 seconds in duration and separated by 1- 10 seconds. Self-induced waveguides can be produced under these conditions but the structures are restricted to millimetre lengths. This system has the disadvantage that the acrylate monomer and polymer absorb UV light, causing attenuation of the propagating beam.

### 4.3.7 Device implications: fibre-on-a-chip

Ours is (to our knowledge) the first report of the creation of a circular waveguide in this manner, supported on a planar substrate. With its roughly circular cross-section, the structure may be described as an "optical-fibre on a chip". Current efforts to miniaturise and integrate optical devices on planar substrates must also account for their interconnection with existing optical-fibre based systems. Several decibels of power loss can be introduced in pig-tailing optical fibres to planar devices. Considerable research effort is being devoted towards resolving this problem. The self-inscribed waveguide described here may be developed into interconnect components between I-O devices and optical fibres. The rounded profile of the channel waveguide is impossible to make with photo-mask techniques. Its smooth walls would minimise scattering losses at sharp edges and offers geometric compatibility with optical fibres. In addition, the ability of the waveguide to support higher order modes indicates its high numerical aperture $N_A$, which is necessary for efficient coupling between optical fibres. Overall, the self-inscribed waveguide presents a strategy of employing light to inscribe its own path and thus define its own propagation conditions between device-device and device-fibre sites. Note also, that the self-focusing event implies that the waveguide has a GRIN profile, especially at the early stages of the process, *i.e.* before $\Delta n_{sat}$ is reached. This is a valuable property that is often used to counter dispersion of propagating pulses in optical fibres[2].

### 4.3.8 The quasi-local photo-response of SAC-01 composites

The diameter ($a$) of the laser beam incident on the SAC-01 planar waveguide was calculated to be approximately 4 μm whereas the diameter ($y$ direction) of its self-inscribed channel waveguide is 10 μm (see Figure 4.11c). This indicates that although the self-focusing beam induced a $\Delta n$ that is symmetric about its propagation axis $z$, the spatial extent of this region is (2.5 times) greater than the beam size. By contrast, $\Delta n$ induced through classical NLO processes such as the Kerr effect is highly localised in space. Here, both the intensity profile and the spatial dimensions of the self-focusing beam are exactly replicated in the medium. Yet, both types of photo-responses support self-focusing laser beams.

The difference in spatial response may be understood by considering the underlying physical mechanisms. As mentioned earlier, the $\Delta n$ induced by the Kerr effect is due to the electronic polarisation – an event that occurs with Å- scale spatial resolution and therefore depends critically on the intensity of the optical field at a particular point in space, *i.e.* $\Delta n$ is proportional to $I(\vec{r})$ (see Equation [4.1]). As a result of this highly localised $\Delta n$, the medium is able to reproduce the shape and the size of the typically micrometer wide beam with Å scale accuracy.

In SAC-01 composites, $\Delta n$ derives from free-radical polymerisation reactions. Here the intensity of the beam serves only to activate the photoinitiator molecules (see Equation 4.21). These then proceed to initiate the free-radical polymerisation of methacrylate substituents in their surrounding volume, which in turn creates a $\Delta n$ in the material. The crucial difference between the Kerr effect and the photochemical system lies here. In the former, the light intensity at a point in space ($I(\vec{r})$) is directly proportional to the photoinduced $\Delta n$ at $(\vec{r})$. In the latter, the intensity of the beam is "sensed" or integrated over the volume in which the free-radical reactions take place. Whereas in a Kerr medium, the $\Delta n$ would exactly replicate a 10 μm wide beam, the photochemical system studied here has a *quasi-local* response, where there is a 2.5-fold "enlargement" of the beam.

The term *quasi-local* signifies that although the photoinduced $\Delta n$ in the SAC-01 composite is not the same size as the beam, it still must have a GRIN profile for self-focusing to take place. As mentioned previously, this requires that the rate of polymerisation ($R_p$) (thus $\Delta n$) maximises at the axial regions and decays symmetrically in the transverse ($y$) direction. It is important to recognise that although the photo-response of the SAC-01 composite is non-local compared to the Kerr effect, the relative spatial confinement of the free-radical reactions in the silica matrix must play a significant role in creating the GRIN lens. In the planar waveguide, the greatest population of titanocene molecules is activated at the most intense, axial region of the beam ($x = 0$, $y = 0$) and it follows that $R_p$ is greatest at here and decreases with $\pm y$. In the silica matrix, these free-radical reactions cannot propagate over large distances and are confined to sub-micrometric lengths. Thus the greatest degree of polymerisation or conversion of methacrylate substituents will always be at the axial regions, with a decay along ± $y$. In this way, the different extents of polymerisation that occur at increasing transverse distances from the axis are registered in the final structure as a gradient in $\Delta n$.

#### 4.3.8.1 Similarities between quasi-local responses in PRCs and SAC-01 composites

Although their molecular origins are vastly different, an analogy may be drawn between the macroscopic photo-responses of SAC-01 composites and photorefractive crystals (PRCs). Refractive index changes in PRCs arise from a space-charge field $E_{sc}$, created when photo-generated charge carriers diffuse and are trapped in the crystal, leaving behind fixed charges of the opposite sign. In this case, the intensity variations in the laser beam determine only the population of charge carriers that are generated. The $\Delta n$ however, due to the $E_{sc}$ that generally relies on the thermal diffusion of these charge carriers over a volume ($\mu m^3$ scale). In PRCs, the photo-response is described as quasi-local because it is integrated over the volume in which diffusion takes place. The gradient in $\Delta n$ arises because the largest population of charge carriers are produced in the most intense (axial) region of the beam where the greatest $E_{sc}$ (thus $\Delta n$) is created. In the SAC-01 composite, the propagation of the free-radical reactions is spatially confined in the silica matrix, allowing the GRIN profile of the $\Delta n$. In PRCs the diffusion of the charge carriers is controlled by irregularities or defects in the material that act as traps. Thus the greatest number of charge carriers are trapped close to the axis with this population decaying along ± $y$, $x$. In this way, the gradient in refractive index required for self-focusing is created. Note that as in the case of the free-radical reactions, if the diffusion of the charge carriers were allowed over much longer distances, the gradient would not be created and the beam would not self-focus. In both SAC-01 composites and PRCs, the inorganic host controls the propagation or diffusion of the events that lead to $\Delta n$.

### 4.3.9 Power-dependence of self-focusing in materials with quasi-local response

In their efforts to bring physical insight into self-focusing phenomena, Snyder and Mitchell[49] pointed out that quasi-local responses to light depend on the intensity of the beam integrated over an area, *i.e.* its power P. The power dependence of the photoinduced $\Delta n$ is then described by the first two terms of a Taylor series expansion in the refractive index. (Only the first two terms were included as the beam, which is smaller than the response would only be affected by $\Delta n$ changes close to its propagation axis):

$$n^2(r,P) = n_0^2 - r^2\alpha^2(P) \qquad [4.23]$$

where r is the transverse distance from the beam centre (y = 0, x = 0) and $\alpha(P)$ is a material property. Equation [4.23] implies that a laser beam propagating in a material with a quasi-local response induces a $\Delta n$ with a parabolic profile, where the maximum $\Delta n$ = n (0,P) coincides with the axis, defined by the initial intensity profile of the beam. The intensity dependent $\Delta n$ in equation [4.11], which describes the propagation of electromagnetic waves in NLO media, may now be replaced with the power dependent one to give:

$$ikn_0\left(\frac{\partial \mathcal{E}}{\partial z}\right) + \tfrac{1}{2}\nabla_\perp^2\mathcal{E} - k^2\alpha^2(P)r^2\mathcal{E} = 0 \qquad [4.24]$$

The mechanical equivalent of this equation is the linear harmonic oscillator. This analogy greatly simplifies the solutions for equation [4.24]. Simple expressions can be found for the propagation of Gaussian shaped laser beams in materials with quasi-local photo-responses. For example, in a medium with a quasi-local photo-response, the radius of a Gaussian beam $I(z) = I_m(z)e^{-x^2/\rho^2(x)}$ (where $I_m$ for a 2-dimensional beam as in our case is $I_m(z) = P/\rho(z)\sqrt{\pi}$ ) varies along $z$ according to:

$$\frac{\rho^2(z)}{\rho_0^2} = \cos^2 qz + \frac{\alpha^2(P_c)}{\alpha^2(P)}\sin^2 qz \qquad [4.25]$$

where $\rho_0$ is the initial beam width, $q = \frac{\alpha(P)}{n_0}$ and the critical power $P_c$ is defined by $\alpha(P_c) = \frac{1}{k\rho_0^2}$.

This model of self-focusing in media with quasi-local responses can account for the behaviour of the SAC-01 composites. It can also complement the model proposed by Monro and co-workers[27]. Although these authors accounted for the temporal delay of the photoinduced Δn in these systems, both this research group as well as others[32] assume that the spatial localisation of Δn due to the free-radical reactions was comparable to that in a Kerr medium.

According to equation [4.24], self-focusing in a system with a quasi-local response may be described as follows. At low P, the photoinduced $\Delta n$ is insufficient to create a GRIN lens and the beam diffracts as it would in a linear medium. As P gradually increases, a radially symmetric parabolic lens is induced in the material and the beam self-focuses. Although the beam self-focuses and propagates without diffraction, at $P < P_c$ and $P > P_c$, Equation 4.25 indicates that the beam radius (ρ) radius varies in a sinusoidal manner as it travels in a straight line along z. Indeed this behaviour is characteristic of Gaussian beams that are focussed though GRIN parabolic lenses. At lower powers, this sinusoidal behaviour may be qualitatively explained by the tendency of the beam to diffract before self-focusing and at higher powers, this may reflect the tendency of the beam to self-focus before diffracting[49]. At $P = P_c$, the self-focusing is exactly balanced by the diffraction and the beam propagates without any changes to its radius, ρ. This is a spatial soliton.

### 4.3.9.1 Power dependence of self-focusing

Equation [4.24] describes self-focusing in a material with a quasi-local, power dependent response to monochromatic light, such as our SAC-01 composites. It also indicates that when these photochemical reactions are carried out at $P_c$, the medium might host spatial solitons. $P_c$ may be identified by monotonically increasing the P of the self-focusing beam to locate the point at which self-focusing is exactly balanced by diffraction.

We examined the self-focusing of the laser beam at various powers (P) in the SAC-01 slab waveguide. At this stage, our objective was not to observe spatial solitons but to probe the power-dependence of the self-focusing event, a crucial step in locating $P_c$. Self-focusing experiments were conducted at P = 5, 25, 100, 250 and 500 mW. In every case, the intensity at the waveguide-output was monitored during self-focusing, as in the example presented in Figure 4.10. The temporal profiles of the output-intensity are presented in Figures 4.12-4.14.

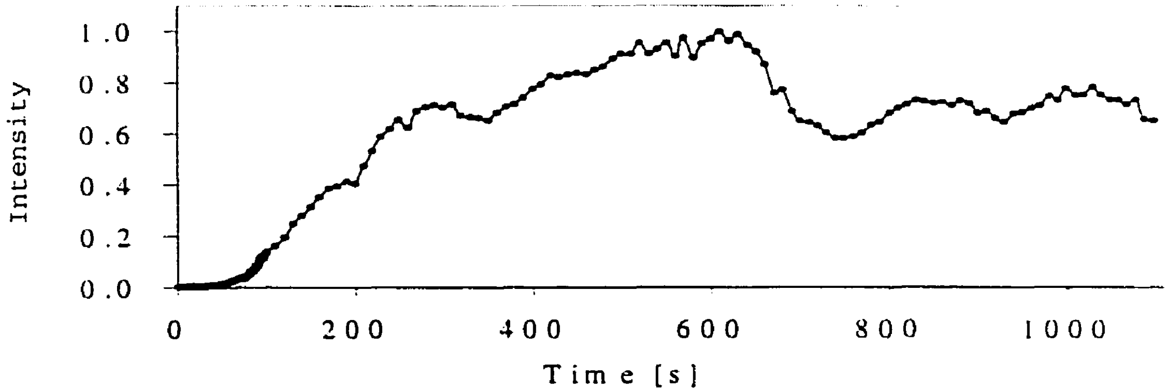

**Figure 4. 12** Time-intensity profile due to self-focusing of light at P = 5 mW

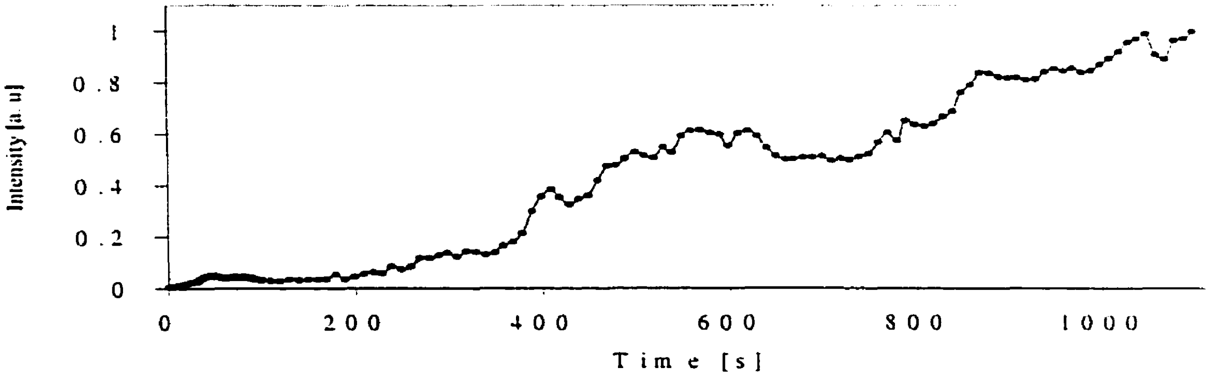

**Figure 4. 13** Time-intensity profile due to self-focusing of light at P = 25 mW

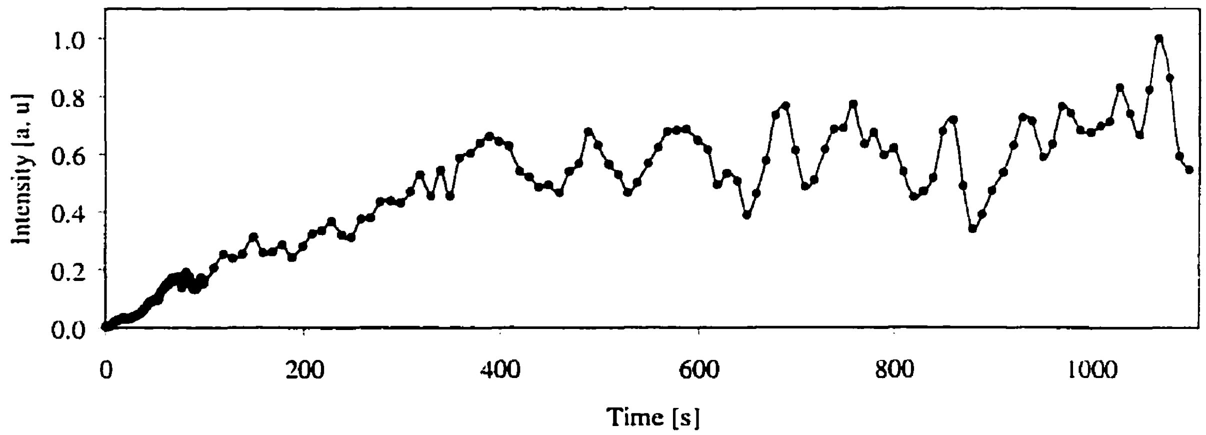

**Figure 4. 14** Time-intensity profile due to self-focusing of light at P = 250 mW

Several trends may be identified by examining Figures 4.12-4.14. At each P, there is an initial increase in intensity due to bleaching of titanocene photoinitiator. As the rate of titanocene activation is proportional to beam intensity, the photobleaching time decreases with increasing P (610 seconds at 5 mW, 40 seconds at 25 mW, 8 seconds at 100 mW). Except for the P = 250 mW, the output signal then flattens for a period of time (500 seconds at 5 mW, 70 seconds at 25 mW, 50 seconds at 100 mw). Following photobleaching, one observes a gradual increase in the output signal. As explained earlier, the increase in intensity signifies the onset of self-focusing of the laser beam, (*i.e.* formation of a channel waveguide in the slab). 300 seconds into the process, the relative intensity increases by 0.14 at 25 mW, 0.30 at 100 mW and 0.40 at 250 mW. At 5 mW, no increase in intensity is observed, and the signal remains relatively constant after photobleaching. This indicates that self-focusing of the beam has not occurred at 5 mW.

Our observations may be explained by considering the power-dependence of the free-radical polymerisation reactions. Recall that for self-focusing to take place the photoinduced $\Delta n$ in the form of a GRIN lens must counter the diffraction of light in the slab, *i.e.* $\Delta n > {}^{n}\!/_{2k^2a^2}$. It is possible that the brief plateau in the signal after photobleaching corresponds to the time that it takes for the polymerisation reactions to induce this required $\Delta n$. The duration of the intensity plateau decreases with increasing P because the rate of polymerisation $R_p$ is proportional to the power of the beam and the $\Delta n$ required for the GRIN lens is achieved at shorter times at greater values of P. Accordingly, in the case of the lowest power, P = 5 mW, the induced $\Delta n$ is too small for self-focusing to occur.

Trends in the waveguide output after the plateau may also be explained by accounting for the effect of the rate of polymerisation on $\Delta n$. For example, at 300 seconds, the greatest increase in intensity has occurred for P = 250 mW, whereas the least is observed for P = 25 mW. At this stage of the process, the greatest $\Delta n$ of the evolving channel waveguide will be at P = 250 mW and the smallest at P = 25 mW. It is well known that the greater the *n* of a channel waveguide, the more efficiently it is able to guide optical modes of a laser beam. Correspondingly, the greatest increase in output-intensity occurs for the channel waveguide induced by P = 250 mW. Similarly, oscillations due to higher order modes are observed only at P = 100 mW and 250 mW. This is also a consequence of the power-dependent polymerisation reactions. At 25 mW, the photoinduced $\Delta n$ is insufficient to introduce additional modes. By contrast at 250 mW where the $\Delta n$ is greatest, the oscillations arrive at 390 seconds whereas at 100 mW, they are observed at a later time (540 s).

#### 4.3.9.2 Self-focusing at P = 500 mW

The evolution of the output-intensity of the SAC-01 waveguide during self-focusing at P = 500 mW (Figure 4. 15) was similar to that observed at P = 100 mW and P = 250 mW. After photobleaching, a gradual increase in the signal was observed (300 seconds into the process the relative intensity was 0.5). This was followed by oscillations corresponding to the onset of higher order optical modes.

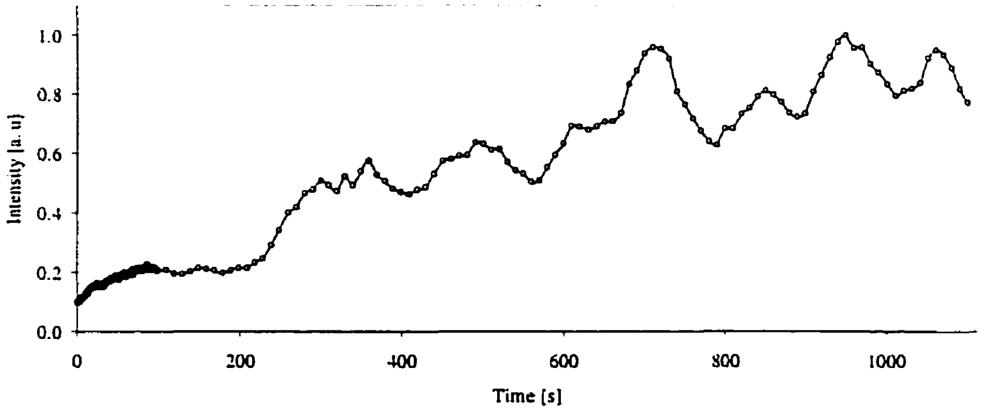

**Figure 4. 15** Evolution of waveguide output signal at during self-focusing at P = 500 mW

When the SAC-01 slab-waveguide was wet-etched after the 500 mW self-focusing experiment, an entire set of self-inscribed waveguides was revealed on the surface (Figure 4. 16 a-c). Significantly, the diameter of each of these structures undergoes a periodic oscillation. As seen clearly in Figures 4. 16 b and c, each waveguide undergoes a periodic (25 μm) change in its width from 10 μm to 5 μm throughout the entire length of the structure.

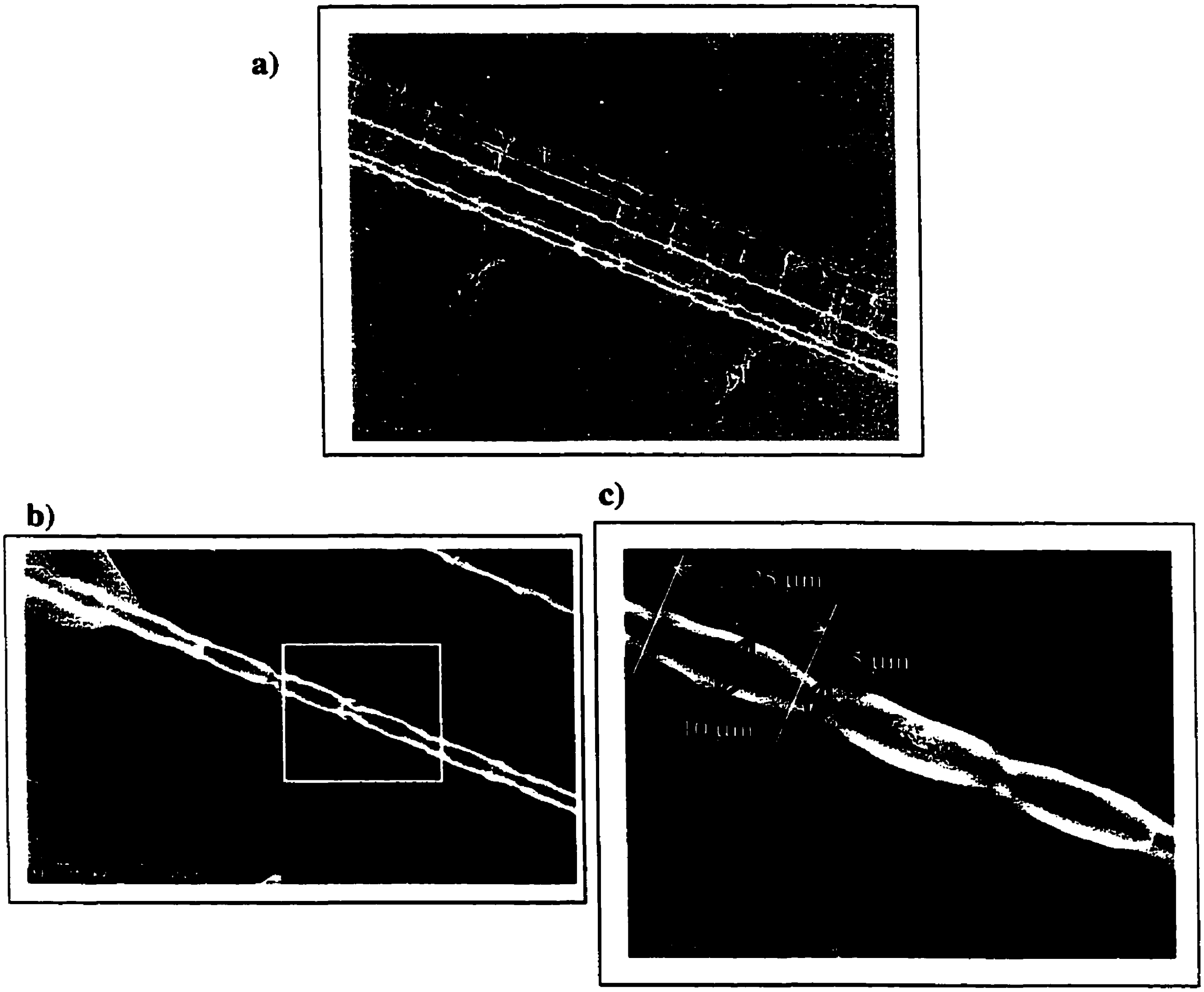

**Figure 4. 16 a**. Set of self-inscribed waveguides – evidence of filamentation at P = 500 mW, **b**. and **c**. "breathing" behaviour of waveguide diameter – oscillation with periodicity of 25 μm

Multiple waveguides created by a single laser beam, as well as the periodic variation in the diameter of these structures are features that correspond to the behaviour of self-focusing beams at powers far from $P_c$, the solution for the spatial soliton[51]. This behaviour is predicted by Equation 4.25, which describes the variation in the width ($\rho$) of a self-focusing beam in a medium with a quasi-local response. Note that when $P \neq P_c$, $\rho$ undergoes a sinusoidal oscillation along the propagation axis z. Figure 4.17[50] illustrates the behaviour of the beam diameter at powers that are equal to, greater or smaller than $P_c$.

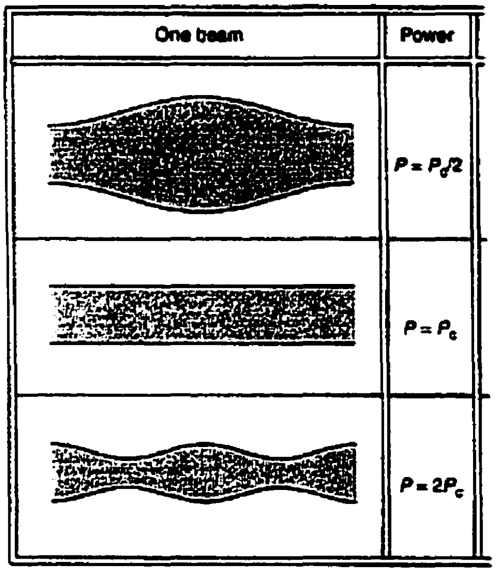

**Figure 4. 17** The power dependent, variation of beam diameter in a medium with a quasi-local photo-response

Note that at the critical power, the diameter of the beam does not vary as it propagates. At $P < P_c$, there is an initial divergence of the beam followed by refraction. The opposite occurs when $P > P_c$ and the beam contracts before diverging, leading to a sinusoidal variation in $\rho$. As shown in Figure 4.17, the "breathing" behaviour of the beam diameter strongly resembles the periodic modulation observed in the self-induced waveguides in our SAC-01 system. From this observation, we can deduce that at P = 500 mW, the self-focusing beam underwent periodic expansion and contraction in the SAC-01 medium, as predicted by equation 4.25 and Figure 4.17. As the photoinitiated free-radical reactions occur in a spatially confined manner in the SAC-01 composite, the resulting polymerised structures *i.e.* the self-induced waveguides faithfully record the spatial variations of the beam, along the propagation axis.

The expansion and compression cycles of the radius of self-focusing beams have also been observed in PRCs at beam powers well removed from $P_c$[50]. Additionally, the simultaneous creation of several waveguides at P = 500 mW, indicates the filamentation or break-up of the beam during the self-focusing process. This too, is characteristic of self-focusing phenomena at high laser powers. For example, the break-up of the beam into several filaments with equal diameters has also been observed at $P > P_c$ in Kerr media[14].

### 4.3.10 The chemistry of self-focusing

#### 4.3.10.1 Photochemical mechanisms underlying self-focusing in hybrid organosilica media

We have argued that self-focusing of light in the SAC-01 medium occurs through a photochemical process, namely the free-radical polymerisation of propyl methacrylate substituents. From the studies described in Chapters 2 and 3, we attribute refractive index changes in films of the SAC-01 composite to photoinduced polymerisation of the organic monomer component and the consequent densification of its silica host. However, as mentioned earlier, there have been some reports of light induced refractive index changes in purely inorganic silica[24]. To prove that self-focusing of light in the SAC-01 medium originates exclusively from the photoinitiated polymerisation of the organic component, the following control experiments were conducted.

##### 4.3.10.1.1 Self-focusing of 514.5 nm light in a silica-acetate slab waveguide

SAC-05 is the "saturated" analogue of SAC-01 derived. The sample was prepared, doped with PMMA and the titanocene photoinitiator. Our aim was to create a hybrid network that was chemically and structurally similar to the SAC-01 composite but that lacked the photo-polymerisable vinyl groups. The precursors chosen for SAC-05 were 3-acetoxy propyltrimethoxysilane, zirconium *n*-propoxide and isobutyric acid. Note that the acetate unit is roughly equivalent to the methacrylate functionality minus the C=C moiety. Similarly, the isobutyric acid is included as a "saturated" analogue of the methacrylic acid complexing agent in SAC-01. Thus, the most significant difference between the two composites SAC-01 and SAC-05, is the absence of the C=C functional group in the latter. Therefore, guided optical waves propagating in SAC-05 waveguides do not initiate the formation of a secondary organic network by photo-induced free-radical polymerisation.

The self-focusing experiment with the 514.5 nm line of an $Ar^+$ laser at P = 100 mW, outlined in Section 4.3.5 for the silica-methacrylate (SAC-01) composite was repeated for the silica-acetate (SAC-05) material. Once the laser beam was in-coupled to the SAC-05 planar waveguide, we monitored the output-signal over time (Figure 4. 18). The temporal evolution of the signal contains no indications of laser self-focusing in the SAC-05 medium. In Figure 4. 18, there is an initial, sharp increase in intensity within the first 14 seconds, due to photobleaching of the titanocene photoinitiator molecules that are present in the matrix. The output-signal then rapidly plateaus and shows neither the significant increase in intensity nor the oscillations due to higher order modes, which are characteristic of a self-focusing beam of light (The random oscillations that are present throughout the graph are due to poor signal to noise ratio values).

The absence of self-focusing in sample SAC-05 demonstrates that laser self-focusing in SAC-01 arise through a spatially localised, free-radical polymerisation process in the hybrid composite.

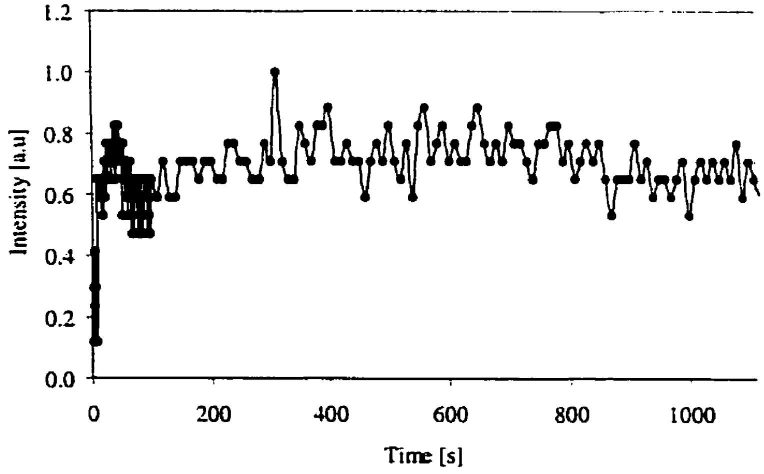

**Figure 4. 18** The evolution of waveguide-output signal in a SAC-05 waveguide

#### 4.3.10.1.2 The role of the different methacrylate species in laser self-focusing

Recall that the SAC-01 composite contains two types of methacrylate species, the propyl methacrylate substituent of the alkoxysilane precursor as well as the methacrylic acid units complexed to the zirconium alkoxide precursor. Our FT-IR spectroscopic studies indicated that both of these species undergo free-radical polymerisation reactions upon UV irradiation (Chapter 2, Section 2.3). To selectively examine the role of each type of methacrylate in the self-focusing process, we designed two other composites, SAC-04 and SAC-03 (Section 4.2.1).

In SAC-04, the zirconium *n*-propoxide precursor was complexed with isobutyric acid so that the only polymerisable groups in the matrix were the propyl methacrylate substituents. Self-focusing of a 100 mW, 514.5 nm laser beam in a SAC-04 planar waveguide is presented in Figure 4. 19. The output-intensity varies significantly over time. From its relative intensity of 0.73 at t = 28 seconds, the signal decreases to a minimum of 0.18 at t = 305 seconds. It then gradually increases to a maximum value of unity at t = 765 seconds, before decreasing to 0.46 at t = 935 seconds. Although this wide oscillation in the output-signal may signify the presence of a higher order mode supported by the self-induced waveguide, the frequency of the oscillation contrasts sharply with the rapid oscillations observed within the same time frame, during self-focusing in the SAC-01 planar waveguide (Section 4.3.5.1). The variation in output intensity of the SAC-04 waveguide indicates that laser induced refractive index changes do take place in the material. However, the change is not sufficient to populate several higher order modes, as is the case in the SAC-01 material.

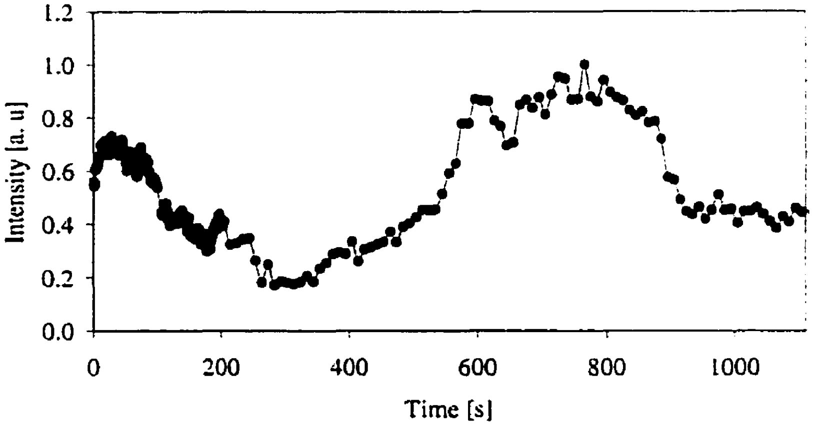

**Figure 4. 19** Behaviour of a 100 mW, 514.5 nm laser beam in a SAC-04 planar waveguide

In sample SAC-03, the 3-acetoxypropyl trimethoxysilane precursor replaced MAPTMS, leaving MAA as the only unsaturated units. The output-intensity of a 100 mW, 514.5 nm laser beam propagating in a SAC-03 waveguide is presented in Figure 4. 20. There is an initial increase in relative intensity from 0.6 at t = 5 seconds to 1 at t = 515 seconds. The signal then decreases to 0.6 at 735 seconds, before remaining approximately constant. Again, the extent of self-focusing is not the same as observed in the SAC-01 composite. The initial increase in intensity in the SAC-04 material may be indicative of a refractive index increase in the medium. However, the 10-fold increases in output intensity as well as the oscillations due to higher order modes that are observed in the SAC-01 material within the same time frame, are absent here.

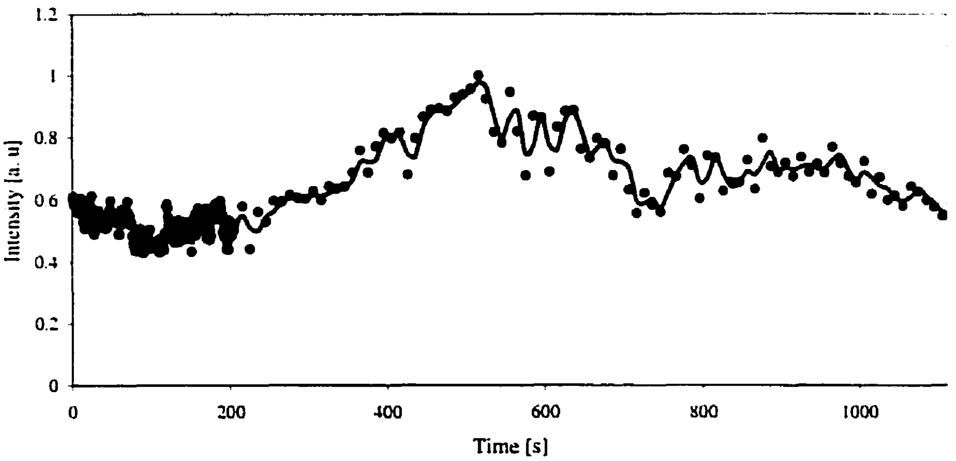

**Figure 4. 20** Behaviour of a 100 mW, 514.5 nm laser beam in a SAC-03 planar waveguide

Overall, both of these experiments indicate that the laser-induced refractive index changes in the SAC-03 and SAC-04 were insufficient (relative to the SAC-01 composite) for laser self-focusing to take place. As both of these experiments were conducted under the same conditions (laser power, time frame) as the SAC-01 self-focusing experiment, we can deduce that the polymerisation of both types of methacrylate groups is necessary for self-focusing to occur.

#### 4.3.10.2 Role of the covalent bond linking the methacrylate groups: guided optical wave polymerisation of free methacrylate monomer in a silica-acetate matrix

Not all free-radical polymerisation processes can give rise to self-focusing of light. We have emphasised that the spatial localisation of photo-induced changes in the SAC-01 composite is one of the key parameters that enables self-focusing to occur. The confinement of free-radical reactions to illuminated areas in the hybrid matrix, arises partly because polymerisable units are covalently linked to either a silicon or zirconium centre, which are themselves part of a cross-linked inorganic network. We studied the importance of the methacrylate units being permanently grafted to a pre-formed inorganic network by examining laser self-focusing in a sol-gel derived silica host doped with *free* methacrylate monomers. SAC-06 consisted of the saturated glass derived from 3-

acetoxypropyltrimethoxysilane and isobutyric acid derivatised zirconia, doped with methacrylic acid.

Figure 4.21 plots the temporal profile of a 100 mW, 514.5 nm beam propagating in a SAC-06 planar waveguide. The evolution of the output-intensity indicates channel waveguide formation and thus laser self-focusing in the silica-methacrylic acid medium. The intensity increases from 0.23 at t = 34 seconds to 0.43 at t = 77 seconds, at which point oscillations in the signal indicate the onset of higher order modes. However, the signal drops significantly from 0.73 at t = 554 seconds to 0.32 at t = 684 seconds.

Self-focusing due to free-radical polymerisation of methacrylic acid monomer in the sol-gel derived silica host occurs at a much faster rate than in the SAC-01 composite with the covalently bound methacrylate units. In Figure 4.21, this is indicated by the rapid onset of higher order modes at t = 77 seconds, relative to t = 540 seconds in the SAC-01 composite. Faster self-focusing dynamics in turn, imply the faster rate of photoinduced refractive index changes (and thus free-radical polymerisation) in the SAC-06 medium. It is evident that the free methacrylic acid monomers would have greater mobility in the SAC-06 matrix than the covalently anchored propyl methacrylate units in the SAC-01 material. Therefore, a greater rate of polymerisation is observed in the former.

However, self-focusing in the SAC-06 seems to be disrupted at t = 554 when there is a significant attenuation in beam intensity. It is possible that rapid organic polymer chain growth in the material leads to phase separation between organic and inorganic components, which could introduce inhomogeneities in the medium. If these phase separated regions have dimensions that correspond to visible light wavelengths, the propagating beam would suffer scattering and thus undergo attenuation in the medium. Indeed, when the SAC-06 was wet-etched, a milky, white residue was observed on the substrate. By contrast, when the SAC-01 waveguides are wet-etched, the self-induced channel waveguide remains transparent to visible light. The covalently bound methacrylate units in the SAC-01 composite thus prevent phase separation by spatially confining polymer chain growth.

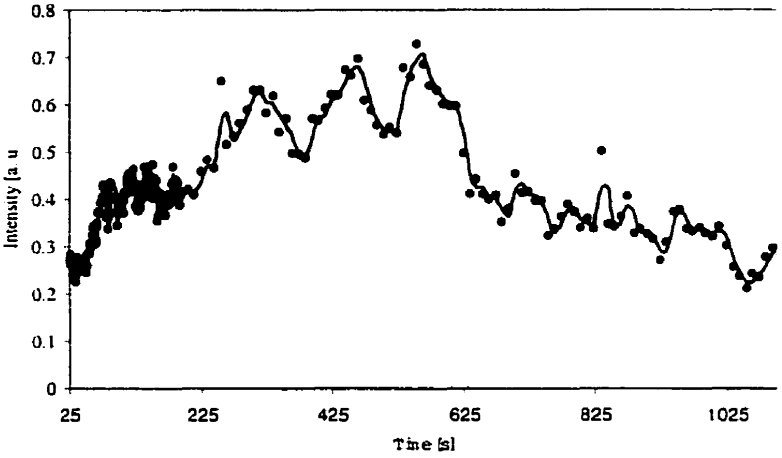

**Figure 4. 21** Behaviour of a 514.5 nm, 100 mW laser beam in a SAC-06 planar waveguide

### 4.3.10.3 Self-focusing of light in other silica-methacrylate waveguides

#### 4.3.10.3.1 Self-focusing in SAC-09 slab waveguides

Laser self-focusing was observed in two other types of sol-gel derived silica-methacrylate composites, SAC-08 and SAC-09. The SAC-09 material was derived from 3-methacryloxypropyldimethoxysilane. We expected the hydrolysis and condensation reactions of the bifunctional alkoxysilane to form a less cross-linked, more open network. The evolution of output-intensity over time of a 514.5 nm, 100 mW beam in a SAC-09 waveguide is presented in Figure 4.22.

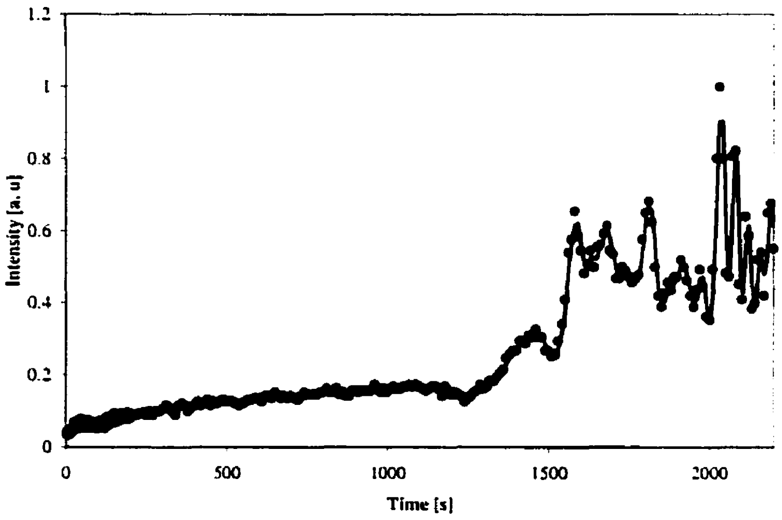

**Figure 4. 22** Temporal evolution of self-focusing laser output-intensity in a SAC-09 planar waveguide

Laser self-focusing is evidenced by an eight-fold increase in relative output-intensity at t = 1460 seconds. Signal oscillations that indicate the population of higher order modes commence at t = 1510 seconds. The principal difference between the self-focusing event in the SAC-01 and SAC-09 networks lies in the response-time scale. Under identical conditions, the output-intensity of the self-focusing beam shows a 10 fold increase at t = 540 s in the SAC-01 waveguide. Oscillations due to higher order modes also begin at this point in time. Note that the corresponding events in the SAC-09 waveguide take place at more than twice these time intervals.

The longer response time of the SAC-09 medium corresponds to the decreased rates of photo-induced, refractive index increase in the material. In turn, this may be traced to the relative rates of free-radical polymerisation in the silica-methacrylate composite. The rate of UV initiated polymerisation of methacrylate units in SAC-09 thin films was monitored through FT-IR spectroscopy. Figure 4.23 graphs the depletion of the ν(C=C) absorbance band with increasing exposure time.

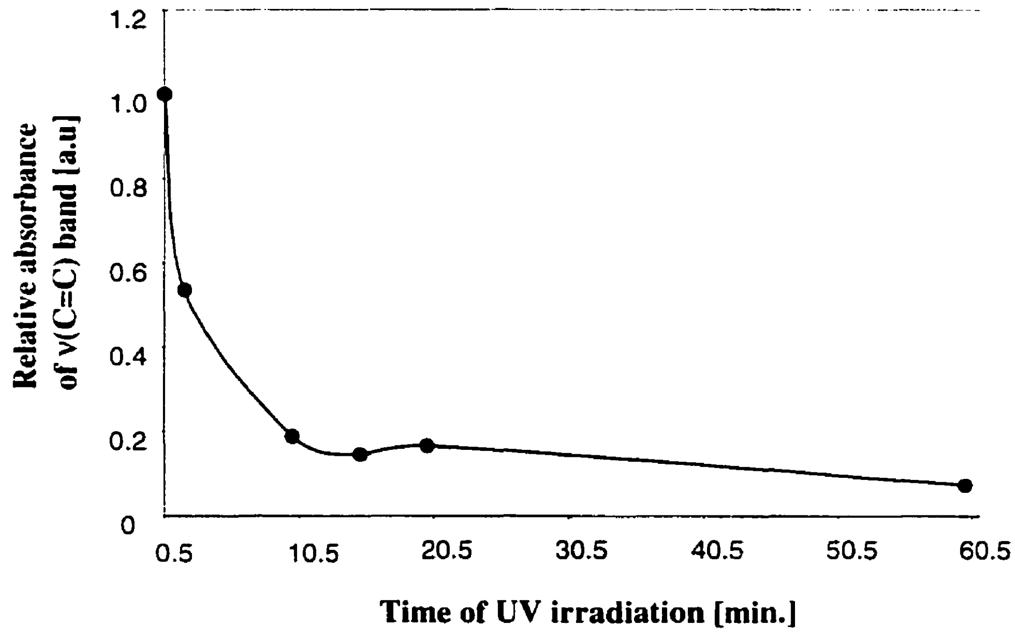

**Figure 4. 23** Consumption of vinyl groups in SAC-09 thin film upon UV irradiation.

The slower rate of free-radical polymerisation in the SAC-09 composite relative to the SAC-01 composite, is evident by comparing the percent conversion of vinyl units during the same period of irradiation. In the case of UV-initiated polymerisation in SAC-01 thin films (Chapter 2, Section 2.3), the relative intensity of the v(C=C) band indicated that 51 % of the methacrylate populations had been saturated within two minutes of UV irradiation. From Figure 4.23, this value is found to be 46 % for the SAC-09 composite.

#### 4.3.10.3.2 Laser self-focusing in SAC-08 slab waveguides

The SAC-08 material was derived from 3-methacryloxymethyltrimethoxysilane, through the same processing conditions as the SAC-01 material. The only difference between the SAC-08 and SAC-01 composites was the alkyl spacer linking the methacrylate functionality to the Si centre. In the former, this is a methyl group whereas a propyl chain links the methacrylate in the latter. Our intention was to probe laser self-focusing in a medium where the photo-polymerisable unit is less flexibility, relative to the SAC-01 medium. We expected the shorter spacer to reduce the flexibility and mobility of the organic substituents in the SAC-01 composite. In turn, this would reduce the rate of light-induced free-radical polymerisation (and refractive index change) in the medium. In the context of laser self-focusing, the reduced rate of refractive index change would correspond to an increase in the "response time" of the material. Figure 4.24 shows a FT-IR of the SAC-08 thin film.

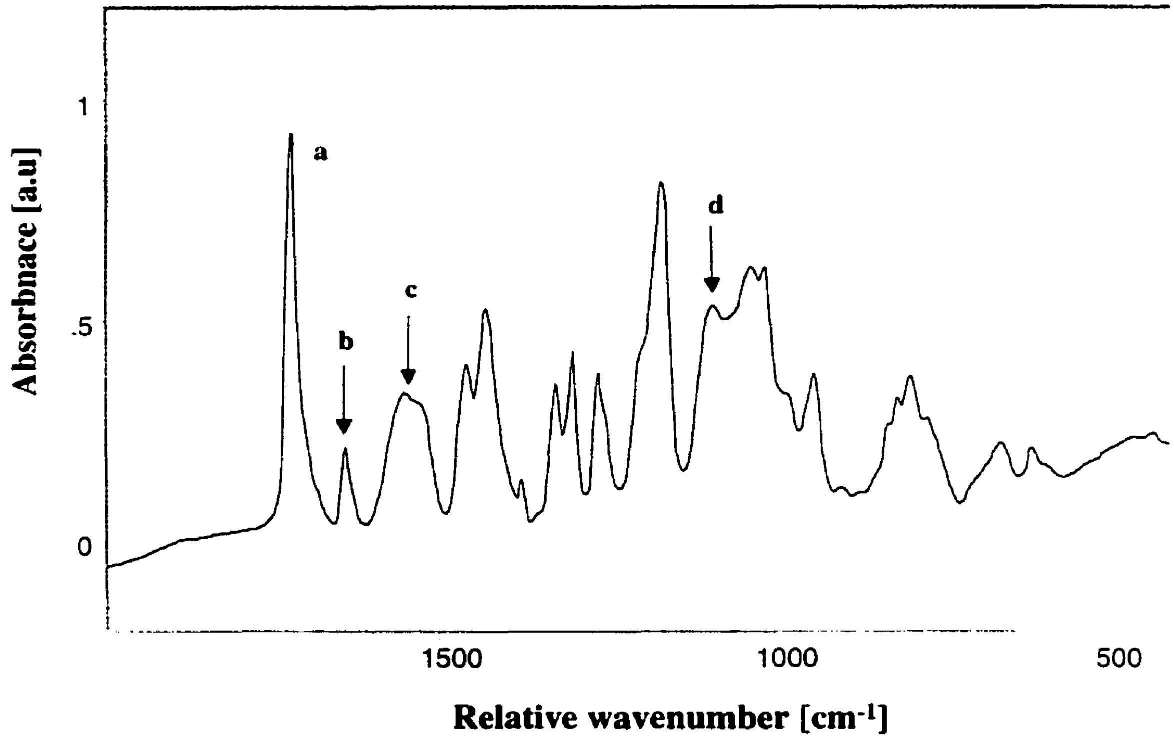

**Figure 4. 24** Mid-IR absorbance of SAC-08 thin film

Bands a and b at 1720 $cm^{-1}$ and 1636 $cm^{-1}$ are assigned to the ν(C=O) and ν(C=C) modes of the propyl methacrylate substituent. The ν(C=O) mode of the methacrylic acid-derivatised zirconia clusters occurs at 1550 $cm^{-1}$ (band c). The relatively narrow $\nu_{as}$(Si-O-Si) band occurs at 1090 $cm^{-1}$. In the SAC-01 composite, this band was broad and occurred at a shorter wavenumber 1060 $cm^{-1}$ (Chapter 2, Section 2.3). The higher energy and the narrow bandwidth of this mode signify a silica network that has a narrow distribution of relatively wide Si-O-Si angles.

Figure 4.25 presents the output intensity of a self-focusing beam (P = 100 mW, 5145. nm) propagating in the waveguide, versus time.

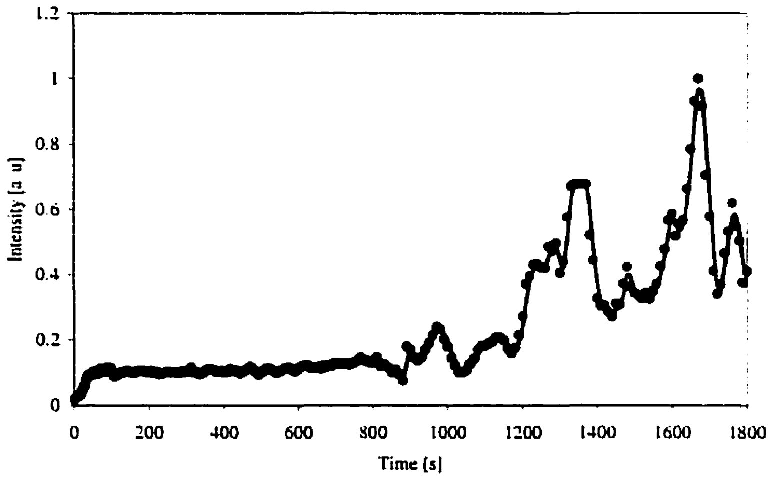

**Figure 4. 25** Temporal evolution of a 100 mW, 514.5 nm laser beam in a SAC-08 planar waveguide

There is a 2-fold increase in output intensity from t = 50 seconds to t = 970 seconds, at which point mode beating is apparent. The slower response time of this medium may also be related to the polymerisation kinetics of the composite. Figure 4.26 plots the depletion of the absorption band of the vinyl substituent (band b) at various times during UV irradiation in SAC-08 thin films. The rate of polymerisation contrasts sharply with that observed in the SAC-01 thin films. In the latter, 32 % of vinyl groups had been consumed after 30 seconds of irradiation. In the SAC-08 matrix, only a 13 % decrease in methacrylate population is observed during the same period. Similarly, after 2 minutes, there is 51 % conversion in the SAC-01 composite and only 26 % in the SAC-08. 68 % conversion has occurred in the SAC-01 matrix after 5 minutes of irradiation whereas in the SAC-08, 51 % conversion has taken place.

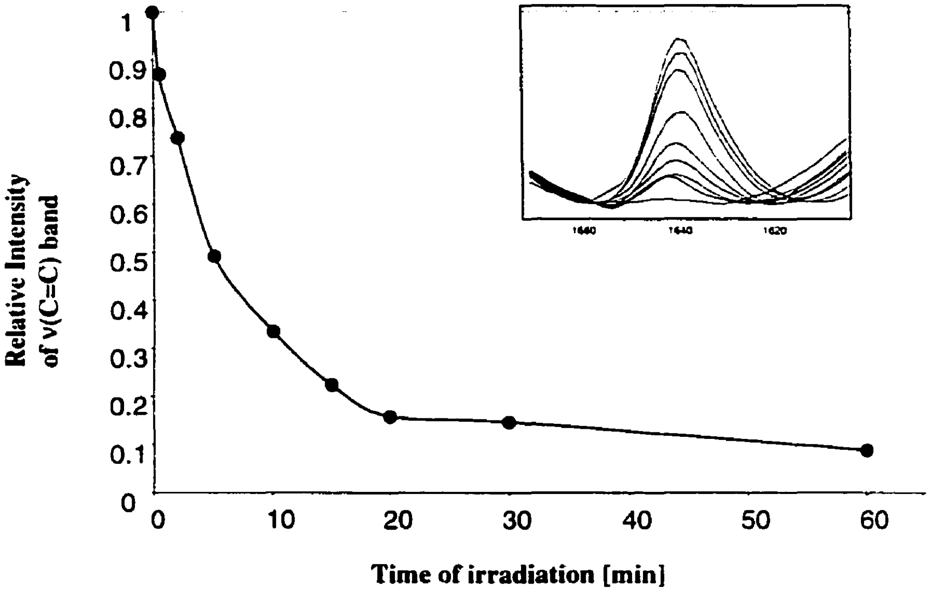

**Figure 4. 176** Decreasing intensity of the v(C=C) band (inset) with increasing time of UV irradiation in SAC-08 thin film.

The experiments collected in the previous Section reinforce our notion that the self-focusing event is mediated by photo-initiated organic polymer chain growth hosted in a silica matrix. Control experiments with "saturated" versions of the SAC-01 composite confirmed that laser-induced refractive index changes are associated with C-C bond formation due to polymerisation in the medium. In addition, our studies indicate that both types of methacrylate species in the SAC-01 are required for laser self-focusing. We have also demonstrated the significance of spatially localised photo-responses to the self-focusing event by studying photo-polymerisation of free methacrylic acid monomer in silica waveguides. Finally, we have shown that temporal evolution of self-focusing may be varied by altering molecular features that influence the rate of polymerisation in the organosilica nano-composites.

### 4.3.11 Self-focusing of incoherent white light in a SAC-01 colloid

The experiments presented thus far in this Chapter described the self-focusing of a monochromatic, laser beam in a planar SAC-01 waveguide. Indeed, the majority of experimental and theoretical studies into self-focusing phenomena has considered only the single-wavelength, coherent laser beam. In 1997 this apparently fundamental tenet of self-focusing and optical spatial solitons was overturned when Mitchell and Segev[52] demonstrated the self-trapping of white light from an incandescent (quartz-tungstenhalogen) bulb in a photorefractive crystal. This broadband, multimode light source produces a temporally and spatially incoherent wave-packet, consisting of a spectrum of wavelengths (380 – 720 nm) with randomly fluctuating phase profiles in space. Yet when this rapidly changing light beam was focussed onto the face of a SBN photorefractive crystal, self-focusing and subsequently self-trapping in the medium was observed. In this Section, we present preliminary evidence for the self-focusing of unpolarised, incoherent white light in a photosensitive SAC-01 colloid.

Theoretical models for the self-trapping of incoherent light beams[52] have identified three principle features that enable this event. These are i) a non-instantaneous, nonlinear response of the medium ii) a multimode waveguide self-induced by the multimode beam iii) the ability of this beam to guide itself in the self-induced waveguide, a requirement termed self-consistency. We now show how all these conditions are satisfied by the SAC-01 composites.

#### 4.3.11.1 Non-instantaneous nonlinear response

This requirement refers to the time interval between irradiation and refractive index change ($\Delta n$), *i.e.* the photo-response time of the medium. Specifically, the response time must exceed the temporal scale at which phase changes occur across the incoherent beam. At a given point in time, phase fluctuations create a random "speckled" pattern of bright and dark spots across the beam. Over time, this pattern undergoes random fluctuations at extremely high rates – on the order of femtoseconds. When the photo-response of the material exceeds this time scale, the material "sees" or responds to only the time-averaged envelope of the incoherent beam. In this way, the $\Delta n$ changes are mutually induced by the superimposed intensity of all the components in the beam. The delayed photo-response of the SAC-01 composites and its effect on the self-focusing of a 514.5 nm laser beam were discussed in previous Sections. Here, the photo-initiated polymerisation reactions that induce $\Delta n$ have reaction times on the order of seconds to minutes, which exceed the femtosecond coherence times of the white light source. Thus the condition of a non-instantaneous nonlinearity is satisfied. In the PRC experiment mentioned above, the required non-instantaneity was achieved with a very low intensity beam of white light (70.8 nW) ensured a long response time from the medium and the self-trapping event occurred over 2.5 hours.

The importance of a non-instantaneous response becomes evident when the alternative is considered. A material with a virtually instantaneous NLO response such as a Kerr medium, would be sensitive to the "speckled" nature of the beam and to its temporal fluctuations. In such a medium each "bright" spot of the beam would self-induce its own GRIN lens and waveguide. In addition, the position of these waveguides would change according to the random spatial and temporal phase fluctuations, leading to filamentation or break-up of the beam of white light.

### 4.3.11.2 Multimode waveguide from a multimode beam

This requirement states that a common waveguide must be induced by all the different frequency components of the incoherent beam. Furthermore, the waveguide must simultaneously guide all of these multimode frequency components, *i.e.* wavelengths from 380 to 720 nm. In most examples of self-focusing and spatial solitons, the self-induced waveguide supports only the fundamental mode of a monochromatic beam. Higher order modes may also be populated in waveguides created in media such as SAC-01 composites and PRCs, which have saturable refractive indices ($\Delta n_{sat}$). As $\Delta n_{sat}$ is approached in a self-inscribed waveguide, its refractive index profile becomes more uniform and the gradient in n, which allowed self-focusing to take place, becomes smaller. In effect, the waveguide becomes "wider", not "stronger" and is able to host multiple optical modes. Previously, we showed that an initially single optical mode photoinduced a multimode channel waveguide in a SAC-01 slab, a precedent that implies that a multimode beam would also induce a multimode waveguide in the SAC-01 medium.

### 4.3.11.3 Self-consistency

This term refers to the ability of the incoherent beam to guide itself in its self-induced waveguide, without changing the refractive index profile of the waveguide. If the modes hosted in a single waveguide are coherent, their interference leads to intensity variations, which may affect the evolving $\Delta n$ profile of the waveguide. A single waveguide may host several modes of the same polarisation if they are mutually incoherent, *i.e.* their interference occurs on a time-scale much smaller than the response time of the medium. For example, multimode waveguides were inscribed in a PRC crystal by combinations of one-dimensional, first and second order and second and third order optical modes of two mutually incoherent visible laser beam[54]. Here, the interference between the optical modes occurred at 0.3 ns intervals whereas the response time of the PRC was 0.1 s. As a result, the waveguide was induced by the superimposed intensity of the modes and was not sensitive to the intensity variations caused by their interference. Thus the modes propagated in their jointly induced waveguide without interference, maintaining their individual intensity profiles. At the output, this was observed through the multiple maxima or "multihumps" in the intensity corresponding to the double and triple amplitude maxima characteristic of second and third order optical modes.

Similarly, the optical modes comprising the beam of white light are incoherent with respect to each other in a medium with a non-instantaneous nonlinearity. Their phase fluctuations occur on a time scale that is much faster than the nonlinearity response of materials such as PRCs and the SAC-01 composite Once again, the medium responds to the superposition of the intensity and is not sensitive to the interference between the modes that occur on a femtoseconds time scale. Thus modes could coexist in the same, self-induced waveguide because of their mutual incoherence. In this way, the white beam may propagate without diffraction or filamentation across the medium with a non-instantaneous nonlinearity. This has been observed in PRCs and as will be described in the following Section, in a SAC-01 composite.

### 4.3.11.4 Self-focusing of white light in a SAC-01 sol

We present preliminary evidence for the self-focusing of white light in a SAC-01 sol. A Hg lamp was used for this experiment. The broadband light (230 nm to 500 nm) from this lamp was collimated into a beam and focussed onto the entrance face of a glass phial containing the SAC-01 sol sensitised with Irgacure 819™. The beam size at the face of the phial was approximately 3 mm and its power, measured at 253.7 nm, was 2 mW-cm$^{-2}$. The self-focusing behaviour of the white beam in the colloid is presented as a sequence of video clips of the event in Figure 4.27.

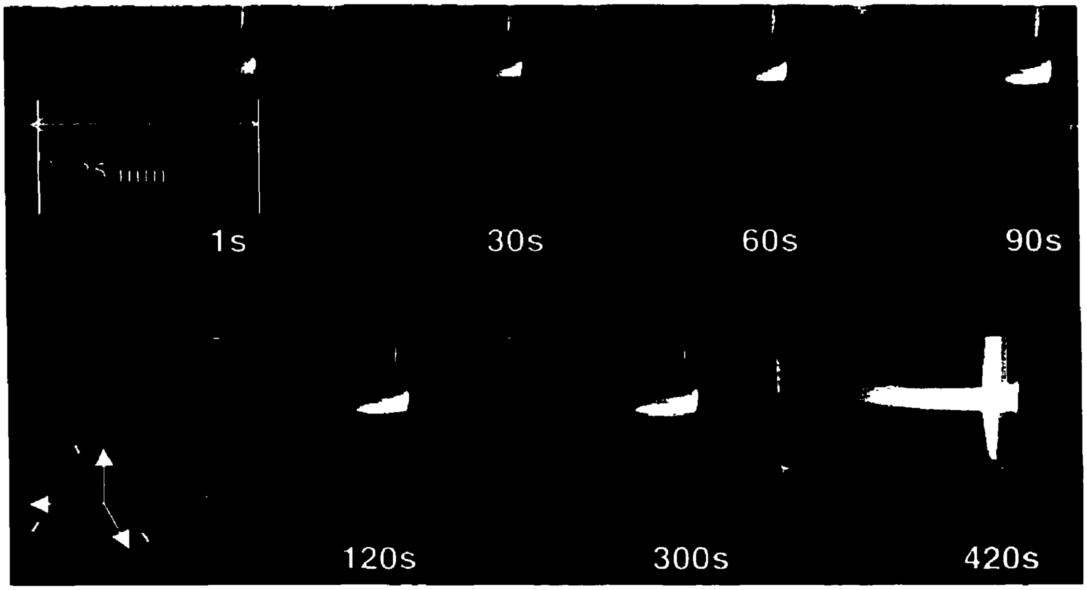

**Figure 4. 18** Self-focusing of white light in a SAC-01 colloid

Initially, the refractive index of the medium may be considered to be homogenous and the maximum of the beam was at the face of the glass vessel. However, within 1 second the beam was focussed along its propagating axis $z$ further into the colloidal medium. (The location and the profile of the beam are evident by its bright white scatter in the medium). The focusing action of the beam in the medium is evident by the narrowing of its beam diameter at the "focal" point which converges at $x = y = 0$. This observation signifies that the beam, through the photo-initiated polymerisation reactions, had induced a GRIN lens in the colloid close to the entrance face, which was able to counter the diffraction of the beam and focus it along $z$.

With time, three events take place: i) The self-focusing action of the white beam persists as it propagates along z. This is seen Figure 4.27 as the advancement of the focal point of the beam. It is important to note that the self-focusing action counters diffraction in both the $x$ and $y$ directions in the fluid medium. ii) The region behind the focal point of the beam evolved into a single waveguide that captured the oncoming white light within its walls. Note that the remainder of the colloidal medium is remarkably inert and remained fluid (unpolymerised) throughout the process. It is evident that some radiation escapes the self-evolving waveguide. However, the intensity of light in the waveguide region suggests that most of the white beam is captured here. iii) In addition to growing along $z$, the waveguide broadened in both the $x$ and $y$ directions.

These observations are qualitatively similar to the sequence of events that characterise self-focusing: the formation of the GRIN lens, the advancement of the beam along $z$ through self-focusing and the simultaneous formation of a channel waveguide. However, the key difference in the experiment described here is the incoherence and polychromatic nature of the self-focusing beam. This experiment indicates that the photo-initiated polymerisation reactions, which underlie $\Delta n$ in the SAC-01 composite, obey the three conditions outlined in the previous Sections. The formation of the GRIN lens and the focusing of the multimode wavepacket, which is spatially and temporally incoherent indicates that the rate of the free-radical reactions is determined by the time-averaged envelope of the beam. As mentioned earlier, this corresponds to the non-instantaneous nonlinearity of the composite. Furthermore, conditions ii and iii are satisfied as the beam induces a single waveguide in the composite that effectively guides all the components of the white beam. As mentioned before, the only previous observation of self-focusing has been in PRCs. This initial study indicates that self-focusing through localised photochemistry may be extended from coherent laser beams to incoherent light sources.

As in the case of self-focusing in the SAC-01 planar waveguide, the waveguide self-induced by the white light beam is permanent (Figure 4.28). The self-inscribed structure protruding from the phial wall is transparent to the naked eye and has smooth, rounded walls. In this sample, the self-focusing process was arrested midway into the phial and the "focal point" of the beam is seen in the resulting structure by the gradually decreasing diameter of the waveguide walls that converge to a rounded, smooth point at a distance ($d_{s.f.}$ = 12 mm) from the entrance. As mentioned earlier, the efficient confinement of the white beam in this self-inscribed waveguide protects the remainder of the colloidal medium from polymerisation. This self-inscribed structure remains suspended in a completely fluid medium. This may be attributed, once again, to the spatial localisation of the free-radical reactions in the SAC-01 medium. For example, when this experiment was carried out in bulk methyl methacrylate liquid, there was no evidence of self-focusing. Instead, the entire liquid polymerised within seconds into a white solid.

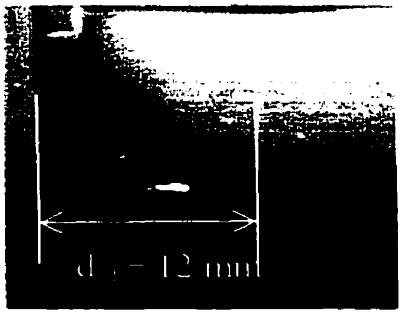

**Figure 4. 19** The waveguide self-induced by the white light

### 4.3.12 Structural reasons for self-focusing

One of the key properties that underlies self-focusing of a laser beam in a SAC-01 composite thin-film, is the spatially localised, photoinduced refractive index change ($\Delta n$) in this medium. In particular, the formation of the gradient index (GRIN) lens was attributed to the spatially confined, free-radical reactions (thus $\Delta n$) in the sol-gel derived silicate matrix. From our previous studies detailed in Chapters 2 and 3, we trace this characteristic to the methacrylate substituent being covalently grafted to the silica network, the growth of the silica matrix that accompanies free-radical polymerisation and the general resistance to mass transport in the viscous thin film medium.

Our observation of the self-focusing of white light (in both the $x$ and the $y$ directions in the SAC-01 sol) implies that photo-initiated free-radical reactions take place with a high degree of localisation even in the colloidal form of the SAC-01 composite. This is a necessary condition for the formation of the GRIN lens and the consequent focusing of the beam of white light along the propagation axis, which is clearly evident in Figure 4.27. This was surprising, as the fluid medium of the sol may be expected to impose less steric hindrance on free-radical diffusion than the viscous medium of a thin film.

#### 4.3.12.1 Evidence of micro-structural organisation in white-light self-induced waveguide

We obtained further insight into the structural character of the SAC-01 composite, by examining cross-sections of the self-induced waveguide (Figure 4.28) at various regions along the propagation axis (*z*). Transmission electron micrographs of cross-sections of the waveguide, made parallel (*zx* plane) and perpendicular (*xy* plane) to the propagation axis are presented in Figure 4.29. A layered or lamellar organisation is evident in the *xy* cross-section closest to the entrance face (sample 1). Each layer is approximately 250 nm wide and shows a certain degree of curvature or undulation. No visible phase separation is evident although dark and light regions, corresponding to electron rich (inorganic) and electron poor (organic), may be identified within each layer. A similar lamellar arrangement is observed in the cross-section made parallel to the propagation axis (sample 2). Closer examination shows that each layer is wider (500 nm) and has straighter walls than the previous sample. Furthermore, the (white) gaps separating each layer are also larger. In the *zx* cross-section made further along *z* (sample 3), the layered form is maintained. A clear distinction can be made between the layers, which alternate as dark and light regions. The latter features are wider (> 500 nm) than the former ones (< 500 nm). The lamellar arrangement has undergone significant disruption in the cross-section made in the *xy* plane closest to the "focal point" or the tip of the self-induced waveguide (sample 4). Although striations that are roughly parallel to each other may be identified here, the sample contrasts sharply with the discrete layers observed in the *xy* plane closest to the entrance face.

The presence of organisation in the SAC-01 composite was unexpected. Silica glasses derived from the acid catalysed sol-gel processing of alkoxysilanes are generally considered to be amorphous, and thus isotropic networks. Therefore it is tempting to attribute the lamellar organisation observed in the SAC-01 composite to some form of photo-orientation that takes place during the self-focusing of white light in the hybrid matrix. It is evident from Figure 4.29 that structural organisation in the composite is disrupted as the self-focusing beam propagates along *z*. This is especially evident by contrasting samples 1 and 4, cross-sections in the *xy* plane, made closest to and furthest away from the entrance face respectively. The high degree of order present in sample 1 is significantly disrupted in sample 4. This suggests that as self-focusing proceeds, the lamellar organisation that is inherent to the SAC-01 colloid, *prior* to irradiation, is gradually distorted.

The presence of self-organisation in the composite might also explain the spatial confinement of the free-radical reactions in this medium. For example, if the lamellar arrangement of inorganic domains is present in the colloidal form of SAC-01, it is likely that the free-radical reactions of methacrylate substituents will be largely intercalated between or within the layers. The unexpected self-organisation observed in the SAC-01 medium and the effects of free-radical polymerisation reactions in the composite will be the subject of investigation and discussion in the following Chapter.

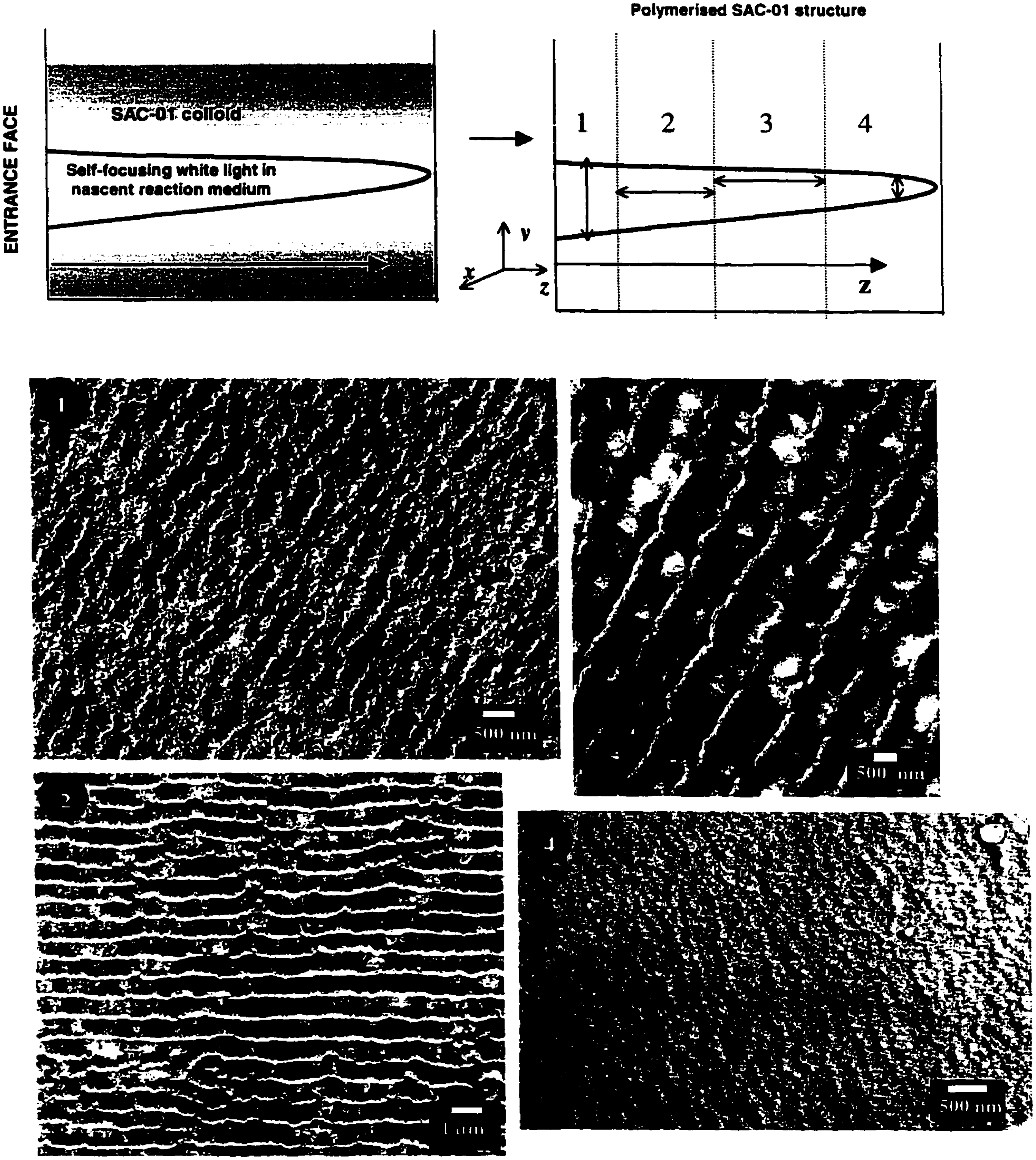

**Figure 4. 29** Cross-sectional transmission electron micrographs of white-light self-induced waveguide in SAC-01 colloid

#### 4.3.13.2 Evidence of micro-structural organisation in thin SAC-01 films

In the previous Section, we described the sub-micrometric, lamellar organisation observed in a waveguide, which was self-inscribed by a beam of white light. Here we describe structural organisation observed in planar SAC-01 waveguides, in which self-focusing of the 514.5 nm laser beam has taken place. Figures 4.30, 4.31 and 4.32 show scanning electron micrographs of regions on the SAC-01 planar waveguide, which have been lightly etched with *iso*-propanol. The thin-film surface consists of a striking, maze-like arrangement of tightly packed, worm-shaped domains. The width of these structures is approximately 200 nm, which corresponds to the dimensions of the layers observed in Figure 4.29. The domains assume several types of patterns on the thin film and as will be detailed below, these arrangements closely follow the path of guided optical modes of 514.5 nm light in the SAC-01 waveguide.

In Figure 4.30, four major forms of domain arrangement may be identified. A linear organisation is observed in the region (a) closest to the channel waveguide (not shown in micrograph). The striations coincide with the long-axis of the channel waveguide and thus the propagation path of the guided optical mode. A higher magnification of this region is presented in Figure 4.31. Another distinct arrangement in Figure 4.30 is the ray-like features that propagate from the bottom left-corner to the top right-corner of the sample. Here too, the domains assume a linear arrangement. Observe however, that these striations have discontinuities, unlike the lines observed in region a, which consist mostly of continuous lines. Furthermore, the regions between these "rays" contain closely packed domains with angular, L-shaped conformations. Smaller regions can also be identified where the domains have a "doughnut" or a circular arrangement (d).

Note that the material is transparent to the laser beam as the width of these domains is much smaller than the wavelength of light (514.5 nm) used in this experiment. Thus, the beam is able to propagate as an optical mode without attenuation (due to scatter) in the SAC-01 waveguide. However, the guided optical mode does initiate the free-radical polymerisation of methacrylate substituents. Therefore as it travels, the beam threads together domains directly in its path through the polymerisation reactions. As a result, the final arrangement of the domains is a close replicate of the path taken by the guided optical mode in the SAC-01 waveguide.

The different conformations of the domains may be understood by considering the intensity of the incident laser beam and the associated rate of polymerisation in these regions. For example, the greatest intensity of the guided optical mode is located where self-focusing takes place, *i.e.* near the self-induced waveguide. It follows that the greatest rate of polymerisation takes place here, linking the domains together in a pattern that closely follows the path of the laser beam. The "rays" on the other hand can be attributed to scattered rays of light, which are lower in intensity. Consequently, the rate of free-radical reactions is also lower in these regions and the domains are not linked to each other in a continuous line. In the regions that experience a still lower intensity of light (c), the domains do not extend into completely linear forms. Rather they exist as angular but partially extended structures that pack efficiently with each other.

It is also interesting to note, the progression of the arrangements from regions that experience high intensities to those with lower intensities of waveguided light. This is evident in the micrograph shown in Figure 4.30. Note that in the regions close to the linear structures, the domains are organised in periodic, angular features. However, in regions that are further away, the organisation seems less rigid, the domains appear "relaxed" and even show some curvature in their arrangements (see also Figure 4.32). Indeed, one of the unique features of the organisation observed here, is the angular and linear structural arrangements that map the path of the propagating optical mode and scattered rays of light in the waveguide. This behaviour reinforces our contention that photoreactions occur in a highly localised manner in the SAC-01 composites. However, the experiments described here do not account for the actual formation of these sub-micrometric domains. The origins of organisation and the chemical identity of these "domains", as mentioned earlier, will be detailed in the following Chapter.

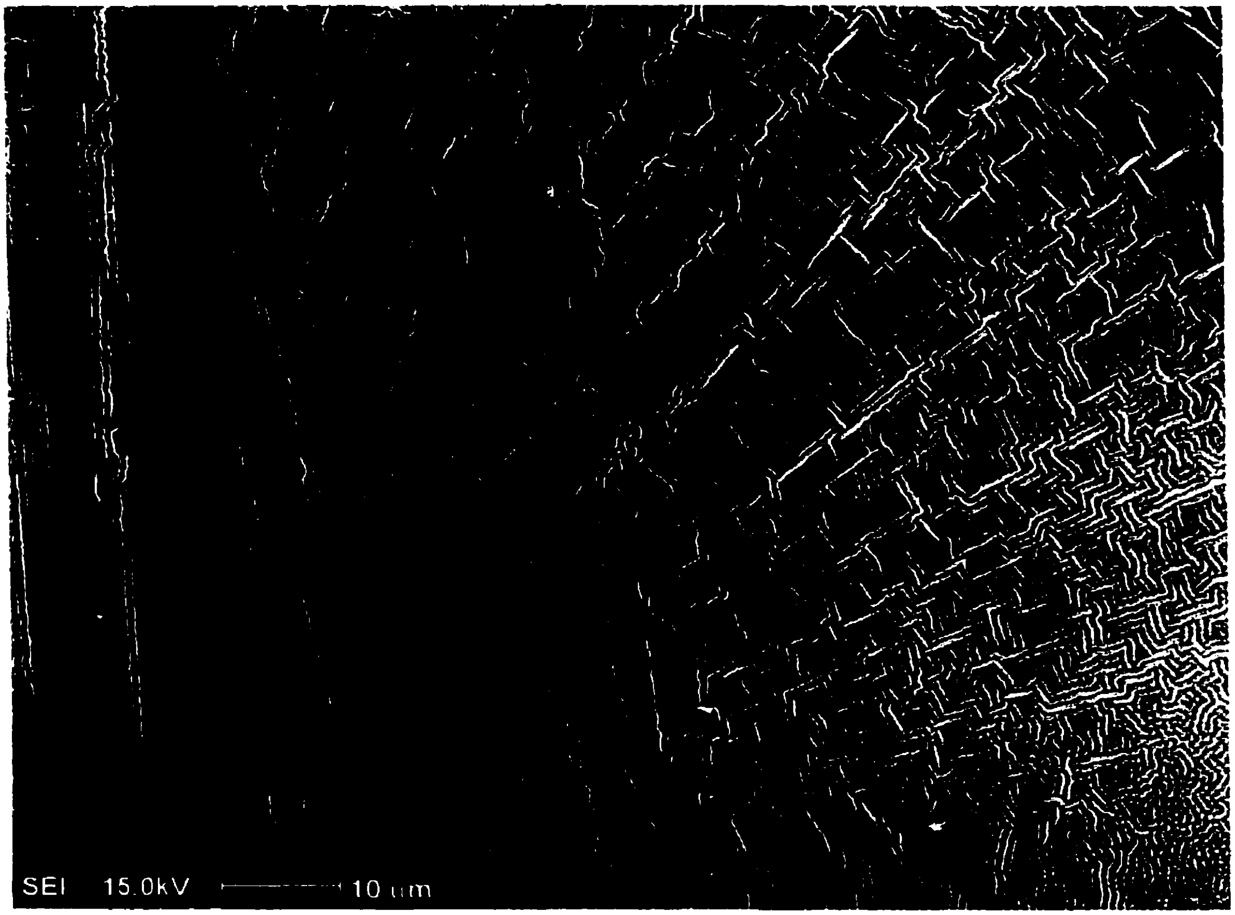

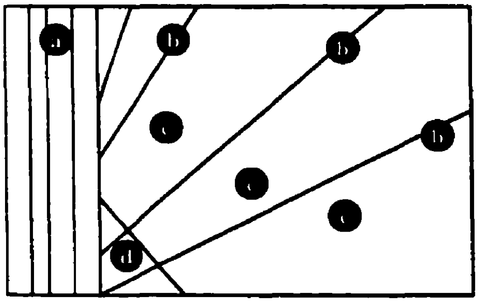

**Figure 4. 30** Guided-mode induced organisation in silica-methacrylate thin films with legend representing various domain arrangements on film.

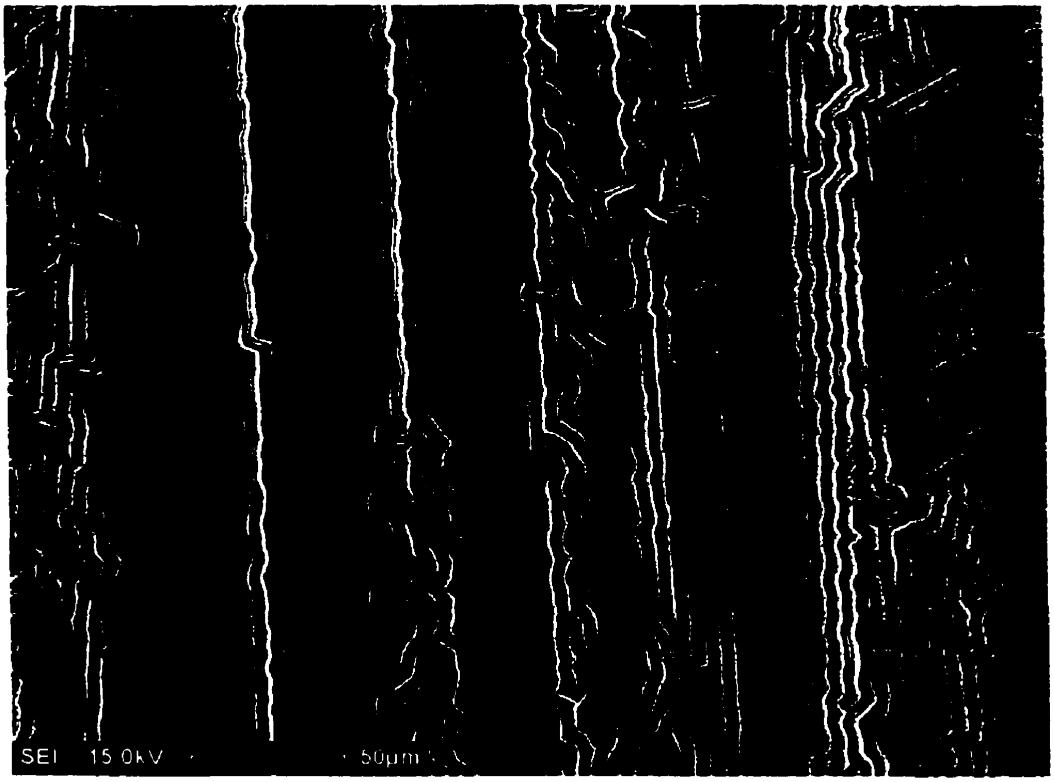

Figure 4. 31 Laser-induced organisation in SAC-01 thin films

Figure 4. 32 Laser-induced changes in silica-methacrylate thin film

## 4.4. CONCLUSIONS

In summary, we have demonstrated the self-focusing of a c.w. 514.5 nm laser beam in a SAC-01 planar waveguide. This is achieved through the guided optical wave polymerisation of propyl methacrylate substituents in the composite thin-film. As it propagates, the guided laser beam initiates the free-radical polymerisation of methacrylate substituents and thus induces a refractive index change in the medium. The spatially localised refractive index changes reproduce the Gaussian intensity profile of the beam, thus forming a lens. As a result, the beam focuses itself along the propagation axis as it traverses the slab waveguide. The alternating lens-formation and self-focusing action of the beam creates a channel waveguide, a narrow region of increased refractive index in the medium. The beam is guided through this self-inscribed waveguide without suffering diffraction. As refractive index changes are permanent in the matrix, once the optical field is removed, the self-inscribed channel waveguide remains on the substrate. This feature has a roughly circular profile and is the first (to our knowledge) fibre-on-a-chip, which has potential as an interconnect between optical fibres to planar integrated optics systems.

Self-focusing of white light was observed in the colloidal form of the SAC-01 composite. Until now, this phenomenon has only been observed in PRCs. In our case, an incoherent, polychromatic beam of light, with random spatial and temporal phase fluctuations, self-inscribed a waveguide and propagated across the fluid SAC-01 medium without diffracting. Transmission electron microscopy of cross-sections of this self-induced waveguide led to the discovery of lamellar organisation in the SAC-01 composite. The degree of organisation diminished with increasing propagation distance of the self-focusing beam of white light. Organisation of domains, that traced the path of waveguided laser light, was also observed in thin films of the SAC-01 composite.

The discovery of structural organisation in the SAC-01 composites is significant for more than one reason. It is to our knowledge, the first report of self-organisation in an acid catalysed, sol-gel derived composite, which have until now been assumed to be isotropic amorphous glasses. There is currently a strong research effort towards finding self-assembled routes to ordered silicate structures and the SAC-01 composites could be a valuable addition to this field. Furthermore, the domain sizes obtained in these composites are on the order of 250 nm and far exceed those obtained with existing

The discovery of structural organisation in the SAC-01 composites is significant for more than one reason. It is to our knowledge, the first report of self-organisation in an acid catalysed, sol-gel derived composite, which have until now been assumed to be isotropic amorphous glasses. There is currently a strong research effort towards finding self-assembled routes to ordered silicate structures and the SAC-01 composites could be a valuable addition to this field. Furthermore, the domain sizes obtained in these composites are on the order of 250 nm and far exceed those obtained with existing approaches. The sub-micrometric features, comparable to the wavelength of visible light, have important implications for photonics application. In addition, the photosensitivity of the self-organised structures opens the possibility of structuring this self-organised matrix with light. The origins and implications of this self-organisation will be the topics of investigation and discussion in the following Chapter.

1. D. Cotter, R. J. Manning, K. J. Blow, A. D. Ellis, A. E. Kelly, D. Nesset, I. D. Phillips, A. J. Poustie and D. C. Rogers, *Science*, **286,** 1523 (1999).
2. A. Hasegawa and F. Tappert, *Appl. Phys. Lett.* **23**, 142 (1973).
3. L. F. Mollenauer, R. H. Stolen and J. P. Gordon. *Phys. Rev. Lett.* **45**, 1095 (1980).
4. F. Fontana, *Photonics Technology News*, July 1998.
5. L. F. Mollenauer, E. lichtman, M. J. Neubelt and G. T. Harvey. *Electron. Lett.* **29**, 910 (1993).
6. R. W. Boyd, *Nonlinear Optics*, (Academic Press Inc. San Diego, CA, 1992), Chapter 4.
7. M. Segev and G. Stegeman, *Physics Today*, August (1998) p.42-48.
8. P. L. Kelley, *Phys. Rev. Lett.* **15**, 1005 (1965).
9. R. W. Boyd, *Nonlinear Optics*, (Academic Press Inc. San Diego, CA, 1992), Chapter 6.
10. R. Y. Chiao, E. Garmire and C. H. Townes, *Phys. Rev. Lett.* **13**, 479 (1964).
11. A. Barthelemy, S. Maneuf, C. Froehly, *Opt. Commun.* **55**, 201 (1985).
12. J. S. Aitchinson, A. M. Weiner, Y. Silberberg, M. K. Oliver, J. L. Jackel, D. E. Leaird, E. M. Vogel and P. W. E. Smith, *Opt. Lett.* 15, 471 (1990).
13. Y. R. Shen, *The Principles of Non Linear Optics*, Chapter 17.
14. G. I. Stegeman and M. Segev, *Science*, **286**, 1518 (1999).
15. J. E. Bjorkholm and A. Ashkin, *Phys. Rev. Lett.* **32**, 129 (1974).
16. G. Khitrova, H. M. Gibbs, Y. Kawamura, H. Iwamura, T. Ikegami, J. E. Sipe and L. Ming. *Phys. Rev. Lett.* **70**, 920 (1993).
17. W. Torruellas, B. Lawrence and G. I. Stegeman, *Electron. Lett.* **32**, 2092 (1996).
18. M. Segev, B. Crosignani, A. Yariv and B. Fisher, *Phys. Rev. Lett.* **68**, 923 (1992).
19. M. D. Iturbe Castillo, P. A. Marquez Aguilar, J. J. Sanchez-Mondragon, S. Stepanov and V. Vysloukh, *Appl. Phys. Lett.* **64**, 408 (1994).
20. M-F Shih, P. Leach, M. Segev, M. H. Garrett, G. Salamo and G. C. Valley, *Opt. Lett.* **21**, 324 (1996).
21. M-F Shih, M. Segev and G. Salamo, *Phys. Rev. Lett.* **78**, 2551 (1997).
22. T. Lehner and N. Auby, *Phys. Rev. E*, **61,** 1996 (2000).
23. T. M. Monro, C. Martijn de Sterke and L. Poladian, *Opt. Comm.* **119**, 523 (1995).

24. K. O. Hill, Y. Fuji, D. C. Johnson and B. S. Kawasaki, *Appl. Phys. Lett.* **32**, 67 (1978).

25. T. Tamir, *Guided-wave optoelectronics*, (Springer-Verlag, Heidelberg, Germany 1988).

26. J. Albert, B. Malo, D. C. Johnson, F. Bilodeau, K. O. Hill, J. L. Brebner and G. Kajrys, *Opt. Lett.* **18**, 1126 (1993).

27. T. M. Monro, D. Moss, M. Bazylenko, C. Martijn de Sterke and L. Poladian, *Phys. Rev. Lett.* **80**, 4072 (1998).

28. H. Hisakuni an K. Tanaka, *Solid State Comm.* **90**, 483 (1994).

29. C. Meneghini and A. Villeneuve, *J. Opt. Soc. Am. B.* **15**, 2946 (1998).

30. E. DelRe, M. Tamburrini, M. Segev, R. D. Pergola and A. J. Agranat, *Phys. Rev. Lett.* **83**, 1954 (1999).

31. S. S. Sarkisov, M. J. Curley, D. E. Diggs, A. Wilkosz, W. W. Grimalsky, G. Adamovsky. *Opt. Eng.* **39**, 616 (2000).

32. A. S. Kewitsch and A. Yariv, *Opt. Lett.* **21**, 24 (1996).

33. S. Shoji and S. Kawata, *Appl. Phys. Lett.* **75**, 737 (1999).

34. M. Mitchell and M. Segev, *Nature*, **387**, 880 (1997).

35. H. Krug, F. Tiefensee, P. W. Oliviera and H. Schmidt, *Proc. SPIE Int. Opt. Eng.* **1758**, 448 (1992).

36. J. Baldwin, N. Schuler, I. S. Butler and M. P. Andrews, *Langmuir*, **12**, 6389 (1996).

37. D. Marcuse, *Theory of Dielectric Optical Waveguides*, (Academic Press Inc. San Diego, CA, 1991).

38. T. M. Monro, C. M deSterke, L. Poladian, *J. Opt. Soc. Am. B*, **13**, 2824 (1996).

39. A. Roloff, K. Meier and M. Riediker, *Pure and Appl. Chem.* **58**, 1267 (1986).

40. B. Klingert, A. Roloff, B. Urwyler and J. Wirz, *Helv. Chim. Acta*, **71**, 1858 (1988).

41. W. Rutsch, H. Angerer, V. Desobry, K. Dietliker and R. Hüsler, *Proceeding of the XIVth International Conference in Organic Coatings Science and Technology*, 11-15th July, 1988, Athens, Greece. p. 423-438.

42. C. Decker and B. Elzaouk, *Current Trends in Polymer Photochemistry*, N. S. Allen, M. Edge, I. R. Bellobono and E. Selli, Eds., (Ellis Horwood, New York).

43. W. Rutsch, K. Dietliker, D. Leppard, M. Köhler, L. Misev, U. Kolczak and G. Rist, *Progress in Organic Coatings*, **27**, 227 (1996).

44. T. M. Monro, C. Martijn de Sterke and L. Poladian, *Opt. Comm.* **119**, 523 (1995).

45. T. M. Monro, C. Martijn de Sterke and L. Poladian, *J. Opt. Soc. Am. B*, **13**, 2824 (1996).

46. J. F. Rybak, *Mechanisms of Photophysical Processes and Photochemical Reactions in Polymers Theory and Applications*, (John Wiley & Sons, Chichester).

47. M. Shih, P. Leach, M. Segev, M. H. Garrett, G. Salamo, G. C. Valley, *Opt. Lett.* **21**, 324 (1996).

48. J. E. Bjorkholm and A. Ashkin, *Phys. Rev. Lett.* 32(4) 1974 129

49. A. W. Snyder and D. J. Mitchell, *Science*, **276**, 1538 (1997).

50. M-f Shih, P. Leach, M. Segev, M. H. Garrett, G. Salamo and G. C. Valley, *Opt. Lett.* **21**, 324 (1996).

51. M. Mitchell and M. Segev, *Nature*, **387**, 880 (1997).

52. M. Mitchell, M. Segev, T. H. Coskun and D. N. Christodoulides, *Phy. Rev. Lett.* 79, 4990 (1997).

53. M. Mitchell, M. Segev, D. N. Christodoulides, *Phys. Rev. Lett.* **80,** 4657 (1998).

# 5. UNEXPECTED SELF-ORGANISATION IN A CLASS OF SOL-GEL DERIVED SILICA-METHACRYLATE COMPOSITES

## 5.1 INTRODUCTION

### 5.1.1 Chemical self-organisation approaches to ordered inorganic structures

There is currently a concerted materials-research effort towards finding simple, chemical pathways to silica and metal-oxides with periodically arranged nano, meso and micro-scale pores. Uniform spherical or channel voids tightly packed into hexagonal close packed (HCP), cubic ($L_3$), lamellar ($L_\alpha$) and face centred cubic (FCC) "unit-cells" in inorganic materials could significantly increase surface areas for adsorption, catalysis, molecular sieve, drug delivery and membrane applications. Composites formed by doping the pores with a second (metallic, organic or inorganic) component, may be expected to have unique electronic and optical properties due to the monodispersity, regular spacing and spatial anisotropy of the pores. Furthermore, each of these narrow channels may serve as an insulated reaction vessel for meso-scale chemistry, providing unique opportunities to design materials with unusual chemical and physical characteristics.

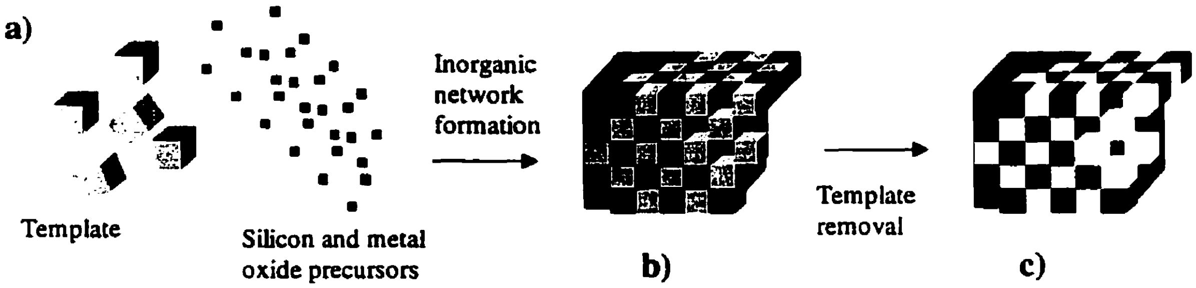

**Figure 5. 1** Schematic of template-guided sol-gel processing of ordered inorganic structures

In the general approach to such ordered structures, the hydrolysis and condensation (sol-gel) reactions of metal and alkoxysilane precursors are initiated in the presence of solutions or liquid crystalline mesophases (HCP, $L_3$, $L_\alpha$) of surfactants, block copolymers or crystalline assemblies of spherical, colloidal particles (as schematised in Figure 5.1a).

The hydrophilic metal-oxo or polysilicate oligomers interact with the amphiphiles through electrostatic, hydrogen (H)-bonding and van der Waals forces. to form hybrid organic-inorganic liquid crystalline phases with long-scale, two or three-dimensional periodicity (Figure 5.1b). These interfacial forces direct (spatially) the inorganic polymerisation reactions, which are confined to the aqueous domains of the supramolecular structure. After glass formation the organic component, removed by pyrolysis or solvent extraction, casts off an ordered inorganic framework, *i.e.* amorphous monolith with pores of uniform geometry and size, regularly spaced at meso and nanometer intervals (Figure 5.1c).

### 5.1.2 Sol-gel processing of inorganic networks

Sol-gel processing is especially suited for this approach because it provides blocks of silicate and metal-oxo species with which to build dense, homogeneous networks around the templates. A wide range of primary structures may be selected through the temperature, concentration and especially the pH of the reactions[1]. For example, base catalysed hydrolysis and condensation of silicon alkoxides lead to charge stabilised. deprotonated and spherical silicate particles whereas acid catalysis is known to form minimally condensed, weakly branched and positively charged oligomeric silicates with fractal dimensions of < 2. Cluster-cluster aggregation of the latter leads to homogeneous and densely packed glasses. The low porosity and compliant nature of these glasses allows them to be moulded into several forms including fibres, films and monoliths[2] and implies their ability to conform to the shape and size of templates. Early examples of organic-templates in sol-gel systems are glasses formed in the presence of methyl orange. Once the dye was removed, the silica structures showed a preferential selectivity for methyl orange over its homologues[3]. Beginning with naturally occurring examples, the following sections will briefly outline the synthetic routes to ordered inorganic structures and some of the applications of this class of materials.

### 5.1.3 Lessons from Nature

Within only the past eight years, several creative and efficient synthetic routes to ordered inorganic structures have been discovered. Yet, the most sophisticated forms of template-guided growth exist in Nature where organic macromolecules regulate the nucleation, growth, morphology and orientation of inorganic crystals. Teeth, cartilage, leaves and shells are remarkable examples of mineral phases grown in the presence of proteins, glycoproteins and polysaccharides[4]. The long-range order imposed by proteins and carbohydrates on amorphous silica is evident in the sheet-like, globular or fibrous structures it assumes in the branches, leaves and hairs of certain plants[5]. Organic and inorganic phases in these bio-systems coexist in exquisitely arranged microstructures, designed to optimise the material's strength and functional specificity. The nacre of the abalone shell in particular, has inspired chemists seeking synthetic routes to laminated, hybrid structures[6]. The shell consists of aragonite sheets interwoven with a strong, fibrous core that causes a 3000-fold increase in its resistance to fracture when compared to a single crystal of $CaCO_3$[7].

The hybrid architecture of Nature spans several length-scales. Although synthetic, template-based self-organisation strategies have been widely successful for ordered nano and meso-scale structures, until the report presented in this Chapter they have (to our knowledge) not been extended to the sub-micrometric scale. On the other hand, many natural colours are not due to dyes or chromophores but to a sub-micrometric periodicity and corresponding refractive index modulation ($\Delta n$) in the biomaterial's microstructure.

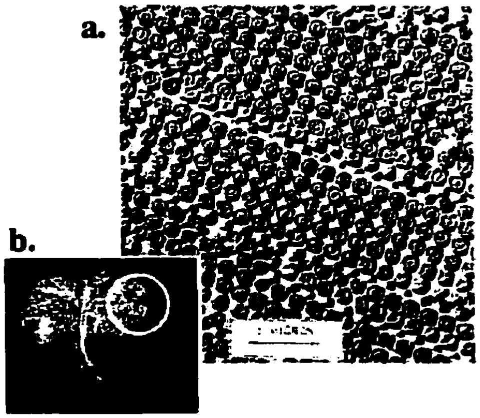

**Figure 5.2a** Scanning electron micrograph of the slightly etched surface of 5.2b. an opal

For example, the wing of the butterfly viewed through a microscope, is an efficient and polarisation sensitive diffraction grating for visible light[8]. In his classic text on the chemistry of silica[9], Iler recognised the opal as a regularly packed crystal of uniform silica particles. The Bragg law of diffraction for optical wavelengths are obeyed by both of these structures, which possess a long-range, refractive index modulation at the sub-micrometric scale. These natural, iridescent materials are encouraging invitations to pursue chemical routes to periodic, hybrid structures that are able to interact with optical fields.

### 5.1.4 Bio-mimetic approaches to hybrid materials

Bio-silicification processes exhibit control over the shape, size and distribution of silica structures. The cell walls of diatoms, for example, are intricately patterned with amorphous, silica nano-spheres, which were created in its membrane vesicles. In the last few years, there have been attempts to identify, isolate and use organic substances responsible for bio-silica formation to create ordered silica structures through sol-gel processing. Polycationic peptides (silaffins) extracted from diatom (*Cylindrotheca fusiformis*) cell walls caused the precipitation of silica spheres from silicic acid solutions within seconds at neutral pH[10]. Silicateins, which are proteins extracted from marine sponges (*Tethya aurantia*), have also catalysed silica formation from tetraethoxysilane under neutral conditions[11]. Synthetic analogues of these proteins, block co-polypeptides with lyseine (water soluble) and cysteine (insoluble) segments, catalysed the hydrolysis and polycondensation reactions of tetraethoxysilane to produce spherical and columnar silica morphologies[12]. Other examples include tubular silica morphologies formed in the presence of low-molecular weight organic gelatiniser fibrils[13] and gnarled and hollow strands of silica templated with fibrous collagen[14].

### 5.1.5 Synthetic approaches to ordered inorganic structures: surfactant templated sol-gel reactions

The most successful and general synthetic route to ordered dielectric- structures was discovered only eight years ago[15, 16]. The approach uses amphiphilic molecules and macromolecules that self-assemble at increasing concentrations into liquid crystalline phases, to spatially direct the sol-gel processed growth of inorganic networks.

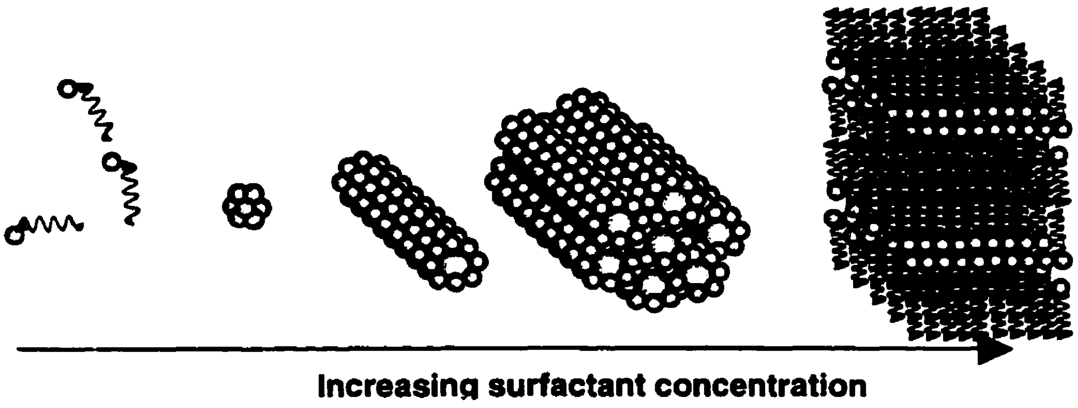

**Figure 5. 3** Liquid crystalline phase behaviour of surfactant molecules

Aluminosilicates formed in the presence of common quaternary ammonium surfactants ($C_nH_{2n+1}(CH_3)_3N^+$) were found to possess a well-ordered, hexagonal close packed (HCP) arrangement of pores. Pore sizes in these mesostructured materials, labelled MCM-41 by researchers at Mobil, could be tuned between 15 and 100 A$^{\circ}$ simply by varying the length of the surfactants' hydrophobic tails.

Quarternary surfactants (e.g. cetyltrimethylammonium bromide (CTAB)) form micellar structures in aqueous solutions[17], where the water-loving cationic heads form the outer surface while their long alkyl chains point towards the micelle centre. This minimises the contact of hydrophobic tails with $H_2O$ and introduces repulsive Coulombic forces between the hydrophilic heads. The balance between these forces determines the stability, local curvature and macroscopic shape of micelles. At the critical micelle concentration (CMC 1) molecules that were initially free in solution, aggregate to form spherical structures. With increasing concentration (CMC 2), these micelles coalesce to form cylinders or rods. As the surfactant concentration is increased further, they progressively pack into HCP, cubic and lamellar liquid crystalline phases.

The hydrolysis and condensation reactions (*i.e.* inorganic network growth) of silicon and metal alkoxides precursors introduced into these systems, are restricted to the aqueous domains. Initially it was assumed that a pre-organised surfactant assembly was necessary to guide the growth of ordered inorganic frameworks. However it soon became evident that MCM-41 type structures could be obtained at surfactant solutions below the CMC 2 *i.e.* in the absence of a pre-formed, organic liquid crystalline phase. Careful NMR, freeze fracture TEM and X-ray diffraction (XRD) studies with cubic octameric silicate anions showed that the precursor ions closely cooperated with the charged surfactant to create new organic-inorganic liquid crystalline phases[18]. These structures termed silicatropic liquid crystalline (SLC) phases, originated from the strong electrostatic interactions at the silicate-surfactant interface. In solution, the polyanionic silicate oligomers replaced the surfactant counterions and complexed with the cationic head groups. The anions screened the Coulombic repulsion between head groups and consequently reduced the local curvature to form hybrid aggregates or liquid crystalline phases.

This liquid crystal template (LCT) approach to ordered materials has been successfully extended to other surfactants and oxides of metals including antimony, W, Mg, Al, Mn, Fe, Co, Ni and Zn[19] and is not restricted to the HCP liquid crystalline phase. The amphiphilic $L_3$ (sponge) phase of cetylpyridinium chloride, a random network of connected bilayer systems, was replicated in tetramethoxysilane (TMOS) derived silicates under acidic conditions[20]. The $L_\alpha \rightarrow L_3$ (lamellar to sponge) intermediate phase, a bilayered vesicular structure was achieved with an electrically neutral, $NH_2$ based gemini-surfactant- silicate system[21]. A silicate mesophase (SBA-8) with an unusual rectangular lattice was obtained by the base catalysed sol-gel reactions of tetraethoxysilane (TEOS) in the presence of rigid bolaform surfactants[22].

Pore sizes have been increased from tens to hundreds of angströms with amphiphilic block co-polymers, which also self-assemble into micellar structures but with larger dimensions corresponding to polymer chain sizes. A family of two-dimensional, HCP mesoporous silicates (SBA-15) have been obtained with various poly (alkylene) oxide triblock copolymers. In their presence and strictly under acidic conditions, the hydrolysis and condensation reactions of TMOS, TEOS and tetrapropoxysilane (TPOS) yield well-ordered, silicate frameworks[23, 24]. In addition, mesostructured aluminosilicates have been obtained with poly (isoprene-b-ethyleneoxide) templates[25] while highly porous silicates with interconnecting, uniform pores were templated with copolymers containing polar polyethylene oxide and apolar polystyrene blocks[26]. In the case of these non-ionic templates, interactions are dominated by H-bonding between the silicate and the hydrophilic blocks of the polymer. In this way, the organisation of the polymer chains (caused by microphase separation due to the different solubilities of the different blocks) is replicated in the silicate morphology.

Many of these template-approaches are controlled by the interactions at the surfactant-inorganic ion interface, which have been classified as $S^+ I^-$, $S^- I^+$, $S^+ X^- I^+$, $S^- X^+ I^-$, S-I and $S^0 I^0$, where S represents the surfactant and I, the inorganic precursor[19]. In the case of the similarly charged surfactants and inorganic precursors, interactions are mediated by counterions, $X^{+/-}$. Empirical examples of $S^+ I^-$, $S^- X^+ I^-$ and S-I (where surfactant and inorganic component are covalently linked) have not been identified.

At the macroscopic level, silica growth guided by the charged surfactants leads to unusual morphologies. For example, tetramethyl ammonium cations were assumed to play an essential role in the formation of layered helical silicate structures from silicon tetraethoxide precursors[27] and hollow, helicoidal or screw-thread structures, due to the differential contraction of silicate-micelle rods, were also observed[28]. The formation of these structures has been attributed to disclinations or defects in the liquid crystalline surfactant-silicate assemblies that are amplified in the macroscopic structure[29].

### 5.1.6 Applications of mesoporous materials

This young class of inorganic materials have had a significant impact on several areas of materials chemistry and physics. A few of these exciting studies are gathered in this section. The large surface area in the mesoporous materials, three times greater than the commercially available samples used for liquid chromatography, is due to their efficiently packed network of uniform pores[30]. The environment of these pores may be tailored to host specific chemical reactions. For example, in a recent report, it was shown that ethene groups integrated into the channel walls during silica synthesis could subsequently be brominated[31]. In another instance, ethene molecules were polymerised in silica channels that were derivatised with titanocene catalysts[32]. In this case the nascent polymer, confined to the structurally anisotropic pores, formed crystalline polymer chains that combined into birefringent fibre-bundles once they emerged from their individual reaction chambers; an unique alternative to orienting polymer performs with physical stretching or extrusion processes. Furthermore, the chemical reactivity of channel surfaces may be tailored to selectively bind and orient atoms and molecules. For example, pore walls were derivatised with tightly packed mercaptopropylsilane monolayers. When contaminated aqueous or organic solutions passed through, the -SH functionalities bound to mercury, silver and lead atoms and efficiently contained them in the 20 nm wide pores[33]. In another case, ruthenium cluster carbonylates were organised along the silicate channels by H-bonding interactions between silanols lining the pore walls and the carbonyl groups[34].

At the macroscopic level, mesoporous materials do not have to be restricted to monolithic or crushed powder forms. Recently it was shown that thin film surfaces could be patterned with ordered silicates by applying micro-moulding techniques to silicate materials templated with colloidal crystals and block co-polymers[35]. Similarly, planar surfaces were patterned with oriented nanotubules of HCP, mesoporous silica[36].

The optically transparent, mesoporous silicates are suitable host media for photophysical studies. The photoluminescence of silicon clusters formed within surfactant-containing HCP silicate channels has been detected[37]. Polarised luminescence studies of semiconducting polymer chains individually confined in 2.2 nm channels have provided valuable insight into their orientation in the hybrid silicate-polymer structures[38].

### 5.1.7 Ordered silica structures with periodicities > 100 nm

Our interest is in the natural, unmodified forms of ordered silicates and metal oxides, which by themselves are fascinating optical materials. The regularly positioned air holes in the dielectric frameworks create a corresponding, long-range, periodic modulation of the refractive index ($\Delta n$). This is an extremely valuable property for the construction of photonic crystals, which are dielectric structures that possess photonic band gaps (PBGs).

According to the nearly free electron model, arrays of atoms in a crystal present a periodic potential to a propagating electron wave. A band gap arises for those wavelengths $\lambda$, comparable to the lattice constant $a$, ($n\lambda/2 = a$, where n is an integer); wavelengths that also satisfy the Bragg diffraction condition for electrons by the lattice. Yablonovitch[39] and John[40] independently pointed out that the diffraction of light waves in dielectric structures with sub-micrometric periodicities would open photonic band gaps (PBGs) at optical energies. Wavelengths in this range incident from any angle would be totally reflected from and forbidden to propagate in such photonic crystals. However light could be trapped[41], guided[42] or reflected[43] by defects or lapses in lattice periodicity.

Creators of photonic crystals are faced with infinite geometric possibilities in their quest for dielectric crystals PBGs. Although aided by theoretical predictions, the search has been largely empirical and has been dominated by micromachining techniques[44]. The first success dubbed the Yablonovite[45] was made by drilling thrice (with a carbide tool bit) through triangular arrays of holes in a mask placed over a dielectric slab. The cross section (Figure 5.4a) of the resulting structure had a refractive index contrast (air/dielectric) periodicity on the order of millimetres and consequently, a band gap of microwave energies. Three-dimensional aluminium oxide cages with period sizes of 66 and 133 μm showing PBGs at 75 and 150 μm respectively, were grown column by column through laser chemical vapour deposition (Figure 5.4b)[46]. Gaps at IR wavelengths of 10 - 14.5 μm were found in structures constructed by repeated deposition and etching of dielectric films (Figure 5.4c)[47].

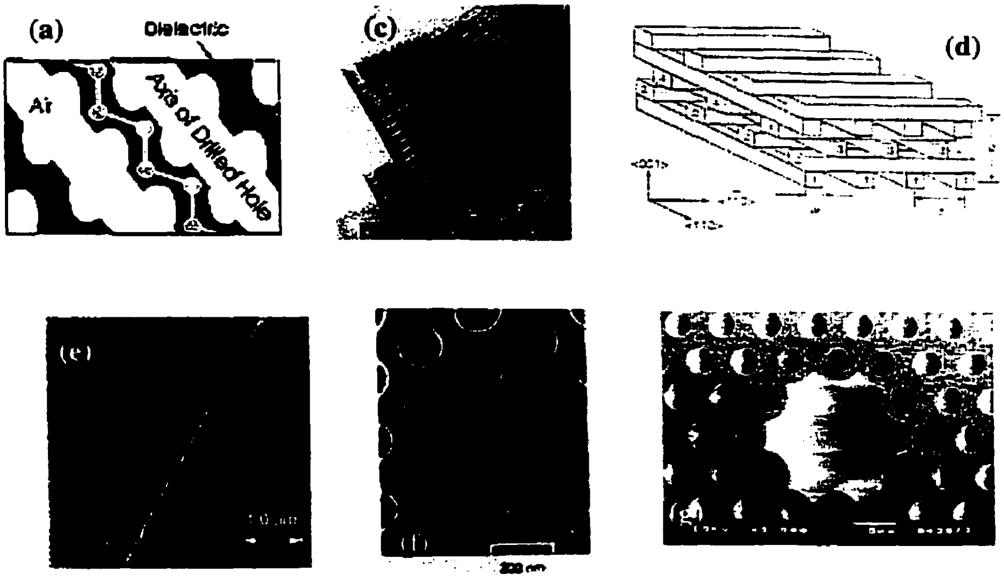

Figure 5. 4 Collection of photonic band gap structures

Air holes drilled 0.22 μm apart with X-ray lithography in a thin strip of Si produced the first PBG at the optical wavelength of 1.56 μm (Figure 5.4 d). Band gaps at even shorter wavelengths (800 - 900 nm) were created in a honey-comb lattice of air holes with a period of 190 nm, etched in AlGaAs with an electron beam (Figure 5.4e)[48]. A similar pattern of air holes spaced 1.9 μm apart in a silica glass fibre (Figure 5.4f) had a band gap for blue (488 nm) and green (528 nm) light[49]. A recent and promising addition has been the development of three-dimensional holographic techniques for the photo-inscription of photonics crystal templates[50].

A close examination of the PBG structures collected in Figure 5.4 shows that they consist of uniform voids arranged in simple geometric patterns in a bulk dielectric medium. Identical structures may be achieved through the template based, chemical pathways that were described in the previous sections. Indeed these would be extremely attractive alternatives to the micro-machining techniques, which are limited with respect to resolution, design flexibility and reproducibility. The chemical self-organisation routes on the other hand, promise long-range order, ease of processing and most importantly the power to control structural parameters through molecular design. However, PBGs at visible or infrared (IR) energies demand crystals with sub-micrometric and micrometric periodicity whereas the length scales of surfactant and block copolymers restrict the dimensions of self-assembled, inorganic frameworks to < 100 nm. Until the work presented in this Chapter, the only self-assembly route to ordered structures with $\Lambda > 100$ nm have been achieved with colloidal crystal templates. Indeed, recently reported silicon structure with a complete PBG at 1.5 μm, was constructed through colloidal templating[51].

### 5.1.8 Colloidal crystals

When spherical, colloidal particles of the same size are concentrated against a flat surface, they pack into a face centred cubic (FCC) form. Silica or metal oxides may be grown in the voids and interstices of a colloidal crystal that has been infiltrated with an alkoxide precursor. When sphere-diameters are on the order of hundreds of nanometers, the periodicity of the dielectric crystals is accordingly raised into the optical wavelength region of the electromagnetic spectrum. Titania, zirconia and alumina structures with 320-360 nm pores have been cast from assemblies of latex spheres[52]. Opalescent titania with pore sizes ranging from 120 to 1000 nm was made through a similar technique[53], which has also been successfully applied to create silica structures with 150 nm to 1000 nm periodicity[54]. At a smaller scale, 18 nm wide gold particles have templated the growth of 7 nm silica shells[55].

Monodisperse, silica spheres themselves organise into FCC arrangements that can diffract visible light[56]. In turn, they have served as templates for porous, photocatalytic $TiO_2$ films[57] and mesoporous carbon with a narrow pore size distribution (12-15 nm)[58]. Strikingly iridescent diamond and glassy carbon structures were cast from jeweller's colloidal crystal templates for synthetic opals (150 to 300 nm periodicity)[59]. Thermal polymerisation of divinyl benzene and ethylene glycol dimethacrylate within $SiO_2$ colloidal crevices have led to organic polymers with ordered mesopores ranging from 15 to 35 nm[60]. Until now, the larger dimensions provided by colloidal spheres has been the only means to achieve periodicities on the order of hundreds of nanometres (sub-micrometric scales), which coincides with the optical wavelength regime. In the following Sections, we will how sub-micrometric organisation may be obtained, in the absence of external templates, in a class of sol-gel derived hybrid silica-acrylate composites.

### 5.1.9 First report of sub-micron scale self-organisation in sol-gel silicates in the absence of external templates

In this Chapter, we report the discovery of self-organisation in a class of hybrid organic-inorganic composites derived from the sol-gel processing of methacrylate-substituted alkoxysilanes. In particular, we examine the composites derived from 3-methacryloxypropyltrimethoxysilane (MAPTMS) and characterise them through a range of techniques including polarised optical microscopy (POM), transmission electron microscopy (TEM), scanning electron microscopy (SEM), NMR and FT-IR microscopy. The microstructure of the hybrid materials consists of a three-dimensionally ordered, periodic and interdigitated arrangement of silica domains. These domains are approximately 250 nm wide and are surface-derivatised with propyl methacrylate substituents. We observed this form of organisation in a range of SAC composites derived from 3-methacryloxymethyltrimethoxysilane, 3-methacryloxypropylmethyldimethoxysilane, 3-acryloxypropyltrimethoxysilane, 3-acetoxypropyltrimethoxysilane and a mixture of MAPTMS and decyltrimethoxysilane.

In the previous Sections of this Introduction, several template-guided pathways to ordered inorganic structures were described. In each one of these procedures, the role of the sol-gel process has been a passive one *i.e.* it simply sculpts an amorphous structure about a *pre-organised* assembly of amphiphiles or colloidal spheres. It is well-known that sol-gel processing of alkoxysilanes, in the absence of external templates, can lead to different silica morphologies, depending on reaction parameters such as pH, concentration and temperature[61]. For example, base catalysed reactions lead to colloidal particles, whereas a fractal, connected gel network is formed through acid catalysis. However, until now, these have been assumed to be inherently amorphous and isotropic networks. The work presented in this Chapter is the first report (to our knowledge) of organised and anisotropic structures created through the sol-gel processing of alkoxysilanes without external amphiphilic templates. In addition, it is also the first example of a self-organised hybrid silica-organic system, where the periodicity approaches the sub-micrometric (and thus the optical wavelength) regime.

To explain these findings, we propose a model based on the amphiphilic effects of the sol-gel precursor itself - the MAPTMS molecules. We surmise that once the hydrolysis reactions are initiated, a microemulsion is formed. These thermodynamically stable systems consist of interwoven aqueous and organic channels separated by an amphiphilic monolayer of hydrolysed MAPTMS molecules – with hydrophobic propyl-methacrylate tails and hydrophilic silicate head groups. Thus, the polycondensation reactions of the hydrolysed MAPTMS molecules are strictly confined to the aqueous domains of the microemulsion and are spatially segregated from the organic phase by the amphiphilic monolayers. Consequently, the final silica structure replicates the interdigitated and organised arrangement of aqueous conduits in the microemulsion. Furthermore, the discrete inorganic domains are surface derivatised and separated from each other by a layer of surface-derivatised propyl methacrylate groups.

In this route to ordered inorganic structures, the self-organisation is inherent to the sol-gel system itself and depends on the phase space of the reaction mixture, consisting of the organic MAPTMS precursor, the amphiphilic hydrolysed MAPTMS species and $H_2O$. As mentioned previously, there has been no empirical evidence of S-I, where the template is covalently attached to the evolving silica network. Our systems indicate that the amphiphilic effects of an organosubstituted alkoxysilane, where the template – the organic substituent is covalently bound to the silica precursor - may indeed lead to organisation.

The self-organising property of this class of materials casts new insight on some of its previously observed optical properties. For example, in each of the previous Chapters, the spatial localisation of free-radical polymerisation reactions in the hybrid composites has been emphasised. This property plays a crucial role in the self-focusing of monochromatic and white light in the colloidal and thin film forms of the composite. It also underlies the sub-micrometric resolution achieved in the photolithography of passive optical devices on thin films. The segregation between the organic and the inorganic phases may underlie the spatial localisation of photo-initiated free-radical polymerisation of methacrylate groups.

The SAC composites combine several features that are valuable for photonic applications: i) silica, the material of choice for several optical applications, ii) self-organisation at the sub-micrometric scales, compatible with optical wavelengths and iii) photosensitivity due to the presence of methacrylate groups, which may be polymerised with visible and UV light. We demonstrate that the organisation present in the colloidal form of these composites may be permanently captured through the UV-initiated free-radical polymerisation of the methacrylate groups into anisotropic, transparent monoliths. We also show that the colloidal silica domains, when confined to planar substrates, arrange themselves into a bicontinuous phase characteristic of amphiphilic macromolecules. Indeed, thin films of these silica structures, due to their sub-micrometric dimensions and organised arrangement, diffract visible light. The significant degree of iridescence makes these composites a valid and new class of candidates for visible photonic band gap materials. Furthermore, the polymerisation of methacrylate substituents in these thin films may be initiated by exposing the film surface to UV light. Polymerisation between the methacrylate substituents links the domains together, in unusual and anisotropic patterns, which depended on the extent of polymerisation of the organic substituents. Polymerisation was also initiated with the guided optical waves from 514.5 nm $Ar^+$ laser beam. As the guided mode propagated, it initiated the polymerisation of methacrylate substituents in its path. In this way, the silica domains were threaded to each other in a pattern that closely followed the path of the laser beam within the waveguide.

## 5.2 EXPERIMENTAL

### 5.2.1 Sample preparation

#### 5.2.1.1 Monoliths

The hybrid organic-inorganic monoliths were prepared from the SAC colloidal series described in Section 4.2, Chapter 4. These were prepared by the procedures described in Chapter 4, section. 10 weight % of the photoinitiator, Irgacure-819®, CIBA-GEIGY, was stirred into each sol, which was then passed through a 0.2 μm PTFE filter. The clear, bright yellow sols were placed in polystyrene cuvettes (1.5 $cm^2$ x 2 cm) and irradiated for 5 to 10 seconds with the focussed beam of a UV lamp (Oriel Corporation, CT. USA). Samples were irradiated from specific directions (Figure 5.5): from only one side (direction A, face 1 for 20 secs), from two sides consecutively (direction A, faces 1 and 2 for 10 secs each); from four sides consecutively (direction A, face 1, 2, 3, 4 for 5 secs each) and directly from above by reflecting the beam with a mirror (direction B for 20 secs). Each window was uniformly irradiated at 5mW-$cm^{-2}$ (measured at the maximum emission wavelength of 253.7 nm).

During irradiation, the initially fluid sols were rapidly converted into transparent solids. The uncovered samples were stored under ambient conditions in the dark for at least 20 hours, after which the non-sticky monoliths could be gently eased out by tapping the cuvette walls with a flat-edged spatula.

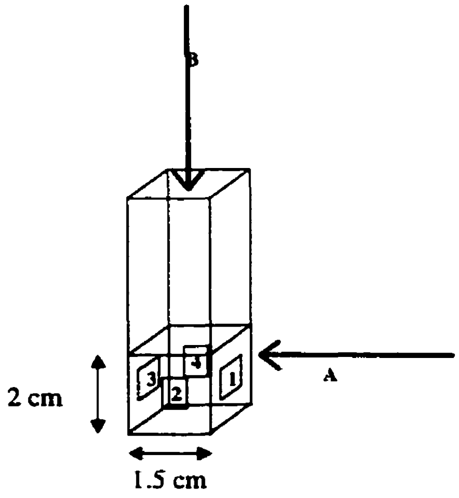

**Figure 5. 5** Irradiation of sols to create monoliths. Each face of the cuvette is numbered. The arrows A and B signify the direction of irradiation

**5.2.1.2 Thin films** were prepared from composite SAC-01, by the method described in Chapter 2. Precursor sols were doped with 1.5 wt % Irgacure-184® and Irgacure-784® for the UV and visible laser irradiation respectively. Free-radical polymerisation of methacrylate groups in the films was initiated with a focussed beam of UV light (irradiance of 8 $mW\text{-}cm^{-2}$ at 253.7 nm for 30 secs). A few drops of *iso*-propanol were placed on the surface of the film, which was then gently dried with a $N_2$ stream. A circular, silvery and highly reflective region corresponding to the irradiated area was revealed on the film.

Polymerisation was also initiated with optical modes that were excited in the thin film, planar waveguides with the 514.5 nm line of an $Ar^+$ laser (please refer to Chapter 4, for a description of the waveguide experimental-set up). After 15 minutes of irradiation at 100 mW, the waveguide was dismounted from its holder and quickly dipped into *iso*-propanol for 10 seconds and dried under a $N_2$ stream. Highly reflective, silvery regions were observed on the film, especially near the output edge of the waveguide. Under a reflection optical microscope, these areas were observed as either a series of microscopic lines that ran parallel to the long-axis of the waveguide or a mosaic of worm-like features arranged in slightly distorted basket-weave patterns.

#### 5.2.1.3 Preparation of iridescent films

Colloid SAC-01 was diluted 20-fold with *iso*-propanol. Films were cast at $5x10^3$ rpm for 5-10 seconds on $SiO_2$ coated Si wafers that had been cleaned by the process outline in Section 2.2, Chapter 2. Directly under sunlight or the emission from a Xe-lamp, the films showed a significant degree of iridescence. Under ambient light, the films had a silvery blue-green colour. Films retained their iridescence qualities even after being heated at 300° C for seven hours.

**5.2.1.4 Ridge and channel waveguides** were photo-inscribed on microscope slides with the photo-mask technique described in Section 2.2, Chapter 2.

### 5.2.1.5 Liquid crystal layering on waveguides

A layer of 4'-pentyl-4-biphenylcarbonitrile (5CB, nematic phase between 22.5 to 35° C, Aldrich) was introduced onto the surface of a set of channel waveguides inscribed on a glass substrate. A cover slip separated by thin Teflon inserts was placed on the film and fixed into place with two bulldog clamps. The entire assembly was stood vertically on a glass slide that had a few drops of 5CB. Once the LC film had formed (through capillarity), the sample was heated above the isotropic transition temperature (35° C) and then allowed to cool down to room temperature before being observed through a polarised optical microscope.

### 5.2.1.6 Thermal treatment of SAC monoliths and films

A Lindberg programmable furnace was used for thermal treatment. Samples (monoliths or thin films) were introduced into the tube-furnace in a quartz boat. Two heating-profiles were used. In one, the temperature was gradually raised from room temperature (RT) at 5° C $min^{-1}$ to 300° C, which was then maintained for 5 hrs. The temperature was then ramped down at a rate of 5° C $min^{-1}$ to R.T. The second profile was similar except the temperature was raised to 700° C, which remained constant for 3 hours. In the former case, both monoliths and films turned a slight orange-brown colour. Although the monoliths were three-dimensionally intact, the 5 μm thick films had fractured into several fragments, some of which had delaminated from the substrate. There were no visible changes in the heated iridescent films. At higher temperatures there was no detectable difference in film behaviour, although the monoliths were now a glossy black. Crushed pieces of the monoliths observed through a microscope, were a rich violet colour. If the temperature was maintained at 700 °C for 7 hrs, the monolith became a pale sandy beige and crumbled when pressure was applied with a spatula, for example. A clean-cleaved face of the latter monolith had an extremely pale bluish green tint.

## 5.2.2 Characterisation methods

### 5.2.2.1 $^{29}$Si NMR of SAC-01 monoliths

NMR spectra were acquired of SAC-01 monoliths prepared were crushed into a fine powder before sample acquisition. Samples were then crushed into fine pieces. Spectra were acquired on a 300 MHz Chemagnetics CMX300 spectrometer.

#### 5.2.2.2 Transmission electron microscopy

Monoliths were microtomed with a diamond tip pen. Slices were made perpendicular to the direction of irradiation. In the case of samples that had been heated at 700° C for 10 hours, monoliths were embedded in a transparent polymer Epon$^{TM}$ matrix before slicing.

#### 5.2.2.3 Scanning Electron Microscopy

A thin Au/Pd layer was evaporated onto thin films. Micrographs were acquired on a JEOL scanning electron microscope.

#### 5.2.2.4 FT-IR microscopy

Transmission IR spectra of thin films were acquired over a range of 400 to 5000 $^{cm^{-}}$1 with a Bruker IFS-48 Fourier transform infrared spectrometer. A Perkin-Elmer wire grid polariser was used for polarised IR spectroscopy.

#### 5.2.2.5 Polarised optical microscopy

A Nikon OPTIPHOT microscope with the UFX-IIA photo-micrographic attachment was used. Photographs were taken with a Nikon F-301 camera.

## 5.3 RESULTS AND DISCUSSION

### 5.3.1 Indications of structural organisation in SAC-01 thin films

Sol-gel derived composites are generally considered to be amorphous glasses, with corresponding isotropic optical properties. Several observations made during the course of our studies of SAC-01 thin films and integrated-optics devices contradicted this assumption and indicated the presence of a high degree of structural anisotropy in the silica-methacrylate materials. These observations are collected in the following Sections.

### 5.3.1.1 Optical anisotropy in SAC-01 ridge waveguides

The birefringence observed in SAC-01 ridge waveguides was one of the earliest indications of the non-random structural arrangement of the composite. A series of ridge waveguides were photo-inscribed on a SAC-01 thin film that was supported on a glass, microscope-slide and observed through crossed polarisers. The polarised micrograph of the devices is presented in Figure 5.6. The 10 μm wide waveguides are clearly visible, giving a qualitative indications that the devices had an anisotropic refractive index profile. The isotropic glass substrate by contrast, is invisible.

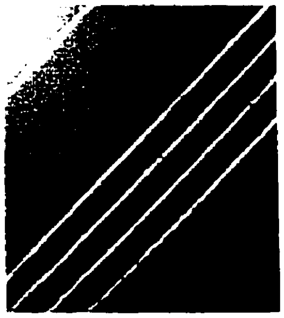

**Figure 5. 6** Polarised optical micrograph of ridge waveguides

#### 5.3.1.1.1 Optical anisotropy

Birefringence often originates from the strict, long-range, structural organisation of materials such as crystals. Several physical properties including the refractive index ($n$) of crystals depend on the direction (or the crystallographic axis) in which they are measured. Excepting cubic crystals, which are optically isotropic, the variations of $n$ in tetragonal, hexagonal, trigonal and other lower-symmetry crystals may be described by an uniaxial ellipsoid (optical indicatrix). An analysis of birefringence must consider the orientation of an incident, plane-polarised beam of light with respect to this indicatrix. As schematised in Figure 5.7, a beam of plane-polarised light will encounter an elliptical cross-section of the crystal's indicatrix at an angle $\alpha$, where the ellipse's major and minor axes represent different $n$ values. The electric field $\vec{E}$ initially vibrating in the plane perpendicular to the ray direction is now resolved into two orthogonal components corresponding to these axes. These components travel at different velocities though the crystal and acquire a different phase (retardation) with respect to each other.

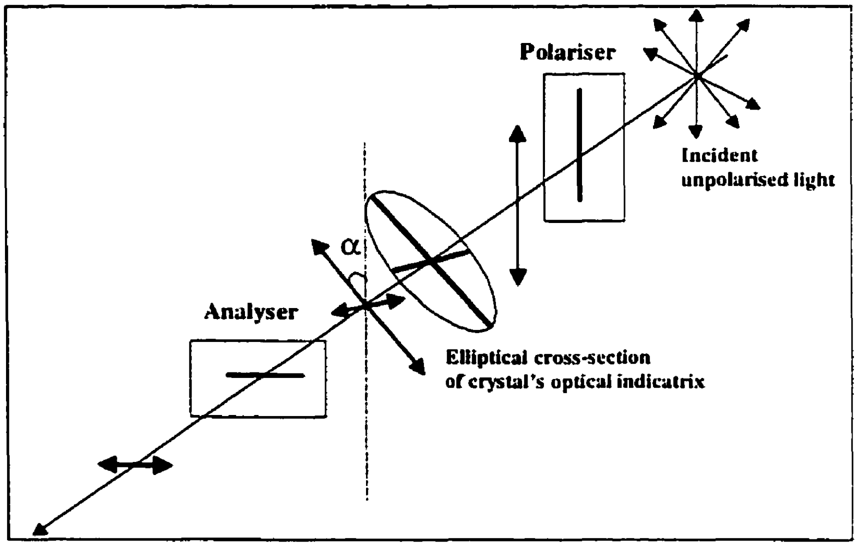

**Figure 5. 7** Schematic of the experimental set-up for the detection of optical birefringence

The beam is now elliptically polarised and has an $\vec{E}$ component that coincides with the crossed polariser (analyser). Anisotropic materials are thus visible through crossed polars. Note that if $\vec{E}$ coincides with either of the two principal axis of the ellipse, the analyser will block it. Two such extinction positions located at 90° to each other (*i.e.* corresponding to each elliptical axis) are always present in anisotropic crystals. Other optically anisotropic media include liquid crystals, polymers oriented by stretching or extrusion and isotropic glasses doped with dichroic chromophores. At the other extreme, the randomness of atomic arrangement and the lack of symmetry in glasses lead to an average *n*, which is independent of the orientation of the amorphous solid. Glasses are thus not visible between crossed polars as the plane of polarisation of the probe light is maintained across these homogenous media. The SAC-01 composites have, until now, been considered amorphous glasses. Their birefringence seen in the ridge waveguides clearly contradicts this assumption.

### 5.3.1.2 Orientation of liquid crystals on SAC-01 ridge waveguides

Figure 5.8 is a polarised optical micrograph of two SAC-01 ridge waveguides coated with a thin layer of the nematic liquid crystalline (LC) phase 4'-pentyl-4-biphenylcarbonitrile (5CB). The LC layer is self-aligned parallel to the long-axes of the two channel waveguides.

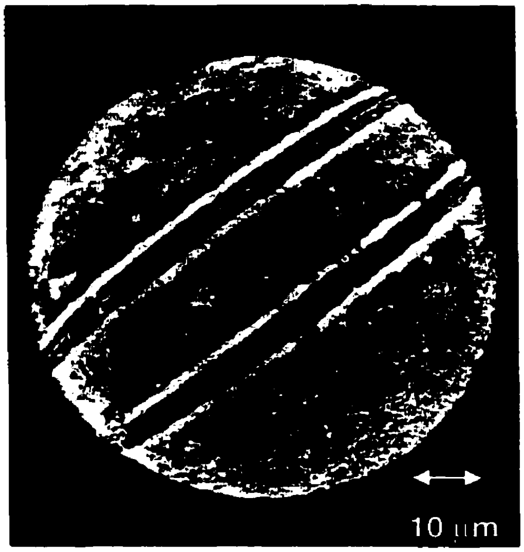

**Figure 5. 8** Polarised optical micrograph of SAC-01 ridge waveguides coated with a layer of 5CB

It is well known that LC layers align themselves along the "rubbing" direction of polymer substrates[62]. However, photo-orientation of substrates is now being examined as an alternative to mechanical rubbing, which often produces static and dust. Luo and co-workers[63] showed that 5CB layers could be aligned along oriented polymer-chains, which were deposited by pulsed laser ablation techniques. The behaviour of the LC layer may in turn, give information about the structural anisotropy of its host medium. For example, liquid crystals that were incorporated into photopolymer formulations (consisting of polymerisable monomer in a plasticiser) self-aligned in the direction of polymer-chain growth in thin films[64]. In this way the liquid crystals, clearly visible between crossed polars, amplified and enabled the optical identification of photo-oriented polymer chains in the matrix.

It follows then that the self-alignment of the 5CB layer along the narrow irradiated surfaces of the ridge waveguides, is a preliminary indication of some form of orientation in the SAC-01 thin film. Furthermore, this behaviour correlates to the birefringence observed in the untreated ridge waveguides and suggests that the optical anisotropy originates from structural organisation in the material.

### 5.3.1.3. Pyrolysis of organic component from SAC-01 to reveal inorganic skeleton

Amphiphile-mediated routes to ordered silica and metal-oxide structures were described in the Introduction. In many of these cases, the organic template is removed (see for example, Figure 5.1c) by heating the composite structure to above 250 °C. In the mesoporous framework that is left behind, the periodically arranged pores or voids represent the regions occupied by the organic component. They also indicate the type of organisational pattern that existed between the inorganic and the organic phases of the hybrid structure. Although there were no external surfactants incorporated in the sol-gel processing of SAC-01 composites (indeed there were no deliberate attempts to induce orientation in the material at this stage), similar thermal treatment of the thin films revealed the micro-structural order inherent to these composites.

In Chapter 2, Section 2.3, we presented scanning electron micrographs of a 5 μm thick SAC-01 film that had been gradually heated to 300 °C and maintained at this temperature for 3 hours. We noted that the edges of each fragment had curvaceous, "scalloped" edge, a feature that was repeated in each of the different pieces of the fractured film. Although there is no immediately evident order or periodicity to the fracture patterns, they are in sharp contrast to the jagged, fracture patterns that randomly propagate in amorphous glasses. The curved and radial morphologies of surfactant-templated silica ("morphokinetics") have been the subject of both theoretical and experimental study[65, 66]. These macroscopic shapes are attributed to defects or disclinations in the silicatropic liquid crystalline (SLC) mesophases, which precede silica formation. The defects, often 2 π disclinations, guide sol-gel processed silica growth and as a result are permanently imprinted in the final structure. The radial edges of the thin films fragments indicated some form of organised silica growth in the SAC-01 composite.

The suspected micro-structural organisation in the SAC-01 thin film was confirmed when the temperature was raised even further (to 700 °C) completely stripping the inorganic matrix of the organic component. Figure 5.9A shows a micrograph of a collapsed fragment of the film. The structure is composed of an array of approximately 0.2 μm wide inorganic rods (Figure 5.9B).

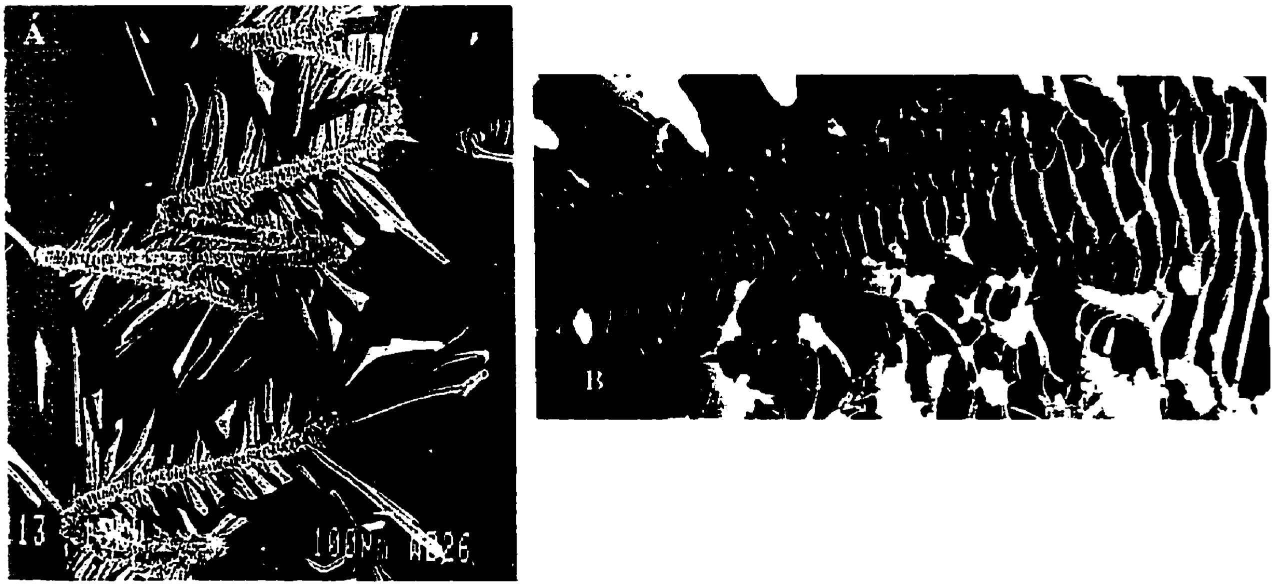

**Figure 5. 9** Scanning electron micrographs of the inorganic "shell" in SAC-01 film, upon removal of organic component.

### 5.3.2 Consequence of organisation in thin SAC-01 films on integrated-optics device fabrication

The zirconia modified, silica-methacrylate SAC-01 composites have been primarily applied in the photolithographic fabrication of passive, integrated-optics (IO) devices[67, 68]. In addition to the ridge waveguides[69] described above, the collection of SAC-01-based micro-optical elements includes laser-patterned optical waveguides[70], Fresnel lenses[71], channel waveguides[72, 73], surface gratings[74, 75], Bragg gratings[76], binary phase zone plates[77], splitters[78], directional couplers[79] and array waveguides (AWG) designed for wavelength division multiplexing (WDM) applications[80]. In each of these optical elements, the refractive index ($n$) profile is the crucial parameter that determines device-optical field interactions. For example, $n$ dictates the wavelengths of light and the number of optical modes ($m$) supported by slab, channel and ridge waveguides. In both surface and Bragg gratings, the size and the period ($\Lambda$) of the refractive index modulation ($\Delta n$) determine grating efficiency and the diffracted wavelength, respectively. Underlying all of these device-fabrication processes is the implicit assumption that the SAC-01 composites are amorphous glasses and therefore optically isotropic, with uniform $n$ profiles. However, the presence of structural anisotropy in the materials implies a corresponding inhomogeneity in $n$.

Conditions change when even a small anisotropy in the $n$ profile is introduced in a waveguide based device. Anisotropic waveguides have non-diagonal dielectric tensors, which cause the coupling between transverse electric (TE) and transverse magnetic (TM) modes propagating in the structure. Several of the devices listed above are designed for data communications or processing applications where such birefringence induced scrambling of polarisation may distort the signal transmitted by linearly polarised light waves. On the other hand, a carefully controllable birefringence is valuable in the design of polarising components such as half- and quarter-wave plates. However, surprisingly little attention has been paid to optical anisotropy in both the fabrication and characterisation of SAC-01 devices. Although Fardad and co-workers[76] noted the slight differences in the reflectivity of transverse electric (TE) and transverse magnetic (TM) polarised light in SAC-01-based Bragg gratings, there have been no detailed studies probing the optical or structural anisotropies of these composites.

In the following Sections, we trace the origins of the organisation observed in these systems to the colloidal form of the composite, which consists of an ordered arrangement monodisperse inorganic domains, surface derivatised with propyl methacrylate substituents.

### 5.3.3 Evidence of self-organisation in sol-gel derived SAC-01 colloids

#### 5.3.3.1 Polarised optical microscopy of SAC-01 monoliths

There is no precedence for any form of self-assembly or structural organisation in the sol or gel formed through the acid-catalysed hydrolysis and condensation of alkoxysilanes. The acid catalysed hydrolysis and condensation reactions of alkoxysilanes occur through bimolecular nucleophilic substitution ($S_N2$) mechanisms. In the hydrolysis step, the protonation of an alkoxide (-OR) group is followed by nucleophilic attack by a $H_2O$ molecule. In the condensation step, silanol (Si-OH) groups react between themselves or with other Si-OR functionalities to form siloxane (Si-O-Si) bonds. Here, Si-OH is protonated before the Si centre is attacked by either a Si-OH or a Si-OR group. As the most basic silanols are located at the ends of chains, acid catalysed sol-gel reactions generally form extended, linear polymeric silicates. Cluster-cluster aggregation between these species leads to an open, mass fractal network, which is by definition structurally isotropic[61]. Our SAC-01 system is based on the acid catalysed sol-gel reactions of the organosubstituted alkoxysilanes, 3-methacryloxy propyl trimethoxysilane. The unique structural character of this system, which contradicts the accepted mass fractal model, is described in the following Sections.

The colloidal form of the SAC-01 composite was studied by first converting it to a monolith. This was achieved by initiating the free-radical polymerisation of methacrylate groups in the network. Within 5 to 20 seconds of UV irradiation, the fluid sol was converted to a crack-free, optically transparent monolith. The dimensions of the composite-block could be as large as 2 x 2 $cm^2$, which remained clear with no visible phase separation over 9 months and suffered approximately 10 % shrinkage due to further condensation reactions in the matrix.

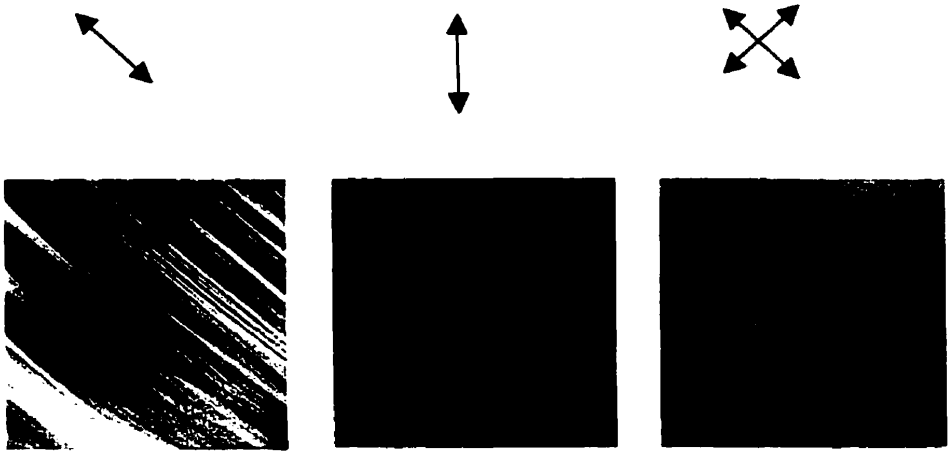

**Figure 5. 10** Polarised optical micrographs of SAC-01 monoliths where a) sample irradiated in single direction b) sample a) rotated by 45° and c) sample irradiated from two opposite directions. Irradiation directions are indicated with double-headed arrows. (magnification x 100)

The optical anisotropy of the monolith became evident when it was observed through crossed polars. The polarised photomicrograph (Figure 5.10) showed a visible, white background that was clearly birefringent, with dark, roughly parallel striations (approximately 1/10 μm wide). The white regions were completely extinguished when the sample was rotated by 45° in both clockwise and anticlockwise directions (Figure 5.10). The dark, narrow lines in the slab were optically isotropic and remained unchanged when the sample was rotated about 360°. However, their alignment across the slab corresponded to the direction in which the sols had been irradiated (see Figure 5.10b). When the square monolith was rotated by 90° and irradiated again, a second set of dark lines was created in this direction. The polarised micrograph of this grid of intersecting lines is presented in Figure 5.10c.

The two most striking features of these observations are i) the spatial localisation and alignment of the free-radical polymerisation reactions in the sol and ii) the apparent anisotropy of the host silicate matrix. Although the monolith was optically transparent (and remained so for more than 6 months), the micrograph indicates that the free-radical reactions were spatially segregated in narrow (approximately 1/10 μm wide), linear regions in the birefringent host. The polymerised regions themselves were optically isotropic but their orientation in the monolith coincided with the direction of irradiation. This sensitivity of the reactions to the direction of the incident UV light was illustrated by the ability to rotate the monolith and photo-inscribe another series of "polymerised lines". This also confirmed that not all the methacrylate units were consumed with the first dosage of UV light; *i.e.* that the free-radical reactions were strongly localised to the regions of irradiation.

The localisation of photoinduced, free-radical reactions in SAC-01 thin films has been consistently emphasised in this thesis. This material property was observed in the photolithography of micro-optical devices, characterised by IR, $^{29}$Si NMR (Chapter 2) and waveguide Raman spectroscopy (Chapter 3) and employed for the self-focussing of monochromatic light (Chapter 4). In thin films, the poly-silicate species exist in a closely packed environment, with low solvent content. Free-radical reactions are restricted here partly because of this highly viscous reaction medium, which decreases diffusion coefficients and consequently the propagation rates of the reactions. Furthermore as described in Section 2.3, Chapter 2, polymeric silicate species are tightly packed on the substrate and as methacrylate substituents link to each other during polymerisation, their Si centres with residual -OH and $-OCH_3$ groups are brought closer together and engage in condensation reactions. The resulting growth and compaction of the silicate host is likely to raise an additional steric barrier against the propagation of the polymerisation reactions.

However, free-radical polymerisation reactions may be expected to be less sterically hindered in a fluid colloidal medium and proceed at rates that may even cause phase separation between the growing organic polymer and its inorganic host. This was observed in tetraethoxysilane derived silicate sols, doped with free methacrylate monomer. Once polymerisation was initiated, the composite became opaque as the poly (methyl methacrylate) phase precipitated out of the silica medium. It may be argued that phase separation in the SAC-01 composites discussed here, is prevented because the polymerisable substituents are covalently linked to their silica host. However, this does not account for the spatially segregated, linear and oriented "polymerised lines" in the monolith. As described previously, the acid catalysed sol-gel process of alkoxysilanes leads to networks that are characterised as fractals, which by definition are isotropic structures. Methacrylate substituents bound to the Si centres would be uniformly distributed in such a structure. Free-radical polymerisation between these substituents would also have no preferred orientation and should produce a composite that is optically isotropic.

The unusual photo-polymerisation characteristics in the SAC-01 composite are reminiscent of those of acrylate monomers hosted in a smectic liquid crystalline (LC) phase[81]. The fluid liquid crystalline (LC) matrix allowed a certain degree of flexibility for the molecular motion and diffusion required by the free-radical reactions. However, its layered structure imposed both spatial and orientational constraints on the photochemical reaction. Simple acrylates such as 1,6 hexanediol diacrylate intercalated themselves between the smectic layers whereas mesogenic monomers aligned themselves within the oriented layers. In the resulting composite, the polymeric component was spatially segregated and had a high degree of orientation.

In light of the above study, the birefringence observed in the SAC-01 medium becomes significant. The optical anisotropy seen here as a "white background" is uniform throughout the sample (3 x 3 $mm^2$) and has two extinction positions located at 90° to each other. This single-crystal like behaviour of the monolith indicates a long-range, periodic structural organisation. The composite's transparency to visible light indicates that the dimensions of this structural arrangement are smaller than the wavelength of visible light (400 nm). Similar optical characteristics have been reported for amphiphile-templated silica with a long-range HCP arrangement of mesoscale pores[82]. Here, the silica sheet was optically transparent to the naked eye but was visible between crossed polars due to the strict structural anisotropy of the HCP arrangement. Transparent, mesoscopically ordered silica monoliths have also been obtained with block copolymer composites[83].

With these considerations, Figure 5.11 presents a possible explanation for the POM observations made here. In the colloidal form (Figure 5.11a), the silica component consists of a 3-dimensional, layered structure with pendant propyl methacrylate groups occupying the interfacial sites. Upon UV irradiation, the free-radical polymerisation reactions of these functional groups are initiated. Due to steric hindrance imposed by the silica scaffold, polymerisation proceeds in a spatially confined manner, with vinyl groups reacting only with their closest neighbours. In the final hybrid monolith, the polymerised regions are intercalated between the silica layers, corresponding to the "lines" observed in the optical micrographs. In turn, the polymerisation of the organic component captures the organisation present in the inorganic network (Figure 5.11b), leading to a structurally and optically anisotropic monolith. As the spatial segregation between the inorganic layers and the methacrylate polymer, occurs below < 400 nm, the monolith is transparent to visible wavelengths.

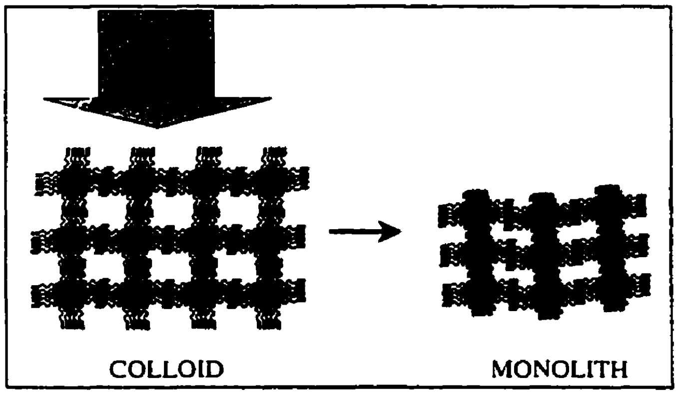

**Figure 5. 11** Schematic of photo-initiated free-radical polymerisation of methacrylate substituents hosted in an organised inorganic host

### 5.3.3.2 Long-range, periodic and sub-micrometric self-organisation in SAC-01 monoliths – evidence from transmission electron microscopy

Clear evidence of long-range, periodic structural organisation in the SAC-01 monolith was obtained through transmission electron microscopy (TEM). Micrographs of cross-sections of the monolith are presented in Figures 5.12 and 5.13. The microtomed section consists of a densely and regularly packed array of layers, each approximately 250 nm wide. Although the arrangement may be superficially described as lamellar, closer examination (Figure 5.13a) reveals that each layer has an undulating or "wavy" edge. Dark and light regions, indicating electron rich (inorganic) and poor (organic) regions may also be identified within each layer, but there are no clear indications of phase separation in the micrographs.

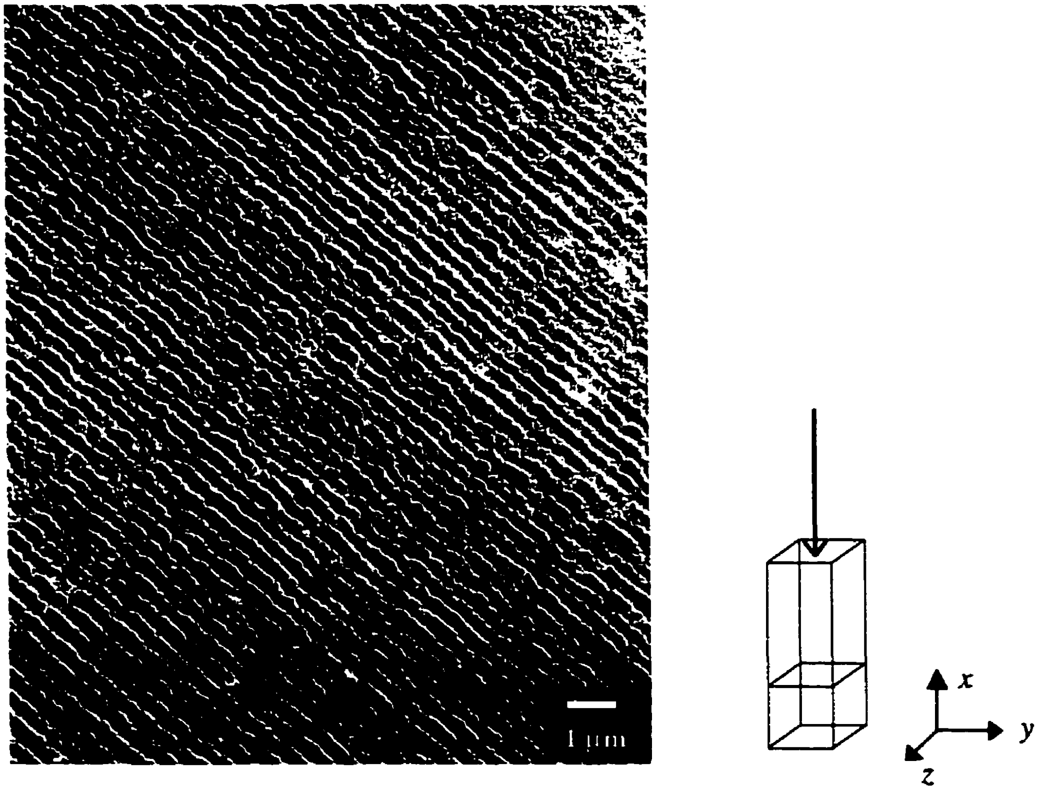

**Figure 5. 12** Transmission electron micrograph of the cross section of a SAC-01 monolith. As schematised, SAC-01 colloids were irradiated in the *x* direction and the cross-section made in the *xy* plane.

Figure 5.13b shows a defect in the sample where three of the layers have separated (due to some strain introduced during sample preparation) from the matrix. The micrograph indicates that each layer is discretely formed and may be easily separated from its neighbours. The exposed edges of the structures are "fuzzy" indicating that a mutual interfacial layer attached them to each other. This is also evident in the framed section of the micrograph, which identifies that a common achesive layer links the two rods. It is possible that this interfacial material is the methacrylate polymer. This correlates to the previous observations made with polarised optical micrographs. As schematised in Figure 5.11, the TE micrographs indicate that the SAC-01 colloid consists of a self-organised layered array of inorganic domains. Once the free-radical reactions are photo-initiated, the methacrylate substituents confined to the interfacial regions between inorganic layers link to each other through the polymerisation reactions. In this way, the free-radical reactions capture the structural organisation present in the SAC-01 colloid. This is further supported by the fact that the powdered form of the SAC-01 monolith is strongly immiscible in aqueous solutions. This is unusual in a sol-gel derived composite, which as indicated by IR and Raman spectroscopy (Chapter 2, 3) is rich in residual, polar silanol groups. The hydrophobicity observed here might be because of the organic methacrylate polymer, which dominates the surfaces of the hydrophilic silicate domains.

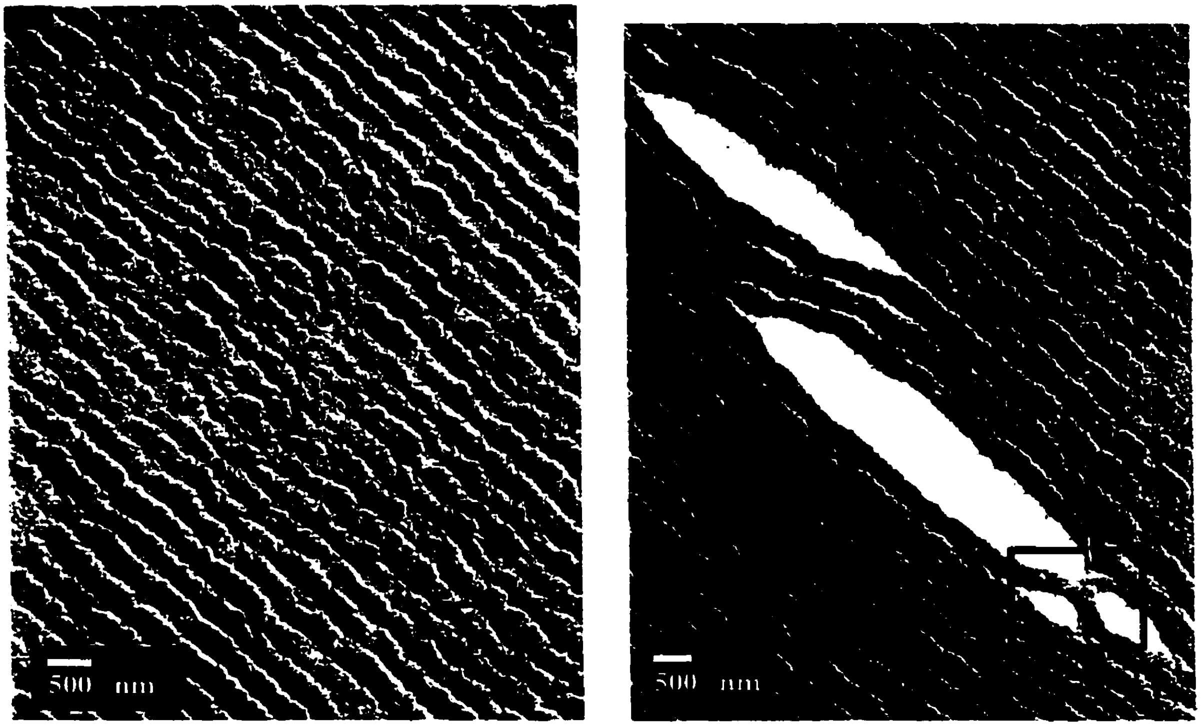

**Figure 5. 13** Higher magnification micrographs of structural organisation in the SAC-01 monolith. Figure 5.13B shows that each layer is discretely formed and is attached to at the interfacial region (see region within black square).

### 5.3.3.3 Role of photo-initiated methacrylate polymerisation reactions

Two different polymerisation processes are involved in the formation of SAC-01 monoliths; the first being the inorganic polymerisation (sol-gel) reactions, which lead to the formation of the inorganic silicate network and the second, the photoinitiated free-radical polymerisation of the methacrylate substituents. The observations made in the previous Sections, suggest that the inorganic polymerisation reactions lead to a self-organised, lamellar arrangement even in the colloidal form of the SAC-01 composite. The role of the second organic polymerisation reactions then is to simply "freeze" or capture this structural anisotropy in the resulting monolith. Indeed, the strategy of polymerising functional groups to immobilise the structural organisation of liquid crystalline mesophases has been employed by other researchers[84].

According to this model, the free-radical polymerisation does not have any direct influence on the structural organisation of the inorganic network. If the polycondensated silicate species exist in a pre-organised assembly in the SAC-01 sol, then the monoliths should have identical structural morphologies, irrespective of the direction from which the sample is irradiated. Figure 5.12 shows the cross-section ($x$-$y$ direction) of the monolith that was irradiated from the $x$ direction. An identical layered morphology with each layer approximately 250 nm wide, is shown in Figure 5.14. This belongs to the cross-section ($x$-$y$ direction) of a monolith that was irradiated from the z direction. The same structure was observed in the micrograph of a monolith that was irradiated in the direction (not shown here). This confirms that the organisation observed in the SAC-01 composite is inherent to the sol-gel stage of the process and that the secondary organic polymerisation does not introduce any form of organisation into the composite.

Conversely, the TE micrographs reveal the layered morphology of the inorganic host, which must impose spatial constraints on the photochemical reactions. This correlates to the observations made through POM, of the spatial segregation of the polymerised regions into layered regions (Figure 5.11). In addition, the preferential orientation of the polymerisation in the direction of irradiation (Figure 5.10) may be due to the spatial localisation of the reactions in the matrix. As the regularly packed inorganic host imposes steric constraints on the free-radical reactions, they are strongly confined to the regions of illumination. The orientation of polymer growth in the direction of irradiation has also been observed in photopolymer compositions[64]. Here, monomer diffusion is limited by the viscous plasticiser host and the free-radical reactions demonstrate a strong localisation to the direction of illumination.

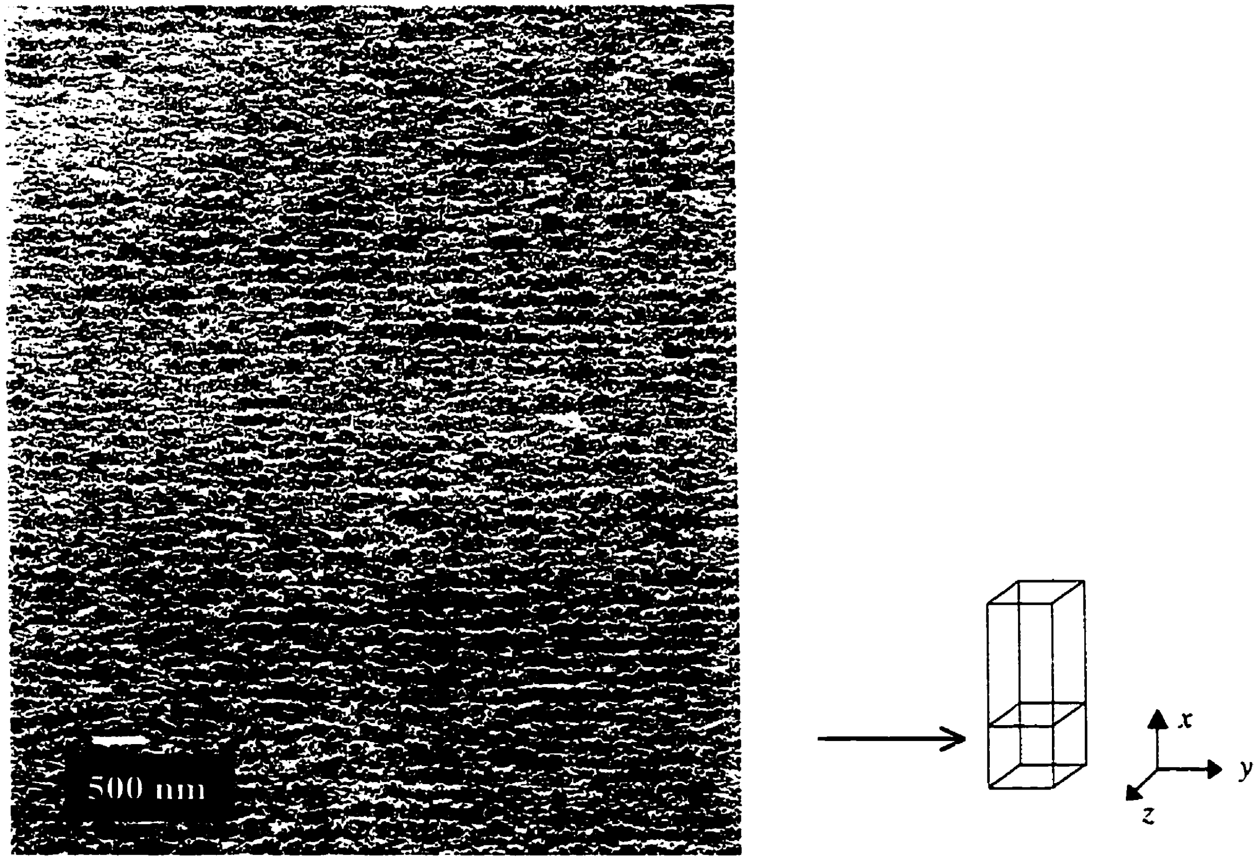

**Figure 5. 14** Transmission electron micrograph of the x-y cross-section of an SAC-01 monolith, which was irradiated from the y direction, *c.f.* Figure 5.12

### 5.3.3.4 Selective removal of organic component to examine inorganic skeleton of SAC-01 composites

In most of the template-based routes to silica (and metal oxide) materials, the organic template is removed from the ordered amphiphile-silica composite by calcination. This is achieved by slowly heating the composite to above 250 °C, thereby pyrolysing away the organic component. The thermally stable inorganic structure left behind is amorphous, but contains an organised array of voids or pores, which represent the regions occupied by the amphiphiles. Generally, there is a slight shrinkage in the resulting structure due to further condensation reactions between residual alkoxide and silanol groups in the inorganic network, during calcination. This is observed in X-ray diffractograms as a slight decrease in the d-spacing of the structure. However, the pattern of structural organisation of the amphiphiles-silicate composite is preserved in the final material.

For our purposes, the gradual removal of the organic, methacrylate component from the SAC-01 composite gave valuable insight into the micro-structural organisation of the material. Figures 5.15-5.21 display TE micrographs of monolith cross-sections that trace various stages of calcination of the matrix. The cross-section of a monolith sample that had been heated at 300 ° C for 3 hours is presented in Figure 5.15. The lamellar morphology that was evident in the non-heated monoliths (Figures 5.12-14) is significantly enhanced in this sample. Observe also, that there is a clear alternation between grey (electron poor) and darker (electron rich) regions, which may be attributed to organic and silica phases respectively. We may assume that upon heating, polycondensation reactions take place in the inorganic network. Simultaneously, there will be a gradual burning out of the organic phase. Thus, there is growth and consolidation of the inorganic framework, with depletion of the organic polymer. These processes, reveal the underlying phase separation between the two components, which was not evident in the unheated monolith.

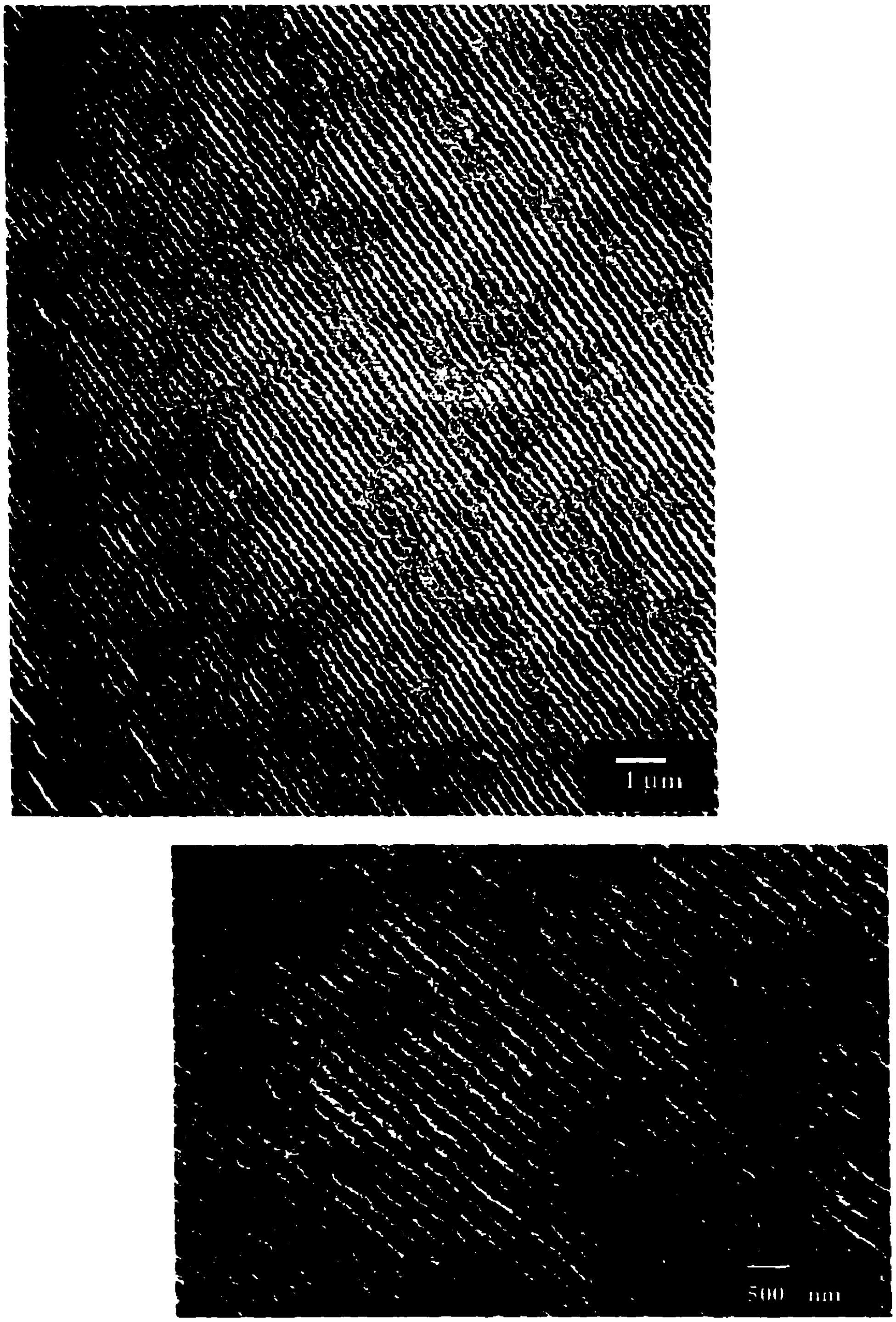

**Figure 5. 15** Cross-sectional transmission electron micrographs of SAC-01 monoliths that have been heated at 300 °C for 5 hrs.

A larger proportion of the organic component is removed upon further heating of the SAC-01 composite. The micrographs presented in Figure 5.16 are cross-sections of a monolith that had been heated at 700 °C for 3 hours. Observe that in all of the cases, the sample now consists of an inorganic "skeleton", composed of rods that are approximately 200 nm wide. Each rod is surrounded with a lighter-coloured layer, most likely residual methacrylate polymer. The voids between the rods represent the regions that were occupied by the organic component, indicating that methacrylate polymer had indeed occupied interfacial regions in the composite, thus serving as an adhesive layer for the inorganic framework. It is also important to not that the spaces between the inorganic rods do not strictly correspond to the dimensions of the organic phase. As the inorganic rods are now quite flexible, they tend to distort easily.

The most striking feature in this set of micrographs is the actual arrangement of the inorganic component. It is clear from the cross-sectional micrographs presented in Figure 5.16 that the hybrid silica-methacrylate composite does not have a simple lamellar morphology, as deduced from previous transmission electron and optical micrographs. The higher magnification micrographs presented in Figure 5.16, reveal that the inorganic rods are not continuous and linear. Rather, they assume an interdigitated arrangement. This "brick-wall" like arrangement of inorganic domains in the composite is clearly evident in Figures 5.16 c and d. Significantly, there is a long-range regularity or periodicity associated with the interdigitated arrangement of the silica-rich regions. It is also evident from Figure 5.16 a and c, that methacrylate polymer must link the inorganic domains to each other at both the interfacial and nodal regions. This feature will be discussed in a later Section.

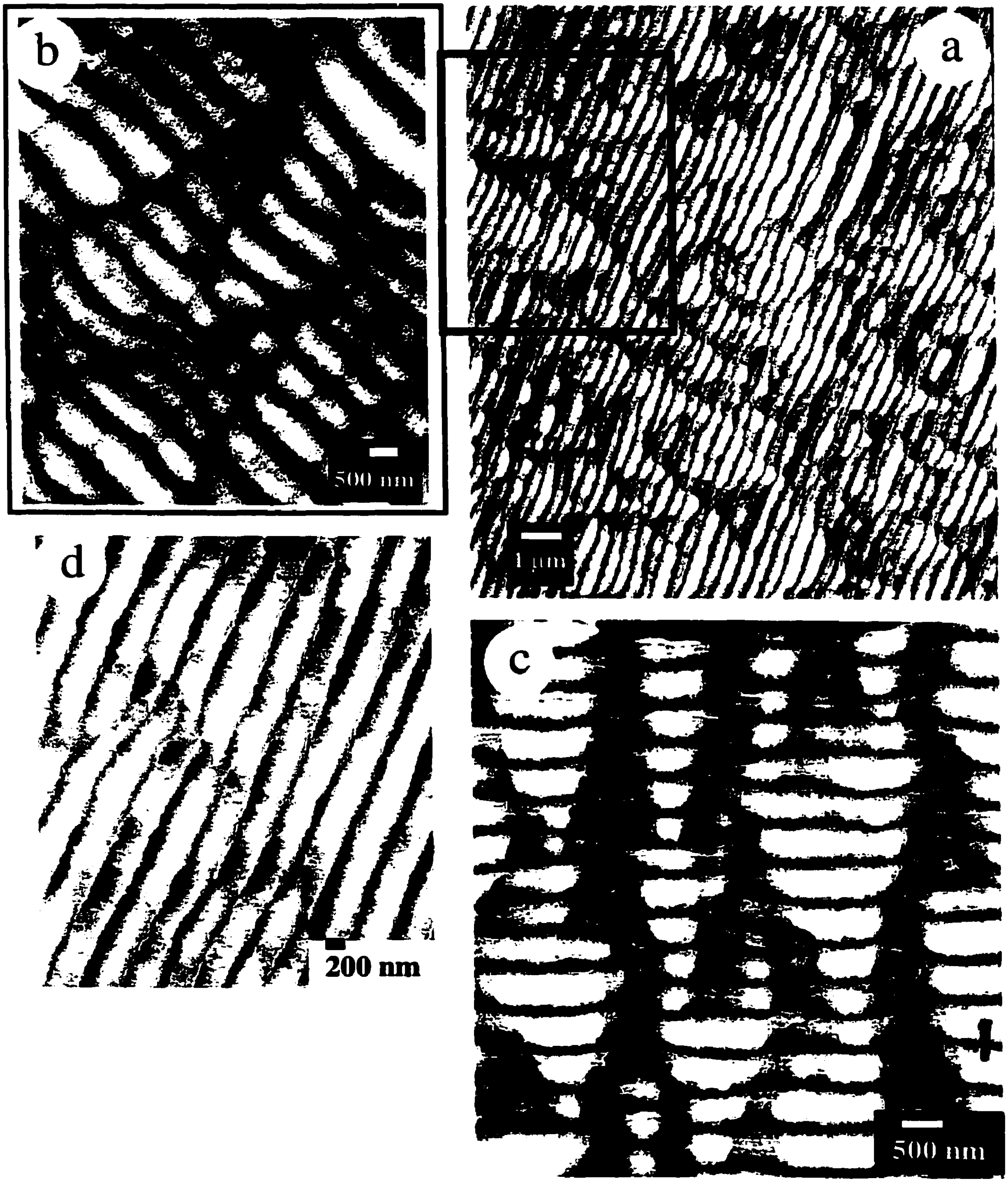

Figure 5. 16 Cross-sectional micrographs of SAC-01 monoliths that were heated at 700° C for 3 hours.

The regularity and periodicity of the interdigitated arrangement was preserved even when the monolith was heated at 700 ° C for 10 hours. In the majority of samples examined through transmission electron microscopy, most of the organic component had removed from the composite at this stage of thermal treatment. Figure 5.17 compares the solid state $^{29}$Si NMR of a SAC-01 monolith that had a) not been heated and b) one that had been heated at 700 ° C for 10 hours. Spectrum (a) contains signals at -58.9 and –66.6 ppm that may be assigned to $T_2$ and $T_3$ Si centres respectively. As mentioned in Section 2.3, Chapter 2, the subscript refers to the number of siloxane bonds present at the Si centre. T signifies the presence of an organic substituent in the trialkoxysilane precursor. Upon pyrolysis of the organic component, spectra (b) indicates that the Si centres present in the matrix correspond to $Q_2$ and $Q_3$ species at –63.9 and 99.3 ppm respectively. Q signifies a tetrafunctional Si centre (*i.e.* without a non-organosubstituted centre). In our case, this confirms that the organic substituent had been removed from the Si centre. Significant changes in the silica matrix are evidenced by FT-IR spectra of the two samples. Figure 5.18 shows that the $v_{as}$(Si-O-Si) mode has shifted from 1080 cm$^{-1}$ to 1018 cm$^{-1}$ upon thermal treatment. In Section 2.3 of Chapter 2, we associated the shift to low energy of the siloxane band to a decrease in the siloxane bond angle, signifying matrix compaction. The significant shift of wavenumber observed here, indicates heat-induced densification takes place in the SAC-01 composite.

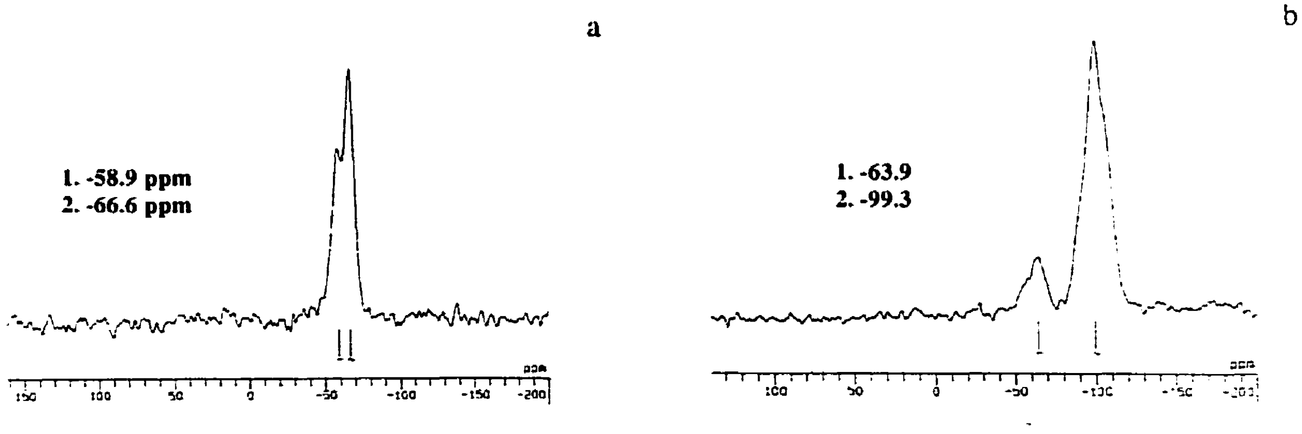

**Figure 5. 17** $^{29}$Si NMR of SAC-01 monolith that was (a) unheated and (b) heated at 700 ° C for 10 hours

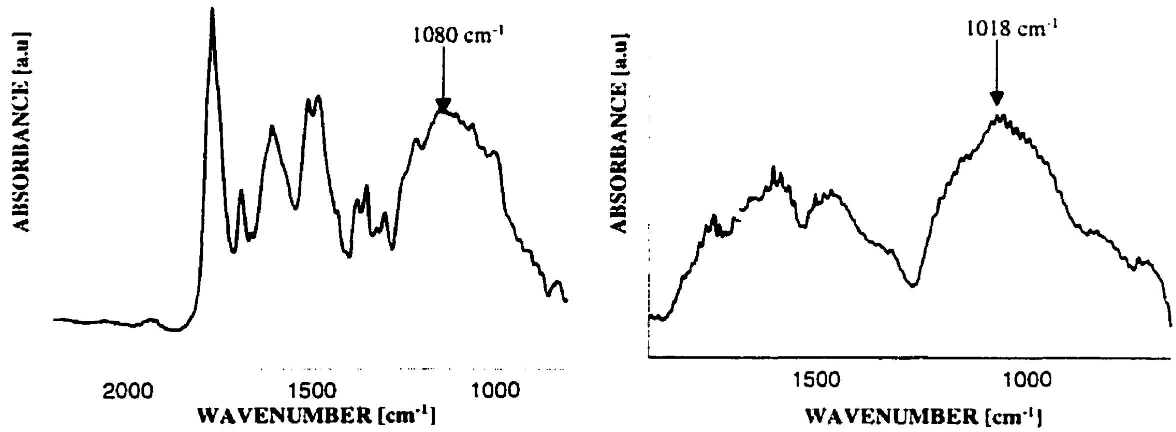

**Figure 5. 18** FT-IR spectra showing $v_{as}$(Si-O-Si) band of SAC-01 monolith that was (a) unheated and (b) heated at 700 ° C for 10 hours

As mentioned earlier, the interdigitated arrangement of inorganic domains was retained as the microstructure evolved with thermal treatment. Cross-sectional micrographs presented in Figure 5.19 show that the inorganic framework separates into filaments as most of the methacrylate polymer is removed from the system. In some regions (Figure 5.19 b, the inorganic filaments, although unconnected to each other, were arranged parallel to each other. In others, the filaments had conglomerated into sheaves during sample preparation. The interdigitated organisation that was evident in Figure 5.16 is also present here. Note that each narrow strip of silica has scalloped walls. It is also evident, that there is an interfacial (lighter coloured) layer along these strips. Closer examination (Figure 5.20) reveals that the scalloped edges of each narrow silica-rich strip, consists of individual inorganic domains that have been linked to each other with the methacrylate polymer. Note that the lighter material namely, the methacrylate polymer is present at the "nodes" as well as the interfacial regions of the silica rods. This reinforces our previous observations that the organic polymer serves as an adhesive that supports the inorganic frame of the SAC-01 monolith. In other regions of the sample (Figure 5.21), there was no evidence of methacrylate polymer although the inorganic filaments were not separated but were arranged with long-range periodicity, in an interdigitated arrangement.

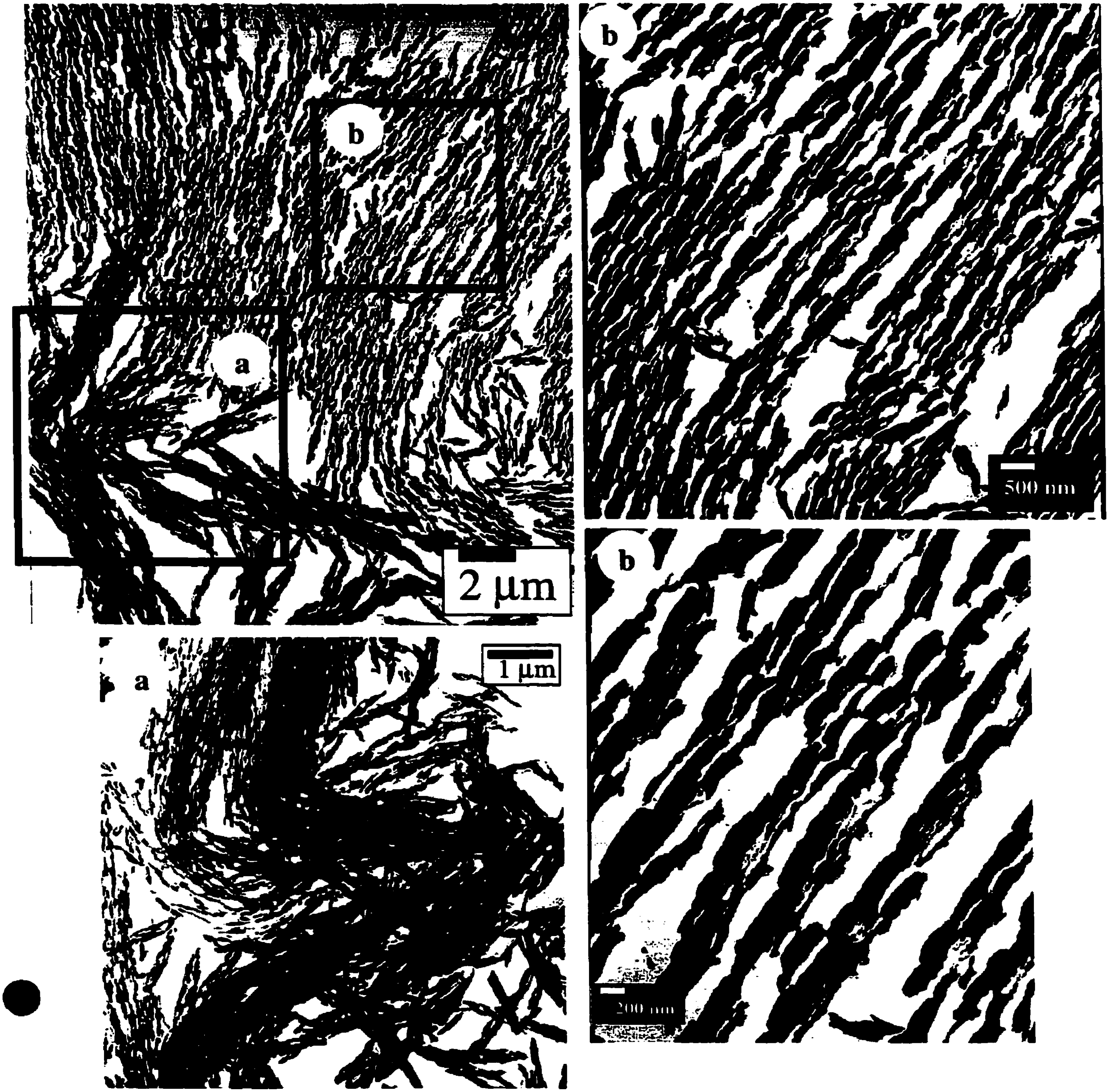

**Figure 5. 19** Cross-sectional transmission electron micrographs of SAC-01 composites that had been heated at 700 °C for 10 hours

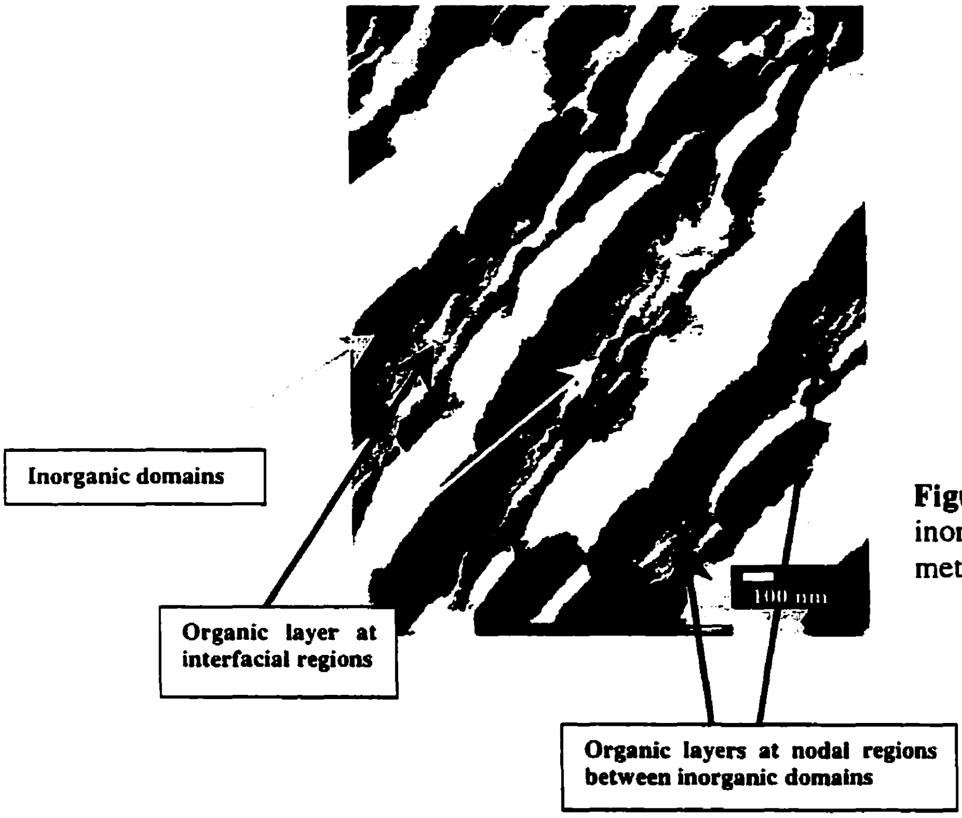

**Figure 5. 20.** TEM showing inorganic domains linked by methacrylate polymer

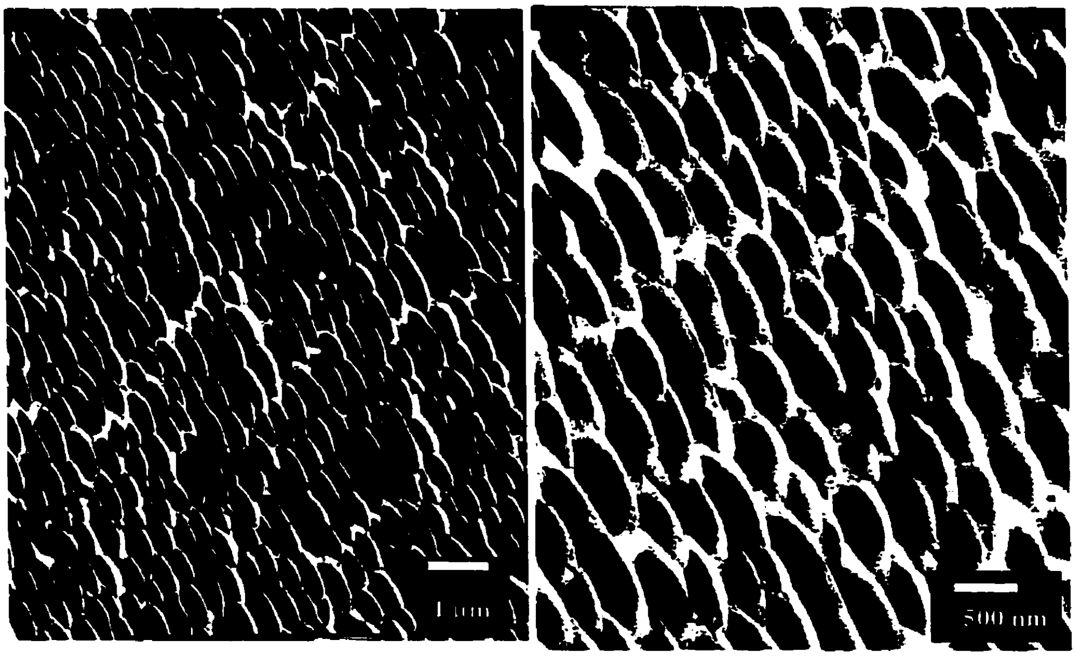

**Figure 5. 21** TEM showing long-range, interdigitated arrangement of inorganic framework

### 5.3.4 Origins of order in sol-gel derived SAC-01 composites

The electron micrographs show that *self*-organisation in the hybrid organic-inorganic composite is based on the spatial segregation of the hydrophilic, sub-micrometric inorganic domains bordered by hydrophobic methacrylate regions. This is a strong, preliminary indication that an amphiphilic mediator was involved in the order-creating process; *i.e.* reducing the interfacial tension and mediating the coexistence of the immiscible hydrophobic and hydrophilic sections. However, in attempting to rationalise the order-creating process and identify a possible mechanism through which it occurs, it is instructive to consider the mechanisms that underlie the conventional amphiphile based synthetic pathways to ordered inorganic structures.

#### 5.3.4.1 Self-assembled amphiphiles as templates for ordered inorganic structures

Until the research presented in this Chapter, synthetic routes to sol-gel derived, ordered mesoporous silica and metal oxides have invariably used *external* "order-directing" templates. As mentioned in the Introduction, these are often aqueous solutions of amphiphilic molecules (surfactants) and macromolecules (block copolymers), which self-assemble into spherical and columnar micelles that have hydrophobic cores and hydrophilic surfaces. With increasing surfactant concentration, the micelles coalesce into liquid crystalline (LC) mesophases with well characterised, HCP, cubic and lamellar geometries. In these systems, the hydrolysis and polycondensation reactions of silicon or metal alkoxide precursors are strictly confined to the aqueous regions of the supramolecular arrays. As a result, the inorganic polymerisation reactions create an amorphous silica or metal oxide structure that is an inverse replica of the organic LC phase. It is important to note that in the case of neutral surfactants and block copolymers templates, no strong chemical interactions take place at the amphiphile-silicate interface during the inorganic polymerisation reactions. Although in some cases, hydrogen-bonding between silicate species and surfactants have been reported[21], the sol-gel process remains largely passive in the "order creating" step, *i.e.* it simply constructs an amorphous cast around a pre-existing organised structure.

### 5.3.4.2 Silicatropic liquid crystals

The existence of a pre-organised liquid crystalling assembly is not necessary for silica growth with ionic surfactant templates. Mesoporous silica structures with long-range HCP organisation form at concentrations of ionic surfactants (e.g. cetyltrimethylammonium bromide (CTAB)) even below the critical micelle concentration (CMC), *i.e.* in the case of ionic surfactants, an organic template with pre-existing, long-range organisation is not a prerequisite to create ordered, mesoporous silica. Indeed, this is a commonly observed feature in biomineralisation and biomimetic processes where a relatively low weight percent of organic species leads to inorganic structures with long-range organisation. The mechanism underlying this process was provided by Firouzi and co-workers[18]. Through a series of elegant experiments complemented by TEM, XRD and NMR characterisation techniques, these researchers demonstrated that cubic octameric silicate anions ($Si_8O_{20}^{8-}$) added to low concentrations of CTAB, displaced the surfactants' counterions and engaged in multi-dentate coordination with the cationic head groups. Such cooperative, molecular level interactions between the inorganic and the organic species led to a unique liquid crystalline (LC) mesophase (termed silicatropic liquid crystalline (SLC) phase) that consisted of both the silicate anions and the surfactant species. This new LC phase attained its own thermodynamic equilibrium and was influenced by parameters such as pH, temperature and ionic strength.

The nature and phase behaviour of the SLC were governed by the coordination, steric effects and charge density at the silicate-surfactant interface. For example, the multidentate binding of the silicate anion reduced both inter and intra micellar aggregate repulsion by shielding the positively charged head groups. In addition, unlike the displaced counterions (e.g. Br- or OH-), the oligomeric silicate anions could simultaneously bind to several surfactant molecules forming "multi-tailed" amphiphilic species, which reduced the curvature of the SLC phase. Collectively, these characteristics encouraged associative interactions between micellar units and shifted the system towards a liquid crystalline phase. Thus, when silicate anions were added to concentrations of surfactants, which by themselves did not form a LC phase, the silicate-surfactant composite species could precipitate out as a SLC with lamellar or HCP organisation.

The work discussed above presented two important, new perspectives to the template-guided growth of ordered silica structures, which are relevant to our SAC-01 systems: i) sol-gel silicates, by forming the SLC phase, were now active participants in the "order creating" process. Here, the "composite silicate-organic" SLC mesophase guides the inorganic polymerisation reactions of the alkoxysilane molecules. The final silica structure is not only an inverse replica of the SLC phase (typically mesoscale HCP arrangement) but its macroscopic (microscale) morphology is strongly influenced by defects and disclinations in the liquid crystalline mesophase[66]; ii) the study also emphasised the critical role played by the silicate-surfactant interface. The strong ionic bonds between the silicate anion and the surfactant essentially creates a new organic-inorganic amphiphile with a hydrophile - silicate head - and a hydrophobe – the long alkyl tail belonging to the surfactant. These amphiphiles are then able to self-assemble into their own liquid crystalline mesophases.

#### 5.3.4.3 Amphiphilic interactions in SAC-01 colloids

Both the features listed above are relevant to the problem at hand – providing an explanation for the order observed in the SAC-01 composite. As mentioned earlier, there were no external templates incorporated into the SAC-01 formulation, which implies that any amphiphilic interactions must be inherent to the sol-gel derived silicates themselves. We reasoned that such an amphiphile might in fact be the hydrolysed product of the alkoxysilane precursor, 3-methacryloxy propyltrimethoxysilane (MAPTMS). Note that initially this is an organic and thus a hydrophobic molecule. However, once hydrolysis is initiated, at least one its methoxide substituents is converted to a hydrophilic silanol group. The MAPTMS molecule thus acquires a hydrophilic "head group" with a seven membered, organic hydrophobic tail (the propyl methacrylate substituent). Whereas in the case of the ionic surfactants discussed above, the silicate species was bound to the surfactant through an ionic bond, here the hydrolysed silicate precursor is covalently bound to a hydrophobic organic group.

The concept of a covalent bond linking silicates to the surfactant, in ordered hybrid structures is not new. The various possible interactions between the surfactant (S) and the inorganic silicate species (I) in template-guided growth processes listed in the

Introduction includes S-I, which signifies a covalent bond linking the two components. Until now however, such interactions have remained unexplored in synthetic routes to ordered silica structures. This is despite the commercial availability of a wide variety of alkoxysilanes with long (up to 18 membered) alkyl chain substituents, reminiscent of the commonly used cetyltrimethylammonium surfactants.

As with neutral amphiphiles, the hydrophobic effect or the tendency of the propyl methacrylate substituent to minimise contact with the polar solvent ($H_2O$) balanced by the preference of the silicate species (the head group) to interact with $H_2O$, may lead to a self-assembled, equilibrium phase of the hydrolysed MAPTMS species such as the one schematised in Figure 5.22.

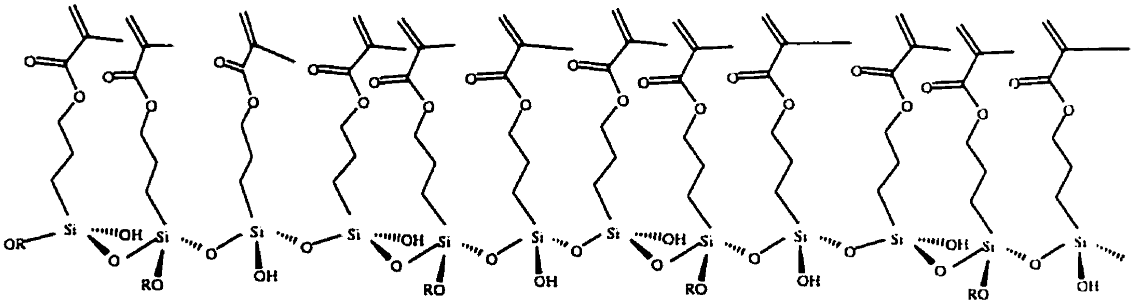

**Figure 5. 22** Schematic of possible amphiphilic layer created by hydrolysed MAPTMS molecules

Such a model must then take into account the simultaneous condensation reactions that take place in the system. Once hydrolysed, the MAPTMS molecules do not remain monomeric but engage in polycondensation reactions with other silanols to form siloxane bonds. A high degree of cross-linking between the polar head groups would impose considerable steric hindrance on the tendency of the amphiphilic species to self-organise. However, it is known that the rate of condensation reactions are minimised in acid catalysed, sol-gel reactions of alkoxysilanes, leading to weakly branched, polymeric silicates. In the SAC-01 composite, this is evident by the residual Si-$OCH_3$ and Si-OH groups observed in the IR and Raman spectra (see Chapters 2, 3). Furthermore, the solid state $^{29}$Si NMR of the monolith shows a significant proportion of $T_2$ species relative to the $T_3$ species, where the subscripts refer to the number of siloxane bonds associated with a

Si centre (T). This indicated that there was a large population of incompletely condensed Si centres – *i.e.* those that had only two siloxane bonds – in the SAC-01 colloid. In fact, these are similar to the "multitailed" oligomeric species observed in the work by Firouzi and co-workers[18], where the multidentate silicate anions simultaneously coordinated to several surfactant molecules. Yet, these oligomeric species self-assembled into a liquid crystalline silicatropic phase. Similarly, the oligomeric silicate species in the SAC-01 colloid, with each Si centre bound to a hydrophobic propyl methacrylate group, may also assemble into an organised mesophase. The possible organisation of these "multitailed" silicate species is schematised in Figure 5.21.

### 5.3.4.4 Microemulsions as order-creating systems

There was no clear evidence of micelle formation in the SAC-01 composite. As seen in the electron micrographs, the SAC-01 material is composed of inorganic domains that are approximately 250 nm wide, interconnected by the organic methacrylate polymer domains. Micellar organisation on the other hand, occurs at the molecular scale and the dimensions associated with these structures are generally on the scale of tens of Angstroms[86] and in the case of polymeric amphiphiles such as block copolymers, do not exceed 30 nm[23]. Even when observed with the electron microscope at higher magnification, neither the untreated nor the calcined SAC-01 monoliths revealed organisation at scales smaller than 250 nm. Furthermore, no Bragg peaks corresponding to the mesoscopic organisation in micelles were detected in small angle x-ray diffractograms (SAXRD) of the powdered SAC-01 monolith. This indicated that the organisation occurred only at the sub-micrometric scale as observed in the transmission electron micrographs. The inorganic domains, themselves were amorphous.

Although a micellar liquid crystalline phase is not present in the SAC-01 composites, the organisation present in the material may be explained by another form of amphiphilic self-assembly – microemulsions. These are generally, three-phase systems consisting of an arrangement of sub-micrometric domains of oil and water, which are separated by an amphiphilic monolayer. Unlike coarse macroemulsions where oil droplets dispersed in an aqueous medium coalesce over time, microemulsions are thermodynamically stable and optically transparent systems. The sharp interfaces between oil and water domains are mediated by monolayers of surfactants, which dramatically reduce the interfacial surface tension between the two immiscible phases by dissolving their hydrophobic tails in the oil phase and immersing their hydrophilic head groups in the aqueous regions.

A microemulsion-based explanation takes into consideration the phase space of the MAPTMS system, which initially consists of two immiscible components – the organic phase (unhydrolysed MAPTMS) and the aqueous phase (acidified $H_2O$, to which sol-gel reactions are confined). A stable microemulsion may be formed if an amphiphilic layer segregates the immiscible phases into sub-micrometric domains. As no external surfactants were added to the system, this amphiphilic interface may indeed consist of the hydrolysed "multitailed" MAPTMS species discussed earlier. As schematised in Figure 5.23, the proposed microemulsion system would consist of organic (MAPTMS) and $H_2O$ domains bordered by a layer of these silicate species with their hydrophilic silicate heads (represented as cubes) anchored in the aqueous region and their propyl methacrylate tails dissolved in the pure MAPTMS phase.

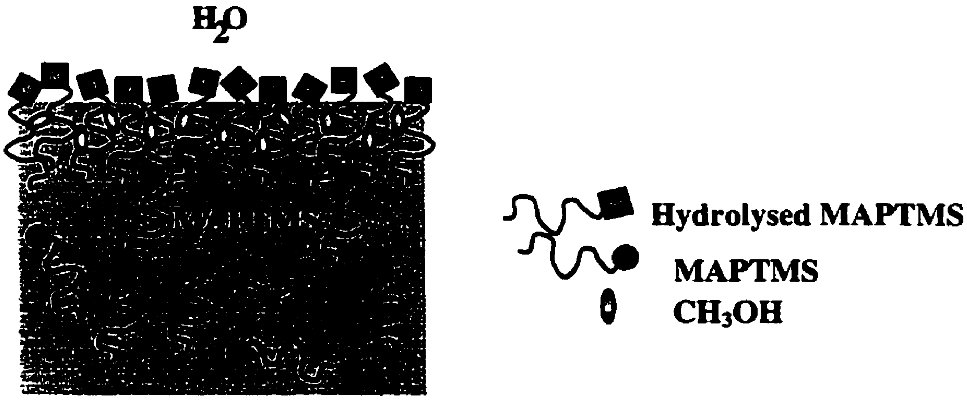

**Figure 5. 23** Schematic of amphiphilic monolayer of hydrolysed MAPTMS species and co-surfactant $CH_3OH$ molecules, segregating the aqueous and organic (MAPTMS) phases of the SAC-01 system.

A key indication of the formation of a microemulsion was observed during the synthesis of the SAC-01 colloid (Section 2.2, Chapter 2). As mentioned earlier, neat MAPTMS is initially a hydrophobic, organic phase. Once the acidified water was added to initiate hydrolysis and condensation of the alkoxysilane, the system became turbid, as a macroemulsion formed between the organic and the aqueous phases. After about 3 minutes of stirring, the system became homogeneous and transparent to visible light. This transition did not occur gradually but swiftly in a single instant – as if the end point in a titration had been reached. This is a critical observation, which often signifies the formation of a microemulsion when short chain alcohol co-surfactants are added to in oil/water/surfactant systems. Indeed, a very similar observation made by Schulman, initiated his pioneering research into microemulsions[85]. He observed that a microemulsion formed when a precise amount of a short chain alcohol was added to a water/oil/ionic surfactant system. The alcohol behaved as a co-surfactant with the ionic surfactant, creating an amphiphilic monolayer that efficiently partitioned the oil and the aqueous domains of the system. As these domain sizes are smaller than the wavelength of light, the formation of a microemulsion is evidenced by the sudden transparency of the system. In the case of the MAPTMS/water system, this transition point may correspond to the formation of the hydrolysed MAPTMS multi-tailed species as well as the by-product of these reactions – methanol. It is possible then that the $CH_3OH$ acts as a co-surfactant and together with the hydrolysed MAPTMS silicate species creates an amphiphilic monolayer that subdivides the aqueous and the organic phases and creates a stable microemulsion system.

### 5.3.4.5 Microstructure of microemulsions

How does the creation of a microemulsion account for the microstructure of the SAC-01 monolith? As with micellar mesophases, microemulsions also have distinct geometries associated with the arrangement of their water and oil domains. Generally, three structural types may be identified: droplets of oil in water and droplets of water in oil systems or a bicontinuous system consisting of interpenetrating oil and water channels[88]. Spherical oil droplets are coated with an amphiphilic monolayer with the hydrophilic head-groups pointing outwards into the aqueous phase. The reverse occurs with the water droplets, which are confined by surfactant monolayers with the hydrophobic functionalities pointing outwards into the oil medium. The electron micrographs of the SAC-01 composite (see Figures 5.12 to 5.14, 5.15-5.21) clearly indicate a bicontinuous, interconnected silica – organic network. Recalling that the formation of silica may only take place in the aqueous channels, the complex 3-D connectivity of the SAC-01's inorganic framework indicates that the microemulsion associated with this system, was bicontinuous and consisted of open channels of $H_2O$ interwoven with hydrophobic organic channels.

Several features of the methacrylate-silicate amphiphiles would make them suitable as the monolayers in the microemulsion, especially of bicontinuous microemulsions. The geometry of the microemulsion is often determined by the spontaneous curvature of the surfactant monolayer. For example, the strong hydrophobicity of surfactants with long alkyl chains lead to highly curved interfaces that are characteristic of spherical domains. Bulky shorter hydrophobic tails are known to form bicontinuous structures, which have relatively flat surfaces[86]. For example, open water channel model unlike the spherically confined reverse micelles has been identified through NMR studies for bis (2-ethylhexyl) phosphoricacid surfactant based microemulsions[87]. Similarly, it is likely that the amphiphilic monolayers based on the relatively short, seven membered propyl methacrylate chains will have low curvatures. In addition, as observed with the silicate anion – surfactant species of the SLC phase[18], the steric bulk of the oligomeric silicate amphiphiles will also contribute to their reduced spontaneous curvature and thus their tendency to form bicontinuous microemulsion systems.

The presence of the co-surfactant $CH_3OH$ also influences the formation of a bicontinuous network. It is known that short chain co-surfactants penetrate the hydrophobic tails of amphiphiles and reduce repulsive interactions between them. It is possible then that the $CH_3OH$ molecules, which are biproducts of the alkoxysilane hydrolysis, incorporate themselves between the amphiphilic hydrolysed MAPTMS silicate species and reduce the repulsion between them. This in turn, is known to reduce the bending rigidity of the monolayer, measured by the elastic moduli $K$, and is necessary for the formation of bicontinuous microemulsions[88].

One of the most distinct and striking features about the SAC-01 composite is undoubtedly its unusual interdigitated mictrostructure and its periodic organisation, created in the absence of external surfactants. Furthermore, the organisation implies that the bicontinuous microemulsion of the MAPTMS/$H_2O$ system itself had the same complex, three-dimensional microstructure. Bicontinuous microemulsions generally have a sponge-like morphology with interconnected aqueous and organic channels but no long-range, periodic organisation. However it is also known that with increasing surfactant concentrations, the sponge-like morphology evolves into more organised, lamellar-like structures[88].

### 5.3.4.6 Sol-gel reactions of MAPTMS– fossilising the microemulsion structure

The formation of the microemulsion in the MAPTMS/$H_2O$ system is coupled to the simultaneous inorganic polymerisation (sol-gel) reactions of the alkoxysilane phase. According to our proposed model, the bicontinuous framework of the microemulsion consists of interwoven aqueous and organic-phase channels, separated from each other by monolayers of the amphiphilic hydrolysed MAPTMS species and the co-surfactant $CH_3OH$ (Figure 5.21). However, the polycondensation reactions of the alkoxysilanes may take place only in the aqueous conduits of the microemulsion. Thus molecules from the hydrophobic MAPTMS phase must diffuse into these channels to participate in the sol-gel reactions. Figures 5.21a-c schematises this process. Silica growth proceeds only in the $H_2O$ channels through the polycondensation reactions of hydrolysed MAPTMS species. The consequent expansion of the hydrophilic regions causes the depletion of the adjacent hydrophobic (MAPTMS) ones (b). The amphiphilic boundary layer dictates the region within which hydrolysis and condensation reactions may take place, *i.e.* the acidified $H_2O$ domains, which may be considered as individual micro-scale reaction chambers for silica growth. In the final structure (c), the amphiphilic layer remains covalently attached to the inorganic domain.

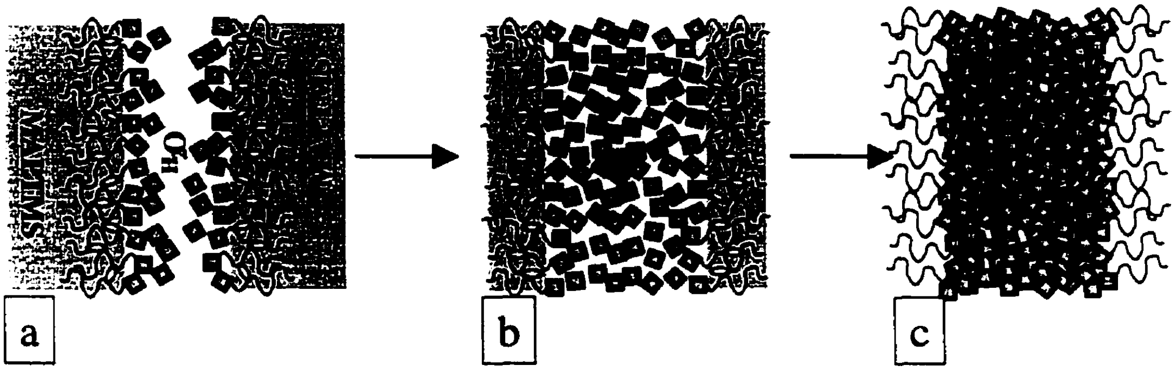

**Figure 5. 24** Schematic of silica formation in the aqueous channels of the SAC-01 microemulsion (a). Note the gradual depletion of the organic MAPTMS layers (b) as silica growth proceeds. In the final structure (c) the amphiphilic boundary layer remains covalently bound to the surface of the inorganic domain.

There have been some reports of *pre-formed* microemulsions, consisting of known quantities of $H_2O$/oil/surfactant, as reaction media for the sol-gel processing of tetra-alkoxysilanes. Here the alkoxysilane precursors, initially borne in the oil phase, undergo hydrolysis and condensation reactions selectively in the $H_2O$ domains. This provides a strategy to control the macroscopic morphology of the final product. For example, base catalysed hydrolysis and condensation of tetraethoxysilane (TEOS) carried out in surfactant coated, $H_2O$ droplets in an oil continuum led to spherical silica particles with remarkably narrow size distributions[89]. Conversely, mesostructured cellular foams (MCF) – strutted silica frameworks with periodic spherical cavities - were created by the sol-gel reactions of TEOS hosted in a oil/water microemulsion consisting of surfactant coated droplets of 1, 3, 5-trimethylbenzene (TMB) in a $H_2O$ medium[90]. Similarly, transparent monoliths of HCP packed pores were formed by polymerising tetramethoxysilane (TMOS) in the liquid crystalline phase of a $H_2O$/octane/polyalkylene oxide + co-surfactant alcohol system. Here, the pore sizes could be tuned by altering the concentration of the surfactant, co-surfactant or oil phase[91].

The above examples rely on the fact that the sol-gel reactions of alkoxysilanes occur exclusively in the aqueous regions of the system. In all these cases, the alkoxysilane precursor, which is initially in the organic phase, must traverse the surfactant monolayer into the aqueous domain to take part in silica growth. Similarly, in our MAPTMS/$H_2O$ system, the MAPTMS molecule must migrate across the amphiphilic monolayer (see Figure 5.24a-c) into the aqueous channels. The ability to allow the molecules to cross the aqueous-organic threshold depends on the flexibility of the amphiphilic monolayer. If this interfacial layer is highly curved (strong head group and tail repulsion, high surface tension) and rigid, then the energetic cost of perturbing the structure to allow the alkoxysilanes through is high, relative to a less rigid layer that has a lower spontaneous curvature.

The flexibility of the surfactant layer is inversely related to its bending rigidity or elastic moduli, *K*. As discussed earlier, it is likely that the *K* of the amphiphilic layer separating the MAPTMS and the $H_2O$ channels would be significantly decreased by the presence of the $CH_3OH$ molecules. These short chain alcohols are known to incorporate themselves within the hydrophobic tail groups of a surfactant monolayer, thus preventing repulsive interactions between them. This decreases *K* (for example from $10k_BT$ to $1k_BT$) and enhances the film's flexibility. This property of alcohol co-surfactants has been noted in other examples of the polymerisation of alkoxysilanes in microemulsions. For example it was shown in the $NH_3$ catalysed polymerisation of TEOS in a water/oil microemulsion that short chain co-surfactant alcohols such as butanol increased the final silica particle size. This was not seen with longer and more rigid alcohols such as hexanol and octanol, which do not significantly reduce *K* of the interfacial film[92]. Ethanol also acted as an efficient co-surfactant that significantly increases TMB oil droplet sizes in acidic water/amphiphile/TMB systems[93]. Both of these examples indicate that the presence of $CH_3OH$ in the interfacial layer of the MAPTMS/$H_2O$ system would facilitate the migration of alkoxysilane molecules from the organic domains into the aqueous ones.

Another feature of the MAPTMS system that may encourage silica growth is associated with the low curvature of its amphiphilic walls, which leads to the non-spherical, open and extended $H_2O$ domains characteristic of a bicontinuous microemulsion. It is evident that silica growth, which occurs through co-condensation reactions between monomers and polymeric silicate species, would be less sterically hindered within the open channels than in the highly curved and rigid environs of a spherical water droplet. This feature has also been observed microemulsions stabilised by shorter tailed surfactants such as poly (oxyethylene) alkylphenyl ether molecules with the chemical structure $5\text{-}H(CH_2)_5Ph(OC_2H_4)_9OH$. This surfactant, with its relatively short hydrophobic tail, forms monolayers with low curvature. Although the microstructure of the system was not directly evaluated, the large conductivity measurements through the aqueous region indicated that it had an interconnected and layered arrangement of aqueous layers. The largest silica particles, through the sol-gel reactions of TEOS, were obtained in this system, compared to those obtained from spherical microemulsions.

### 5.3.4.7 Microstructure of SAC-01 composite – role of the covalent bond

The efficiency of silica growth in the SAC-01 system is evident in the final microstructure of the composite, which consists of a tightly packed arrangement of 250 nm wide inorganic domains (Figures 5.12 and 5.14). Neither the micrographs nor the $^{29}Si$ NMR spectrum of the material reveal the presence of any unpolymerised MAPTMS molecules. This confirms that the organic phase was entirely consumed for silica growth. One of the most remarkable features of the final microstructure is the discrete nature and the uniform size of the inorganic domains that compose the complex, interdigitated, periodic, three-dimensional framework of the SAC-01 monolith.

The careful organisation in the composite is especially evident in Figure 5.21, which shows the approximately 200 nm wide domains arranged with long-range, periodicity in a fish-scale pattern (that incidentally bears a likeness to the interdigitated microstructure of nacre). The preservation of this structural order during the sol-gel process may be explained by the presence of the methacrylate polymer layer around the inorganic domains (Figure 5.20). This organic region, according to the microemulsion model, corresponds to the amphiphilic layer that initially separated the aqueous and the organic domains (Figure 5.24). Recall that this interfacial film consists of hydrolysed silicate species and the $CH_3OH$ co-surfactant. In the actual SAC-01 monolith, the organic layer completely surrounds every inorganic domain and is also present at the nodes and interfaces that link these domains together (Figure 5.20). This indicates that although the organic phase is consumed by the inorganic polymerisation reactions, the microemulsion boundaries dictated by this amphiphilic monolayer are still highly respected, *i.e.* the aqueous channels did not fuse during the inorganic polymerisation. In this way, the original arrangement of the aqueous and the organic phases in the microemulsion has been faithfully reproduced in the final microstructure of the SAC-01 monolith.

The series of transmission electron micrographs presented here, are microtomed cross-sections of the SAC-01 monoliths. Thus, they give only a two-dimensional representation of the bicontinuous structure of the composite and the original microemulsion. However, from the arrangement of the organic and the inorganic phases in the SAC-01 composite, we can deduce that the microemulsion consisted of aqueous and organic channels that were interwoven into a three-dimensional, periodic structure. Figure 5.25 shows a transmission electron micrograph (the negative is shown for better contrast) of a microtomed section of the SAC-01 monolith, where the organic component has been selectively removed. The sample gives some insight into the three-dimensional structure of the microemulsion as it contains two interwoven layers of the inorganic skeleton. Each layer consists of silica "ribbons" of uniform width, threaded to the other into a basket-weave pattern.

**Figure 5. 25** Evidence of intercalation in SAC-01 composites

The uniform widths of the inorganic domains and the manner in which they interpenetrate each other indicate that the structure of the microemulsion is carefully reproduced in the SAC-01 composite. They further emphasise the role of the amphiphilic layer in preserving the organic-inorganic boundary throughout the inorganic polymerisation reactions. Recall that at the interface the methacrylate substituents point away from the aqueous phase and are dissolved into the MAPTMS phase whereas the hydrophilic silicate "head group" is anchored in the nascent silica medium. As mentioned earlier, at the early stages where the hydrolysis reactions of the MAPTMS molecules predominate, the low curvature and flexibility of the amphiphilic layer probably enabled the transfer of MAPTMS molecules from the organic phase into the aqueous channels. However, it is important to note that once the condensation reactions between the monomers take place, the amphiphilic layer becomes covalently bound, through its "head group" to the evolving inorganic network.

The significance of the covalent bond amphiphile-silicate interface in our SAC-01 system may be understood by considering another example of silica growth templated by a bicontinuous microemulsion composed of tetra and hexadecane/$H_2O$/didodecyldimethylammonium bromide (DDAB)[94]. Here, TEOS initially borne in the oil medium underwent acid catalysed hydrolysis and condensation in the aqueous channels. The resulting networks were composed of ribbons and filaments, which reproduced the *random* morphology of the bicontinuous network. However, the connectivity of the structure could only be obtained when the reactions were hosted in a frozen microemulsion. At room temperature, the silica did not reproduce microstructure of the microemulsion. Once again, the interface between silicate and the surfactant discussed earlier becomes significant. Here only van der Waals forces exist between the ionic surfactant DDAB and the silicate species (no SLC phases were detected at this concentration). Therefore at room temperature, it is possible that once the silica is formed it easily deforms the surfactant monolayer and thus disrupts the bicontinuous arrangement of the system. At lower temperatures, the rigidity of the interface is increased and silica growth is dictated by the structure of the microemulsion. In our case, self-organisation in the SAC-01 monoliths are obtained at room temperatures. The disruption of the

$H_2O$/MAPTMS interface by the growing inorganic network is unlikely because the structure-directing amphiphilic layer is covalently bound to the growing silica medium and therefore forms a strong boundary around the aqueous regions. In this way, it is able to confine silica growth to the aqueous regions and preserve the original structure of the microemulsion.

(Note that although there is evidence of an amphiphilic layer consisting of hydrolysed MAPTMS, between the aqueous and organic regions, not all the organic substituents occupy interfacial sites (this would lead to micellar self-assembly). Methacrylate units are also incorporated within the amorphous silica network evolving in the aqueous channels of the microemulsion. This has been observed in the co-polycondensation reactions of MAPTMS and TEOS hosted in a water/toluene/*iso*-propanol microemulsion. In the resulting product, the methacrylate groups were buried within the silica spheres and were not accessible (except for roughly a monolayer) at the surface.[95].)

#### 5.3.4.8 Summary

The microemulsion-based route to self-organisation in the SAC-01 composites is schematised in Figure 5.26. The addition of acidified $H_2O$ to MAPTMS, leads to a bicontinuous microemulsion (a), where the aqueous and the organic channels are bordered by an amphiphilic monolayer, which consists of hydrolysed MAPTMS species and $CH_3OH$ co-surfactant molecules (insets). Sol-gel reactions are strictly confined to the aqueous regions, which eventually consume the entire organic MAPTMS phase. In this way, the long-range, periodic, structural organisation of the microemulsion (a) is replicated in the SAC-01 colloid (b). UV initiated, free-radical polymerisation of the methacrylate substituents in the colloid consolidate the self-organised system (b) into a monolith (c). Essentially, the structure of the microemulsion is fossilised by two polymerisation reactions; first the inorganic polymerisation, which is confined to the aqueous domains then the free-radical polymerisation, which link the amorphous inorganic domains together. Note that the organic polymerisation serves to capture the periodic arrangement of the inorganic domains into a structurally anisotropic monolith. Cross sections of the SAC-01 monolith (d) clearly show methacrylate polymer regions at the nodes and interfaces of the inorganic domains, linking them to each other. After monolith formation, the organic component may be thermally removed. The inorganic skeleton that is left behind (e) retains its interdigitated, periodic microstructure

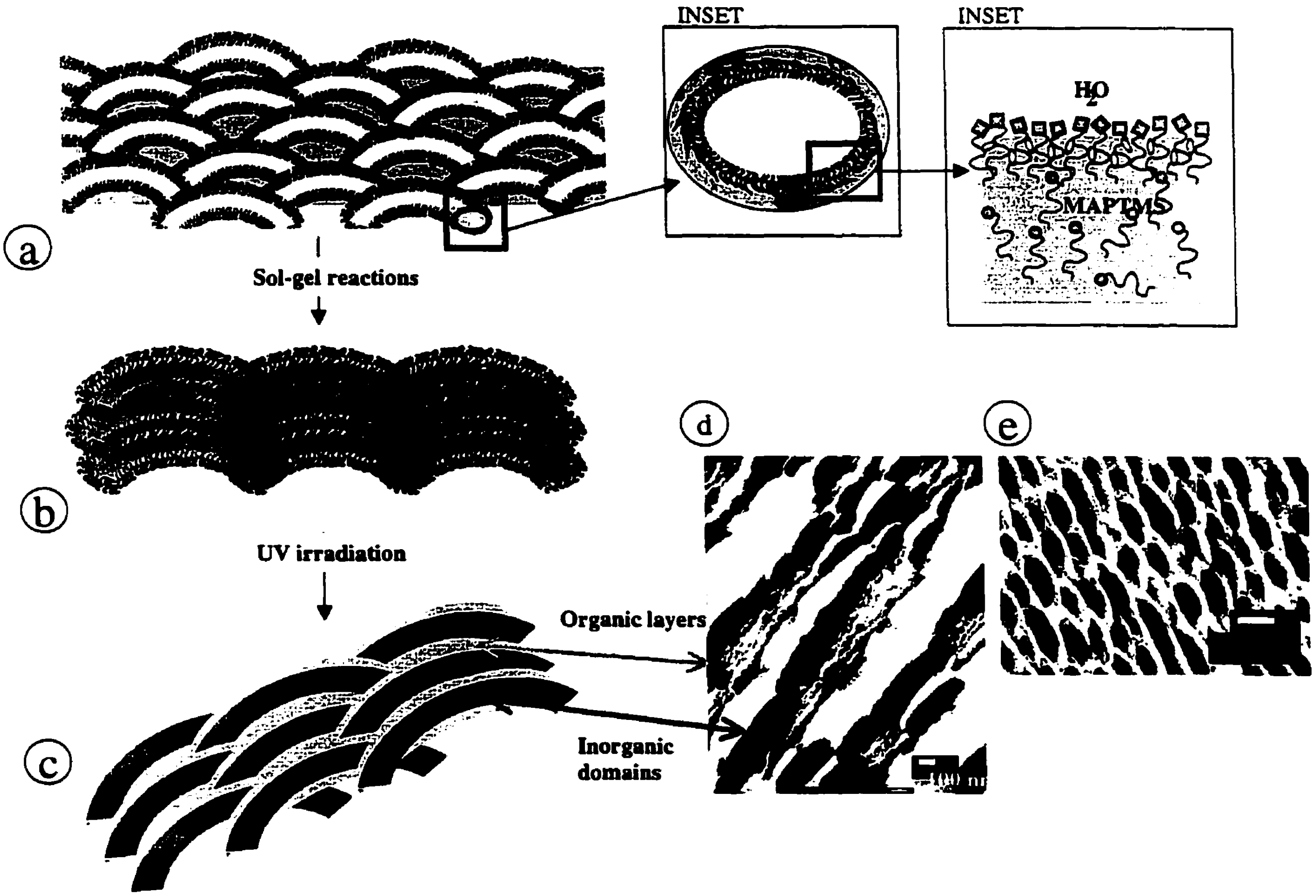

**Figure 5. 26** Schematic of the origins of self-organisation in the SAC-01 composite. A microemulsion is formed, consisting of periodic, interpenetrating aqueous and organic (MAPTMS) channels (a) separated by an amphiphilic layer (INSETS). Sol-gel reactions proceed in the aqueous channels and the structure of the microemulsion is preserved in the SAC-01 colloid (b). UV initiated polymerisation of the methacrylate substituents forms a monolith (c), where the organic polymer permanently links the inorganic domains together (d). The organic component may be thermally removed from the monolith to reveal an inorganic skeleton, with a periodic, interdigitated microstructure (e).

### 5.3.5 Evidence of self-organisation in the SAC series of composites

Self-organisation discussed in the previous Sections was not restricted to the SAC-01 composite alone. We observed self-organisation in several members of the silica-acrylate composite (SAC) series introduced in Section 4.3 of Chapter 4. All colloids consisted of alkoxysilane precursors with slightly varying chemical structures. For sol preparation, the same compositions were used. Thus the systems had similar "phase structures". Our reasoning in examining the microstructure of monoliths derived from different precursors, was to examine the effect of molecular-scale features on the final structure. As in the case of micellar organisation, microemulsions are also influenced by parameters such as hydrophilicity of head group, bulk of hydrophobe as well as the phase composition of the system. Our observations of self-organisation in the SAC series are described below.

Self-organisation was observed in colloids derived from 3-methacryloxymethyltriethoxysilane (MAMTES), 3-methacryloxypropyldimethoxysilane (MAPDMS) and 3-acryloxypropyltrimethoxysilane (ACTMS). Cross sectional transmission electron micrographs of each monolith presented in Figure 5.27. These monoliths had been heated at 300 °C for 5 hours. Similar features to those observed in the SAC-01 system are evident here. In general, the microstructure consists of inorganic "rods" or layers that are interconnected with organic polymer. Inorganic domain widths are approximately 200 nm. The structure of monoliths derived from ACTMS and MAPDMS are remarkably similar. Note that MAPDMS is a dialkoxysilane. The observation of organisation in its system, supports our model of an amphiphilic layer based on hydrolysed propyl-methacrylate substituted alkoxysilane molecules. We argued that the low degree of condensation in the trialkoxysilane precursor enabled the formation of the amphiphilic walls of the microemulsion. According to our model, the dialkoxysilane molecules with a maximum of only 2 siloxane bonds form the amphiphilic layers in the microemulsion.

It is also interesting to note that "filamentation" of the methacryloxymethylsilane precursor occurs at an earlier stage in the thermal process. Recall that this was observed only upon heating at 700 ° C. This is a qualitative indication that organic polymer is removed at a faster rate in the MAMTMS system, where the methacrylate is attached to the Si centre with a single methyl group.

Self-organisation was also observed in systems derived from 3-acryloxypropyltrimethoxysilane doped with methacrylic acid. The cross-sectional transmission electron micrograph of this monolith is presented in Figure 5.28a. The relative "disorder" in the arrangement of the inorganic framework is most evident in this composite. Note, that although the inorganic rods that are now characteristic of these organosilica systems is seen, their arrangement contrasts sharply to the parallel, uniaxial organisation observed in the SAC-01 as well as the monoliths obtained from the other methacrylate substituted alkoxysilane precursors described above. The lower degree of organisation in this system highlights the importance of the covalently bound polymerisable substituent in the composite. Note that this composite is the "saturated" analogue of SAC-01. According to our microemulsion model, hydrolysed acryloxypropylalkoxysilane precursor should also exhibit amphiphilic character, leading to microemulsion formation. However, the structure of the microemulsion is not faithfully reproduced in the monolith because organic polymerisation is carried out with free methacrylic acid monomer. We have argued earlier that free-radical reactions are spatially localised in SAC-01 composites partly due to the fact that they are covalently anchored to the inorganic matrix. It is possible that the localisation of polymerisation in the SAC colloids allows the structure of the microemulsion to be preserved in the monolith. The high degree of organisation observed with other methacrylate substituted alkoxysilanes reinforces this notion. In the case of the "saturated" monolith, organic polymerisation involves methacrylic acid monomers that are introduced into the colloid. It is possible that as organic chain growth occurs in a non-local fashion, it does not retain the structural organisation present in the microemulsion.

The cross-sectional micrograph of a SAC-01 colloid, where exactly half the molar amount of MAPTMS has been replaced with decyltrimethoxysilane is presented in Figure 5.28b. Note that similar form of layered organisation is obtained here. It is interesting to note however, that the width of the organic layer intercalated between the inorganic domains is actually wider in this composite. It is possible that a larger volume is occupied by the organic phase in this microemulsion due to the long, hydrophobic tail of the alkoxysilane precursor. This is an encouraging observation that indicates that monolith microstructure may be influenced by tailoring the molecular precursors of the microemulsion.

Finally, we also observed self-organisation in a SAC-01 colloid where the zirconia component had been replaced with titania (Figure 5.28c). The ability introduce other transition metal oxides into this organised system presents the possibility of tuning the refractive index of the composite and even introducing functionality into the monoliths, by dispersing semiconductor, colloidal metal particles into the microemulsion system.

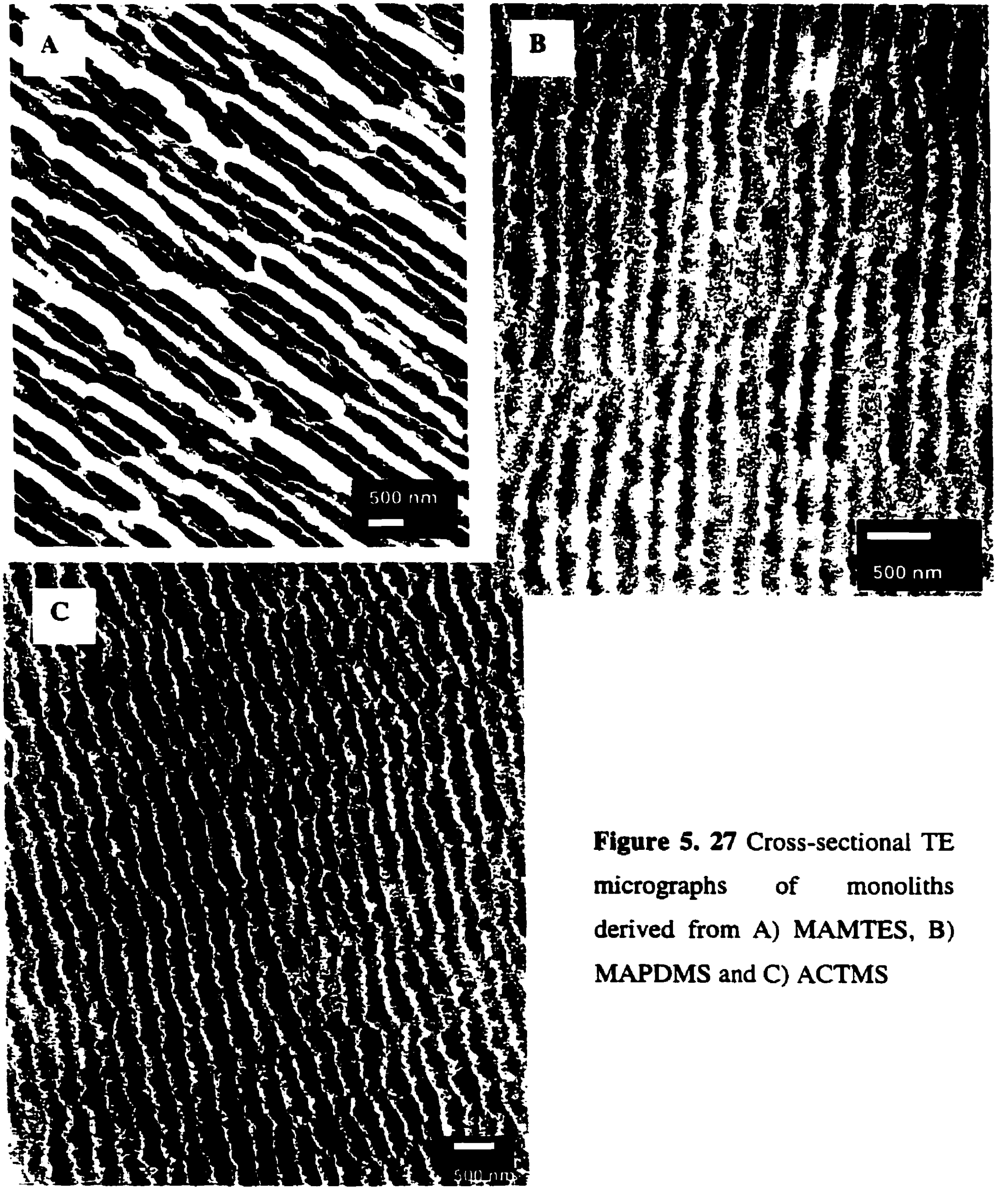

**Figure 5. 27** Cross-sectional TE micrographs of monoliths derived from A) MAMTES, B) MAPDMS and C) ACTMS

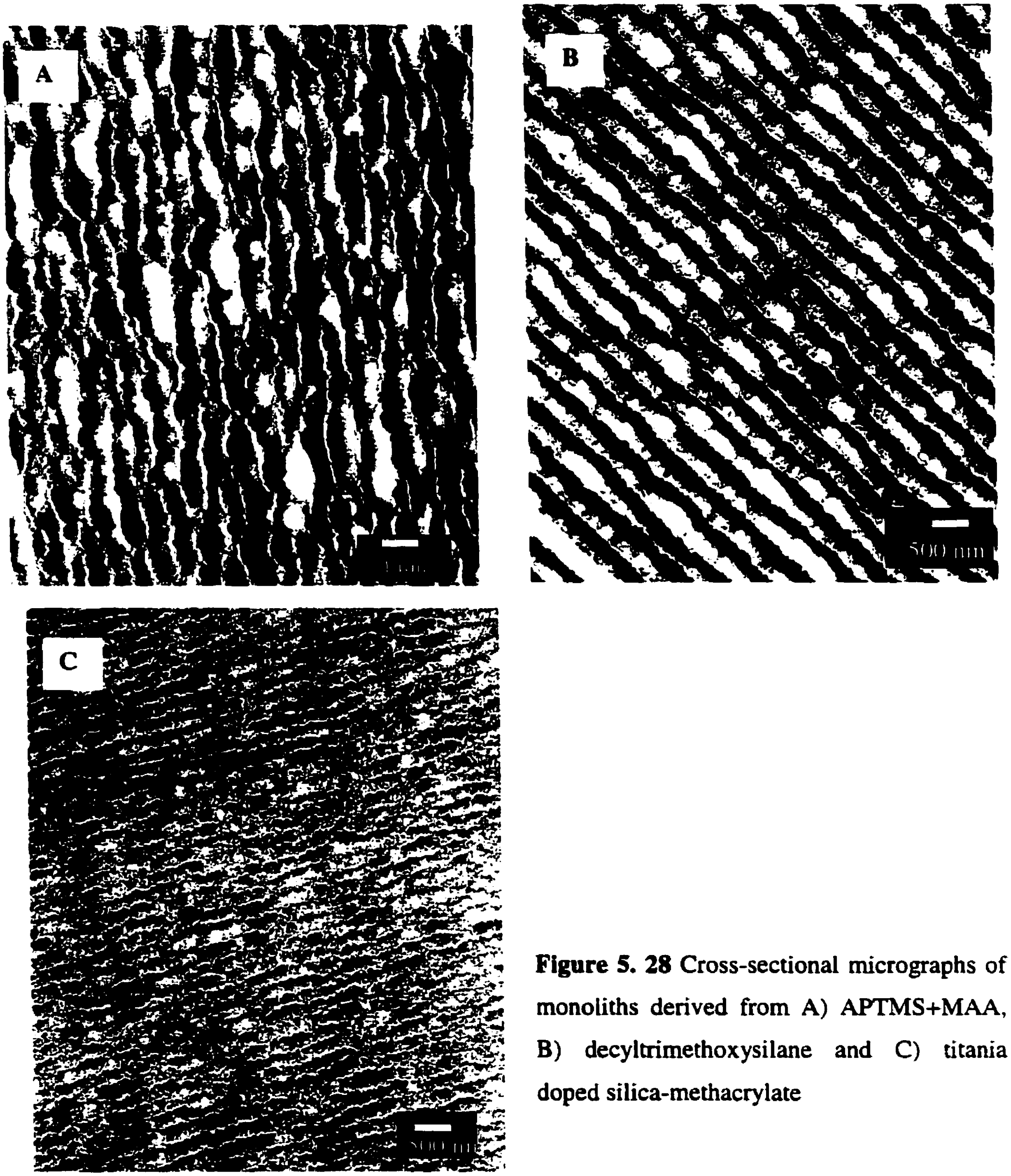

**Figure 5. 28** Cross-sectional micrographs of monoliths derived from A) APTMS+MAA, B) decyltrimethoxysilane and C) titania doped silica-methacrylate

### 5.3.6 Organisation of the organic phase in a organosilica material

In the previous Sections, we described self-organisation in hybrid sol-gel derived silica-methacrylate composites through a microemulsion model. In suggesting this model, we emphasised the role of the covalently bound methacrylate substituent in the trialkoxysilane precursor in creating the microemulsion. As mentioned earlier, covalently bound template strategies towards ordered sol-gel derived structures have remained largely unexamined. Here, we develop this notion further by creating an organosilica composite with an oriented organic phase.

Our contention is that silica-template interactions can be significantly enhanced by covalently linking the organic group to the alkoxide precursor. There are also other advantages to substituent-templates: the Si-C bond survives the mild conditions of sol-gel processing such that after network formation, there is a uniform distribution of the template. Furthermore, organic substituents have been shown to enhance the hydrolysis reaction kinetics and the homogeneity of the silica phase[96]. The ability of sol-gel processed silica to conform to substituent-templates has been very recently observed in microporous materials research[97]. The size of the pores on the order of angstroms was correlated to the methacrylate functional group. Of course, in this case the pores were randomly distributed.

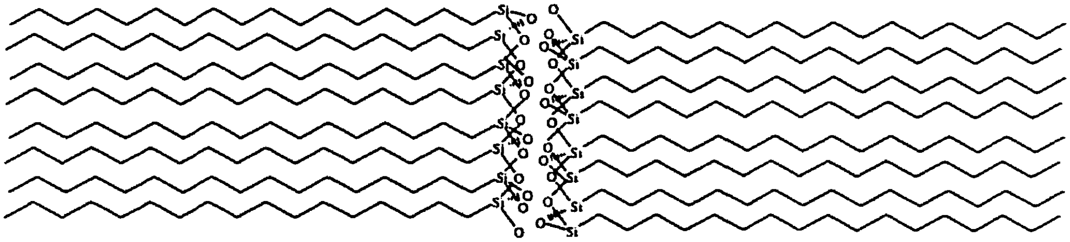

**Figure 5. 29** Organisation of organic substituent in organosilica material

In creating organised structures, the substituent-template although covalently bound to the silicate matrix, must show a phase separation; *i.e.* interactions between the organic substituents must be encouraged. These have been previously reported for hybrid glasses. π-π interactions between covalently bound ligands have been noted in phenyl trimethoxysilane glasses[98]. The pore sizes in silsesquioxane templated with rigid paraphenylene rods have been accounted for by aggregation of the organic units in the glass[99]. Self-organisation within organic spacers in xerogels was recently reported for glasses with similar phenylene substituents[100].

### 5.3.6.1 Dodecyltrimethoxysilane-derived birefringent composites

For our purpose of creating composites with an organised organic component, such phase separations must occur in an ordered fashion on the nanometer scale. These may be induced in long, alkyl chained precursors, such as the commercially available n-(6-aminohexyl) aminopropyl trimethoxysilane and n-octadecyl trimethoxysilane reagents. Their long hydrocarbon links, reminiscent of surfactants' hydrophobic tails are likely to induce organisation of alkoxide molecules in solution.

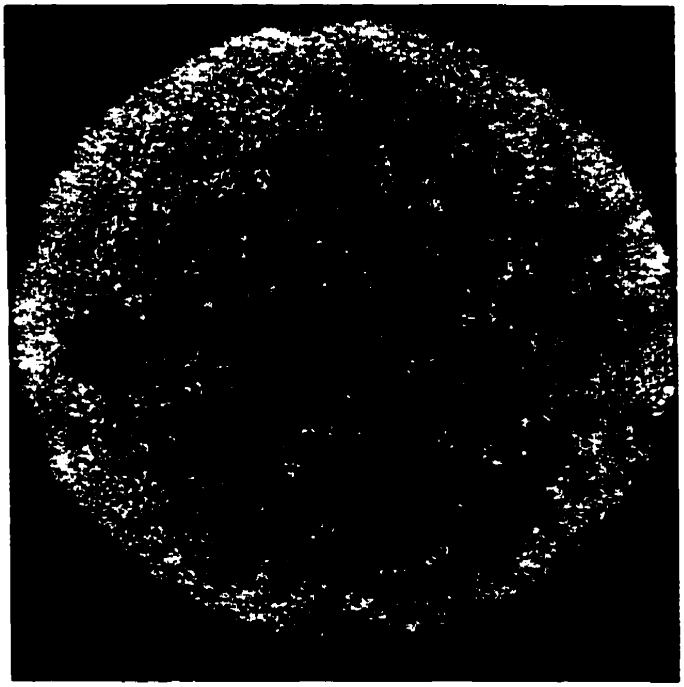

**Figure 5. 30** Polarised optical micrograph of composite derived from dodecyltrimethoxysilane

For this initial study, we demonstrate that orientation in a composite that was derived from the hydrolysis and condensation reactions of a trimethoxysilane with a 18-carbon substituent. The dodecyltrimethoxysilane precursor underwent acid catalysed hydrolysis and condensation reactions, to yield a waxy white solid. Significantly, the solid was not "sticky" as is characteristic of colloids or gel derived from tetraalkoxysilanes. Additionally, the material dissolved easily in solvents such as methanol and iso-propanaol. This indicated that some form of macromolecular association was taking place in the composite. We probed for organisation in this material through polarised optical microscopy and polarised infrared spectroscopy.

The polarised optical micrograph of this white, waxy solid that was smeared on a glass substrate is presented in Figure 5.30. The micrograph is in sharp contrast to observations made with amorphous sol-gel derived glasses. Figure 5.30 shows a material with an inherent and high degree of birefringence, evidenced by the bright white "speckles" that are dispersed throughout the picture. These regions may be due to oriented or organised micro-phase separated regions in the composite, such as the long-alkyl chains substituents of the alkoxysilane.

The origins of this organisation were confirmed through polarised infrared spectroscopy. Figure 5.31 shows the polar plot of absorbance of thev(CH) stretch at 2954 cm$^{-1}$ belonging to the alkyl chain versus input polarisation. The significant variation in absorbance intensity versus the electric field of the excitation light, clearly that the organic chains in the composite have a preferred orientation.

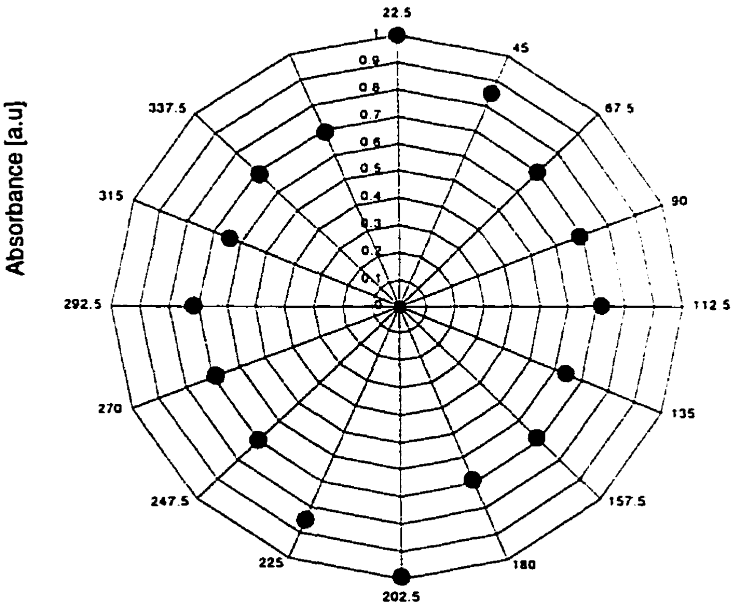

**Figure 5. 31** **Polarised infrared absorbance of v(CH) of composite derived from dodecylalkoxysilane**

The significance of this observation lies in the possibility of covalently bound templates for ordered silica growth. If organised phases could be encouraged in the organosubstituted alkoxysilane precursor itself, then growth of the silica structure will be guided by this organised phase. Whereas the current approach uses external surfactant assemblies to introduce order in sol-gel derived structures, covalently bound templates may create organised template phases that are inherent to the alkoxysilane molecules themselves.

### 5.3.7 Bicontinuous arrangement of methacrylate-derivatised silica domains on thin films – photo-manipulation opportunities

In closing this Chapter, we describe some interesting optical properties of thin films derived from the SAC-01 colloid. According to our microemulsion model, prior to irradiation with UV light, the SAC-01 colloid consists of a periodic arrangement of interpenetrating, bicontinuous silica domains. As we have mentioned previously, thin photosensitive films may be cast from the SAC-01 colloid. During film formation, the silica domains in the microemulsion are concentrated on a Si surface. We observed a bicontinuous arrangement of methacrylate derivatised silica domains, in a thin film derived from the SAC-01 colloid

Scanning electron micrographs showing the bicontinuous arrangement of methacrylate derivatised silica domains on a Si substrate is presented in Figure 5.32. The film surface consists of a densely packed arrangement of silica domains. Observe that the domain sizes correspond to those observed in the transmission electron micrographs presented previously. In both cases, domain widths are on the order of 250 nm. Although, there is no clear periodicity in the structure, the sub-micrometric length scales associated with the features cause the diffraction of visible light at the film surface. Figure 5.33 is a photograph of the opalescence exhibited by such a film under morning sunlight. As mentioned earlier, one of the most exciting aspects of our self-organised silica composite is its sub-micrometric length scale, which approaches the wavelength of visible light.

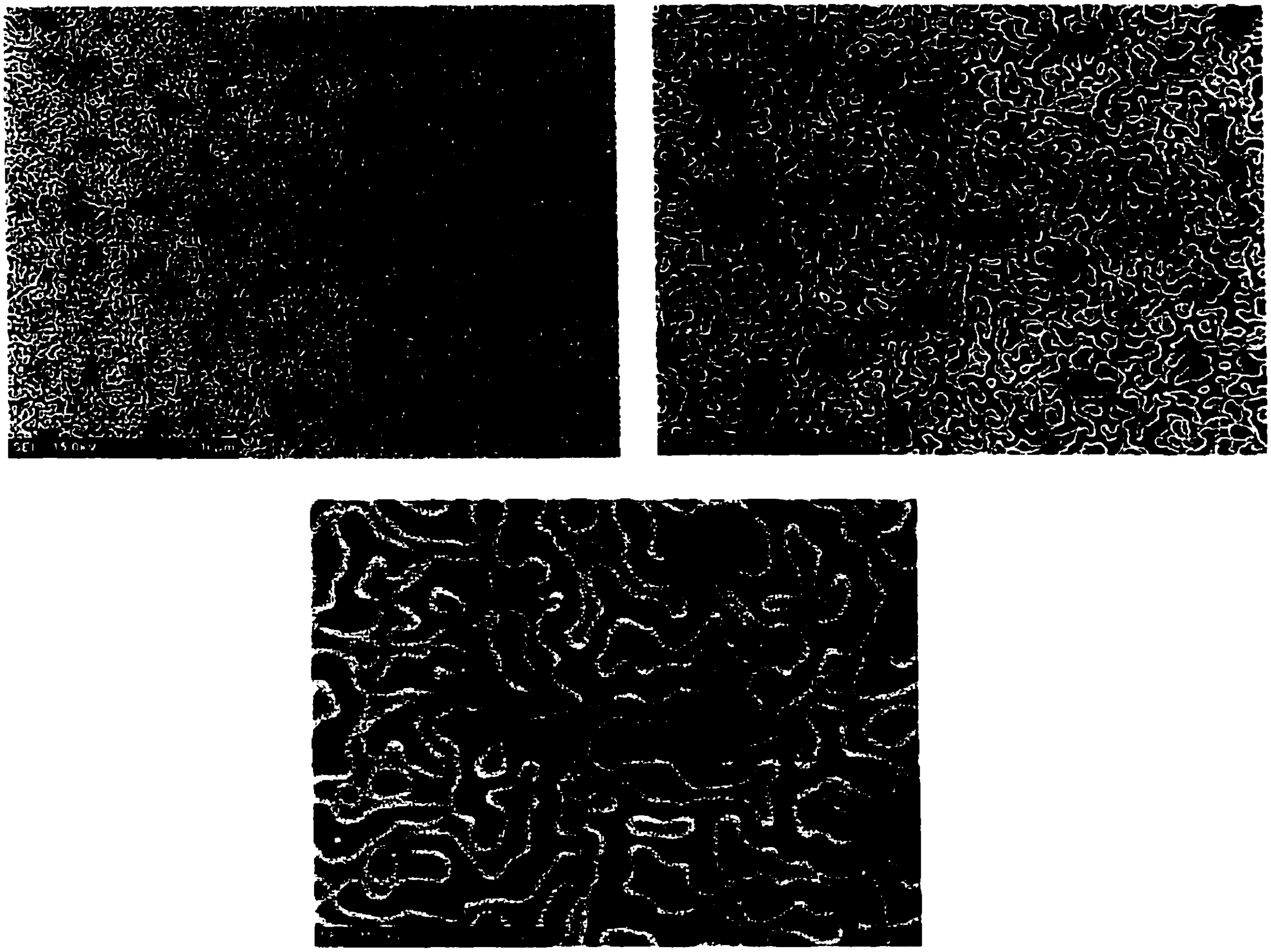

**Figure 5. 32** Thin films showing bicontinuous arrangement of methacrylate derivatised silica domains

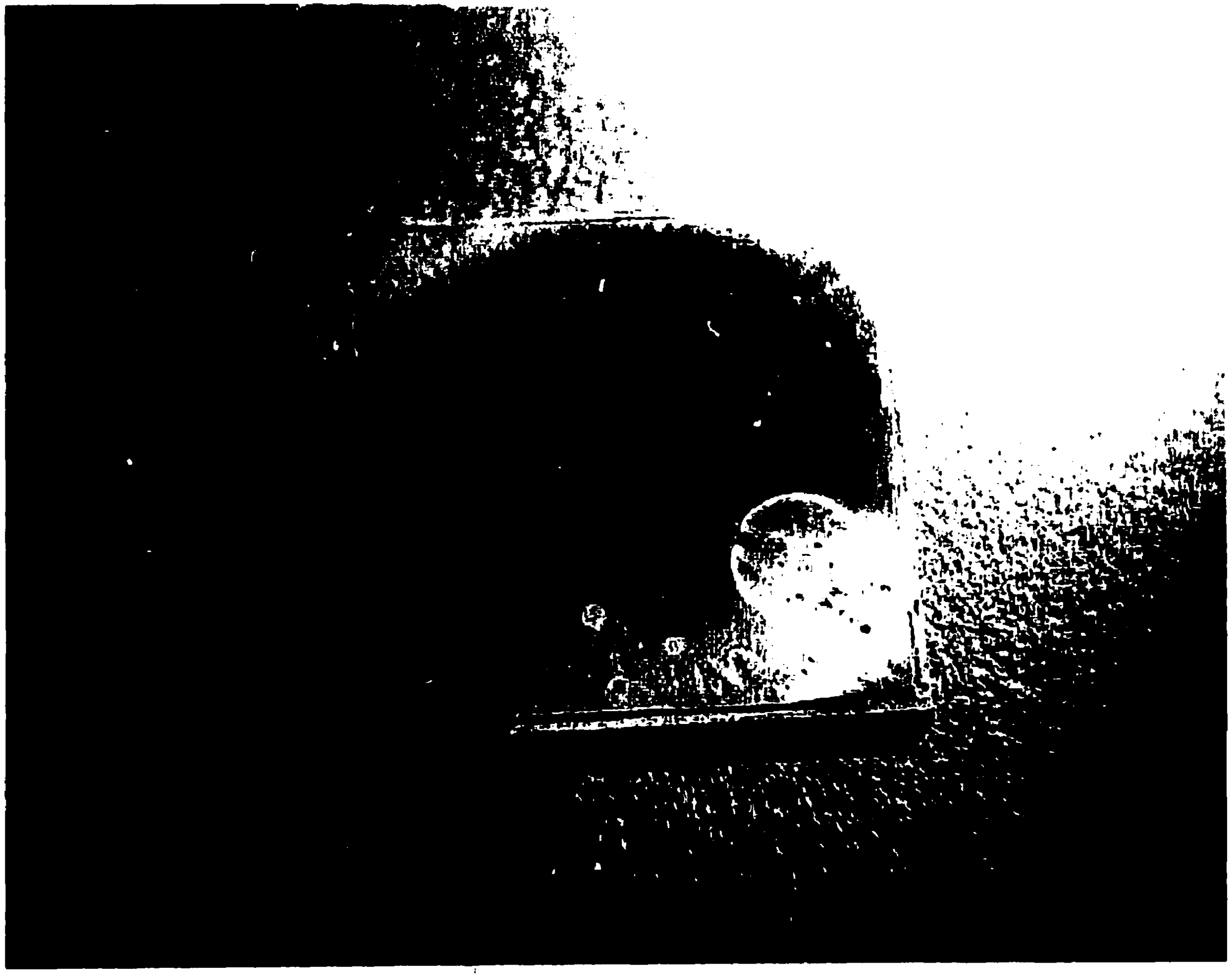

Figure 5.33. Opalescence of silica-methacrylate thin films.

Thin films also have interesting photochemical properties. Recall that silica domains are derivatised with propyl methacrylate substituents. Simply irradiating the film with UV light, causes the domains to link in unusual arrangements. The degree of connection between the inorganic domains may be controlled with the irradiance. The sequence of micrographs presented in Figure 5.34 trace the degree of polymerisation from the centre (a) of the focuseed spot of UV light to its edges (d). As can be seen, the highest degree of polymerisation and thus the highest degree of linkage between the inorganic domains occurs in A. Photo-manipulation of thin films may also be achieved with guided optical modes. As we showed in Chapter 4, laser light links domains as it propagates as an optical mode within the film. This creates a dramatic change in the arrangement of silica domains on the thin film (Figure 5.35).

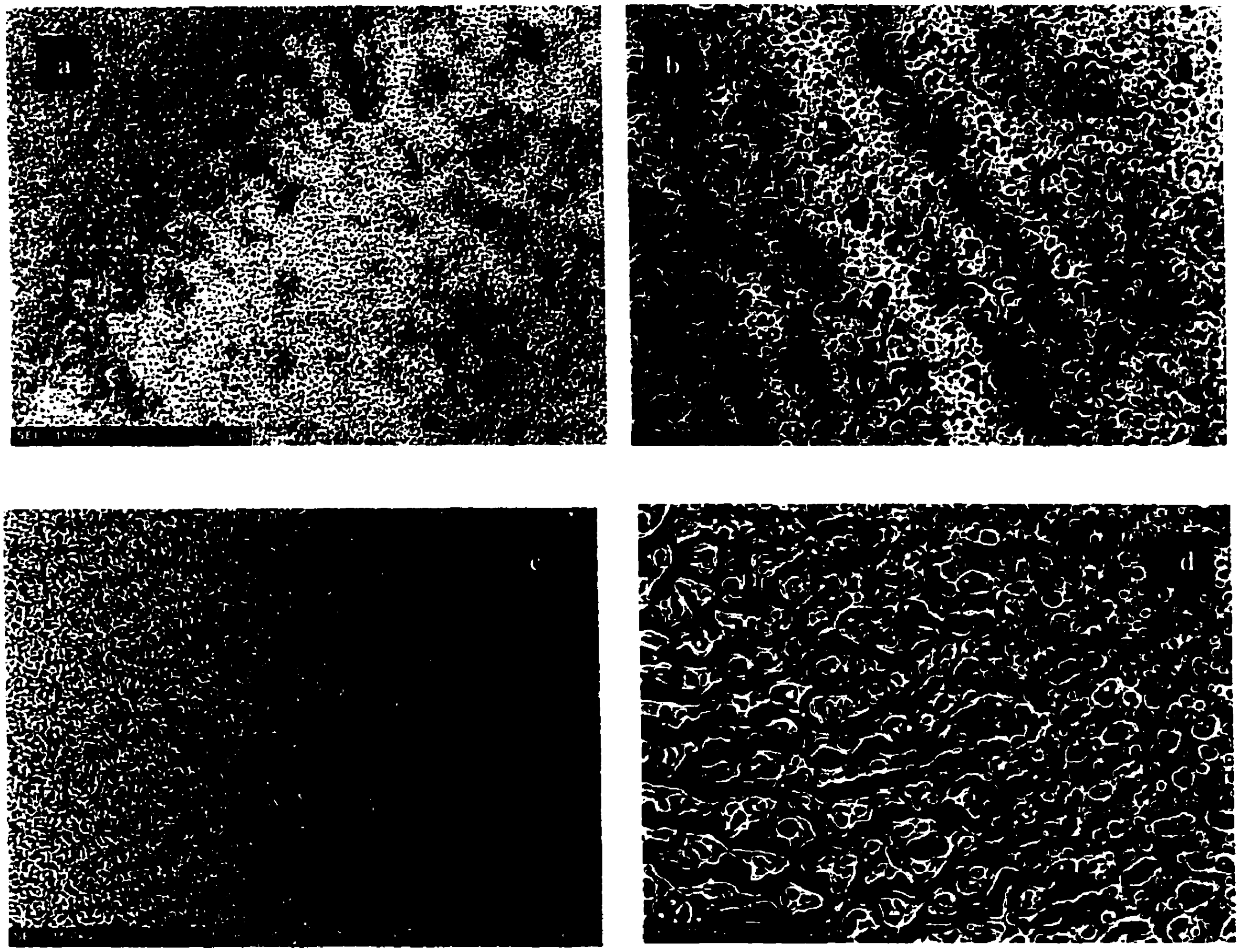

**Figure 5. 34** Scanning electron micrographs of silica-methacrylate thin films with various stages of organic polymerisation

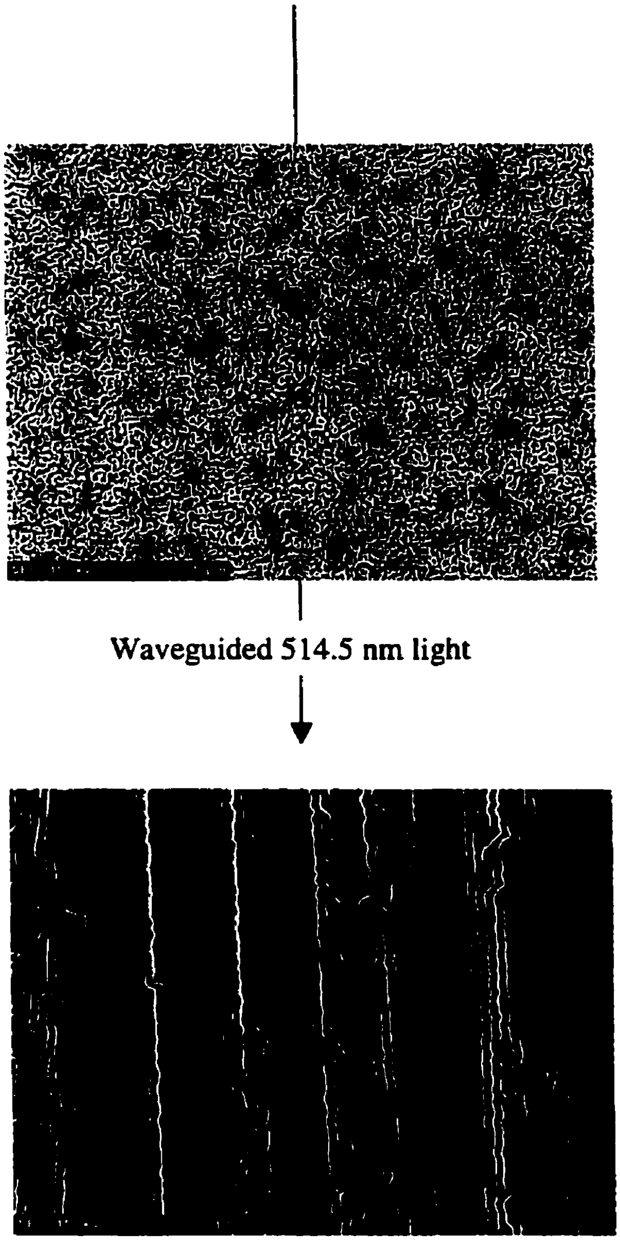

**Figure 5. 35** Effect of guided optical wave on silica-methacrylate thin film

## 5.4 CONCLUSIONS

We have observed, for the first time, long range, periodic organisation in a sol-gel derived organosilica composite, formed in the absence of external surfactants. The microstructure of silica-methacrylate monoliths derived from 3-methacryloxypropyltrimethoxysilane consisted of an interdigitated arrangement of silica-rich domains that were approximately 200 – 250 nm wide. The domains were linked to each other through polymerisation of methacrylate substituents. We propose a model for this observation based on the amphiphilic nature of hydrolysed MAPTMS molecules. We argue that a microemulsion is formed in the MAPTMS/$H_2O$/$CH_3OH$ system, where the MAPTMS and co-surfactant methanol molecules erect amphiphilic walls to segregate aqueous and organic phases in the system. Acid catalysed condensation reactions are strictly restricted to the aqueous regions and the microstructure of the microemulsion is reproduced in the final inorganic framework that is created. Free-radical polymerisation of the methacrylate substituents captures the organised microstructure into anisotropic monoliths. On the other hand, our initial studies show that thin films cast from the silica-methacrylate colloid consist of a bicontinuous arrangement of the methacrylate derivatised domains. Polymerisation, in these cases, may be initiated with UV light or waveguided optical beams.

In rationalising the order and periodicity observed in our SAC system, we advance the notion of covalently bound organic templates, which direct silica growth into organised structures. Organisation in organoalkoxysilanes was also demonstrated with trimethoxysilanes that had long, 18-membered carbon chains. Both polarised optical microscopy and infrared spectroscopic studies confirmed that long-alkyl chains showed preferential orientation in the composites.

---

1. C. J. Brinker, *ACS Advances in Chemistry Series*, **234,** 361 (1994).
2. L.C. Klein, *Annu. Rev. Mater. Sci.* **23**, 437 (1993).
3. F. H. Dickey. *Proc. Natl. Acad. Sci. U.S.A.* **35** 227 (1949).
4. P. Szuromi. *Science*. **277**, 1183 (1997).
5. S. I. Stupp and P. V. Braun, *Science,* **277**, 1242 (1997).
6. C. J. Brinker, Y. Lu, A. Sellinger and H. Fan, Adv. Mat. **11**, 579 (1999).
7. B. L. Smith, T. E. Schäffer, M. Viani, J. B. Thompson, N. A. Frederick, J. Kindt, A. Belcher, G. D. Stucky, D. E. Morse and P. K. Hansma, *Nature*, **399**, 761 (1999).
8. P. Vukusic, J. R. Sambles and C. R. Lawrence, *Nature*, **404**, 457 (2000).
9. R. K. Iler, *The Chemistry of SIlica, Solubility, Polymerization, Colloid and Surface Prcperties, and Biochemistry,* (John Wiley and Sons, Inc. U.S.A 1979).
10. N. Kröger, R. Deutzman and M. Sumper, *Science*, **286**, 1129 (1999).
11. Y. Zhou, K. Shimizu, J. N. Cha, G. D. Stucky and D. E. Morse, *Angew. Chem. Int. Ed.* **38**, 780 (1999).
12. J. N. Cha, G. D. Stucky, D. E. Morse and T. J. Deming, *Nature*, **403**, 289 (2000).
13. Y. Ono, K. Nakashima, M. Sano, Y. Kanekiyo, K. Inoue and J. Hojo, *Chem. Commun.* 1477 (1998).
14. Y. Ono, Y. Kanekiyo, K. Inoue, J. Hojo, M. Nango and S. Shinkai, *Chemistry Lett.* 475 (1999).
15. C. T. Kresge, M. E. Leonowicz, W. J. Roth, J. C. Vartulli and J. S. Beck. *Nature*, **359**, 710 (1992).
16. J. S. Beck, J. C. Vartuli, W. J. Roth, M. E. Leonowicz, C. T. Kresge, K. D. Schmitt, C. T-W Chu, D. H. Olson, E. W. Sheppard, S. B. McCullen, J. B. Higgins and J. L. Schlenker. *J. Am. Chem. Soc.* **114**, 10834 (1992).
17. N. K. Raman, M. T. Anderson and C. J. Brinker, *Chem. Mater.* **8** 1682 (1996).
18. A. Firouzi, D. Kumar, L. M. Bull, T. Besier, P. Sieger, Q. Huo, S. A. Walker, J. A. Zasadzinski, C. Glinka, J. Nicol, D. Margolese, G. D. Stucky and B. F. Chmelka, *Science,* **267**, 1138 (1995).
19. Huo, D. I. Margolese, E. Ciesla, P. Feng, T. E. Gler, P. M. Petroff, F. Schüth and G. D. Stucky, *Nature*, **368**, 317 (1994).

20. K. M. McGrath, D. M. Dabbs, N. Yao, I. A. Aksay and S. M. Gruner, *Science*, **277**, 552 (1997).
21. S. Su Kim, W. Zhang, T. J. Pinnavaia, *Science*, **282**, 1302 (1998).
22. D. Zhao, Q. Huo, J. Feng, J. Kim, Y. Han and G. D. Stucky, *Chem. Mater.* **11**, 2668, (1999).
23. D. Zhao, J. Feng, Q. Huo, N. Melosh, G. H. Fredrickson, B. F. Chmelka and G. D. Stucky, *Science*, **279**, 548 (1998).
24. N. A. Melosh, P. Lipic, F. S. Bates, F. Wudl, G. D. Stucky, G. H. Frederickson and N. F. Chmelka, *Macromolecules*, **32**, 4332 (1999).
25. M. Templin, A. Franck, A. Du Chesne, H. Leist, Y. Zhang, R. Ulrich, V. Schädler, U. Wiesner, *Science*, **278**, 1795 (1997).
26. C. G. Göltner, S. Henke, M. C. Weissenberger and M. Antonietti, *Angew. Chem. Int. Ed.* **37**, 613 (1998).
27. Y. Akiyama. F. Mizukami, Y. Kiyozumi, K. Maeda, H. Izitsu and K. Sakaguchi. *Angew. Chem. Int. Ed.* **38**, 1420 (1999).
28. S. M. Yang, I. Sokolov, N. Coombs, C. T. Kresge and G. A. Ozin. *Adv. Mater.* **11**, 1427 (1999).
29. S. M. Yang, H. Yang, N. Coombs, I. Sokolov, C. T. Kresge and G. A. Ozin, *Adv. Mater.* **11**, 52 (1999).
30. K. W. Gallis, J. T. Araujo, K. J. Duff, J. G. Moore and C. J. Landry, *Adv. Mater.* **11**, 1452 (1999).
31. T. Asefa, M. J. MacLachlan, N. Coombs and G. A. Ozin, *Nature*, **402**, 867 (1999).
32. K. Kageyama, J. Tamazawa and T. Aida, *Science*, **285**, 2113 (1999).
33. X. Feng, G. E. Fryxell, L. Q. Wang, A. Y. Kim, J. Liu, K. M. Kemner, *Science*. **276**, 923 (1997).
34. W. Zhou, J. M. Thomas, D. S. Shephard, B. F. G. Johnson, D. Ozkaya, T. Maschmeyer, R. G. Bell, Q. Ge, *Science*, **280**, 705 (1998).
35. P. Yang, T. Deng, D. Zhao, P. Feng, D. Pine, B. F. Chmelka, G. M. Whitesides and G. D. Stucky, *Science*, **282**, 2244 (1998).
36. M. Trau, N. Yao, E. Kims, Y. Xia, G. M. Whitesides and I. A. Aksay, *Nature*, **390** 674 (1997).

37. Ö. Dag, G. A. Ozin, H. Yang, C. Reber and G. Bussière, *Adv. Mater.* **11**, 474 (1999).

38. T. Nguyen, J. Wu, V. Doan, B. J. Schwartz, S. H. Tolbert, *Science*, **288**, 652 (2000).

39. E. Yablonovitch, *Phys. Rev. Lett.* **58**, 2059 (1987).

40. S. John. *Phys. Rev. Lett.* **58**, 2486 (1987).

41. J. S. Foresi, P. R. Villeneuve, J. Ferrera, E. R. Thoen, G. Steinmeyer, S. Fan, J. D. Joannopoulos, L. C. Kimerling, H. I. Smith and E. P. Ippen, *Nature*, **390**, 143 (1997).

42. S. Lin, E. Chow, V. Hietala, P. R. Villeneuve and J. D. Joannopoulos, *Science*, **282**, 274 (1998).

43. J. D. Joannopoulos, P. R. Villeneuve and S. Fan, *Nature*, **386**, 143 (1997).

44. E. Yablonovitch, *J. Mod. Opt.* **41**, 173 (1994).

45. E. Yablonovitch, T. Gmitter and K. Leung, *Phys. Rev. Lett.* **67**, 2295 (1991).

46. M.C. Wanke, O. Lehmann, K. Müller, Q. Wen and M. Stuke, *Science*, **275**, 1284 (1997).

47. S. Y. Lin, J. G. Fleming, D. L. Hetherington, B. K. Smith, R. Biswas, K. M. Ho. M. M. Sigalas, W. Zubrzycki, S. R. Kurtz and J. Bur, *Nature*, **394**, 251 (1998).

48. T. F. Krauss, R. M. De La Rue and S. Brand, *Nature*, **383**, 699 (1996).

49. J. C. Knight, J. Broeng, T. A. Birks, P. St. J. Russell, *Science*, **282** 1476.

50. M. Campbell, D. N. Sharp, M. T. Harrison, R. G. Denning and A. J. Turberfield. *Nature*, **404**, 53 (2000).

51. A. Blanco, E. Chomski, S. Grabtchak, M. Ibistate, S. John, S. W. Leonard, C. Lopez, F. Meseguer, H. Miguez, J. P. Mondia, G. A. Ozin, O. Toader and H. M. van Driel, *Nature*, **405**, 437 (2000).

52. B. T. Holland, C. F. Blanford and A. Stein, *Science*, **281**, 538 (1998).

53. J. E. G. J. Winjhoven and W. L. Vos, *Science*, **281**, 802 (1998).

54. O. D. Velev, T. A. Jede, R. F. Lobo and A. M. Lenhoff, *Nature*, **389**, 447 (1997).

55. S. R. Hall, S. A. Davies and S. Mann, *Langmuir*, **16**, 1454 (2000).

56. H. Míguez, F. Meseguer, C. López, Á. Blanco, J. S. Moya, J. Requena, A. Mifsud and V. Fornée, *Adv. Mater.* **10**, 480 (1998).

57. S. I. Matsushita, T. Miwa, D. A. Tryk and A. Fujishima, *Langmuir*, **14**, 6441 (1998).

58. S. Han and T. Hyeon, *Chem. Commun.* 1955 (1999).

59. A. A. Zakhidov, R. H. Baughman, Z. Iqbal, C. Cui, I. Khayrullin, S. O. Dantas, J. Marti and V. G. Ralchenko, *Science*, **282**, 897 (1998).

60. S. A. Johnson, P. J. Ollivier and T. E. Mallouk, *Science*, **283** 963 (1999).

61. C. J. Brinker and G. W. Scherer. *Sol-Gel Science, The Physics and Chemistry of Sol-Gel Processing*. (Academic Press, Inc. San Diego, CA, U.S.A, 1990).

62. R. Hasegawa, Y. Mori, H. Sasaki, M. Ishibashi, *Mol. Cryst. Liq. Cryst.* **262**, 77 (1995).

63. Q. Luo, X. Chen, Z. Liu, Z. Sun and N. Ming, *Applied Surface Science*, **108**, 89 (1997).

64. V. V. Krongauz, *Processes Photoreact. Poly.* 260 (1995).

65. S. M. Yang, H. Yang, N. Coombs, I. Sokolov, C. T. Kresge and G. A. Ozin. *Adv. Mater.* **11**, 52 (1999).

66. I. Sokolov, H. Yang, G. A. Ozin, *Adv. Mater.* **11**, 636 (1999).

67. H. Schmidt, M. Popall, *Proc. SPIE-Int. Soc. Opt. Eng.* **1328**, 249 (1990).

68. H. Krug and H. Schmidt, *New J. Chem.* **18**, 1125 (1994).

69. A. Fardad, M. Andrews, G. Milova, A. Malek-Tabrizi. I. Najafi, *Appl. Opt.* **37**, 2429 (1998).

70. H. Schmidt, H. Krug, R. Kasemann and F. Tiefensee, *Proc. SPIE-Int. Soc. Opt. Eng.* **1590**, 36 (1991).

71. P. W. Oliviera, H. Krug, H. Kuenstle, H. Schmidt, *Proc. SPIE-Int. Soc. Opt. Eng.* **2288**, 554 (1994).

72. P. Coudray, J. Chisham, A. Malek-Tabrizi, C-Y Li, M. P. Andrews, N. Peyghambarian and S. I. Najafi, *Opt. Commun.* **128**, 19 (1996).

73. P. Etienne, P. Coudray, Y. Moreau, J. Porque, *J. Sol-Gel Sci. Technol.* **13**, 523 (1998).

74. J. E. Chisam, M. P. Andrews, C-Y Li, S. I. Najafi, A. Malek-Tabrizi, *Proc. SPIE-Int. Soc. Opt. Eng*. **2695**, 52 (1996).

75. S. Pelissier, D. Blanc, M. P. Andrews, S. I. Najafi, A. V. Tishchenko and O. Parriaux. *Appl. Opt*. **38**, 6744 (1999).

76. M. A. Fardad, T. Touam, P. Meshkinfam, R. Sara, X. M. Du, M. P. Andrews and S. I. Najafi. *Electron. Lett*. **33**, 1069 (1997).

77. J. T. Rantala, P. Äryäs, R. Levy, S. Honkanen, M. R. Descour and N. Peyghambarian, *Opt. Lett*., **23**, 1939 (1998).

78. P. Coudray, J. Chisham, A. Malek-Tabrizi, C. Y. Li, M. Andrews and S. I. Najafi, *Proc. SPIE-Int. Soc. Opt. Eng*. **2695**, 92 (1996).

79. C-Y Li, J. Chisham, M. Andrews, S. I. Najafi, J. D. Mackenzie and N. Peyghambarian, *Electron. Lett*. **31**, 271 (1995).

80. E. J. Lerner, *Laser Focus World*, **33**, 119 (1997).

81. C. Allan Guymon, E. N. Hoggan, N. A. Clark, T. P. Rieker, D. M. Walba and C. N. Bowman, *Science*, **275** 57 (1997).

82. R. Ryoo, C. H. Ko, S. J. Cho and J. M. Kim, *J. Phys. Chem. B*, **101**, 10610 (1997).

83. N. A. Melosh, P. Davidson and B. F. Chmelka, *J. Am. Chem. Soc*. **122**, 823 (2000).

84. R. C. Smith, W. M. Fischer, D. L. Gin, *J. Am. Chem. Soc*. **119** 4092 (1997).

85. P. Kumar, K. L. Mittal Eds., *Handbook of Microemulsion Science and Technology* (Marcel Dekker Inc. New York, 1999), p. 1.

86. B. Jönsson, B. Lindman, K. Holmberg and B. Kronberg Eds., *Surfactants and polymers in aqueous solution* (John Wiley & Sons, Chichester, 1998) Chapter 18.

87. R. D. Neuman and T. H. Ibrahim, *Langmuir*, **15**, 10 (1999).

88. W. M. Gelbart, A. Ben-Shaul, *J. Phys. Chem*. **100**, 13169 (1996).

89. C-L Chang, H. S. Fogler, Langmuir **13**, 3295 (1997).

90. P. Schmidt-Einkel, W. W. Lukens Jr., P. Yang, D. I Margolese, J. S. Lettow, J. Y. Ying and G. D . Stucky, *Chem. Mater*. **12**, 686 (2000).

91. P. Feng, X. Bu, G. D. Stucky and D. J. Pine, *J. Am. Chem. Soc*. **122**, 994 (2000).

92. J. Esquena, Th. F. Tadros, K. Kostarelos and C. Solans, *Langmuir*, **13**, 6400 (1997).

93. P. Schmidt-Winkel, C. J. Glinka and G. D. Stucky, *Langmuir*, **16**, 356 (2000).

94. S. D. Sims, D. Walsh and S. Mann, *Adv. Mater.* **10**, 151 (1998).

95. P. Espiard, A. Guyot and J. E. Mark, *J. Inorg. Org. Polym.* **5**, 391 (1995).

96. J. Sanchex, S. E. Rankin and A. V. McCormick. *Ind. Eng. Chem. Res.* **35**, 117 (1996).

97. Y. Lu, G. Cao, R. P. Kale, S. Prabakar, G. P. López and C. J. Brinker. *Chem. Mater.* **11** 1223 (1999).

98. R. Tamaki. K. Samura and Y. Chujo, *Chem. Commun.* 1131 (1998).

99. P. Chevalier, R. J. P. Corriu, P. Delord, J. J. E. Moreau and M. W. C. Man, *New J. Chem.* **22**, 423 (1998).

100. B. Boury, R. J. P. Corriu, V. Le Strat, P. Delord and M. Nobili, *Angew. Chem. Int. Ed.* **38** 3172 (1999).

# 6. ORIENTED POLYMER GROWTH WITH POLARISED, SELF-FOCUSING LIGHT IN SILICA-METHACRYLATE WAVEGUIDES

## 6.1 INTRODUCTION

In Chapter 4, we identified and characterised laser self-focusing in hybrid silica-methacrylate (SAC-01) planar waveguides. In this process, a guided mode of a continuous wave, visible (514.5 nm), $Ar^+$ laser beam initiates free-radical polymerisation of propyl methacrylate substituents in the composite. Photo-responses of the SAC-01 medium are highly localised in space and depend critically on the intensity profile of the beam. As a result, a lens-like, refractive index profile is created in the medium, through which the beam focuses itself along the propagation axis. Diffraction is suppressed and laser self-focusing leads to anomalously high optical field intensities in the material.

Sequential lens-formation and self-focusing actions of the beam lead to a channel waveguide in the SAC-01 medium, which could be elaborated on the silicon substrate through a simple wet-etching step. A scanning electron micrograph of the surface of such a channel waveguide is presented in Figure 6.1. Careful observation reveals that the surface of the structure is patterned with a series of linear features. The striations have sub-micrometric widths, and run along the long-axis of the waveguide, *i.e.* they coincide with the path travelled by the guide optical mode in the SAC-01 waveguide. The observation suggests a form of structural orientation is induced in the SAC-01 medium by the self-focusing laser beam.

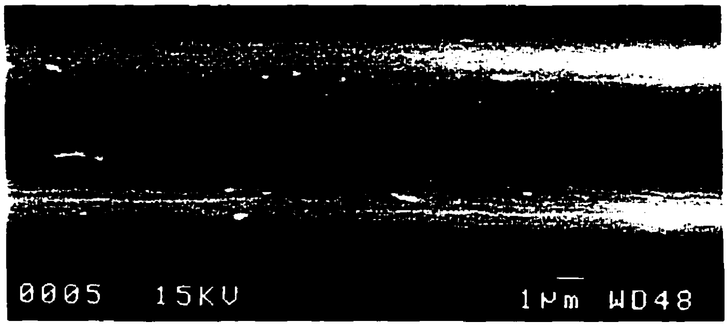

**Figure 6. 1** Scanning electron micrograph of self-inscribed channel waveguide, showing striations parallel to the waveguide long-axis.

In this Chapter, we examine laser-induced orientation in SAC-01 composites. Specifically, we study free-radical, methacrylate chain growth with linearly polarised, self-focusing laser beams and characterise the effect of laser-polarisation on the optical anisotropy in self-inscribed channel waveguides. Laser induced birefringence in SAC-01 planar waveguides was first discovered by T. Kanigan[1], through a series of careful polarised Raman spectroscopic studies.

In the following Sections, we apply our understanding of laser self-focusing and self-organisation in silica-methacrylate composites, to further investigate laser-induced anisotropy in SAC-01 planar waveguides. We propose a mechanism based on photo-oriented chain growth in the nonlinear optical and *anisotropic* reaction field provided by a linearly polarised, self-focusing laser beam. In our view, anisotropy of the reaction field, imparts orientation to the nascent methacrylate chains, during free-radical polymerisation. This concept may be compared to other examples of polymer growth in asymmetric reaction media. For example, birefringent, crystalline fibres of polyethylene were grown in the channels of mesoporous silica host[2]. In this case, channels arranged in a periodic, hexagonal pattern, served as highly oriented, reaction vessels for chain growth. In another instance, polyacetylene fibres with clockwise and anticlockwise helical structures was synthesised in the presence of chiral, nematic liquid crystals[3]. In our case, the polarisation direction of the laser beam presents a net anisotropy over the reaction medium.

Our characterisation of laser self-focusing in SAC-01 planar waveguides examines the scalar effects of refractive index change in the composite. To characterise photo-orientation in SAC-01 waveguides, we focus on the vector effects of refractive index change. Accordingly, we use polarised light techniques such as polarised waveguide Raman spectroscopy and optical birefringence measurements to characterise photoinduced anisotropy in the medium.

## 6.2 EXPERIMENTAL

### 6.2.1 Self-focusing with linearly polarised guided optical waves

The optical assembly used for self-focusing experiments, described in Section 4.2, Chapter 4, was used. The polarisation of the laser beam prior to in-coupling was specified with a half-wave retardation plate. As shown in Figure 6.2, photo-initiated free-radical polymerisation of methacrylate groups was carried out with transverse electric (TE), transverse magnetic (TM) and TE+TM polarised light. Self-focusing experiments were carried out with laser intensities ranging from 250 mW – 500 mW. At various intervals during self-focusing, "readings" of laser-induced birefringence in the self-inscribed channel waveguide were made with waveguide Raman and optical birefringence measurements. The same $Ar^+$ laser beam served as the excitation and probe beams. The intensity of the beam was lowered to 100 mW and 5 mW for the waveguide Raman and the optical birefringence measurements, respectively.

### 6.2.2 Polarised waveguide Raman spectroscopy

The set-up or waveguide Raman spectroscopy described in Section 3.2 of Chapter 3, was used. For polarised spectra, an analyser (dichroic sheet linear polariser with a 10. 000 to 1 extinction ratio (Spindler and Hoyer) was inserted between the two collection lenses. To compensate for grating polarisation sensitivity, a wedge depolariser was placed immediately before the holographic filter used for exclusion of the excitation beam wavelength. The polarisation of the excitation beam (514.5 nm line of an $Ar^+$ laser) was specified with a half-wave retardation plate in the $y$ or the $z$ directions. Spectra were acquired at laser intensities of 100 mW. Acquisition times ranged from 8 to 30 seconds for each spectral window of 600 $cm^{-1}$ and 30 scans were averaged for each spectrum.

### 6.2.3 Measurements of photo-induced birefringence

Growth and apparent erasure of photo-induced birefringence in self-inscribed channel waveguides were monitored as follows. Self-focusing was carried out with 514.5 nm, 500 mW, TE+TM polarised light for 30 minutes. Optical birefringence of the self-inscribed waveguide was measured by placing a polarisation analyser at the waveguide output. The power of the in-coupled laser beam was then reduced to 5 mW and its polarisation was set to TE ($y$) orientation. The analyser was oriented in the TM ($z$)

direction. The waveguide output was captured by a fibre optic bundle that delivered light intensity to a spectrograph (MultiSpec, Oriel Corporation, Stratfield, COT. USA) equipped with a photodiode charge coupled device (PCCD) detector. Intensity measurements were made at 514.5 nm with an acquisition time of 2 seconds. The evolution of optical birefringence in the structure was monitored by exposing the waveguide to TE, TE+TM light, TM, TE+TM light, in that sequence. Optical birefringence measurements were made at intervals by reducing the power of the laser beam and following the procedure outlined above.

### 6.2.4 Measurement of axes of birefringence

The optical set-up described in the previous Section was used. Axes of birefringence were located by varying the polarisation of the input probe beam from 0° to 180° with respect to the $z$ and $y$ axes of the waveguide (Figure 6.2), where 0° and 180° correspond to the TE polarisation and 90° to TM polarised light. For each input polarisation, output measurements were made with the analyser oriented in the $z$ (TM) and the $y$ (TE) directions. The degree of polarisation of the output light was then calculated according to Equation 6.1. The same measurements were made after the waveguide had been irradiated with TE+TM waveguided light and then with TE polarised light.

## 6.3 RESULTS AND DISCUSSION

In our investigations of laser self-focusing in SAC-01 planar waveguides, the polarisation of the laser beam was always maintained in the TE+TM (transverse electric + transverse magnetic) orientation, where the electric field of the beam is oriented at 45° to the $z$ and $y$ geometric axes of the waveguide (Figure 6.2). In these experiments, we examined the scalar effects of refractive index change in the medium. The waveguided beam induced spatially, localised and intensity dependent refractive index changes index that enabled it to focus along its propagation axis, without suffering diffraction. The self-action of the beam created a long, narrow channel waveguide in the SAC-01 slab, which had an enhanced refractive index relative to unexposed regions. In this Chapter, we examine the influence of the polarisation of the laser beam on the refractive index profile of the self-inscribed channel waveguide. We achieve this by probing optical anisotropy in self-inscribed channel waveguides through polarised light techniques. We relate the orientation of this birefringence to the polarisation of the self-focusing laser beam. Whereas in Chapter 4, we focussed on the scalar effects of refractive index change, here we probe its vector effects.

### 6.3.1 Free-radical polymerisation in SAC-01 planar waveguides with linearly polarised guided waves – polarisation dependent laser self-focusing

We examined self-focusing with the laser beam linearly polarised along three different axes of planar SAC-01 waveguides. Laser polarisation directions with respect to the geometric axes of the SAC-01 waveguide are shown in Figure 6.2. Accordingly, free-radical polymerisation of methacrylate substituents in the silica-methacrylate medium, was carried out with (a) transverse electric (TE) and (b) transverse magnetic (TM) polarised light, where the electric field vector oscillates in the *y* and the *z* directions, respectively and with (c) TE + TM polarisation where it oscillates at a 45° angle to the *z* and *y* axes. The power of the 514.5 nm laser beam was maintained at 250 mW for all three samples.

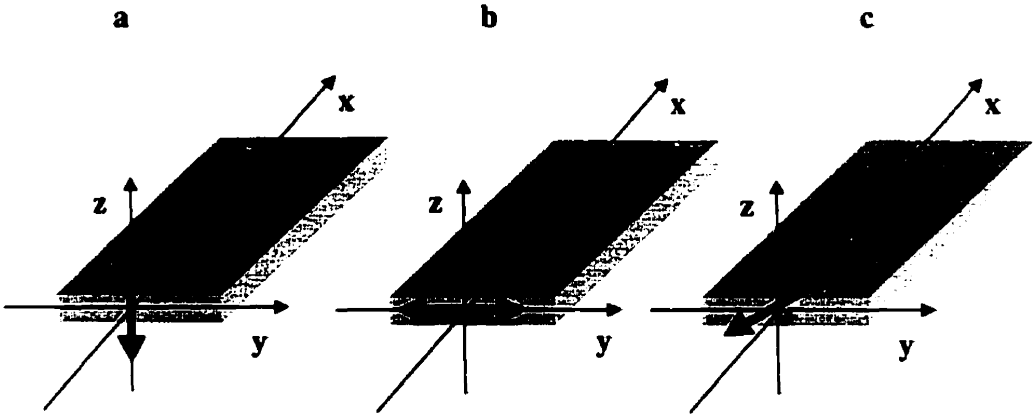

**Figure 6. 2** Free-radical polymerisation in SAC-01 waveguide with laser beam linearly polarised in the a) *z* direction (TM) b) *y* direction (TE) and c) 45° to the *z* and *y* axes (TE+TM)

Laser self-focusing in the SAC-01 waveguides was characterised by monitoring the slab waveguide output-intensities over time (Chapter 4). The temporal evolution of the output signal for the three different laser polarisations are presented in Figures 6.3-5.

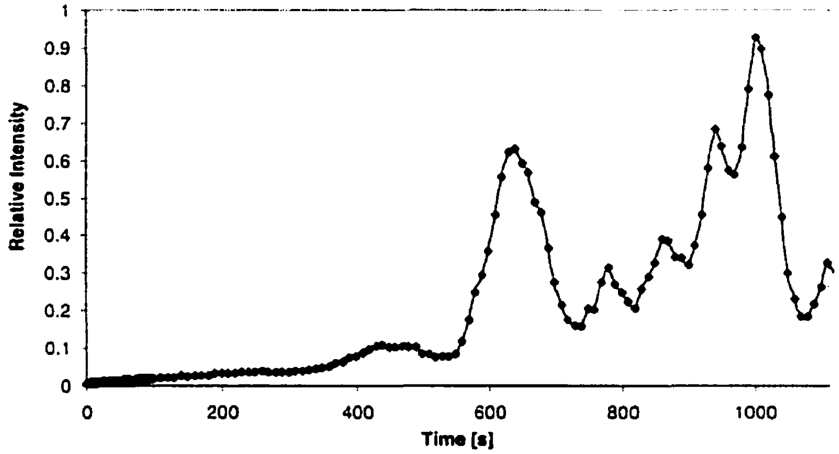

**Figure 6. 3** Temporal evolution of SAC-01 waveguide output of a TM, 514.5 nm, 250 mW beam.

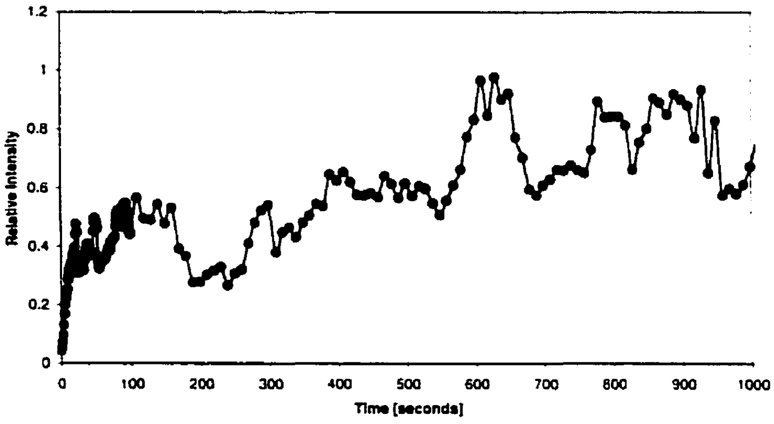

**Figure 6. 4** Temporal evolution of SAC-01 waveguide output of a TE, 514.5 nm, 250 mW beam.

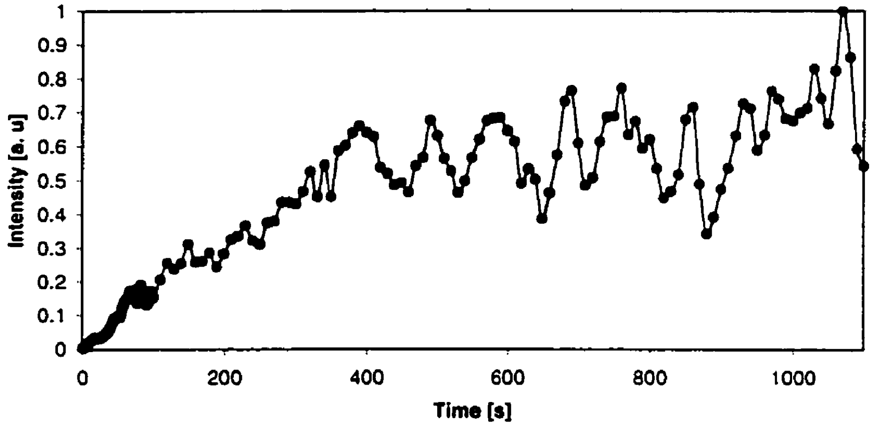

**Figure 6. 5** Temporal evolution of SAC-01 waveguide output of a TE + TM, 514.5 nm, 250 mW beam.

The above Figures show a distinct output-intensity profile for each polarisation of the in-coupled laser beam. Self-focusing is evident for both TM (Figure 6.3) and TE+TM (Figure 6.5) polarised laser light. In the former, after the initial photobleaching of the titanocene photo-initiator, there is as a gradual 17-fold increase in intensity over 450 seconds. This time period signifies the formation of a channel waveguide in the SAC-01 medium. The self-inscribed channel waveguide guided the propagating laser beam and suppresses diffraction in the *y* direction. Signal oscillations that commence at t = 540 seconds are caused by the onset of higher order optical modes in the channel waveguide. Self-focusing is also evident in the case of TE+TM polarised light, where the electric field vector oscillates in the plane that is at a 45° angle to the *x* and *y* axes of the SAC-01 waveguide. This specific experiment was also described in Section 4.3 of Chapter 4. Here, refractive index changes in the SAC-01 medium are indicated by an initial 33-fold increase in intensity from t = 30 – 390 seconds. Mode beating commences at t = 390 seconds. The output intensity of TE polarised light behaves differently (Figure 6.4). There is an initial 10-fold increase in intensity followed by rapid oscillations of the signal. Over time, the output intensity exhibits random oscillations and by t = 1050 seconds, has increased two-fold.

The only variable in the three experiments described above was the polarisation of the guided optical mode. As described above, the waveguide output-intensity profile is significantly different for each linear polarisation and suggests that laser self-focusing in the SAC-01 medium is a polarisation-sensitive event. Previously (Chapter 4) we have shown that self-focusing depends critically on photo-induced refractive index changes in the hybrid silica-methacrylate medium. As it propagates, the waveguided laser beam induces spatially localised and intensity-dependent refractive index changes ($\Delta n$), which create a gradient index lens in the medium. The laser beam then self-focuses through this lens along its propagation axis. The lens-forming and self-focusing action of the beam leads to a uniform channel waveguide in the medium, which confines the beam and suppresses diffraction. In identifying and characterising this phenomenon, we emphasised the intensity-dependence and the spatial modulation of the photoinduced Δn in the SAC-01 medium. In effect, we considered the scalar aspects of refractive index change in our hybrid organosilica system.

On the basis of our initial observations of polarisation sensitive self-focusing, we inferred that photo-induced refractive index changes in the SAC-01 composite do not occur in a homogenous, isotropic manner. In the case of an isotropic refractive index profile, all orientations of the electric field vector (all angles of linear polarisation) will be subjected to the same propagation conditions in the medium. In such an instance, the self-focusing action of the beam, monitored through the evolution of the waveguide output-intensity, should be identical for all laser polarisations. It is evident from Figures 6.3-6.5 that self-focusing kinetics varies significantly with laser polarisation. In turn, this implies that an anisotropy is associated with the photo-induced refractive index profile of the SAC-01 waveguide, namely $\Delta n$ varies according to the axis along which it is measured. In such a case, the refractive index profiles of the self-inscribed channel waveguides should be anisotropic, *i.e.* the waveguides should be birefringent.

### 6.3.2 Origins of optical anisotropy in SAC-01 waveguides

With these initial, qualitative observations of polarisation-sensitive refractive index changes in the SAC-01 waveguide, two origins of structural (thus optical) anisotropy in the medium must be considered. The discovery of self-organisation in the SAC-01 colloids was detailed in Chapter 5. The long-range, three-dimensional, periodic arrangement of methacrylate derivatised silica domains is permanently captured by UV initiated, free-radical polymerisation of methacrylate substituents. The monoliths, although transparent to visible wavelengths, exhibited a high degree of optical anisotropy when observed between crossed polars. We also showed that thin films cast from SAC-01 colloids consisted of a bicontinuous arrangement of methacrylate-derivatised silica domains. A visible laser beam coupled into the SAC-01 film propagates as a guided mode and initiates free-radical polymerisation of methacrylate functionalities in its path. Carbon-carbon bond formation between organic substituents effectively links silica domains to each other. As free-radical reactions occur in a spatially localised manner in the SAC-01 medium (Chapter 2), the resulting arrangement of silica domains faithfully traces the uniaxial path of the visible laser beam within the waveguide (Figure 6.6(i) and (ii)). Indeed, the striations that are observed along the long axis of the final, self-inscribed channel waveguide (Figure 6.1) correspond to these linear silica-domain arrangements. A possible explanation for polarisation-sensitive self-focusing lies here. The structurally anisotropic, uniaxial arrangement of silica domains that occurs during laser self-focusing, may in turn give rise to an anisotropic refractive index profile.

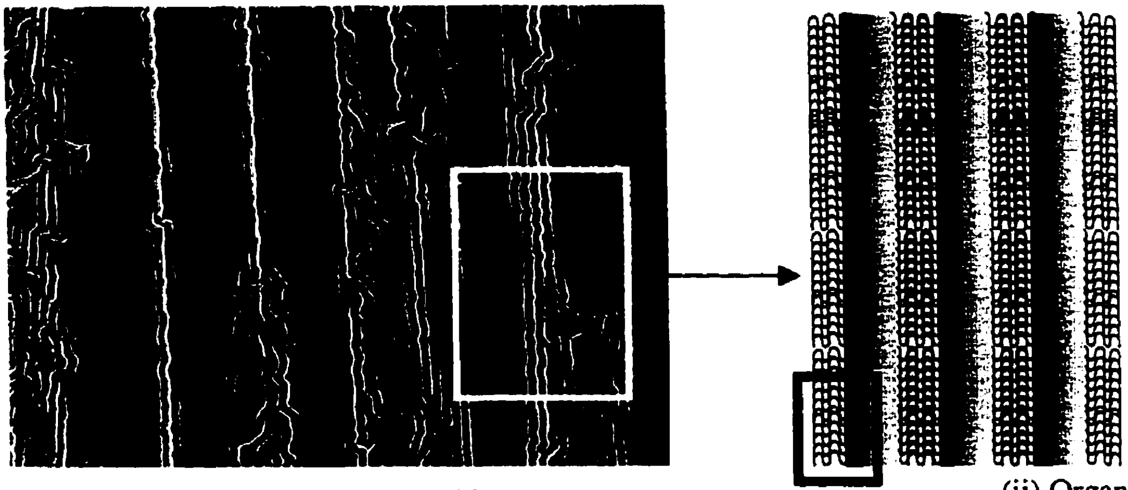

(i) Surface of a SAC-01 waveguide

(ii) Organised methacrylate derivatised silica domains

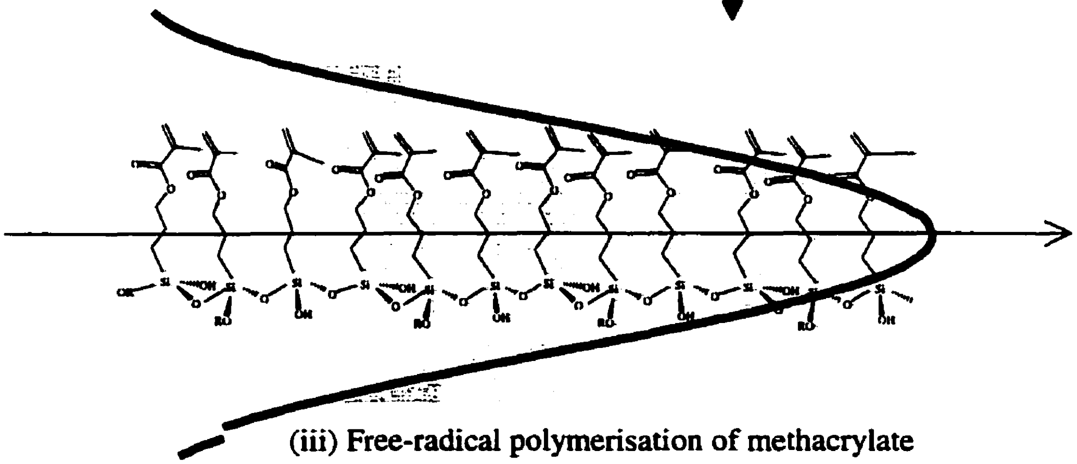

(iii) Free-radical polymerisation of methacrylate functionalities by a linearly polarised guided optical wave

**Figure 6. 6** Guided wave free-radical polymerisation in SAC-01 waveguides: (i) Scanning electron micrograph of uniaxial arrangement of methacrylate-derivatised silica domains in SAC-01 waveguide (ii) schematic showing methacrylate functionalities and (iii) their polymerisation with linearly polarised guided optical waves.

On the other hand, birefringence may arise from laser-initiated polymerisation of the organic component in the SAC-01 medium. This is schematised in Figure 6.6 (iii). AS mentioned previously, photo-initiated free-radical reactions in the SAC-01 waveguide are carried out in the nonlinear and anisotropic reaction field provided by a linearly polarised, self-focusing laser beam. Furthermore, we have shown that methacrylate polymerisation occurs in a spatially confined manner in the sol-gel derived silica medium. Under such conditions, orientation of molecular units by the intense and linearly polarised optical field will be permanently "locked" into place by the polymerisation process. Such photo-oriented, organic chain growth will also give rise to a refractive index anisotropy in the final self-inscribed channel waveguide.

In the following sections, we use techniques such as polarised waveguide Raman spectroscopy and optical birefringence measurements to probe the origins and characterise the vector component of laser-induced $\Delta n$ changes in SAC-01 waveguides.

### 6.3.3 Polarised waveguide Raman spectroscopy of SAC-01 waveguides

Optical anisotropy in channel waveguides that were self-inscribed with linearly polarised guided optical waves was first examined through polarised waveguide Raman spectroscopy. A schematic of the experimental set-up used for this study is presented in Figure 6.7.

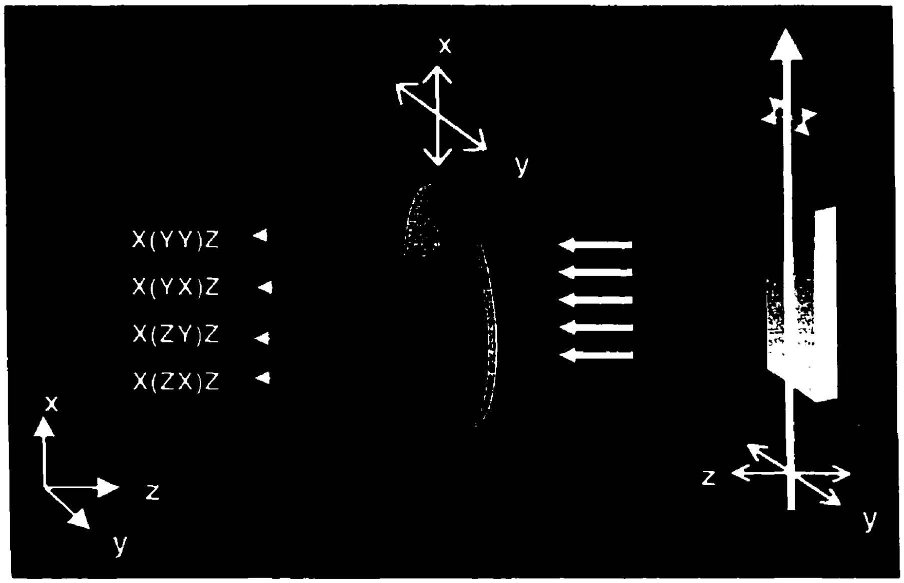

**Figure 6. 7** Schematic of polarised waveguide Raman spectroscopy experiment

According to laboratory frame coordinates specified in Figure 6.7, the excitation source (514.5 nm line of an $Ar^+$ laser) is coupled into the planar waveguide and propagates along the $x$ axis. The polarisation of the laser beam may be set along the $z$ (TM) or the $y$ (TE) axes using a half-wave retardation plate. As the visible laser beam travels as a guided optical wave in the planar waveguide, it excites Rayleigh and Raman scatter along its path. According to conventional 90° scattering geometry, collection of Raman scatter occurs along the $z$ direction. An analyser placed in the $z$ axis selects the polarisation of the intensity, either in the $x$ or the $y$ directions.

With these combinations of excitation polarisation and analyser directions, four different Raman spectra of the waveguide sample may be acquired. As shown in Figure 6.7, these may be classified according to Porto's notation[4] as X(YY)Z, X(YX)Z, X(ZY)Z and X(ZX)Z. Here, the first and the last letters correspond to the axes of excitation and collection respectively. The first letter inside the parenthesis specifies the polarisation of the excitation source and the second corresponds to the orientation of the analyser.

In the case of a three-dimensionally isotropic system, the intensity contributions to each of these Raman spectra may be expressed in terms of the orientationally invariant terms δ and ρ, derived from the molecular polarisability tensor[5], where, δ and ρ represent the symmetric and anisotropic components of the spectral intensity (Table 6.1).

**Table 6. 1** Symmetric and anisotropic contributions to Raman spectral intensity

| | **ROTATIONAL INVARIANT** | |
|---|---|---|
| | **symmetric** | **anisotropic** |
| X(YY)Z | δ | $4\gamma^2/45$ |
| X(YX)Z | δ | $\gamma^2/15$ |
| X(ZY)Z | δ | $\gamma^2/15$ |
| X(ZX)Z | δ | $\gamma^2/15$ |

where $\partial = \frac{1}{3}\sum_{i=1}^{3}\alpha_{ii}$ and $\gamma^2 = \frac{1}{2}\sum_{i<j}[(\alpha_{ii} - \alpha_{jj})^2 + 6\alpha_{ij}{}^2$.

Generally, the intensity ratio between the polarised spectrum X(YY)Z and one of the depolarised spectra X(ZY)Z gives the depolarisation ratio, which is used to distinguish symmetric from asymmetric bands in the Raman spectrum. In our case, the polarisation sensitive spectra gave the first indication polarisation rotation in the SAC-01 waveguide.

### 6.3.3.1 Evidence of photo-induced anisotropy in SAC-01 channel waveguides

Polarised Raman spectra were acquired of self-inscribed channel waveguides in the SAC-01 medium. In these experiments, the 514.5 nm line of the $Ar^+$ laser was used for both self-focusing and as the excitation source for Raman spectroscopy (details of the experimental set-up used for self-focusing and waveguide Raman spectroscopic studies were detailed in Section 4.2 of Chapter 4). Thus the visible laser beam served to both "write" and "read" photo-induced anisotropy in the SAC-01 waveguide. In the "write" step, the linearly polarised laser beam self-inscribed a channel waveguide in the SAC-01 film. In the subsequent "read" step, the beam (with reduced intensity) propagating in the newly formed channel waveguide provided vibrational spectroscopic information about the self-inscribed structure.

Figure 6.8 contains the set of polarised and depolarised waveguide Raman spectra of a channel waveguide that had been self-inscribed with TE polarised light. Raman spectral assignments of the SAC-01 planar waveguide were detailed in Chapter 3. We focus here on the C-H stretching region of the spectrum that ranges from 2800 to 3200 $cm^{-1}$.

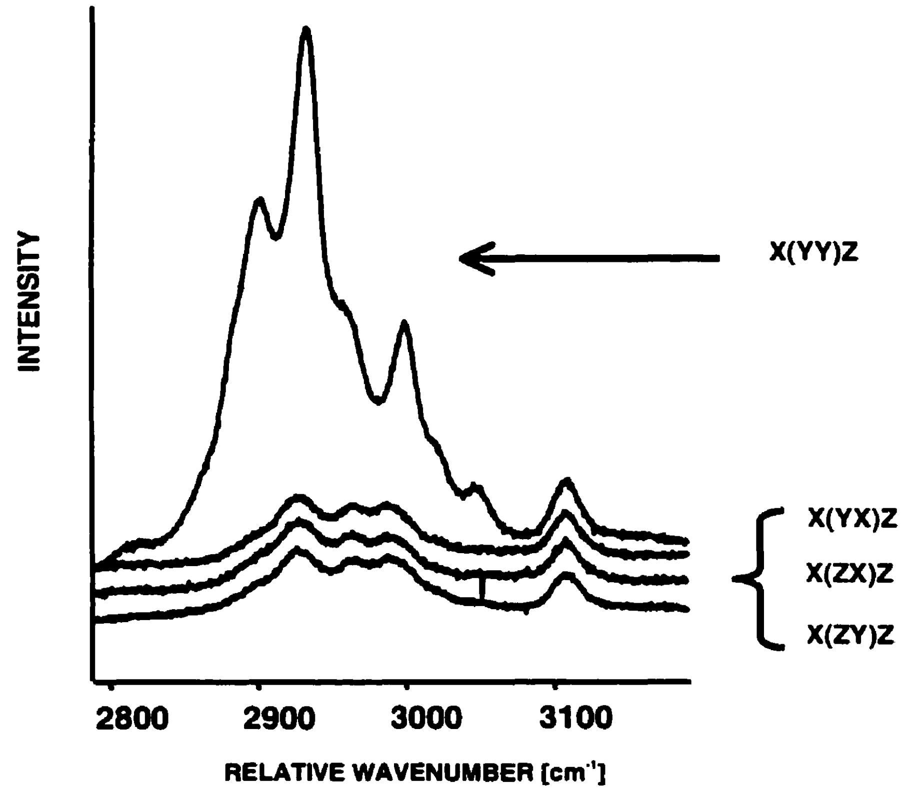

**Figure 6. 8** Polarised and depolarised waveguide Raman spectra of SAC-01 waveguide

Bands in the 2800 to 3200 cm$^{-1}$ region of the Raman spectrum may be assigned as follows: $\nu_s(CH_3)$ at 2899 cm$^{-1}$, $\nu_s(CH_2)$ of = $CH_2$ at 2929 cm$^{-1}$, $\nu_{as}(CH)$ of Si-$OCH_3$ at 2958 cm$^{-1}$, 2996 cm$^{-1}$, $\nu_s(CH)$ of = $CH_2$ at 3045 cm$^{-1}$ and $\nu_{as}(CH_2)$ of = $CH_2$ at 3105 cm$^{-1}$. According to Table 6.1, contributions from the invariant symmetric component of the molecular polarisability tensor are contained only in the polarised spectrum denoted X(YY)Z. Accordingly, bands $\nu_s(CH_3)$, $\nu_s(CH_2)$ of = $CH_2$ and $\nu_s(CH)$ of = $CH_2$ are present only in the polarised spectrum in Figure 6.8. The three depolarised spectra are qualitatively similar and contain contributions from the anisotropic components. This series of spectra obtained from the channel waveguide self-inscribed with TE polarised light contain no indication of anisotropy. Indeed, the spectra correspond to the Raman scatter activities of a structurally and thus optically isotropic medium.

Self-focusing with the TE+TM polarisation was then carried out in a non-exposed region of the same SAC-01 planar waveguide. The set of polarised and depolarised Raman spectra of the resulting channel waveguide is presented in Figure 6.9.

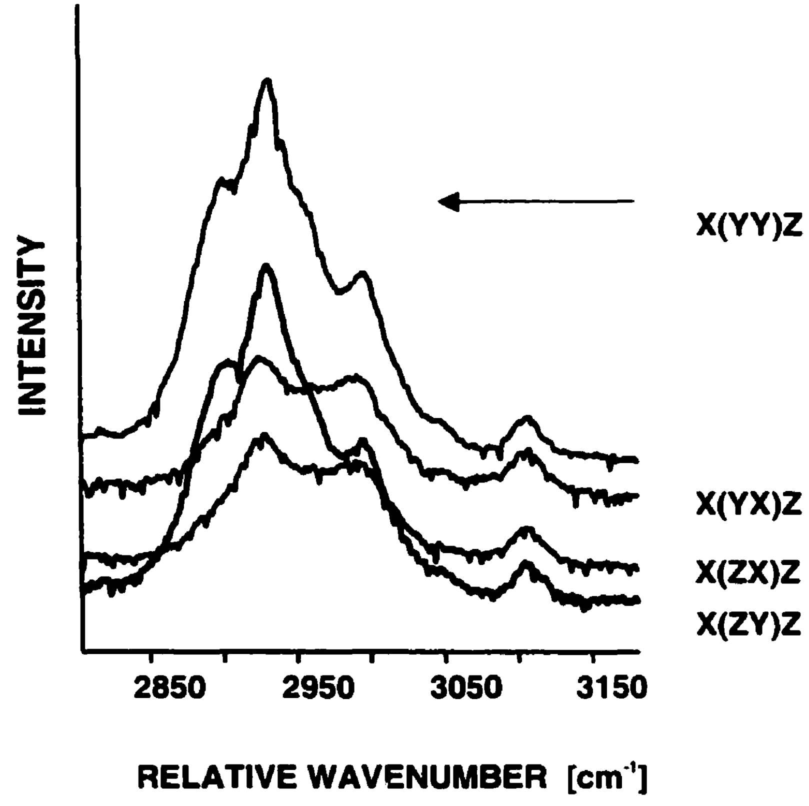

**Figure 6. 9** Polarised and depolarised waveguide Raman spectra of channel waveguide self-inscribed with TE+TM polarised light

A striking difference is immediately observable in the series shown in Figure 6.9. Spectral intensity in one of the depolarised spectra, namely (X(ZY)Z), now contains contributions from the rotationally invariant symmetric component of the molecular polarisability tensor. Note that all of the symmetric stretches that are present in the polarised spectrum X(YY)Z, can be identified in the X(ZY)Z spectrum shown in Figure 6.9. In fact, both spectra are qualitatively identical, a strong indication that rotation of the linearly polarised excitation beam was taking place in the channel waveguide that was self-inscribed by TE+TM polarised light.

In polarised Raman spectroscopic studies, it is assumed that the linear polarisation of the excitation beam is preserved throughout the sampling volume. In the case of planar waveguides, this is true for samples with isotropic refractive index profiles. Polarisation scrambling may occur in birefringent waveguides, which in the simplest case have two different indices of refraction oriented along two different axes of the waveguide. If the polarisation of the probe laser beam is not perpendicular or parallel to and thus does not coincide with one of these axes of birefringence, polarisation scrambling occurs. In this case, the linearly polarised laser beam encounters both components of the refractive index. The electric field vector is resolved into two components that propagate at different speeds and thus acquires a phase difference with respect to each other. In effect, there is conversion from linear to elliptical polarisation of the laser beam.

Such a case may be used to explain the anomalous depolarised spectrum in Figure 6.9. Assume that in the "write" step, self-focusing with TE+TM polarised light introduces an anisotropy in the refractive index profile (*i.e.* an axes of birefringence ) along the self-inscribed channel waveguide. In the "read" experiment, the probe polarisation of the excitation source is initially linearly polarised along $z$. However, as it propagates in the birefringent channel waveguide, the laser beam becomes elliptically polarised. The electric field vector now acquires components in the $y$ direction. Note that in the case of the X(ZY)Z depolarised spectrum, the analyser is set along the $y$ axis. As mentioned previously, in this experimental set-up the polarised Raman spectrum with the symmetric contributions is obtained only with the X(YY)Z configuration, where the probe polarisation coincides with the analyser orientation. In the case of the birefringent channel waveguide, polarisation scrambling of the $z$-polarised probe beam allows the scattering activity of the symmetric component of the molecular polarisability tensor to be detected in the X(ZY)Z spectrum.

Interestingly, photo-induced anisotropy in the SAC-01 channel waveguide was reversible. The sequence of spectra (a) - (h) presented in Figure 6.10 monitor the X(ZY)Z spectrum of a waveguide that was initially self-inscribed with TE light and subsequently exposed to different polarisations of light. (Laser polarisation with respect to the $x$ and $y$

geometric axes of the SAC-01 waveguide (Figure 6.2) is represented by double-headed arrows adjacent to the spectra.) Spectrum (a) corresponds to the channel waveguide that was self-inscribed with a 500 mW TE polarised beam. The spectral intensity contains contributions only from anisotropic, vibrational bands with no evidence of photo-induced anisotropy. Spectrum (b) was acquired after exposing the same channel waveguide to TE+TM light also at 500 mW. The "switching on" of the anisotropy is immediately evident in the X(ZY)Z spectrum, which now resembles its polarised X(YY)Z counterpart. The birefringent channel waveguide was subsequently exposed to TM polarised light. Spectra (c)-(e) monitor the evolution of the X(ZY)Z spectrum at various stages of exposure to TM light. The gradual removal of the symmetric contributions to the X(ZY)Z spectrum can be observed here, indicating that the birefringence induced with TE+TM light is effectively erased by exposure to TM polarised light. The "write-erase" cycle of the birefringence may be recommenced by exposing the waveguide to the TE+TM polarisation. As revealed by spectra (f) and (g), birefringence was rewritten in the channel waveguide through exposure to TE+TM polarised light. The absence of symmetric stretches in spectrum (h), which was acquired after exposing the channel waveguide to TE polarised light, indicates that in addition to TM polarised light, the birefringence may also be erased with TE polarisation.

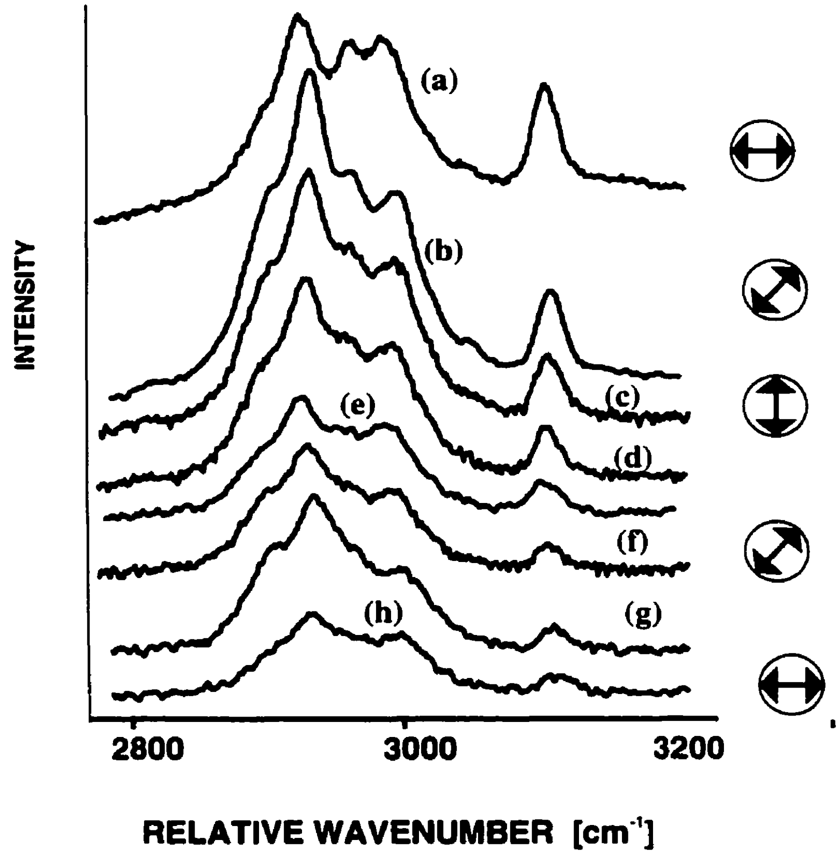

**Figure 6. 10** Write and erase cycles of photo-induced anisotropy in self-inscribed SAC-01 channel waveguides

The polarised waveguide Raman spectroscopic studies described above indicate that a self-focusing, TE+TM polarised, laser beam inscribes a birefringent channel waveguide in the SAC-01 medium. The studies also indicate the *apparent* reversibility of photo-induced birefringence by subsequent exposure of the channel waveguide to TE or TM polarised light. From our examination of laser self-focusing in the SAC-01 medium (Chapter 4), we have demonstrated that this process occurs through free-radical polymerisation of methacrylate functionalities in the material. Evidence of anisotropy in the refractive index of the self-inscribed channel waveguide indicates that some form of photo-orientation takes place during this reaction. In this context, the observation of birefringence "erasure" is puzzling. Carbon-carbon bond formation that takes place during free-radical polymerisation is permanent and "reversal" of this process, which implies bond cleavage, is not possible with the low energy, visible laser beam used here.

Taking this into consideration, it is probable that exposure of the birefringent waveguide to TE or TM light does not erase the anisotropy but rather *re*-inscribes a new axis of birefringence oriented parallel or perpendicular to the TE (y) or the TM (z) directions. Note that the birefringence axes induced by the TE and TM polarised light, coincide with the geometric axes (*z* and *y*) of the SAC-01 planar waveguide. In such a case, the photo-induced birefringence cannot be detected by polarised Waveguide Raman spectroscopic measurements. This may be understood by considering the orientation of the photo-inscribed birefringence axes with respect to the polarisation of the probe laser beam. As will be shown below, polarisation scrambling of the probe beam does not occur when the axis of the birefringence coincides with the waveguide geometric axes.

The linear polarisation of a laser beam becomes elliptically polarised as it propagates in a birefringent waveguide. Viewed through crossed polars, the degree of polarisation of elliptically polarised light at the waveguide output, is represented by[6]:

$$P = \frac{E_{max}^2 - E_{min}^2}{E_{max}^2 + E_{min}^2} = \frac{I_{max} - I_{min}}{I_{max} + I_{min}} \qquad [6.1]$$

where $E_{min}$ and $E_{max}$ are the minimum (crossed polarisers) and maximum (parallel polarisers) values of the electric field amplitude of the elliptically polarised light. In a birefringent waveguide, the degree of polarisation at the output of a linearly polarised laser beam is also given by:

$$P = [1 - \sin^2(2\theta)\sin^2\delta]^{1/2} \qquad [6.\,2]$$

where $\theta$ is the angle of the incident linearly polarised light with respect to the $x$ axis of birefringence and $\delta$ is the retardation. When $\theta$ equals $N\pi$ (where N is an integer), the linear polarisation of the input beam is preserved as it propagates. This represents the case when the probe polarisation is parallel or perpendicular to the birefringent axis of the waveguide.

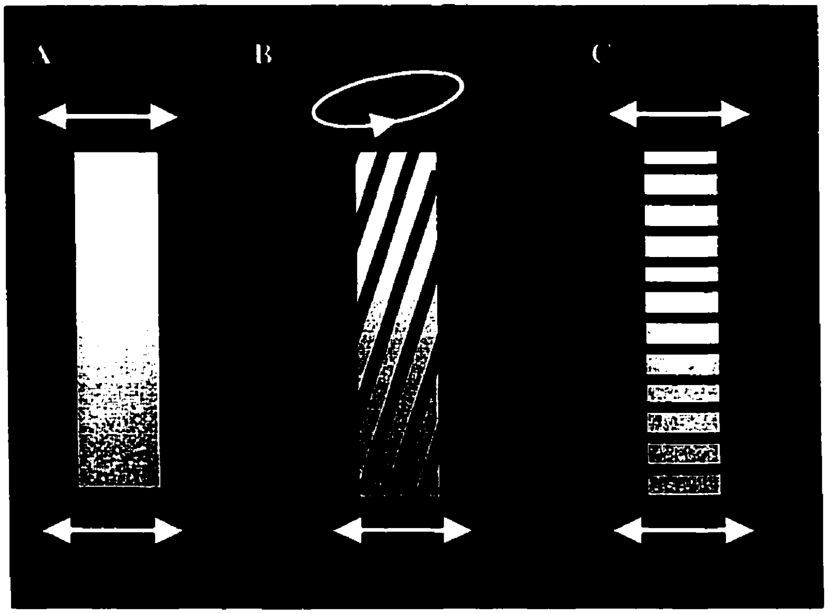

**Figure 6. 11** Behaviour of linearly polarised light in A) isotropic medium B) in a medium where it is oriented at 45° to and C) where it coincides with the birefringence axis.

With these considerations, an explanation for our observation of anisotropy in the polarised waveguide Raman spectra of SAC-01 waveguides is presented in Figure 6.11. Figure 6.11A represents a SAC-01 waveguide with an isotropic refractive index. A probe laser beam initially polarised along the $z$ axis (represented by the double-headed arrow), retains its polarisation as it propagates through the structure. Laser self-focusing with a TE+TM polarised beam in the SAC-01 waveguide introduces an anisotropy in the refractive index. Figure 6.11B represents the resulting birefringent channel waveguide. Observe that the axis of photo-induced birefringence is located at a 45 ° angle to the $z$ and $y$ geometric axes of the waveguide. Now, the linear polarisation of the probe beam is oriented at a 45 ° angle to the birefringent axis and according to Equation [6.2] becomes elliptically polarised as it propagates. In this way, the electric field vector of the laser beam acquires components in the $y$ direction. As a result, the spectral intensity of the depolarised Raman spectrum X(ZY)Z of the birefringent waveguide contains contributions from symmetric components that are characteristic of the polarised X(YY)Z spectrum. Exposure of the birefringent waveguide to TM light, now re-inscribes an axis of birefringence along the $z$ axis (Figure 6.11C). It is important to note that here too, there is an anisotropy in the refractive index. However, the axis of birefringence now coincides with the geometric axis of the waveguide. The polarisation of the probe beam (along $z$) now coincides with the waveguide axis of birefringence. Thus according to Equation [6.2], it is preserved as it propagates through the birefringent waveguide. Accordingly, the X(ZY)Z spectrum of the waveguide contains contributions from only the anisotropic bands and photo-induced birefringence is not detected in this case. The same reasoning may be applied to explain the apparent erasure of anisotropy with TE polarised light.

### 6.3.4 Characterisation of photo-induced anisotropy through birefringence measurements in SAC-01 channel waveguides

Direct evidence of tuneable, photo-induced birefringence in the SAC-01 waveguide was obtained by monitoring its output through crossed polarisers. Figure 6.12 plots the evolution of the waveguide output-intensity between crossed polarisers. Self-focusing was carried out with TE+TM, TE, TE+TM, TM, TE light, in that sequence. The birefringence was monitored at intervals by reducing beam power to 5 mW, setting the probe polarisation with a half wave plate to TE and observing the output through a crossed polariser (TM) placed at the waveguide output.

At t = 0 seconds, the waveguide initially inscribed with TE+TM light has a relative birefringence of 0.46. This value is decreased to 0.05 over the next 3480 seconds by exposure to TE polarised light. This time period signifies the inscription of a new axis of birefringence that coincides with the *y* axis of the waveguide. Subsequent illumination with TE+TM polarised light, re-introduces the birefringence in the waveguide. Within the next 570 seconds (t = 4050 seconds), the birefringence reaches a maximum value of 1. Subsequent exposure to TM polarisation rapidly reduces the birefringence to 0.03 in the next 1230 seconds (t = 5880 seconds). Exposure to TE+TM polarisation re-introduces the birefringence, which increases to 0.95 in the next 360 seconds. Notice also that the TM polarisation reverses the anisotropy at a faster rate than TE polarised light. Whereas, 3480 seconds of exposure to TE light reduces birefringence from 0.46 to 0.05, TM polarised light reduces birefringence from 1 to 0.03 in almost a third of this time, 1220 seconds.

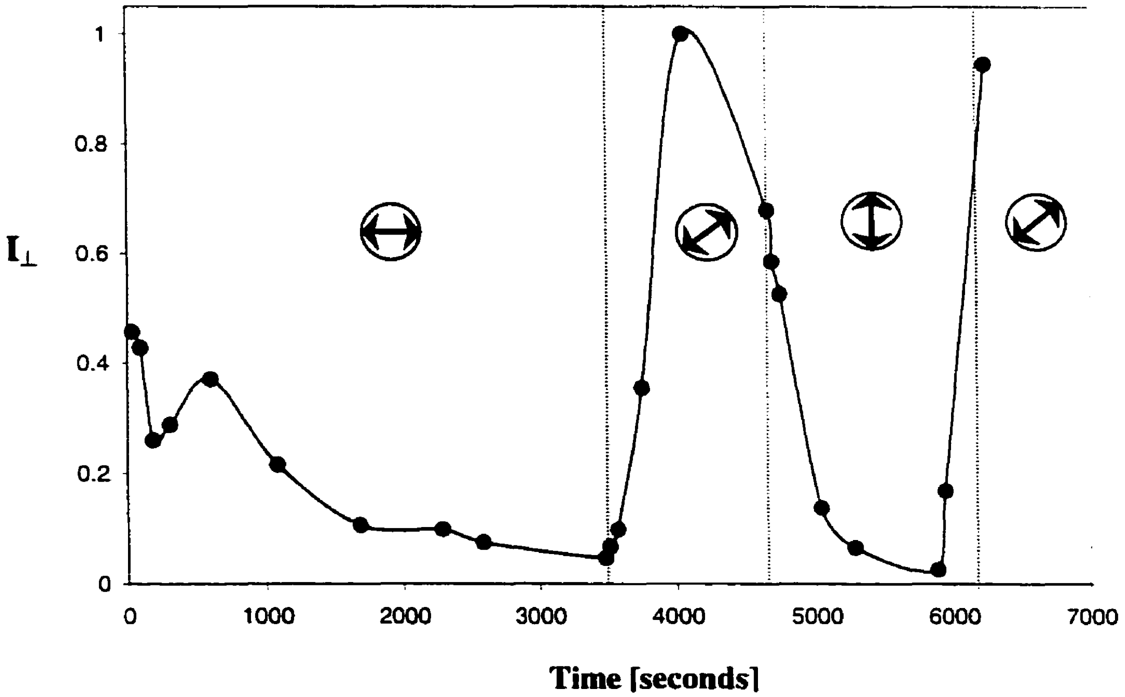

**Figure 6. 12** Evidence of laser-tuneable birefringence in the SAC-01 waveguide

### 6.3.5 Photo-inscription of axes of birefringence in SAC-01 channel waveguides

The above studies indicate that linearly polarised light introduces orientation in the self-inscribed waveguide, which is parallel or perpendicular to the electric field vector (polarisation) of the incident laser beam. In turn, this creates an anisotropy in the refractive index (birefringence) in the resulting channel waveguide. The axes of photo-induced birefringence in the SAC-01 waveguide may be located by measuring the degree of polarisation of elliptically polarised light at the waveguide output, according to Equation [6.2]. In these measurements, the input polarisation of the probe laser beam was varied from 0 to 180°, where 0° and 180° correspond to TE polarised light, parallel to the $y$ axis of the waveguide and 90° corresponds to TM polarised light, parallel to the $z$ axis of the waveguide. The TE+TM polarisation of the probe beam then corresponds to 45° and 135°. During the measurements, the orientation of the analyser at the waveguide output was maintained in the $z$ direction. The degree of polarisation at the output was calculated according to Equation [6.2].

A plot of the degree of polarisation [P] versus input polarisation for a non-irradiated SAC-01 waveguide is presented in Figure 6.13. Note that the greatest P values 0.98 and 0.99 occur for the TE and the TM orientations respectively (as denoted by the double-headed arrows), which coincide with the geometric $z$ and $y$ axes of the waveguide. The same measurements were repeated after the waveguide was exposed to TE+TM light (Figure 6.14). Observe that P for both TE and TM light has decreased to 0.90 and 0.95 respectively. TE+TM light inscribes a birefringence that is oriented at 45° to the $z$ and $y$ axes of the SAC-01 waveguide. In such a case, the TE and TM polarisations become elliptically polarised as they propagate in the birefringent structure, which is seen as a decrease in P at the waveguide output. The waveguide was now exposed to TE light, during which an axes of birefringence that coincides with the $z$ axis is written in the waveguide. Measurements of the degree of polarisation measurements made after this step are presented in Figure 6.15. The P values have now increased to 0.99 for both TE and TM probe polarisations, indicating that polarisation scrambling no longer occurs in the waveguide.

The above measurements clearly indicate that the electric field vector of the visible laser beam, induces a net anisotropy in the refractive index of the SAC-01 composite. The axes of this birefringence coincide with the polarisation of the incident beam. Subsequent exposure of the waveguide to an alternate polarisation, re-inscribe the birefringence in this orientation.

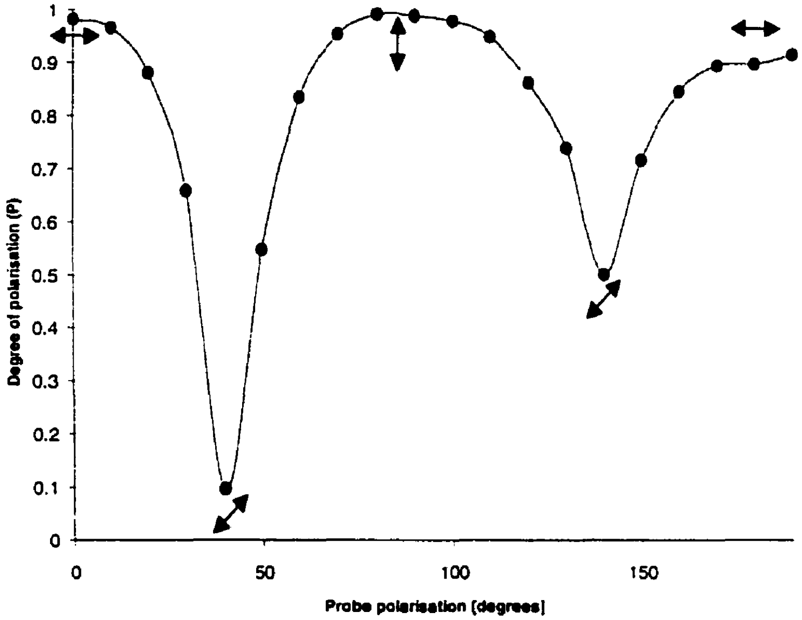

Figure 6. 13 Degree of polarisation versus probe polarisation for non-irradiated SAC-01 planar waveguide

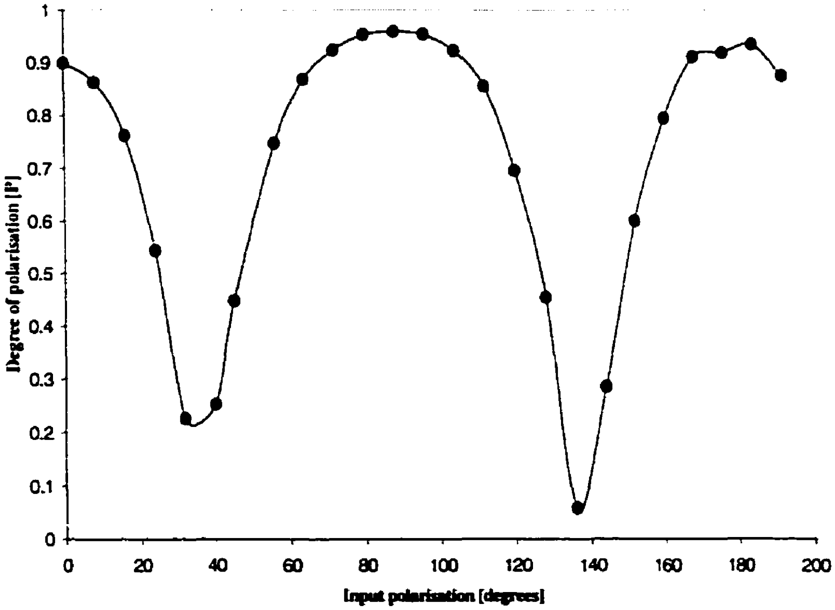

Figure 6. 14 Degree of polarisation versus probe polarisation in channel waveguide self-inscribed with TE+TM light

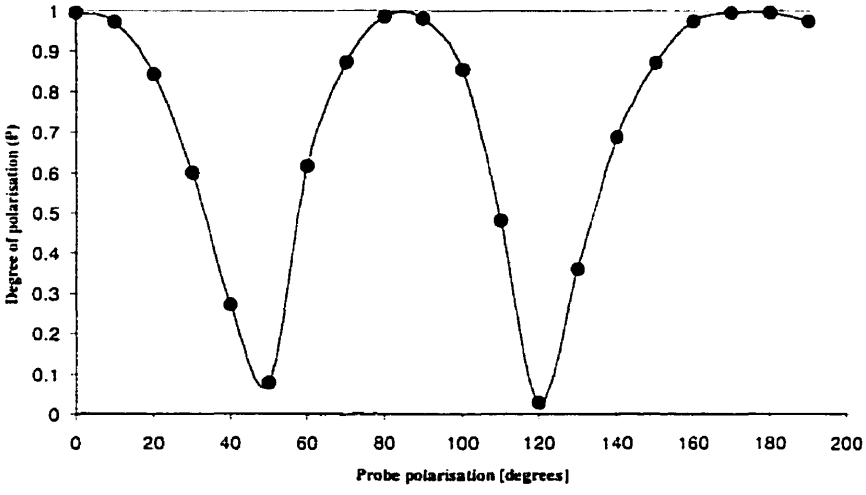

**Figure 6. 15** Degree of polarisation [P] versus probe polarisation for SAC-01 channel waveguide in Figure 6.12 exposed to TE light

### 6.3.6 Microscopic origins of photoinduced anisotropy in the SAC-01 medium

The studies described in the previous Sections confirm that refractive index changes ($\Delta n$) induced by a self-focusing laser beam in a SAC-01 waveguide have both scalar and vector effects. In Chapters 2, 3 and 4, we examined the scalar effects of photo-induced $\Delta n$ in the composite. Through spectroscopic studies we learnt that photo-initiated, free radical polymerisation of methacrylate substituents trigger polycondensation reactions in the silica host. The resulting growth and compaction of the matrix leads to an increase in refractive index. This scalar effect of refractive index change is used in photolithography of integrated-optics devices in SAC-01 substrates. In Chapter 4, we applied the same property to elicit self-focusing of a visible, continuous wave, laser beam in SAC-01 planar waveguides. This phenomenon also relies on the scalar effects of photo-induced Δn. Intensity-dependent and spatially localised ($\Delta n$) in the SAC-01 medium create a lens-like refractive index profile in the path of the beam, which is a prerequisite for laser self-focusing. In this process, the $\Delta n$ changes induced by the self-focusing beam lead to a self-inscribed channel waveguide in the SAC-01 medium.

The polarised light techniques described in the previous Sections of this Chapter, identified a *net* anisotropy in the refractive index profile of such self-inscribed waveguides. The self-focusing beam inscribes an axis of birefringence that coincides with the polarisation of the incident beam, suggesting that this was an electric-field induced effect. These observations of bulk optical birefringence raise the question about the microscopic origins anisotropy in the hybrid silica-methacrylate medium.

In Section 6.3.2, we considered two possible reasons for structural and thus optical anisotropy in the SAC-01 material. The first was based on laser-induced organisation of methacrylate-derivatised silica domains in SAC-01 thin films. We proposed that optical birefringence could originate from the uniaxial arrangement of silica domains, created as waveguided light propagates through the SAC-01 slab. However, this explanation does not account for the ability to tune birefringence with linearly polarised light. The other possible mechanism is associated with light-induced, organic chain growth in the medium. As mentioned earlier, polymerisation of methacrylate substituents in the sol-gel derived silica host is conducted in the nonlinear optical environment of a self-focusing beam. Significantly, the linear polarisation of the beam provides a highly anisotropic reaction field, which may influence or introduce orientation in the nascent polymer chains.

In order to confirm that birefringence in the self-inscribed waveguides was directly associated with free-radical polymerisation, we conducted control experiments with waveguides prepared from the "saturated" analogue (SAC-02) of the SAC-01 composite. SAC-02, derived from 3-acetoxypropyltrimethoxysilane (see inset, Figure 6.16, consists of an organically modified silica matrix without any photo-polymerisable vinyl functionalities. As such, it enables the photo-responses of the inorganic host to be selectively examined in the absence of free-radical polymerisation. This material was introduced in Chapter 2 and was used for other control studies in Chapters 2, 4 and 5.

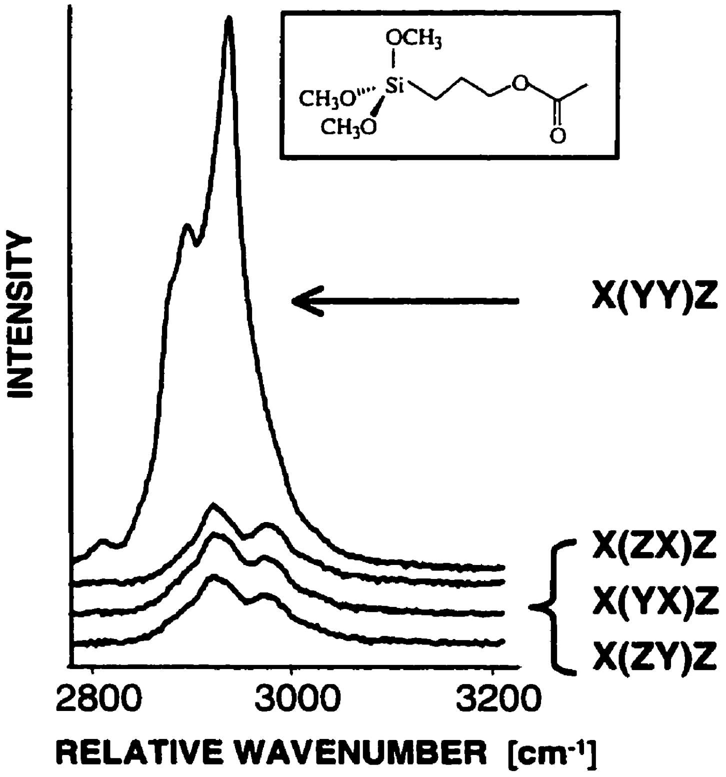

**Figure 6. 16** Polarised and depolarised waveguide Raman spectra of SAC-02 waveguide

We probed for photo-induced anisotropy in SAC-02 waveguides through polarised waveguide Raman spectroscopic measurements. The C-H stretching region of polarised and depolarised Raman spectra of an SAC-02 waveguide is presented in Figure 6.16. The symmetric mode, $v_s$(CH) of $-OCH_3$ is present only in the polarised X(YY)Z spectrum. No changes to any of the four spectra presented were observed after exposure of the medium to TE, TM or TE+TM polarised, waveguided light. Figure 6.17 monitors the behaviour of the X(ZY)Z spectrum, which was diagnostic of anisotropy in the SAC-01 medium, after the SAC-02 waveguide was exposed to TE, TE+TM and TM light. This spectrum remains unchanged, indicating that the SAC-02 medium remains isotropic even after exposure to linearly polarised light. From this control experiment, we can infer that anisotropy in the SAC-01 medium originates from the photo-initiated free-radical polymerisation of methacrylate functionalities in the SAC-01 matrix.

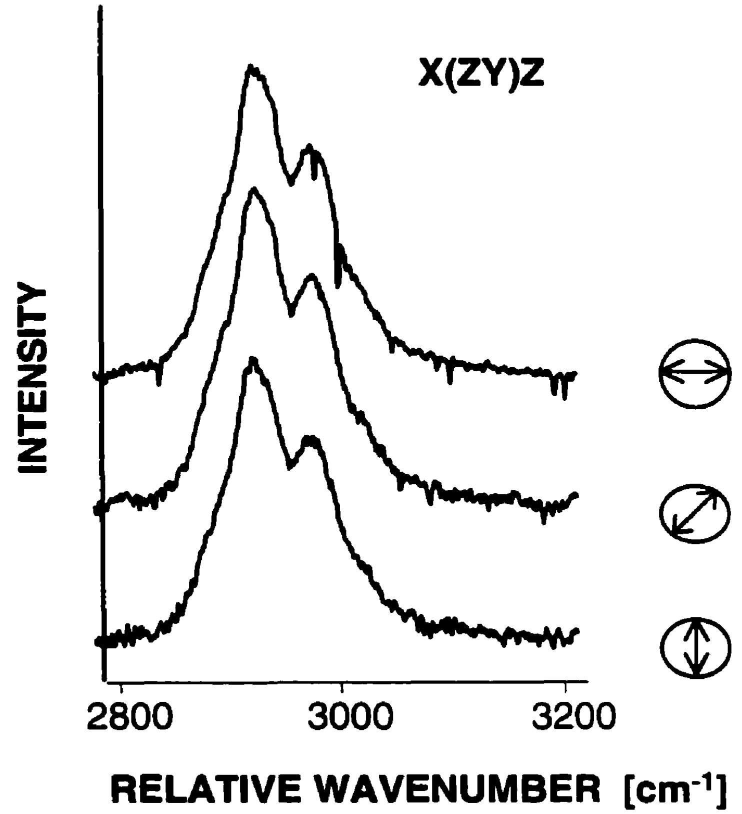

**Figure 6. 17** Behaviour of the X(ZY)Z depolarised Raman spectrum of SAC-02 waveguide after exposure to TE, TE+TM and TM light

We have identified free-radical polymerisation of methacrylate groups as the process during which orientation is introduced in the SAC-01 medium. This together with the observations of optical anisotropy in the self-inscribed waveguides indicate that the electric field vector of the laser beam causes the organic units to align parallel or perpendicular to its electric field vector. Simultaneous free-radical polymerisation then links the oriented organic units to each other. In this way, the "memory" of the orientation is retained in the channel waveguide.

With this information, Figure 6.18 gives a simplified, two-dimensional schematic of the distribution of methacrylate functionalities before and after exposure to linearly polarised light. We assume that prior to irradiation, there is no preferred orientation of the organic group. (Indeed, our measurements of polarised infrared spectroscopy and dichroic UV-Vis spectroscopy of SAC-01 thin films did not reveal any preferred orientation in the bands associated with the methacrylate functionality.) In such a model, we can regard the methacrylate units as micro-volumes, which are randomly distributed in the material and have no order with respect to each other. Linearly polarised light, through some interaction with the electric field and the molecular level anisotropy, orients each micro-volume parallel to the polarisation of the incident light. As schematised in Figures 6.18A, B and C, TE, TM and TE+TM polarisations induce macroscopic orientation along the $y$, $z$ and 45° between these axes, respectively. Note that each micro-volume in the sample is oriented along a common axis. Thus a net or bulk anisotropy is created in the medium. Recall that simultaneous to this "poling" process, laser-initiated free-radical polymerisation links the oriented micro-volumes to each other with carbon-carbon bonds. In this way, the net anisotropy of the SAC-01 medium is permanently captured, such that the SAC-01 medium retains the "memory" of orientation even after the incident laser beam is removed. The anisotropy gives rise to the optical birefringence that was characterised in previous Sections of this chapter with polarised light techniques.

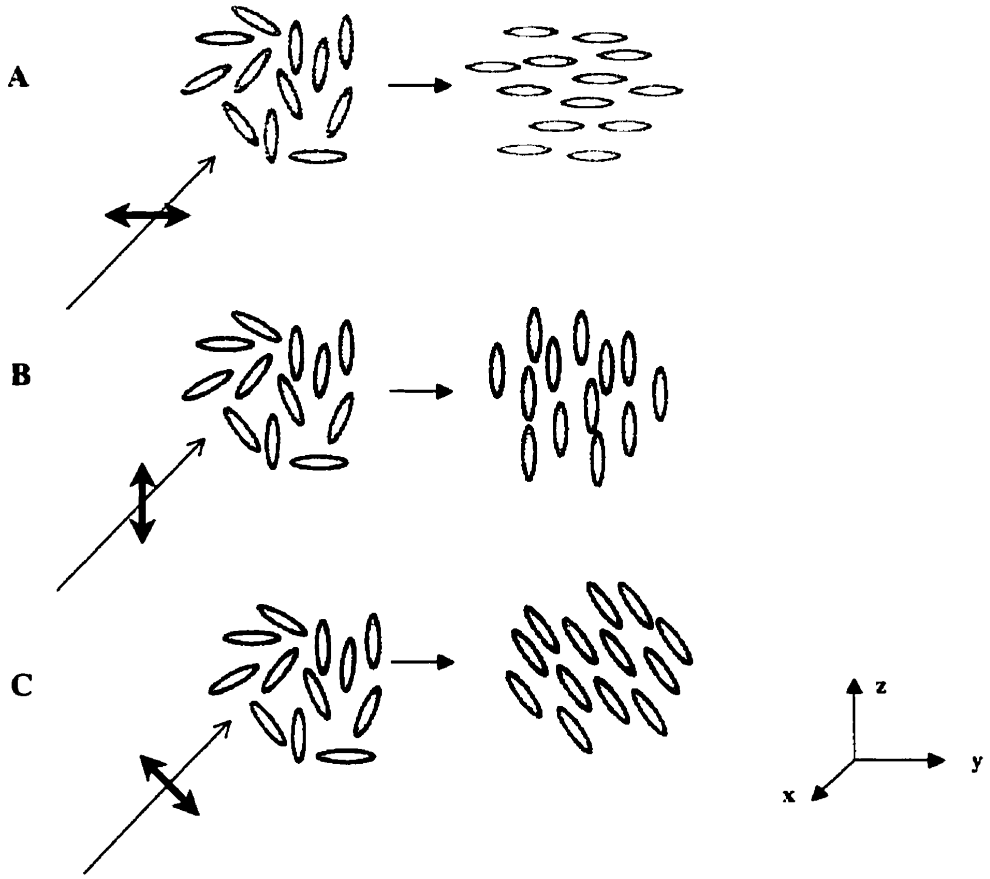

**Figure 6. 18** Schematic depicting possible orientation of methacrylate units by TE, TM and TE+TM polarised beams, leading to macroscopic anisotropy in the medium.

In order to better understand the origins of anisotropy in our system, it is instructive to consider other examples of photo-induced birefringence. The discovery of light-induced refractive index changes in germanosilicate optical fibre[7] was soon followed by reports of photo-induced birefringence in the material[8a-e, 11]. When silica is implanted with Ge ions, colour centres form in the material, as indicated by the growth of an absorption band at 240 nm. Linearly polarised UV or visible laser light selectively photo-bleaches the colour centre dipoles that are oriented along the electric field axis. In this way, dichroism is introduced in the material, which then leads to a refractive index anisotropy. UV-laser induced birefringence has also been observed in glass doped with nano-crystalline ZnS and Cu-ion co-dopants. Here, birefringence was thought to arise from an anisotropic distribution of trapped charges following excitation with linearly polarised laser beams. Extensive research has also been conducted on photo-induced anisotropy in chalcogenide glasses[9a-d] where anisotropy is thought to originate from the excitation of lone pair electrons of the chalcogen atoms. Photo-induced anisotropy has also been studied in azo-dye doped systems, where linearly polarised light selectively activates cis-trans isomerisation of chromophores[10]. In most of these examples, the material consists of a random distribution of transition dipoles. Linearly polarised light then selectively excites transition dipoles along its electric field vector[11]. In the caseswhere there is a photochemical reaction as a result of this interaction, (e.g. photo-isomerisation, photo-bleaching), the anisotropy is permanently imprinted in the medium, even after the incident beam is removed.

An explanation based on transition dipoles cannot be used in the case of the SAC-01 medium. The silica-methacrylate material is transparent at the 514.5 nm wavelength used for self-focusing experiments as neither the methacrylate unit nor the saturated methacrylate polymer absorb at visible wavelengths. A possible explanation may be given by considering the unusual conditions under which polymerisation is carried out in the SAC-01 planar waveguide. It is known that the self-focussing action of laser beams can lead to anomalously high optical field intensities[12]. It is also known that at sufficiently high laser intensities, all dielectric materials are driven into the nonlinear optical regime[13]. The electric field of an intense laser beam can induce a nonlinear distortion or polarisation of electronic charge distribution in a medium. Microscopically, this may be described as a contribution from the third order susceptibility $\chi^3$, of a material to nonlinear polarisation ($P^{NL}$). At the bulk level, this causes an increase in the index of refraction in the material. In classical experiments conducted in nonlinear optical media, it is this nonlinear behaviour of the refractive index that facilitates laser self-focusing. Conversely, in SAC-01 media, laser self-focusing occurs through the refractive index changes caused by photo-initiated polymerisation reactions. However, it is important to note that regardless of the mechanism underlying the process, laser self-focusing leads to high optical field intensities in the SAC-01 medium. These intensities may in turn elicit nonlinear polarisation responses from the organic substituents in the SAC-01 composite, which then leads to a nonlinear increase in the refractive index of the material, expressed through:

$$n = n^L + n_2(I)I \qquad [6.3]$$

where $n^L$ is the linear refractive index and $n_2(I)$ is the nonlinear refractive index coefficient that is dependent on the intensity (I) of the optical field. The nonlinear refractive index in turn, originates from the nonlinear, third order polarisation term ($P^{NL}$), which is a function of the third order susceptibility of the molecule.

In explaining photo-orientation in the SAC-01 medium, we must consider the anisotropy that is associated with the nonlinear optical response described by Equation 6.3. The nonlinear response of non-spherical atoms and molecules often involves the reorientation and redistribution of molecules along the electric field of a laser beam. Due to their anisotropic susceptibilities, a linearly polarised beam will tend to orient such molecules parallel to its electric field, by inducing a dipole moment along the most polarisable axis of the molecule and then exerting a torque on it. This orientation effect is further enhanced by induced dipole-dipole interactions between the molecules themselves, which will rearrange themselves to minimise the free-energy of the system. In this case, there is a net anisotropy introduced in the system, which leads to optical birefringence. The light-induced birefringence can change the polarisation of a probe beam propagating in the medium. The birefringence may be described through:

$$\delta n_{\Pi} - \delta n_{\perp} = \frac{9\pi\chi^{(3)}}{4n^{L}}|E|^{2} \qquad [6.4]$$

Equation 6.4 represents the optical Kerr effect, which forms the basis of several spectroscopic techniques used to measure nonlinear optical responses of systems. The Equation relates optical birefringence to the third order susceptibility term and the intensity of the optical field.

According to the mechanism described above, the intense optical field provided by the self-focusing beam, drives the SAC-01 into the nonlinear optical regime. Nonlinear polarisation responses of the anisotropic methacrylate substituents cause their orientation along the electric field vector of the propagating laser beam. In this way, a net anisotropy and thus birefringence is introduced in the system following Equation 6.4. In our system, free-radical reactions take place in concert with the optical Kerr effect. Carbon-carbon bonds link the oriented methacrylate units to each other. The self-focusing laser beam thus serves two purposes – to introduce orientation and refractive index increase in the SAC-01 planar waveguide. As a result, the self-inscribed channel waveguide has a permanent, anisotropic refractive index profile.

Our observations may be compared to a recent report of an unusual photophysical event in supersaturated solutions of urea in water[14]. A linearly polarised, IR laser beam, triggered nucleation and crystallisation in the solution. It was observed that the crysallites were oriented parallel to the polarisation of the incident beam. In order to explain this phenomenon, the authors invoked the optical Kerr effect and suggested that the laser beam oriented pre-nucleating urea clusters in the solution, increasing the chances of nucleation. Crystal growth then follows the initial laser-induced cluster orientation, which in effect reduced the entropic contribution to the activation of nucleation. Whereas in this system, photo-orientation of molecules by an intense optical field is amplified in the final structure through crystallisation, in the SAC-01 medium, bulk anisotropy is "locked" into place by free-radical polymerisation.

The proposed mechanism of photo-oriented methacrylate chain growth in the SAC-01 medium, requires considerable flexibility of the organic free-radical, in order to align itself with the electric field vector of the laser beam. It is possible that the propyl linkage attaching the methacrylate unit to the Si centres, confers some mobility to the group. Electron spin resonance studies of the early stages of polymerisation of methacrylic acid monomer have shown that the free-radicals have considerable rotational mobility[15]. On the other hand, it is also important to realise the significance of spatially localised photoreactions in the SAC-01 medium. Recall, the free-radical reactions are strongly confined to the regions of illumination in SAC-01 composites. This must play a significant role in preserving the orientation of methacrylate units. Consider for example, the same experiment in a bulk monomer liquid. It is unlikely that free-radical reactions initiated with intense, linearly polarised laser beam in this medium, will lead to a net anisotropy. Rapid polymer chain growth in the system will strongly inhibit the rotational mobility of the monomer units and their ability to align parallel to the electric field of the laser beam. In the case of the SAC-01 composite, the strict spatial confinement of free-radical reactions is likely to preserve the orientation associated with methacrylate functionalities, leading to a net anisotropy of the material. Such a case may be represented by the schematic presented in Figure 6.19, where the net orientation of the system derives from the inherent anisotropy associated with each micro-volume.

We observed that "new" axes of birefringence could be introduced in the system simply by exposing the waveguide to light with a different polarisation. It is possible that not all the methacrylate units are polymerised with the first "dosage" of light. This is supported by our infrared spectroscopic studies (Chapter 2), which indicated that unsaturated methacrylate units remain in the material even after extensive irradiation. It is possible that with each irradiation step with a different polarisation, a new axes is created through the orientation and polymerisation of the residual methacrylate monomers.

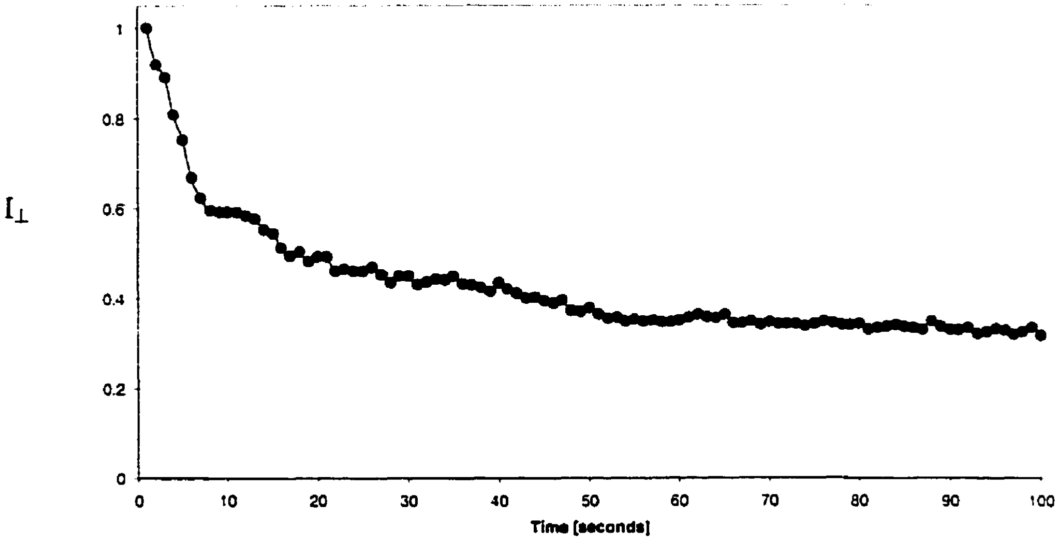

**Figure 6. 19** Birefringence decay in a SAC-01 waveguide formed with TE+TM light

A strong indication that some form of poled-order was achieved in the material was obtained by actually monitoring the relaxation of the photo-induced birefringence. Figure 6.19 measures the birefringence decay from the point that the laser beam was turned "off". There is a steep decrease in the first 10 seconds to almost half its initial value. It then decreases more gradually, and finally reaches a plateau. The non-exponential decay behaviour indicates that there is a complex relaxation process taking place, as the "poled" methacrylate units attempt to relax back to their isotropic equilibrium state. However, it is possible that relaxation kinetics are complicated by the fact that the organic units are actually linked to each other. It is also important to note that there is a significant residual birefringence in the waveguide. In other experiments, we have observed that the birefringence is retained in the waveguide over periods longer than 24 hours.

## 6.4 CONCLUSIONS

We have characterised photo-induced birefringence in self-inscribed SAC-01 channel waveguides with polarised waveguide Raman spectroscopy and optical birefringence measurements. Linearly polarised, self-focusing laser beams inscribe axes of birefringence in the SAC-01 material. Through control studies with the silica-acetate based, "saturated" analogue of the silica-methacrylate medium, we have confirmed that anisotropy originates from free-radical polymerisation of methacrylate functionalities in the sol-gel derived medium. We propose a mechanism where the anomalously high optical field intensities provided by the self-focusing laser beam induce nonlinear polarisation responses from methacrylate substituents. In the nonlinear optical regime, methacrylate functionalities are photo-oriented along the electric field axis of the linearly polarised, self-focusing beam. Simultaneous free-radical polymerisation links these oriented groups to each other, thus preserving the net anisotropy of the system. According to this model, the birefringence caused by the optical Kerr effect is permanently captured in the resulting SAC-01 channel waveguide.

---

1. T. Kanigan, Ph. D. Thesis, McGill University, 1995.
2. K. Kageyama, J. Tamazawa and T. Aida, *Science* **285**, 2113 (1999).
3. K. Akagi, C. Piao, S. Kaneko, K. Sakamaki, H. Shirakawa and M. Kyotani, *Science* **282**, 1683 (1998).
4. D. J. Gardiner and P. R. Graves, Eds., *Practical Raman Spectroscopy* (Springer-Verlag, Berlin, 1989).
5. N. E. Schlotter and J. F. Rabolt, *J. Phys. Chem.* **88**, 2062 (1984).
6. A. Wang, S. Zhou, K. A. Murphy and R. O. Claus, *Opt. Lett.* **19**, 460 (1994).
7. K. O. Hill, Y. Fuji, D. C. Johnson and B. S. Kawasaki, *Appl. Phys. Lett.* **32**, 67 (1978).
8. a) S. Bardal, A. Kamal and P. St. J. Russell. *Opt. Lett.* **17**, 411 (1992), b) T. Meyer, P. A. Nicati, P. A. Robert, D. Varelas, H. G. Limberger and R. P. Salathé *Opt. Lett.* **21**, 1661 (1996), c) A. Kamal and P. St. J. Russell. *J. Opt. Soc. Am. B.* **11**, 1576 (1994) d) D. Wong, S. B. Poole and M. G. Sceats. *Opt. Lett.* **17**, 1772 (1992), e) D. P. Hand and P. St. J. Rusell, *Opt. Lett.* **15**, 102 (1990).
9. a) P. Krecmer, A. M. Moulin, R. J. Stephenson, T. Rayment, M. E. Welland and S. R. Elliot, *Science* **277**, 1799 (1997), b) V. K. Tikhomirov and S. R. Elliot, *Phys. Rev. B.* **51**, 5538 (1995), c) K. Tanaka, K. Ishida and N. Yoshida, *Phys. Rev. B.* **54**, 9190 (1996), d) V. Lyubin, M. Klebanov, V. Tikhomirov and G. Adriaenssens, *J. Non.Cryst Solids*, **198-200**, 719 (1996).
10. For example, P. A. Blanche, Ph. C. Lemaire, C. Maertens, P. Dubois and R. Jérôme, *Opt. Comm.* **139**, 92 (1997).
11. J. Albert, B. Malo, D. C. Johnson, F. Bilodeau, K. O. Hill, J. L. Brebner and G. Kajrys, *Opt. Lett.* **18**, 1126 (1993).
12. See for example, R. W. Boyd, *Nonlinear Optics*, (Academic Press Inc. San Diego, 1992).
13. J. F. Reintjes, *Nonlinear Optical Parametric Processes in Liquids and Gases*, (Academic Press, New York, 1984).
14. B. A. Garetz, J. E. Aber, N. L. Goddard, R. G. Young and A. S. Myerson, *Phys. Rev. Lett.* **77**, 3475 (1996).

15. B. Rånky and J. F. Rabek. *ESR Spectroscopy in Polymer Research.* (Springer-Verlag, Berlin, 1977).

# 7. CONCLUSIONS, SUGGESTIONS FOR FUTURE RESEARCH AND CONTRIBUTIONS TO ORIGINAL KNOWLEDGE

## 7.1 SUMMARY OF RESEARCH AND SUGGESTIONS FOR FUTURE WORK

The research presented in this thesis has advanced our understanding of certain aspects of sol-gel derived hybrid organosilica composites. In the following Sections, we summarise our studies, which identified and characterised some structural and optical properties of these materials. We also make suggestions for future work.

### 7.1.1 Free-radical polymerisation and co-densification in SAC-01 thin films

We examined photo-induced process in sol-gel derived silica-methacrylate (SAC-01) thin films, which are used for the photolithography of integrated-optics devices. Light-initiated reactions were studied through a variety of techniques including UV-Vis, FT-IR and $^{29}$Si NMR spectroscopy. Photoreactions in SAC-01 thin films were also monitored *in situ* through waveguide Raman spectroscopy. In this instance, guided optical modes of a visible laser beam excited Raman scatter from a SAC-01 planar waveguide, which was simultaneously irradiated with UV light. Light-induced changes to macroscopic properties of the composite, including index of refraction and film thickness, were measured with *m*-line spectroscopy and profilometry respectively.

From these studies, our understanding of photoreactions in the composite thin films is as follows. UV light initiates free-radical polymerisation of methacrylate functionalities in the SAC-01 composite. These reactions do not proceed in isolation in the sol-gel derived, cross-linked silica host. Our spectroscopic studies indicate that organic chain formation triggers polycondensation reactions between residual silanol and silicon alkoxide groups, which in turn lead to growth and compaction of the host silica matrix. A possible mechanism for this behaviour is schematised in Figure 7.1. Polymerisation of propyl methacrylate substituents decreases the distance between silicon centres, bearing reactive hydroxy and alkoxy functionalities. Condensation reactions between the moieties ensue, leading to additional siloxane bonds and growth of the silica network. The mechanism of silica co-densification through organic polymerisation in our *hybrid* system contrasts sharply to purely inorganic silica networks, where significantly higher photon energies (vacuum UV) are required for matrix densification.

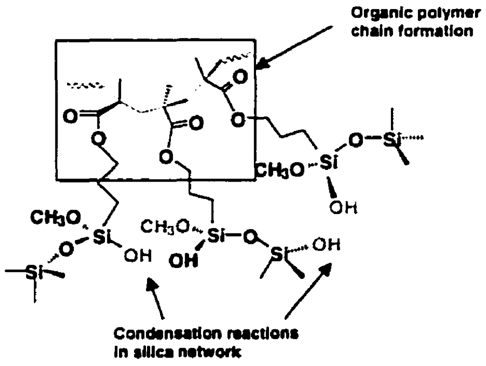

**Figure 7. 1** Model for collateral densification of silica in hybrid silica-methacrylate composite

We correlated molecular scale matrix densification and compaction to spatially localised increases of the index of refraction. Emphasis was placed on the spatial localisation of photo-induced refractive index change. This was dramatically illustrated in Bragg grating fabrication, which consisted of a long-range, sub-micrometric modulation in the index of refraction. Free-radical reactions are strongly confined to regions of illumination in the composite because organic polymerisation is hosted in a cross-linked silica network, where the polymerisable organic units are covalently grafted to silicon centres and the growth of the silica network accompanies organic chain growth.

#### 7.1.1.1 Suggestions for future work: silica densification with visible light

The ability to densify silica at low optical energies implies that device lithography may be shifted to even lower energies simply by selecting an appropriate photo-initiator. The methacrylate moiety in the SAC-01 composite has electronic excitation bands in the UV region, which coincide with currently employed UV lithographic wavelength. The inherent UV absorption of the thin film, causes attenuation of the inscribing beam and therefore reduces curing depth. In addition, extensive irradiation may cause degradation of polymer chains in the composite. We anticipate that by selecting a photo-initiator that is activated with visible light, problems associated with light attenuation and polymer degradation will be alleviated. In this case, the only absorbing species would be the photoinitiator, which upon irradiation would initiate free-radical reactions. Furthermore, as reactions proceed and photo-initiator molecules are consumed, material transparency to the inscribing beam would actually improve.

### 7.1.2 Self-focusing of light in SAC-01 composites

We have identified and characterised self-focusing of a continuous wave, visible laser beam in SAC-01 planar waveguides. Guided optical mode of the laser beam initiates free-radical polymerisation of methacrylate substituents in the SAC-01 slab. As it propagates in the nascent reaction medium, the beam encounters a continuously changing refractive index. Refractive index changes in the SAC-01 composite are strongly localised in space and are proportional to the optical field intensity. Consequently, a refractive index gradient develops with a maximum at the axial (most intense) region of the beam. This lens-like profile continuously focuses on-coming light and traps it in a narrow region of enhanced refractive index. The reciprocal action of self-focusing and lens-formation creates a channel waveguide, which guides the beam across the medium and suppresses diffraction. Refractive index changes in the SAC-01 medium are permanent and wet-etching of the slab with an organic solvent revealed the channel waveguide, inscribed by the self-focusing laser beam. As shown in Figure 7.2, this is a narrow, roughly cylindrical structure with a diameter of approximately 10 μm. This "optical fibre on a chip" has potential as an interconnect between optical fibres and planar integrated optics systems.

**Figure 7. 2** Self-inscribed channel waveguide in SAC-01 medium

In classical examples, self-focusing was observed in the nonlinear optical regime, where intense (Megawatt) laser pulses induced anharmonicity in electronic polarisation. This led to spatially localised and intensity dependent refractive index changes in dielectric media, which in turn elicited laser self-focusing. We emphasise that self-focusing in the SAC-01 composite occurs through refractive index changes caused by a photochemical reaction, namely the photo-initiated polymerisation of methacrylate functionalities in the hybrid network. We have examined the power dependence of self-focusing in SAC-01 media. The rate of free-radical reactions (and thus refractive index change) are greater at higher laser powers. In turn, self-focusing is achieved at earlier times with increasing laser power. We have also obtained evidence of beam filamentation or break up at laser powers of 500 mW. In addition to the SAC-01 medium, we have examined self-focusing in a range of newly synthesised sol-gel derived organosilica composites. In each of these cases, the kinetics of self-focusing could be correlated to the rate of photo-initiated free-radical polymerisation in the material.

We have also observed self-focusing of white light, a spatially and temporally incoherent wavepacket, in SAC-01 colloids. The beam induces a gradient in the refractive index and propagates without diffraction in the fluid colloidal medium. We attribute this phenomenon to the principally to the non-instantaneous response time of the system – *i.e.* there is a delay between irradiation and refractive index increase in the system. The rates of free-radical reactions occur on the scale of milliseconds to seconds in the SAC-01 composite. Thus, the medium is not sensitive to the femtosecond phase changes of the polychromatic, "speckled" white beam. Rather, it "sees" a time-averaged spatial and temporal intensity of the beam, which then propagates in its self-induced waveguide. As in the case of SAC-01 planar waveguides, refractive index changes in the colloidal medium are permanent. Transmission electron micrographs of cross-sections of the self-inscribed waveguide revealed a remarkable degree of organisation in the SAC-01 medium, which have until now been considered amorphous glasses.

Our observation of laser self-focusing through organic chain growth presents a new perspective to a field that has been dominated by photophysical mechanisms. Significantly, laser-induced refractive index changes are permanent in our hybrid network and may be elaborated through a simple wet-etching step. By contrast, refractive index changes in nonlinear optical media are transient and relax once the optical field is removed. In our case, laser induced refractive index changes persist in the material even after the optical field has been removed, and as shown in Figure 7.2, provide "structural" insight into light-matter interactions during the self-focusing event. Furthermore, laser self-focusing due to free-radical polymerisation presents a unique tool to the polymer chemist, namely the ability to examine organic chain growth in the highly nonlinear optical environment provided by a self-focusing beam.

#### 7.1.2.1 Suggestions for future work: spatial solitons in SAC-01 composites

Laser self-focusing is a prerequisite for spatial soliton formation in nonlinear optical media. At a critical power, the self-focusing effect of a monochromatic beam precisely counterbalances its tendency to diffract in the medium. Under this condition, the spatial profile of the laser beam is preserved as it propagates in the material. This is a spatial soliton. We have observed that laser self-focusing in the SAC-01 medium is a power dependent process. The critical power must be located at which spatial solitons are formed in our photochemical system. With our current experimental set-up, we are able to monitor the output-intensity of self-focusing light. In order to observe spatial solitons in our system, the optical assembly must be complemented with a CCD beam profiler, which enables the three-dimensional intensity profile of the input and the output beams to be accurately monitored over time.

There is currently significant interest in the interactions between spatial solitons. As mentioned in Chapter 4, studies have already identified repulsion, attraction, spiralling and fusion between these solitary waves. In all of these cases, soliton interactions have been characterised through optical methods, *i.e.* by monitoring the spatial and temporal behaviour of the output beams. Refractive index changes that give rise to spatial solitons would be permanently imprinted in the SAC-01 medium. This presents the exciting possibility of obtaining "frozen" images of solitons as well as interactions between them.

### 7.1.3 Self-organisation and photo-manipulation of sub-micrometric methacrylate-derivatised silica domains

We have identified and characterised self-organisation in composites formed from the controlled hydrolysis and polycondensation reactions of methacrylate-substituted alkoxysilanes. Resulting organosilica colloids consist of a long-range, periodic, interdigitated arrangement of methacrylate-derivatised silica domains. To our knowledge, this is the first report of self-organisation in sol-gel derived silica formed in the absence of external, liquid crystalline organic templates. Significantly, the periodicities associated with the organised structures are approximately 250 nm. Such dimensions, which approach optical wavelengths, cannot be achieved with conventional techniques of sol-gel derived silica grown in the presence of liquid crystalline templates.

We propose a microemulsion model to explain these observations. Hydrolysis of 3-methacryloxypropyltrialkoxysilane (MAPTMS) precursor leads to an amphiphilic species with an organic tail and a hydrophilic silanol bearing head. A thermodynamically stable microemulsion results, where monolayers of these amphiphiles separate the aqueous and the organic (MAPTMS) regions in the system. The microstructure of the system consists of a bicontinuous, interdigitated, periodic arrangement of aqueous and organic conduits. As silica growth is strictly confined to the aqueous regions of the system, the structure of the microemulsion is "fossilised" in the composite. Subsequent, UV-irradiated free-radical polymerisation of the methacrylate moieties in the composite, permanently captures the sub-micrometric order of the microemulsion in a transparent but structurally anisotropic monolith. The polymerised acrylate component can be selectively pyrolysed, leaving a three-dimensionally intact, periodic inorganic shell.

Thin films cast from the colloid, consist of a bicontinuous arrangement of methacrylate derivatised silica domains. We have observed that these thin films exhibit significant iridescence. Diffraction of visible light occurs due to the sub-mictrometric arrangement of the domains. Thin films of silica-methacrylate composites offer unique photo-initiation possibilities with a laser beam, which restricts free-radical polymerisation to its focussed beam spot. Figure 7.3 is a scanning electron micrograph that traces the radially symmetric polymerisation effects on a silica-methacrylate film surface. Alternatively, if the laser beam is injected into the transparent film, its waveguide modes

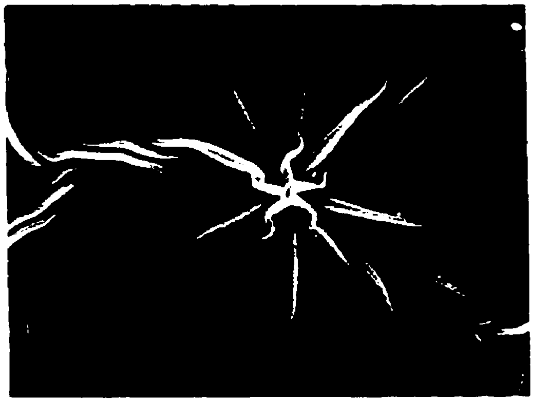

**Figure 7. 3** Laser-induced changes in silica-methacrylate thin film

Our inherently organised composites are valuable options for two and three-dimensionally ordered silica nanostructures. Considerable materials research effort is currently directed towards artifical, microstrucutred silica materials for catalytic, sensor, medical and photonic applications. The principal strategy in these attempts has been surfactant-templated growth of silica. However, long-range order is limited by weak silicate-micelle interactions and is restricted to the number of micellar phases available.

### 7.1.3. 1 Suggestions for future work: covalently bound templates for organised silica growth and optical properties of silica-methacrylate composites

The model that we propose to explain self-organisation in the MAPTMS system is based on the amphiphilic nature of a hydrolysed organosubstituted alkoxysilane. The concept of introducing order in a sol-gel derived system through a covalent substituent must be examined further There are several organo-substituted alkoxysilane precursors that are readily available commercially. A systematic study can thus be conducted, identifying the effects of substituent length, volume and hydrophobicity on the final structure of the composite. Phase diagrams must be created to probe the effects of parameters such as concentration, temperature and pH on the structure. It would also be interesting to monitor the structure of the microemulsion with time, to assess if it undergoes changes as silica growth proceeds in the system.

As mentioned earlier, one of the most exciting aspects of our observation is the periodicity associated with self-organisation. The compatibility of these silica-based materials with optical wavelengths, the ability to create both three and two-dimensional organised structures, the presence of a photosensitive methacrylate substituent as well as the potential of tuning the refractive index of the structures (by doping with other metal alkoxides) are features that make these materials attractive for photonic applications. The diffraction properties of these structures at optical wavelengths must be investigated further in order to examine their potential as photonic band gap materials.

### 7.1.4 Photo-oriented polymerisation with linearly polarised, self-focusing laser beams in SAC-01 planar waveguides

We have characterised photo-induced birefringence in self-inscribed channel SAC-01 waveguides through polarised waveguide Raman and optical birefringence studies. In order to explain these effects, we have proposed a mechanism of photo-oriented, free-radical polymerisation of methacrylate substituents. Organic chain growth is carried out under the anomalously high intensities provided by a self-focusing laser beam. It is possible that under the intense optical field, methacrylate monomer units exhibit nonlinear polarisation responses. In such a case, linearly polarised light will induce a dipole along the most polarisable axis of the methacrylate unit and cause it to align parallel to the electric field of the laser beam. A net anisotropy is created in the material, which is oriented parallel to the polarisation of the incident beam. Simultaneous free-radical reactions that take place in the network, link the oriented methacrylate units to each other. In this way, the net anisotropy created by the nonlinear optical response of the methacrylate units is preserved in the SAC-01 waveguide.

#### 7.1.4.1 Suggestions for future studies: modelling birefringence decay and photo-induced orientation with other organic substituents

Careful study and modelling of birefringence decay in self-inscribed channel waveguides will give more information on the "poled" order in the SAC-01 systems. It is also suggested that photo-orientation of polymerisable units other than methacrylate substituents are examined. In this way, the effect of the electronic distribution and consequent nonlinear polarisation on the photo-induced birefringence may be examined. It would also be interesting to examine the effects of a circularly polarised, self-focusing laser beam on the photo-induced birefringence in the SAC-01 medium.

## 7.2 CONTRIBUTIONS TO ORIGINAL KNOWLEDGE

1) Our understanding of photo-processes in sol-gel derived silica-methacrylate thin films – in the context of integrated-optics device photolithography - has been advanced. A process in which light-initiated free-radical polymerisation of methacrylate substituents trigger the growth and densification of their silica host was identified for the first time. This presents the possibility of achieving silica-densification in hybrid organosilica materials with low-energy, optical wavelengths.

2) The application of waveguide Raman spectroscopy for monitoring photo-processes in planar waveguides *in situ* was demonstrated for the first time. *In situ* studies of UV-light and visible laser induced photo-processes in silica-methacrylate planar waveguides provided additional insight into photo-initiated free-radical reactions and collateral silica densification in the medium.

3) Laser self-focusing was identified and characterised in SAC-01 waveguides. Guided optical modes at 514.5 nm, initiate free-radical polymerisation as they propagate in the silica-methacrylate medium. The resulting refractive index changes lead to laser self-focusing. We have emphasised that this phenomenon, typically observed in nonlinear optical materials, occurs due to a photochemical reaction in our hybrid composite. By examining self-focusing in various silica-methacrylate materials, we have demonstrated that self-focusing kinetics may be qualitatively related to the rate of photo-initiated polymerisation in these media.

4) Refractive index changes in the silica-methacrylate composite are permanent. Thus, the channel waveguide inscribed by the self-focusing beam could be revealed in the silica-methacrylate medium with a simple wet-etching step. This allowed for the first time, the "visualisation" of self-focusing light-matter interactions even after the optical field was removed. The self-inscribed waveguide is also, to our knowledge, the first example of a cylindrical waveguide supported on a planar substrate. The passive device has potential as an interconnect between optical fibres and planar integrated-optics modules.

5) We have observed self-focusing of white light in silica-methacrylate colloids. A beam of spatially and temporally incoherent white light was observed to propagate without diffraction, through a self-inscribed waveguide. We attribute this phenomenon primarily to the non-instantaneous and quasi-local photo-response of the silica-methacrylate medium. This is only the second report of white-light self-focusing. The first was observed in photorefractive crystals.

6) Long-range, periodic, three-dimensional self-organisation was identified in a series of sol-gel derived silica-methacrylate composites. A model based on an organised microemulsion system was proposed, where silica growth takes place exclusively in the aqueous regions, thus preserving the microstructure of the microemulsion. This is the first example of self-organisation observed in sol-gel derived composites in the absence of external liquid crystalline templates. Furthermore, the periodicity associated with organisation is approximately 250 nm, which exceeds the dimensions that may be obtained with existing template-based strategies towards ordered silica structures.

7) Our understanding of photo-induced anisotropy in SAC-01 waveguides has been advanced. Linearly polarised, self-focusing laser beams in silica-methacrylate waveguides induce optical anisotropy in self-inscribed channel waveguides. In accounting for photo-induced birefringence, we propose that the anomalously high intensities created by a self-focusing laser beam drive the system into the nonlinear optical regime. A net anisotropy is created through the optical Kerr effect of the methacrylate monomer units, which is "frozen" through the free-radical polymerisation reactions. Thus, the final structure retains the optical birefringence induced by a nonlinear optical process. We have advanced the notion that the linearly polarised optical field presents an anisotropic reaction medium, which imparts orientation into the growing polymer chains.